Terms and Conditions of Use of Digitised Theses from Trinity College Library Dublin

Copyright statement

All material supplied by Trinity College Library is protected by copyright (under the Copyright and Related Rights Act, 2000 as amended) and other relevant Intellectual Property Rights. By accessing and using a Digitised Thesis from Trinity College Library you acknowledge that all Intellectual Property Rights in any Works supplied are the sole and exclusive property of the copyright and/or other IPR holder. Specific copyright holders may not be explicitly identified. Use of materials from other sources within a thesis should not be construed as a claim over them.

A non-exclusive, non-transferable licence is hereby granted to those using or reproducing, in whole or in part, the material for valid purposes, providing the copyright owners are acknowledged using the normal conventions. Where specific permission to use material is required, this is identified and such permission must be sought from the copyright holder or agency cited.

Liability statement

By using a Digitised Thesis, I accept that Trinity College Dublin bears no legal responsibility for the accuracy, legality or comprehensiveness of materials contained within the thesis, and that Trinity College Dublin accepts no liability for indirect, consequential, or incidental, damages or losses arising from use of the thesis for whatever reason. Information located in a thesis may be subject to specific use constraints, details of which may not be explicitly described. It is the responsibility of potential and actual users to be aware of such constraints and to abide by them. By making use of material from a digitised thesis, you accept these copyright and disclaimer provisions. Where it is brought to the attention of Trinity College Library that there may be a breach of copyright or other restraint, it is the policy to withdraw or take down access to a thesis while the issue is being resolved.

Access Agreement

By using a Digitised Thesis from Trinity College Library you are bound by the following Terms & Conditions. Please read them carefully.

I have read and I understand the following statement: All material supplied via a Digitised Thesis from Trinity College Library is protected by copyright and other intellectual property rights, and duplication or sale of all or part of any of a thesis is not permitted, except that material may be duplicated by you for your research use or for educational purposes in electronic or print form providing the copyright owners are acknowledged using the normal conventions. You must obtain permission for any other use. Electronic or print copies may not be offered, whether for sale or otherwise to anyone. This copy has been supplied on the understanding that it is copyright material and that no quotation from the thesis may be published without proper acknowledgement.

An investigation into the role of substrate stiffness and oxygen availability in the regulation of stem cell differentiation during tissue regeneration

Darren Paul Burke BA BAI

A thesis submitted to the University of Dublin in partial fulfilment of the requirements for the degree of

Doctor in Philosophy

Trinity College Dublin

October 2013

Supervisor

Dr Daniel J. Kelly

External Examiner

Prof Liesbet Geris

Internal Examiner

Prof David Taylor

Declaration

I declare that this thesis has not been submitted as an exercise for a degree at this or any other university and it is entirely my own work.

I agree to deposit this thesis in the University's open access institutional repository or allow the library to do so on my behalf, subject to Irish Copyright Legislation and Trinity College Library conditions of use and acknowledgement.

ke

Summary

Mesenchymal stem cells (MSCs) are multipotent cells which can differentiate down multiple lineages and potentially generate tissues such as cartilage, bone or adipose tissue. It is becoming increasingly clear that mechanical cues also play a key role in determining the fate of such cells. Extrinsic mechanical stimuli such as tissue deformation, fluid flow and hydrostatic pressure have often been implicated as regulators of tissue differentiation *in vivo*. It has been possible to test different hypotheses for mechano-regulated MSC differentiation by attempting to simulate regenerative events such as bone fracture repair, where repeatable spatial and temporal patterns of tissue differentiation occur. More recently, *in vitro* studies have identified other environmental cues such as substrate stiffness and oxygen availability as key regulators of MSC differentiation; however it remains unclear if and how such cues determine stem cell fate *in vivo*. For example, the stiffness of the local matrix elasticity has been shown to be intimately linked to MSC differentiation, where an osteogenic phenotype is promoted by a stiff substrate, while adipogenesis is enhanced by exposure to a soft substrate. Oxygen availability is another known regulator of MSC differentiation. Both adipogenesis and osteogenesis have been shown to be diminished under low oxygen conditions, whereas chondrogenesis is promoted by hypoxia.

This thesis employed a computational mechanobiological approach to explore the role of substrate stiffness and oxygen availability as regulators of stem cell fate *in vivo*. Undertaking such an approach involves the development of a predictive computational framework in which the rules for stem cell differentiation can be input. Predictions of tissue distributions during a regenerative event are output by the model. The validity of a potential differentiation rule is assessed by determining if simulations produce accurate temporal and spatial predictions of tissue phenotypes. As part of this thesis, a computational framework was developed to test the hypothesis that substrate stiffness and oxygen availability regulate stem cell differentiation during tissue regeneration. Rather than assuming mechanical signals act directly on stem cells to determine their differentiation pathway, it was postulated that they act indirectly to regulate angiogenesis and hence partially determine the local oxygen environment within a regenerating tissue. Chondrogenesis of MSCs was hypothesized to occur in low oxygen regions, while in well vascularised regions of the regenerating tissue a soft local substrate was hypothesised to facilitate adipogenesis while a stiff substrate facilitated osteogenesis.

This bioregulatory model of tissue differentiation was applied to a number of different regenerative scenarios, with predictions compared to both experimental data and to predictions from another well established computational mechanobiological model where tissue differentiation is assumed to be regulated directly by the local mechanical environment. When

applied to the fracture healing regenerative event, the model successfully predicted all the major events of fracture repair, including cartilaginous bridging, endosteal and periosteal bony bridging and bone remodelling. The model was also applied to fracture repair in Thrombonspondin-2 (TSP2)-null mice, where a significantly altered pattern of healing is observed versus wild type controls in spite of the mechanical environment remaining similar. Model predictions successfully identified increased angiogenic progression as a result of TSP2 deletion as the key driver of the altered healing pattern. In the context of testing such tissue differentiation hypotheses within an *in silico* framework, the greater the number of scenarios in which the underlying model hypothesis is subjected to attempted falsifiability [1], but ultimately corroborated, the stronger the hypothesis becomes.This thesis next tested the hypothesis that substrate stiffness and oxygen availability could predict MSC differentiation *in vivo* in a different regenerative event, the implanted bone chamber. The model successfully predicted key aspects of MSC differentiation, including the correct spatial development of bone, marrow and fibrous tissue within the unloaded bone chamber. The model also successfully predicted chondrogenesis within the chamber upon the application of mechanical loading.

At the heart of the tissue differentiation hypothesis proposed by this thesis is the assumption that mechanical stimuli have an indirect (rather than a direct) effect on tissue differentiation. This was explored by developing novel mechano-regulation models to investigate how mechanics regulate neovascularisation. This work highlighted a mechanism by which mechanics may regulate blood vessel growth directionality, and hence play a key role in determining stem cell fate in vivo. Support for the hypothesis that the direction of minimum principal strain acts as a mechanical guiding stimulus for directionality of neovascularization was provided via successful prediction of spatial blood vessel progression during large bone defect healing.

In conclusion, this thesis provided corroboration for the hypothesis that tissue differentiation is regulated by substrate stiffness and oxygen availability during a number of different regenerative scenarios. It is extremely difficult to design and perform *in vivo* studies to accurately isolate and relate specific stimuli, such as those identified in previously mentioned *in vitro* studies, to the temporal and spatial patterns of tissue differentiation that occur during regenerative events. *In silico* studies such as those performed in this thesis, however, can be used to predict the state of the local environment experienced by MSCs during complex regenerative scenarios. Such corroboration and/or rejection of tissue differentiation hypotheses provide improved understanding of the regulation of MSC fate. The therapeutic potential of MSCs is substantial. The results of this thesis enhance current knowledge and understanding of MSC behaviour and will bring us closer to exploiting their full potential in regenerative medicine.

Acknowledgements

Firstly, I would like to sincerely thank Danny for his guidance, motivation and endless positivity over the past four years. I left every meeting with a positive outlook on my research and where it was going (or at least "something to think about").

I'd also like to thank everyone in TCBE for making my time here such an enjoyable experience. Much appreciation has to go to Alanna, Eamon and Tariq who I have had the pleasure of spending 4 years with, who were always there to keep each other sane, especially during those tough thesis write up times (even if that meant doing online personality tests at 11pm on a Friday night!). Thanks also to Thomas and Adam- the computational crew, always on hand for nerdy discussion or trip down to TCHPC! Thanks to Tat, Steve and Eoghan who made me feel at home upon starting and showed how it should be done in terms of finishing! To my founding partner of 4sies Grainne! Further thanks to Yuroung (Feel better man!!), Lu ("The Big Cat"), Simon, The "Beautiful" Henrique, Katey, Rebecca, Mike, Mark, Amy, Laura, Jake, Pedro, Raj, Binu, Conor, Alan, Lara, Olivier, Gill, Steve [2], Steve (Whelan), Gar, Liam, Tommy, Susan, Andy (American), Andy (Newbie), Mirka, Masooma (Back of the head buddies), Hanifeh (don't we need to pin a paper on a certain door?) and all the other postgraduates for providing excellent companionship over the past four years. I must also thank DUAFC and all the football lads (In particular Drico (still doesn't get it), who went through the same four years as I did and was always on hand to have tactical PhD discussion).

The assistance of Joan, Melanie, June and Judy has been invaluable throughout the past four years.

To Gormo, Chrissy, Deano, Iano, Liamo and all the rest of the lads who provided solid banter (which is invaluable for those times when the research doesn't go to plan!)

Finally, I must thank my family for all their support throughout the years!!

Table of contents

List of figures

List of tables

Nomenclature

The nomenclature contains some of the abbreviations used in this thesis. It is not a full list of all abbreviations and symbols used - they will be explained in the text whenever used.

Ang	angiopoietin
bFGF	basic fibroblast growth factor
BMP	bone morphogenic protein
CC	calcified cartilage
CSK	cytoskeletal
dpf	days post fracture
EC	endothelial cell
ECM	extracellular matrix
FE	finite element
FGF21	fibroblast growth factor 21
HIF1	hypoxia-induction-factor
HP	hydrostatic pressure
HUVEC	human umbilical vein endothelial cell
IFS	interfragmentary strain
LEGI	local excitation/global inhibition
MSC	mesenchymal stem cell
NMM	nonmuscle myosin
OFF	oscillatory fluid flow
SMC	smooth muscle cell
TAZ	transcriptional coactivator with PDZ-binding motif
TNF-α	tumour necrosis factor-α

TSP2	thrombospondin-2
VEGF	vascular endothelial growth factor
VOI	volume of interest
WT	wild type
YAP	yes-associated protein

Publications and conference contributions

Publications

Burke, D.P. and D.J. Kelly, *Substrate Stiffness and Oxygen as Regulators of Stem Cell Differentiation during Skeletal Tissue Regeneration*: A Mechanobiological Model. PLoS One, 2012. **7**(7): p. e40737.

Burke, D., M. Dishowitz, M. Sweetwyne, E. Miedel, K.D. Hankenson, and D.J. Kelly, *The role of oxygen as a regulator of stem cell fate during fracture repair in TSP2-null mice. Journal of orthopaedic research* : official publication of the Orthopaedic Research Society, 2013. In press.

Burke, D., Khayyeri, H., D.J. Kelly, *Substrate Stiffness and Oxygen Availability as Regulators of Mesenchymal Stem Cell Differentiation within a Mechanically Loaded Bone Chamber*. Under review.

Burke, D., D.J. Kelly, *A Mechanobiological Model of Endothelial Cell Migration and Proliferation*. Under review.

Conference contributions

Burke, D., D.J. Kelly, 2011. *Could substrate stiffness and oxygen tension regulate stem cell differentiation during fracture healing?* Proceedings of Bioengineering in Ireland, the Annual 17th Conference of the Section of Bioengineering of the Royal Academy of Medicine in Ireland. National University of Ireland Galway, Galway, Ireland. (Presentation).

Burke, D., D.J. Kelly, 2011. *Could substrate stiffness and oxygen tension regulate stem cell differentiation during fracture healing?* 14th Annual Sir Bernard Crossland Symposium - University of Ulster, Belfast, Northern Ireland. (Presentation representing Trinity College Dublin).

Burke, D., D.J. Kelly, 2011. *Could substrate stiffness and oxygen tension regulate stem cell differentiation during fracture healing?* Proceedings of the ASME 2011 Summer Bioengineering Conference. Nemacolin Woodlands Resort, Famington, Pennsylvania, USA. (Presentation).

Burke, D., Dishowitz, M., Sweetwyne M., Miedel, E., Hankenson, K., Kelly, D.J., 2012. *The Role of Oxygen Tension as a Regulator of Stem Cell Differentiation during Fracture Repair in TSP2-Null Mice*. Proceedings of Bioengineering in Ireland, the Annual 18th Conference of the Section of Bioengineering of the Royal Academy of Medicine in Ireland. Queens University, Belfast, Northern Ireland. (Presentation).

Burke, D., Dishowitz, M., Sweetwyne M., Miedel, E., Hankenson, K., Kelly, D.J., 2012. *The Role of Oxygen Tension as a Regulator of Stem Cell Differentiation during Fracture Repair in TSP2-Null Mice*. 18th Congress of the European Society of Biomechanics, Instituto Superior Técnico (IST), Lisbon, Portugal. (Presentation).

Burke, D., Khayyeri, H., D.J. Kelly, 2013. *Substrate Stiffness and oxygen availability as regulators of stem cell differentiation in the implanted bone chamber.* Proceedings of Bioengineering in Ireland, the Annual 19th Conference of the Section of Bioengineering of the Royal Academy of Medicine in Ireland. Trinity College Dublin, Dublin, Ireland. (Presentation).

Burke, D., Khayyeri, H., D.J. Kelly, 2013. *Substrate Stiffness and oxygen availability as regulators of stem cell differentiation in the implanted bone chamber.* 21st Annual Symposium on Computational Methods in Orthopaedic Biomechanics, University of Texas, San Antonio, Texas. (Presentation and Poster).

Burke, D., Kelly, D.J., 2013. *Integrating computational mechanobiological methods and transgenic mouse models to eludicate the role of environmental factors in regulating stem cell fate during fracture repair.* Annual Meeting of the Orthopaedic Research Society 2013, Gonzalez Convention Center, San Antonio, Texas, USA. (Poster).

Chapter1: Introduction

This chapter will firstly introduce and provide a brief background of mechano-regulation of mesenchymal stem cell (MSC) differentiation. A similar background will then be provided for mechano-regulation of angiogenesis. Next, the global objective of the thesis is presented and motivated. The global objective is subsequently divided into a number of subobjectives which are introduced at the end of this chapter.

1.1 Mechano-regulation of stem cell differentiation

The analysis of regenerative events, such as fracture healing in long bones, has led to the development of a number of theories on how the mechanical environment regulates mesenchymal stem cell (MSC) differentiation *in vivo*. Over 50 years ago, Pauwels [3] hypothesised that distortional shear stress is a specific stimulus for collagen fibres and that cartilage formation is induced by a compressive stress stimulus. Bone formation could only occur after soft tissues had ensured sufficient stabilisation. Further theories of mechano-regulated tissue differentiation inspired by Pauwels initial hypothesis have suggested alternative mechanical stimuli as regulators of stem cell fate. Such theories have been investigated by employing a computational mechanobiological approach [4]. Carter *et al* [5] suggested hydrostatic stress and tensile strain or octahedral stress as regulators of tissue differentiation. They provided support for this hypothesis using finite element (FE) analysis and by demonstrating a correlation between the magnitudes of these stimuli and the appearance of specific tissue types within a fracture callus [6]. Claes and Heigele [7] proposed a similar regulation mechanism using quantified limits for strain and hydrostatic pressure as stimuli. Prendergast [8] hypothesized tissue differentiation was regulated by a combined stimulus of octahedral shear strain and relative fluid velocity. This model has been shown capable of predicting stem cell differentiation during multiple regenerative events such as fracture healing [9-11], osteochondral defect repair [12, 13], distraction osteogenesis [14], bone chamber [15-17], neoarthrotis formation [18] and others [19-21] providing strong corroboration for this hypothesis. Sole mechanical stimuli such as deviatoric strain, volumetric strain and principal strains have also been investigated as potential regulators of stem cell differentiation during fracture repair [9, 22, 23].

In addition to such mechanical cues, it has been demonstrated that extracellular matrix elasticity (or substrate stiffness) directs stem cell differentiation [24-26]. Soft matrices that mimic brain tissue were shown to be neurogenic, stiffer matrices that mimic muscle tissue were found to be myogenic, while more rigid matrices that mimic collagenous bone were demonstrated to be osteogenic [24]. Similar results were obtained in a bipotential model which permits osteoblast and adipocyte differentiation [25]. Adipogenesis was induced

in cells exposed to softer substrates while osteogenesis was induced in cells exposed to stiffer substrates. To date computational mechanobiological models have not been used to explore how substrate stiffness might regulate MSC fate *in vivo*.

1.2 Mechano-regulation of angiogenesis

In addition to mechanical stimuli, other environmental cues have been identified by in vitro studies as regulators of MSC differentiation. Oxygen availability is one such environmental cue. Severe impairment of adipogenic and osteogenic pathways has been demonstrated at low oxygen availability [27-29]. On the other hand, enhanced chondrogenesis has been shown under hypoxic conditions [30-32]. In addition, an increase in cartilage formation has been demonstrated in vivo in hypoxic fractures [33].

An inherent assumption of the previously mentioned tissue differentiation hypotheses is that mechanical signals act directly on MSCs to regulate their differentiation pathway. In conjunction, or perhaps alternatively, the local mechanical environment could also act indirectly to regulate MSC differentiation. For example, mechanical cues may regulate angiogenesis and hence the supply of oxygen and other factors to the wound site. This can lead to development of hypoxic regions within a regenerating tissue, which may repress some differentiation pathways while promoting others as previously mentioned. The possibility that mechanics act indirectly in this manner to regulate MSC fate has not previously been explored using *in silico* approaches.

Mechanical stimuli have been implicated to regulate angiogenesis in a number of ways. Firstly, the rate of blood vessel growth has been demonstrated to be influenced by the magnitude of mechanical stimuli experienced. A high mechanical stimulus may rupture capillary growth [34-38] decreasing the rate of blood vessel progression but a stimulus lower in magnitude has been implicated in promoting endothelial cell (EC) migration and proliferation increasing blood vessel growth rates [39-41]. In addition, application of mechanical stimuli has been demonstrated to regulate EC proliferation and migration direction [41-45], and hence bias blood vessel growth directionality. For example, it has been demonstrated that the application of mechanical stretch can influence neovessel

sprouting orientation, regulating blood vessel network morphometry [43]. It is therefore plausible that mechanics may regulate blood vessel growth directionality *in vivo* also.

Angiogenesis is vital to numerous regenerative scenarios [38, 46-48]. In spite of its importance, many tissue differentiation modeling frameworks have not included a model of angiogenesis [5, 7, 10, 49]. In those that have, angiogenesis has been regulated by biochemical cues, which could influence both blood vessel growth rate and directionality, or has been regulated by mechanics which influence only blood vessel growth rate [21, 50-53]. A modeling framework that describes mechanically driven blood vessel growth directionality during tissue differentiation has yet to be developed.

1.3 Objectives

The objective of this thesis is to explore an alternative hypothesis for how environmental factors regulate stem cell differentiation during regenerative events such as fracture repair. It is hypothesized that stem cell differentiation is regulated by substrate stiffness and oxygen availability during tissue regeneration. Rather than assuming mechanical signals, such as matrix deformation, act directly on stem cells to determine their differentiation pathway, it is postulated that they act indirectly to regulate angiogenesis and hence the local oxygen availability within a regenerating tissue. This hypothesis has been motivated by *in vitro* observations reported in the literature of how these factors in isolation regulate stem cell differentiation [24, 25, 27-32, 54]. It will be tested by developing a computational tissue differentiation model based on this hypothesis and applying it to various regenerative events in order to test its predictive capability. This work will employ a computational mechanobiological approach. Undertaking such an approach involves the development of a predictive computational framework in which the rules for stem cell differentiation can be input. Predictions of tissue distributions during a regenerative event are output by the model. The validity of a potential differentiation rule is assessed by determining if simulation predictions produce *"realistic tissue structures and morphologies"* [4].

The developed modelling framework will be initially applied to explore stem cell fate during fracture healing. Spatial and temporal predictions of tissue

differentiation generated by the model will be compared with both averaged histological images of tissue distributions during the different stages of fracture repair [55] and to simulation predictions generated from a well established tissue differentiation hypothesis regulated by shear strain and fluid velocity [8].

To further test the hypothesis, a study will be undertaken to determine if this model can predict changes in stem cell fate in a scenario where the callus mechanical environment remains similar. Thrombospondin-2 (TSP2) is a multifactorial matricellular protein, affecting many aspects of cell physiology [33]. Upon deletion of TSP2, the mouse fracture callus contains significantly more bone and less cartilage during fracture repair versus wild type controls under similar mechanical conditions [33]. This study will apply the proposed tissue differentiation model to explore fracture repair in TSP2-null mice and investigate potential mechanisms which may be driving such changes in tissue differentiation.

A robust test of a given hypothesis requires undertaking multiple experiments attempting to falsify the hypothesis. In the context of testing such tissue differentiation hypotheses within an *in silico* framework, the greater the number of scenarios in which the underlying model hypothesis is subjected to attempted falsifiability, but ultimately corroborated, the stronger the hypothesis becomes [56]. The third study of this work will test the hypothesis that substrate stiffness and oxygen availability can predict stem cell differentiation in a different regenerative event, the implanted bone chamber. Comparisons will be made between model predictions and experimental data of tissue distribution patterns in both loaded and unloaded conditions.

The next phase of this thesis will consider the possibility that mechanical cues might not act to prevent angiogenesis, but that the local mechanical environment could regulated blood vessel directionality. To begin to address this hypothesis, the mechano-regulation of angiogenesis and EC behaviour *in vitro* will first be explored. For this study, a computational model (specifically a lattice based model) will be developed capable of describing EC migration and proliferation in response to alterations in the mechanical environment. The model will be tested by attempting to simulate EC behavior under altered mechanical environments *in vitro* [42] . A number of hypotheses for how mechanics might

regulate EC physiology will be tested based on ability to predict experimental outcomes.

The final study of this thesis will test different hypotheses for mechano-regulation of angiogenesis (and subsequent stem cell differentiation regulated by substrate stiffness and oxygen availability) *in* vivo during stabilized and unstablized fracture repair. The hypothesis that a mechanical stimulus guides blood vessel directionality will be explored. Model predictions with blood vessel directionality guided by various mechanical stimuli will be tested for their validity by comparison with experimentally observed differences in vascular response under varied loading conditions [40]. Subsequently, the full modeling framework of angiogenesis and MSC differentiation will be applied and predictions compared to experimental assessment of tissue distributions during stabilized and unstabilized fractures.

By performing such investigations, this thesis will test the hypothesis that substrate stiffness and oxygen availability regulate stem cell differentiation in multiple regenerative scenarios. At the heart of this hypothesis is the assumption that mechanical stimuli have an indirect (rather than a direct) effect on tissue differentiation. This will be explored by developing novel mechano-regulation models to investigate how mechanics regulate neovascularisation.

Chapter2: Literature review

This chapter will provide a thorough background to this work by reviewing the applicable scientific literature. Firstly, mesenchymal stem cells (MSCs) will be introduced, followed by a review of how various environmental factors regulate stem cell differentiation (including mechanical signals, cell shape, substrate stiffness, oxygen availability and biochemical regulators). Next, a similar summary of how different environmental factors regulate angiogenesis will be provided. Finally, fracture healing and implanted bone chamber experiments are reviewed from a computational mechanobiological perspective.

2.1 Mesenchymal stem cells

Mesenchymal stem cells (MSCs) have the capacity to pursue numerous differentiation pathways and ultimately produce mesenchymal tissues such as bone, fat, adipose tissue, muscle, tendon and marrow stroma [57]. Friedenstein's [58] detailed investigations into the stem cells of bone marrow nearly 40 years ago led Caplan [59] to propose the term 'mesenchymal stem cell' to describe the earliest progenitor cell of this lineage. Five stages are proposed in the mesengenic process (Figure 2-1). Firstly, MSCs undergo mitosis and proliferate. This is followed by commitment to one of many potential stem cell lineages. Lineage progression precedes differentiation. The differentiated stem cell then matures and begins producing mesenchymal tissue.

Pittenger *et al* [57] performed investigations into MSC potential and found that stem cells could be induced to pursue adipogenic, osteogenic or chondrogenic lineages (Figure 2-1). Skin fibroblasts were also exposed to identical adipogenic, osteogenic or chondrogenic induction conditions but did not undergo any such differentiation. Primary fibroblasts, which are mature differentiated cells of the mesenchymal lineage, lack the differentiation capacity which is observed in human MSCs.

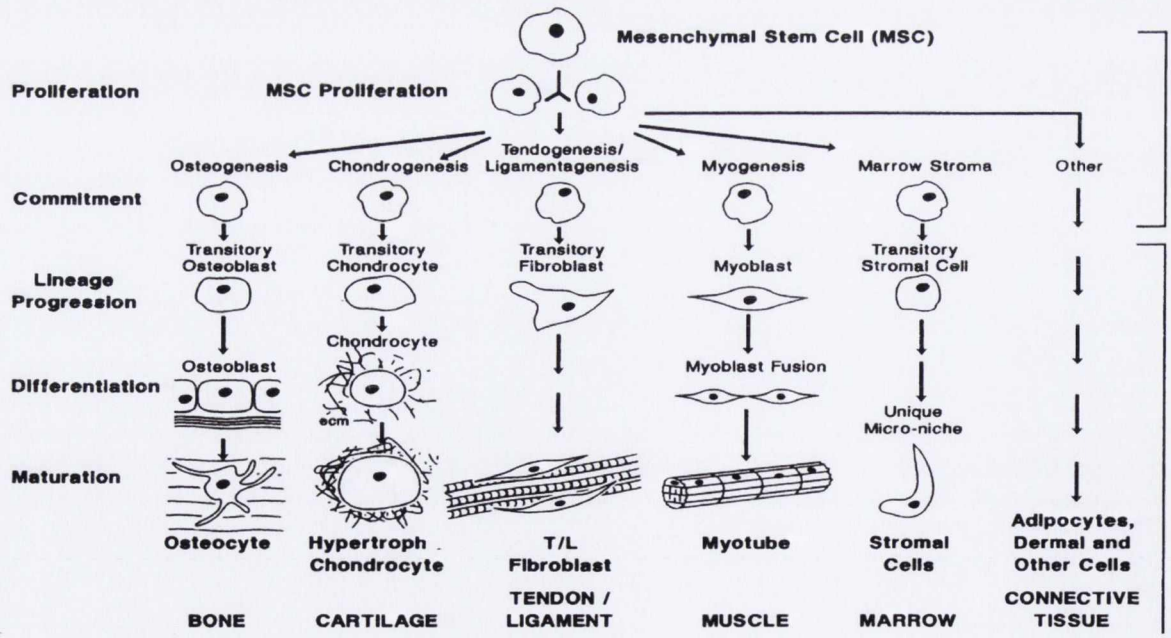

Figure 2-1.The pluripotential of mesenchymal stem cells [59]

Environmental cues will dictate lineage commitment of a stem cell. However, the specific environmental conditions that drive differentiation *in vivo* are not well understood. Substrate stiffness [24, 60, 61], cell shape [62, 63], mechanical forces [3, 5, 7, 64], oxygen tension [27, 28, 31, 54, 65] and biochemical cues [46, 57, 66] have all been implicated as factors which may influence MSC fate *in vivo*. Details of studies investigating many of these factors are discussed later in this review. Since MSCs have the potential to regenerate several important muscoskeletal tissues, greater understanding of how some or all of these factors are influencing the regulation of stem cell differentiation has significant implications in many (if not all) disciplines of regenerative medicine. Such information could allow the development of sensible and accurate strategies for the treatment of bone fracture, osteochondral defects, osteoarthritis, in the design of implant prosthesis and in many other areas.

2.2 Environmental factors regulating stem cell differentiation

Many factors have been implicated as possible regulators of stem cell differentiation. This section will review a number of such factors including mechanics, oxygen availability, substrate stiffness, biochemical cues and cell shape.

2.2.1 Mechanical signals

Extrinsic mechanical signals inflicted on a cell by its extracellular environment are thought to influence MSC fate. This section of the literature review will begin with early observations of the role of mechanics in regenerative events such as fracture repair, progress onto the first hypotheses of how mechanics may potentially regulate MSC fate and finally look at recent *in vitro* studies which investigate the influence of specific mechanical signals (compression, tension, hydrostatic pressure and fluid flow) on stem cell fate.

2.2.1.1 Early mechano-regulation theories

Fracture repair has been a commonly investigated regenerative event for many years. Experiments have demonstrated that mechanics have a significant influence upon fracture healing outcomes. Stronger and more compliant fracture healing with cyclic compression versus static compression has been demonstrated in a

rabbit model [67]. Application of cyclic loading results in greater callus size and stiffness at 8 weeks post fracture in an ovine model [68]. Excessive levels of strain lead to greater inflammation and a decrease in bone formation which ultimately hinders the normal healing process [69]. An interesting point is that for the same level of interfragmentary strain (IFS), larger fracture gap sizes heal more poorly than smaller gap sizes [69]. In an oblique fracture model, it was found that shear increased cartilage differentiation in rabbit fracture healing [70]. Such studies show the influence of mechanics on cell fate during regenerative events such as fracture repair. Observations such as these have led to a number of hypotheses of how mechanics may be directly regulating stem cell differentiation.

Over 60 years ago, Pauwels [3] put forward a theoretical framework proposing that mechanical deformation of regenerating tissue, as a result of mechanical forces, determined tissue differentiation. He hypothesised that distortional shear stress is a specific stimulus for collagen fibres and that cartilage formation is induced by a compressive stress stimulus following examination of the processes of fracture repair (Figure 2-2). He postulated that bone formation could only occur after soft tissues, such as cartilage and fibrous tissue, had provided sufficient stabilisation [3].

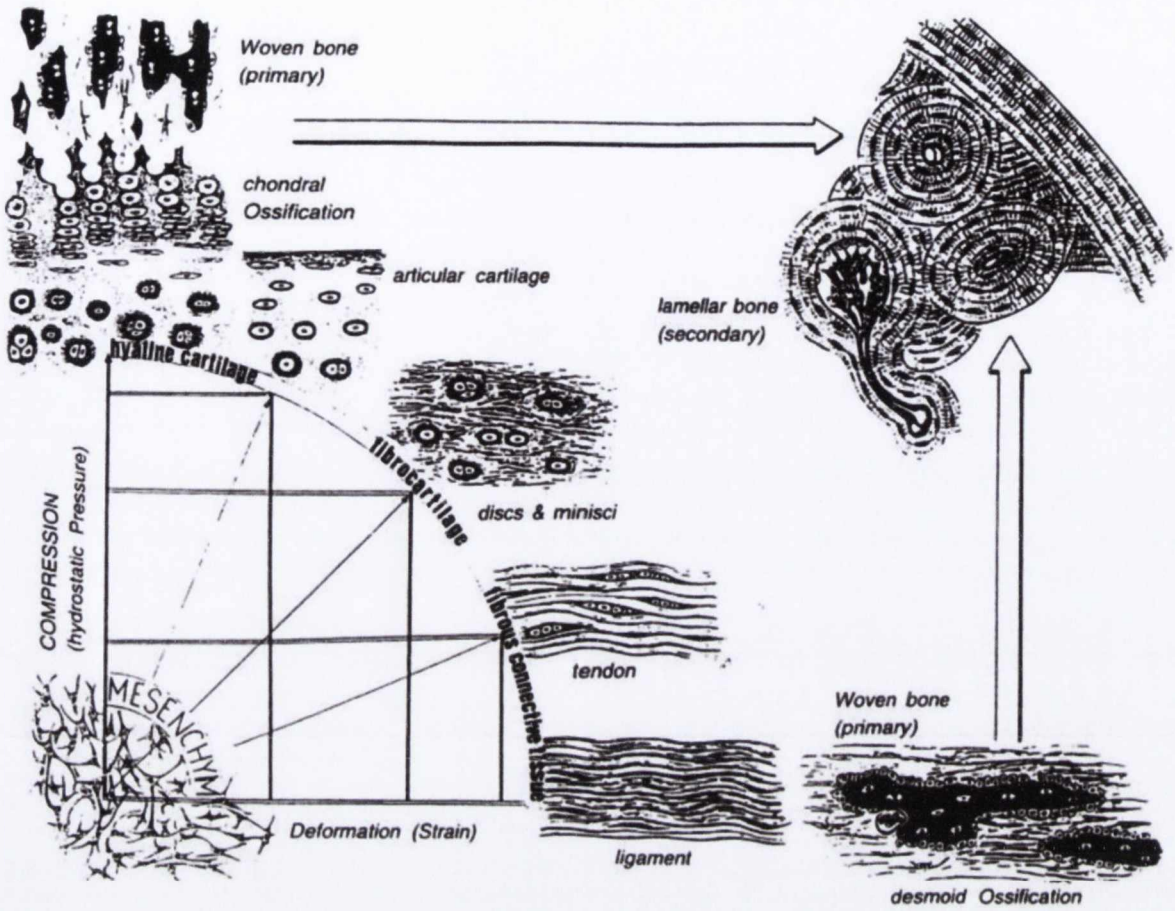

Figure 2-2. Pauwels theory of regulation of tissue differentiation (as illustrated by [71])

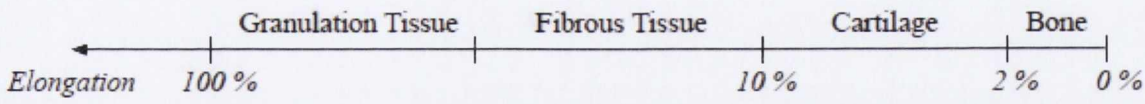

Figure 2-3. Elongation tolerences of fracture healing tissues [72]

Perren [72], motivated by Pauwels' work, proposed that tissue differentiation could be predicted via a process determined by whether or not the rupture strain of that tissue has been exceeded. In other words, a tissue is unable to form in a region where the level of strain exceeds that tissue's failure strain (Figure 2-3).

For example, if the local strain is 6%, cartilage would form in that region. The rupture strain for bone is approximately 2% and therefore bone cannot form in that region. It was suggested that tissue differentiation during fracture healing

could be explained by the level of IFS (Equation 2.1). Due to the very different rupture strains of the tissues, healing occurs by a progressive tissue differentiation from initial granulation tissue and fibrous tissue, which have very high tolerances for elongation, next is cartilage and finally bone is formed when the fracture has been sufficiently stabilized by the other soft tissues.

$$Interfragmentary\ Strain = \frac{Interfragmentary\ Motion}{Fracture\ Gap\ Size} \quad \text{(Equation 2.1)}$$

The interfragmentary theory has the advantage of being simple and convenient. Interfragmentary motion and gap size can both be obtained easily. However, there are limitations. Firstly, the callus is modelled as one dimensional entity ignoring the 3 dimensional complexity of a real callus. The interfragmentary strain theory is also limited in terms of predicting some aspects of fracture repair. For example, the theory predicts, for a given interfragmentary movement, better results with increasing gap size which does not agree with experimental results [69, 73]. Further theories of tissue differentiation inspired by the theories Pauwels and Perren based upon mechanical stimuli are summarised in Section 2.5 Computational Mechanobiology.

2.2.1.2 Mechanosensation

The processes of how MSCs sense their mechanical environment is complex and as of yet not fully understood. Cellular mechanosensors are required to analyse the mechanical environment and mechanotransduction is necessary to convert a mechanical stimulus into chemical activity. There are a number of potential cellular mechanosensors and mediators of mechanotransduction (Figure 2-4). Recent work [62] has highlighted the importance of the cytoskeletal network as a medium for cell mechanosensation of mechanical signals. Both intrinsic and extrinsic mechanical signals may alter tension in the cytoskeletal network of a cell. Cytoskeletal tension is a key component in determining cell shape, which itself is known as a regulator of MSC differentiation (see Section 2.2.2 Cell Shape). Cytoskeletal changes (which may be inflicted by mechanical stimulation or otherwise) have been demonstrated to initiate a cascade of biochemical events within a cell which lead to changes in gene expression and ultimately differentiation [62].

Integrins are transmembrane receptors which mediate the attachment between a cell and its local environment, which may include extracellular matrix (ECM) or other cells. It is possible that integrins experience mechanical stimuli and act as a cell's mechanosensors forming the link and possibly transferring tension to the cell's cytoskeletal network [74]. Local matrix stiffness can also play an important role and has been demonstrated to regulate integrin binding and the organization of adhesion ligands [75] (see Section 2.2.3 Substrate stiffness).

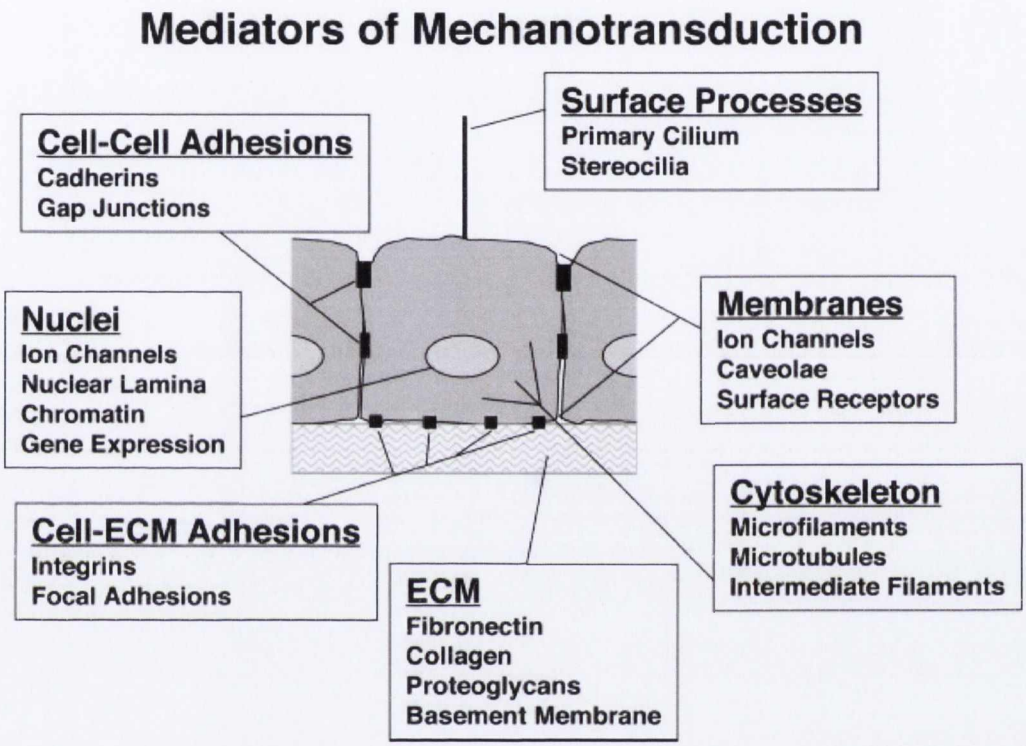

Figure 2-4. Mediators of cellular mechanotransduction [76]

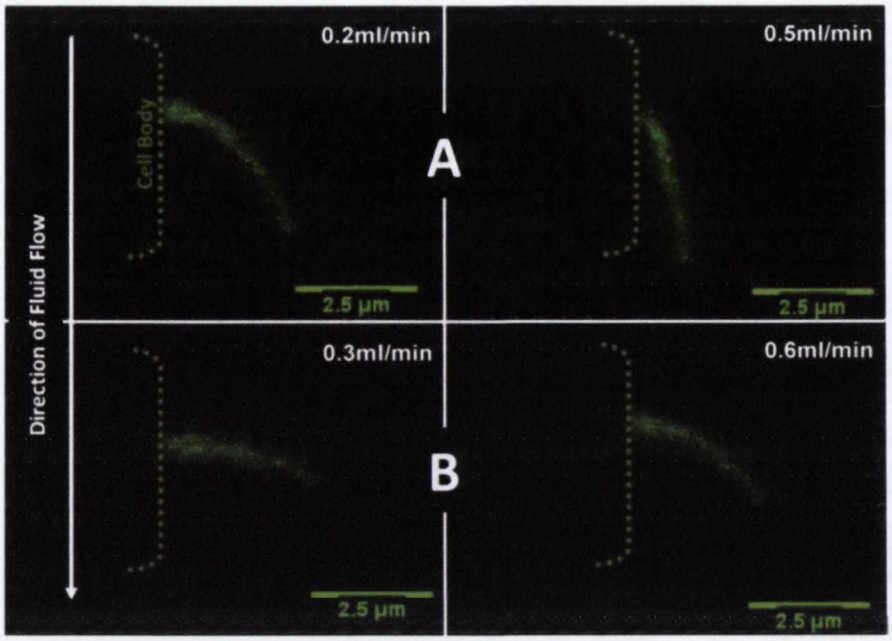

Figure 2-5. Primary cilia response to fluid flow. Following an initial period of bending due to applied fluid flow (A) and a rest period of 15 minutes, a decreased degree of bending is observed (B) despite higher flow rate. This would indicate that the mechanics of the primary cilium habe altered with time and possibly in response to the initial loading [77]

Primary cilia are solitary immotile microtubule-based slender structures that project out from the much larger cell body into its extracellular environment. They are thought to serve as dual sensory organelles capable of both mechanosensation and chemosenstation coordinating essential cell differentiation signaling pathways [78]. In terms of mechanosensation, primary cilia are believed to act as flow meters responding to oscillatory fluid flow (OFF) [79]. Hoey *et al* [79] demonstrated that the mechanics of the primary cilium change in response to OFF and that the cilia has a pro-osteogenic mechanosensory role (Figure 2-5).

Gap junctions have also been proposed as possible mechanisms of cellular mechanosensation [80]. A gap junction is an intracellular network of protein channels that permits cell-to-cell communication via the interchange of hormones, neurotransmitters and ions. Application of mechanical stimuli may initiate changes in intracellular communication and growth factor and other molecular secretion by physical stretching of the junction [81, 82]. Cellular mechanosensation could also be facilitated by similar mechanisms in Adherens junctions. For example, Janssen *et al* [83] demonstrated that stretch can activate mechanoreceptor TRPV4 (transient receptor potential vanilloid 4 channel), in

Adherens junctions of bladder cells. Whether such a mechanism exists regulates stem cell differentiation is to be determined.

2.2.1.3 In vitro studies

Recent *in vitro* bioreactor studies have provided a greater insight into how stem cell differentiation is regulated by mechanical signals. This next section of the literature review will investigate how different mechanical stimuli may promote or inhibit differentiation pathways.

Static compressive loading has been shown to promote chondrogenesis of mice embryonic limb bud MSCs [84]. Dynamic compression has also been shown to upregulate chondrogenic gene expression in human bone marrow-derived MSCs [85]. However, this relationship is not as simple as it may appear. The response of MSCs to compression is dependent upon the time of load application. Mouw *et al* [86] found, in a study of bovine bone marrow stromal cells, that application of dynamic compressive loading at early time points (8 days) has little effect on chondrogenic gene expression while loading applied at later time points (16 days) significantly upregulates chondrogenic gene expression. This would suggest that the mechanosensivity of MSCs is altered dependent upon the stage of chondrogenesis a stem cell is currently at and also potentially on the stage of development of a pericellular matrix.

While compression may favour chondrogenesis, other types of mechanical stimulation may promote other differentiation pathways. Haudenschild *et al* [87] found that bone marrow-derived MSCs embedded in alginate gels do not respond equally to the application of dynamic compression versus dynamic tension. It was demonstrated that while chondrogenic gene expression was upregulated under application of compression, the application of dynamic tensile loading regulated osteogenic and fibrogenic gene expression [87]. The authors suggest that tension caused increases in β-catenin signalling thereby repressing the chondrogenic pathway. β-catenin has also been shown to be necessary for osteogenesis [88]. Day *et al* [88] demonstrated that the knockout of β-catenin leads to a reduction in osteogenesis and the promotion of chondrogenesis, even in osteogenic culture conditions. Sumanasinghe *et al* [89]demonstrated that application of tensile strain can induce osteogenic differentiation without the addition of osteogenic induction

factors in human bone marrow-derived MSCs, providing further support for the role of tension in osteogenesis. In that study, tensile strain caused the upregulation of bone morphogenic protein (BMP)-2 which has previously been shown to promote osteogenesis [90].

Oscillatory fluid flow (OFF) is another mechanical stimulus that has been shown to regulate of MSC differentiation. OFF can induce changes in cell shape, alter cytoskeletal tension or may be sensed by primary cilia. Li *et al* [91] found that MSCs experiencing OFF displayed upregulated gene expression of osteopontin and osteocalcin (both osteoblastic markers). Another study found that OFF induced upregulation of Sox9 (indicative of chondrogenesis), Runx2 (associated with the osteogenic pathway) and PPARγ (an adipogenic marker) demonstrating the potential of OFF to influence multiple lineage pathways [92]. The same study demonstrates that OFF develops tension in a cell's actin cytoskeleton which in turn activates RhoA and ROCKII. It was previously shown that cells with activated RhoA or ROCKII have the potential to undergo osteogenesis but if this pathway is inhibited an adipogenic pathway is pursued instead [62]. Inhibition of the RhoA/ROCK II pathway has also been demonstrated to increase Sox9 expression and hence, to enhance chondrogenic differentiation [93].The same authors also demonstrated that OFF regulates Wnt β -catenin signaling [94] which is important in both osteogenic and chondrogenic pathways [95]. The stability of β-catenin, shown necessary for osteogenesis, is dependent on this pathway. Without Wnt ligands, β -catenin is tagged for degradation. Prendergast predicted the influence of fluid flow in a tissue differentiation algorithm [8] (see Section 2.5 Computational mechanobiology).

Hydrostatic pressure (HP) is another mechanical stimulus which has been shown to have a strong effect on differentiation. Angele *et al* [96] showed that the application of hydrostatic pressure increases the formation of cartilaginous matrix of bone marrow-derived mesenchymal progenitor cells undergoing chondrogenic differentiation. The same authors also demonstrated that the magnitude of hydrostatic pressure differentially regulated chondrogenesis [97]. However, other studies have shown that HP has little or no effect on expression of chondrogenic genes or matrix accumulation [98, 99]. Therefore, the role of HP in the regulation of MSC fate remains unclear.

2.2.2 Cell shape

Cell shape is an important component in the regulation of MSC fate. According to Caplan [63]:

"*the key factor in the conversion of a mesenchymal cell to a chondrocyte is maintaining the progenitor cell in a round, unspread confirmation.*"

To further support the role of cell shape in differentiation, McBeath et al [62] demonstrated that adipogenesis was promoted when MSCs were only permitted to maintain a spherical unspread morphology but underwent osteogenesis upon being allowed to spread and flatten. RhoA and ROCK signalling pathways have been shown to be key in such fate determination with greater activity in spread cells than in unspread cells [62]. Activation of the RhoA pathway enhanced osteogenic differentiation in spread cells while deactivation in unspread cells induced adipogenesis, indicating the dependence of RhoA signalling on cell shape [62] (Figure 2-6). Furthermore, ROCK signalling induced osteogenesis in both round and spread cells indicating its independence of cell shape [62]. RhoA-Rock in combination with cell shape has also been demonstrated to regulate chondrogenesis [93].

Cell shape is predominantly determined by the state of a cell's actin cytoskeleton. Zhang *et al* [100] demonstrated that cytochalasin, a cytoskeletal disrupting agent, disrupts actin filament organisation resulting in a more rounded cell morphology and enhanced chondrogenesis. Cytoskeletal (and hence cell) shape is controlled through a force balance between microfilaments, microtubules and ECM [76]. Further insights into the influence of stiffness of ECM and other substrates are discussed in the next section.

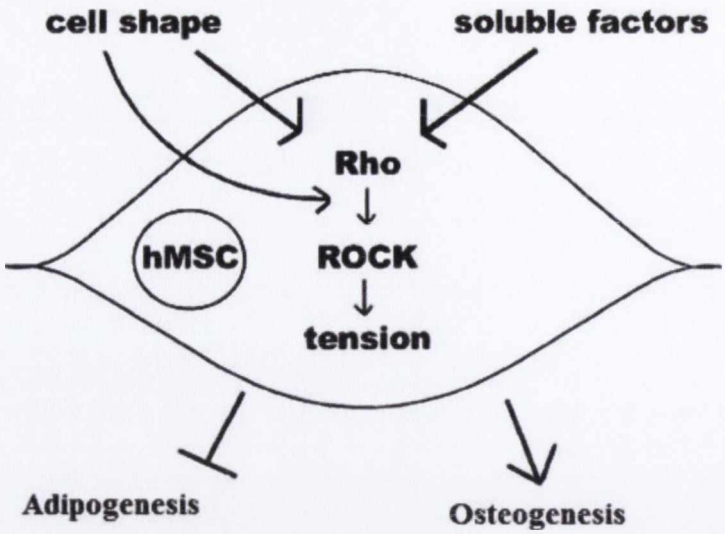

Figure 2-6. Role of cell shape in the regulation of MSC differentiation via cytoskeletal tension and RhoA and ROCK signalling pathways. (Figure from [101] who adapted from [62])

2.2.3 Substrate stiffness

Previous sections of this review looked at the influence of extrinsic mechanical signals inflicted on the cell by its extracellular environment on cell fate. It is also probable that intrinsic mechanical stimuli generated within a cell in response to its local extracellular environment regulate MSC differentiation

Engler *et al* [24] demonstrated that the stiffness of an adjoining substrate directed stem cell differentiation. They demonstrated that MSCs tended to pursue a lineage that produced a tissue of similar stiffness to the substrate the cell was exposed to during culture (Figure 2-7). Cells on collagen-coated gels of similar elasticity to brain cells (0.1 – 1 kPa) undertook a spread neurogenic morphology in combination with upregulation of neurogenic transcription factors. Cells exposed to substrates of similar elasticity to myogenic tissue (8-17 kPa) were likely to undergo myogenesis as evidenced by spindle shaped morphology (similar to myoblasts) and higher expression of myogenic markers. Matrices of stiffness mimicking the elasticity of osteoid (25 - 40 kPa) induced MSCs to take on an osteoblastic-like morphology and increase osteogenic gene expression. The authors suggested that nonmuscle myosin (NMM), a key structural component of the actin cytoskeleton which is also central to the control of cell adhesion, regulates this mechanism. Inhibition of NMM withdrew spreading, branching and

elongation of MSCs independent of substrate exposure, demonstrating the importance of NMM regulation of MSC differentiation via local matrix elasticity. As the stiffness of the local matrix was increased, so did the level of myosin expression and also cell adhesion. The authors concluded that the stiffness within a cell's own actin cytoskeleton itself increases in accordance with an increase in local matrix elasticity [24]. As was previously mentioned in this review, tension build up in the actin cytoskeleton activates RhoA and RockII. Activation of these pathways allows cells to have osteogenic potential [62].

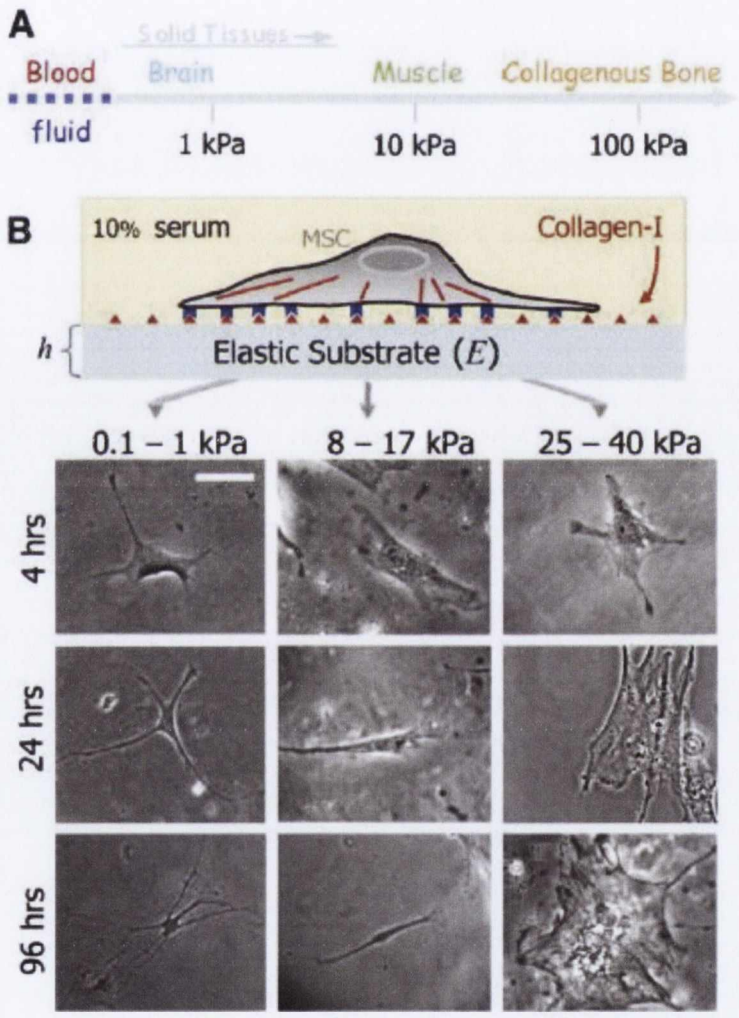

Figure 2-7. Substrate stiffness influence upon tissue differentiation. MSCs are are exposed to gels of varying stiffnesses which results in varying cell morphologies and eventual differentiation pathways [24]

Park *et al* [60] also found a significant influence of substrate stiffness on the chondrogenic and adipogenic differentiation pathways. It was found that a soft

substrate induced both chondrogenesis and adipogenesis more prominently than a stiff substrate. Guvendiren and Burdick further investigated the key role of matrix stiffness in MSC differentiation in a dynamic bipotential model which permits osteoblast and adipocyte differentiation [25]. The dynamic nature of the system better mimics many natural processes such as development, wound healing and disease [25]. Gels could be stiffened (from soft to stiff) at different time points and the effect on differentiation compared to statically stiff and soft controls. Similar to Engler *et al* [24], cells exposed to soft substrates maintained a round morphology inducing adipogenesis while stiff substrates caused a spread morphology and eventual osteogenesis (Figure 2-8). Not all cells differentiated simultaneously and remaining uncommitted cells could be differentiated according to a dynamic or changed stiffness (osteogenesis with stiff substrate and adipogenesis with a soft substrate) while cells which had already committed, to undergoing adipogenesis for example, did not change pathway according to current matrix elasticity resulting in a mixed population (Figure 2-9).

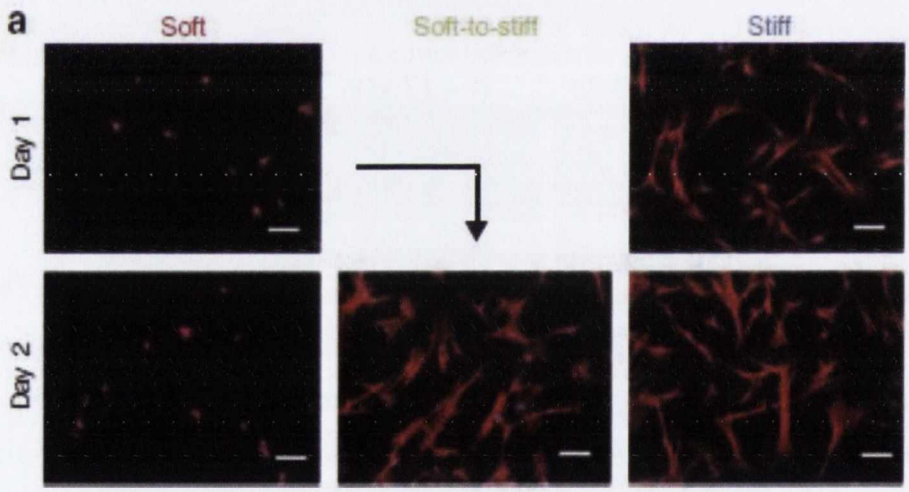

Figure 2-8. Flourescent images of MSCs cultured on soft (3kPa), stiff (30kPa) or soft-stiff (3-30kPa) gels. Scale bars are 100 μm [25].

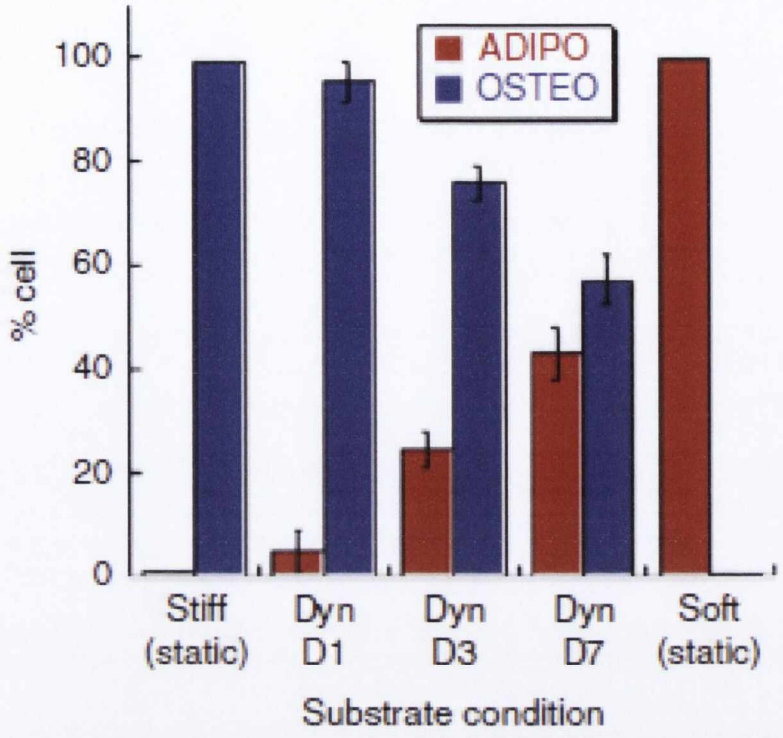

Figure 2-9. The influence of matrix stiffening at various time points upon tissue differentiation (measured at day 14). The stiff group had a stiff substrate for the full 14 days (and similarly for the soft group with a soft substrate). The Dyn D1 group had a soft substrate which was dynamically stiffened on day 1 and remained stiff until day 14. Similary for the Dyn D3 and Dyn D7 groups which were soft substrates initially but were stiffened on day 3 and day 7 respectively [25].

The question then arises of how a cell might sense local matrix elasticity? Focal adhesions may provide a means for MSCs to feel their microenvironment. Cells may "feel" their adjoining matrix via a push or a pull and respond with the generation of biochemical activity via mechanotransduction [102]. Integrins act as mechanoreceptors for the transmission of mechanical signals to the cytoskeleton [102]. Inhibition of integrin binding disrupts substrates stiffness driven differentiation providing confirmation of the role of integrin bonds [75].

It is also found that treatment with bebbistatin (a myosin II inhibitor), Y-27632 (which prevents myosin activation) or Cytochalasin (a cytoskeletal disrupting agent, disrupts actin filament organisation) prevented the osteogenic differentiation of uncommitted cells even upon exposure to stiff substrate [25]. This indicates that the increase in cytoskeleton tension, potentially from increased traction forces exhibited by the cell on its surrounding stiff substrate, is as a key factor in regulation of (in this case osteogenic) differentiation.

The pull or contractility of MSCs can be assessed as a cellular prestress, which balances the tractions stresses exerted on the substrate by the cell [103]. A linear increase of traction/prestress with matrix stiffness has been reported [24, 25] (Figure 2-10). Soft substrates resulted in weaker adhesions [24, 60] which could be important for the underlying mechanism behind regulation of stem cell differentiation by substrate stiffness.

The mechansim behind regulation of differentiation via substrate stiffness may be coupled to cell shape as mentioned in the previous section. Increasing cytoskeletal tension (perhaps as a result of increased ECM rigidity) results in cell flattening, bundling of actin filaments and buckling of some microtubules (Figure 2-11). On the other hand, decreasing cytoskeletal tension (perhaps as a result of decreased ECM rigidity) leads the cell being unable to bear cell traction forces. This results in internal force transfer to microtubules causing buckling, bending and stress fiber disassembly. A rounded cell is the result.

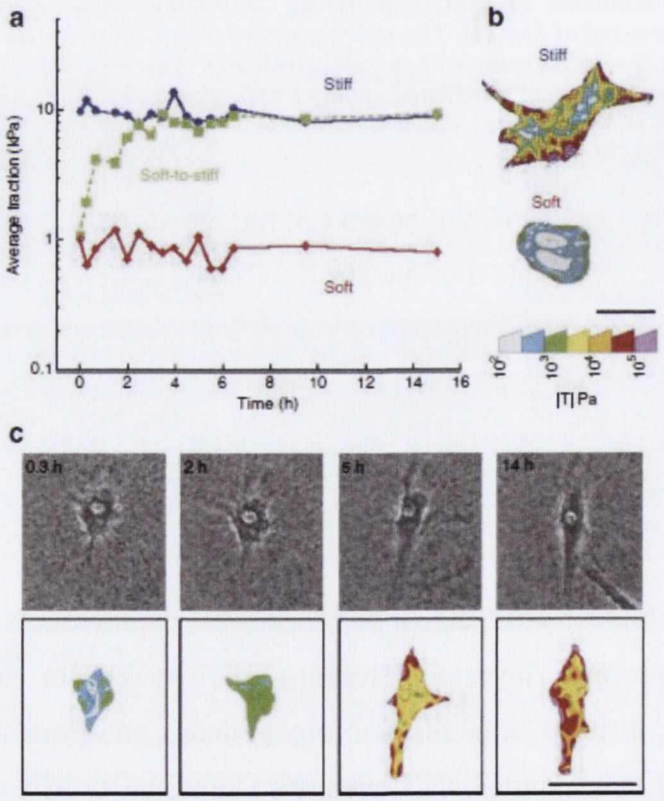

Figure 2-10. (a) Change in traction force with time for soft, stiff and dynamically stiffening (soft to stiff) hydrogels. (b) Colour traction maps (of spatial traction forces) for representative cells from soft and stiff hydrogels (scalebar is 25 μm) (c) Change in cell shape (with accompanying traction maps) of a cell exposed to a stiffening hydrogel (adapted from [25]).

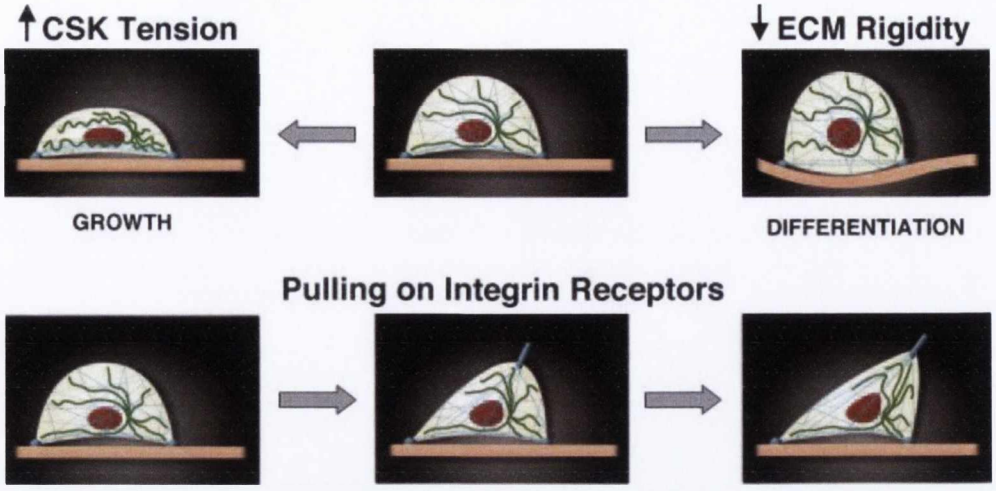

Figure 2-11. Mechanical force balance between ECM, microtubules and microfilaments dictate cell shape and stability. Top: Increased cytoskeletal (CSK) tension is postulated to maintain cellular growth whereas decreasing ECM rigidity is thought to promote cell differentiation. Bottom: Influence of integrin receptor tension on cell shape [76].

A molecular mechanism for ECM stiffness regulation of MSC differentiation has been demonstrated by Dupont *et al* [26]. Yorkie homologues Yes-associated protein (YAP) and transcriptional coactivator with PDZ-binding motif (TAZ), known also as WWTR1, were identified as essential nuclear relays of mechanical stimuli exerted by substrate stiffness and cell shape [26] . YAP/TAZ transcriptional activity is regulated by ECM rigidity, with greater activity occurring due to growth on a stiff substrate (40kPa) versus a soft substrate (0.7kPa) (Figure 2-12). Cell shape was also demonstrated as a regulator of YAP/TAZ with greater activity occurring in cells with spread morphology versus spherical morphologies (Figure 2-12). Consistent with observations from previous studies, osteogenesis occurred in spread cells and cells exposed to stiff substrates while adipogenesis occurred in spherical cells and cells exposed to soft substrates. The authors successfully induced adipogenesis in cells growing on a stiff substrate by knocking down YAP/TAZ and also induced osteogenesis in cells growing on a soft substrate by overexpression of YAP/TAZ (Figure 2-13) providing strong evidence for the role of YAP/TAZ in mechanotransduction during the regulation of stem cell differentiation by ECM rigidity and cell shape.

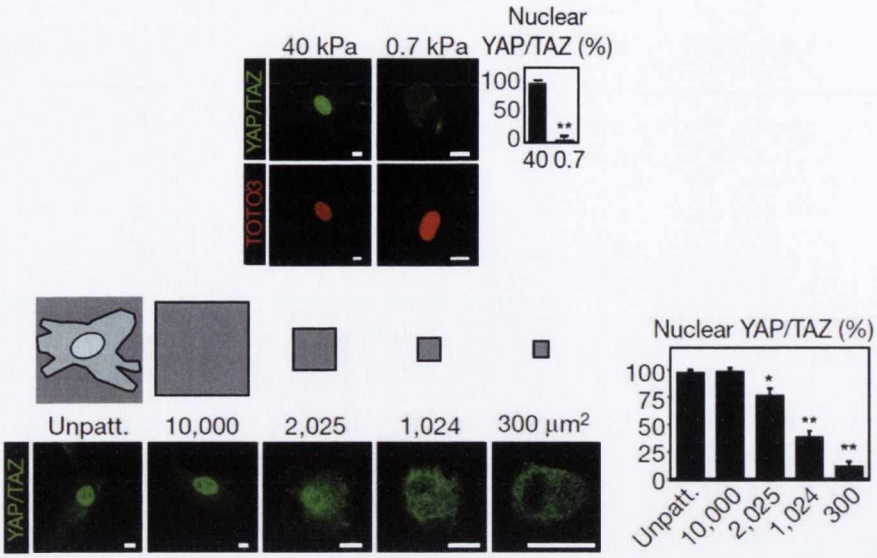

Figure 2-12. Top: Confocal immunofluorescence images showing greater YAP/TAZ activity in cells on the stiffer substrate, particularly in the region of the nucleus. Bottom: Microprinted fibronectin islands of different sizes determine cell shape which in turn regulates nuclear YAP/TAZ activity. Image adapted from [26].

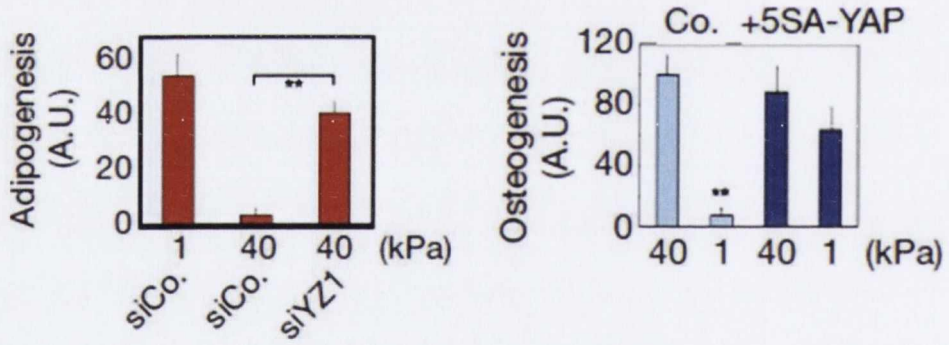

Figure 2-13. Left: Adipogenesis occurring at high levels in cells on a stiff substrate (40kPa) upon YAP/TAZ knockdown. Right: Osteogenesis occurring at high levels in cells on a soft substrate upon YAP/TAZ overexpression. Image adapted from [26].

2.2.4 Oxygen availability

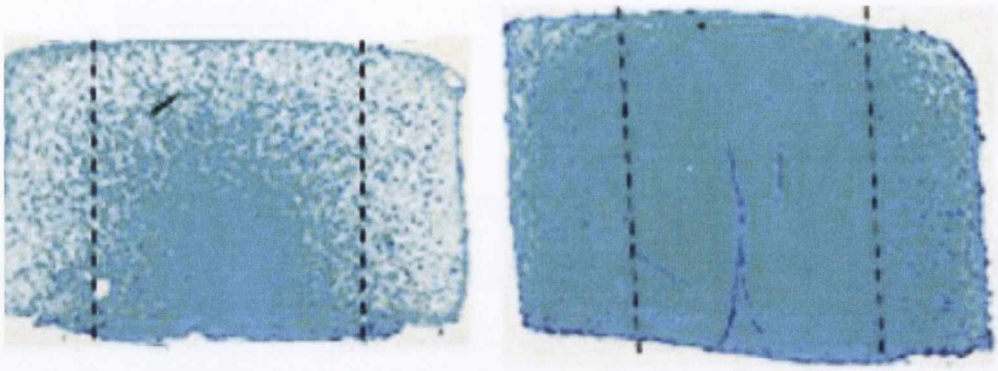

High oxygen tension **Low oxygen tension**

Figure 2-14. Alcian blue staining for sulphated proteoglycan (marker of chondrogenesis). Deeper staining at low oxygen tension shows more prominent chondrogenesis [31].

Oxygen availability is vital to almost all lifeforms and as such, it is intuitive that the presence (or lack) of oxygen would influence the regulation of cellular mechanisms such as MSC differentiation. Some stem cell differentiation pathways are repressed in hypoxic conditions [27, 28]. Holzwarth *et al* [27] showed that adipogenic and osteogenic pathways are severely impaired at 1% oxygen tension. Fehrer *et al* [28] found similar impairment of osteogenesis and adipogenesis at 3% oxygen tension. Yun *et al* [29] also demonstrated impairment of adipogenesis under hypoxia (Figure 2-15). On the other hand, it has been shown that the chondrogenic pathway is more prominent under hypoxic conditions [30-32]. Meyer *et al* [31] demonstrated that low oxygen availability was a more potent promoter of chondrogenesis than a mechanical stimulus, dynamic compression (Figure 2-14). Osteogenic precursor cells have been shown to pursue a chondrogenic lineage under low oxygen tension [30, 32]. Hirao *et al* [32] found greater chondrocytic differentiation and matrix sythesis at 5% oxygen tension versus 20 % oxygen tension. Kanichai *et al* [30] demonstrated greater chondrogenesis, as evidenced by increased proteoglycan deposition and upregulation of collagen II and Sox 9, at 2% oxygen tension versus 20% oxygen tension.

Recent work has provided insights into the mechanisms of oxygen related regulation of stem cell fate. It has been demonstrated that variations in oxygen availability strongly affect gene expression in differentiating osteoblasts [104].

When oxygen is sparse, a triggered response in mammals is to increase expression of a large number of genes including vascular endothelial growth factor (VEGF) and glycolytic enzymes [105]. Salim *et al* [106] demonstrated that downregulation of BMP-2 and RunX2 expression as a result of exposure to low oxygen conditions inhibits osteogenesis. It has already been mentioned in this review that BMP-2 has osteogenic stimulation properties [90]. Runx2 is a member of the runt family of transcription factors. It is both necessary and sufficient for osteogenesis [107]. Runx2 binds to responsive elements within the promoters of collagen I, osteocalcin and osteopontin enhancing their expression [108].

Hypoxia-induction-factor (HIF1), which contains the HIF1-α and HIF1-β subunits, is responsible for the transcriptional induction of most hypoxia-related genes [109]. The role of HIF1- α as a key mediator of hypoxia induced chondrogenesis was demonstrated by an siRNA knockdown approach which eliminated the pro-chondrogenic effect of low oxygen tension [30]. The HIF complex binds to hypoxia responsive elements and initiates the transcription of Sox 9 and aggrecan [110]. Upregulation of Sox 9 and aggrecan are central to chondrogenesis [111]. There is also data available demonstrating the role of HIF1 in the hypoxia-induced inhibition of adipogenesis. The HIF1 regulated gene *DEC1/Stra13* inhibits the activation of the adipocyte-specific transcription factor *PPARγ2* which is necessary for adipogenesis [29] (Figure 2-15). It has been suggested that HIF1- α mediates a metabolic switch with cells fueling themselves primarily through anaerobic glycolysis rather than through aerobic respiratory mechanisms under hypoxia [112]. Such metabolic differences may explain the prevalence of chondrogenesis over osteogenesis and adipogenesis, for example, when oxygen is in paucity. Interestingly, however, Sahai *et al* [105] found that HIF-1 does not play a role in inhibition of osteogenesis under hypoxia by blocking HIF-1 activity which did not have a significant impact on osteogenic gene expression.

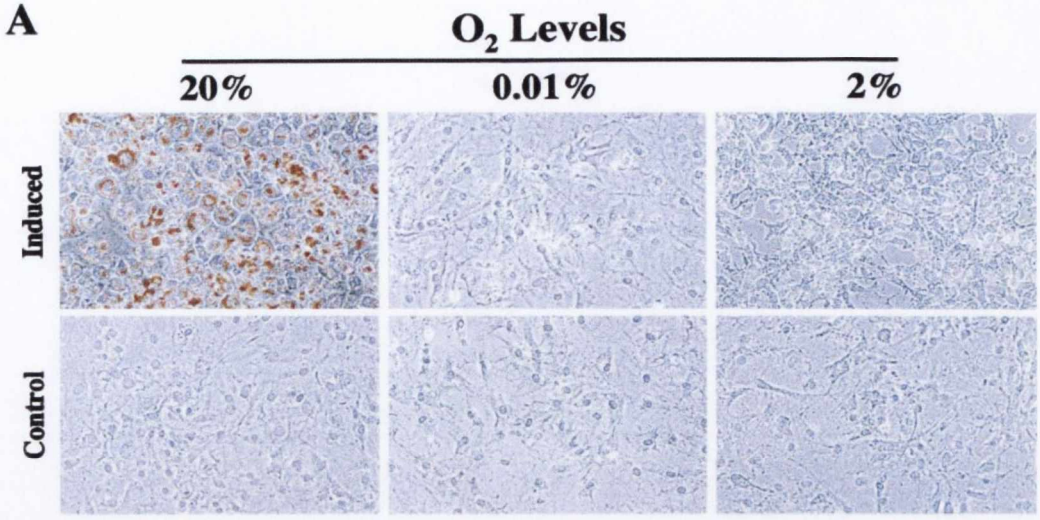

Figure 2-15. Oil Red O staining for lipid droplets. The Induced group of 3T3-L1 (L1) cells, which were treated with a standard cocktail of adipogenic hormones, containing insulin, dexamethasone, and 3-isoglycolysis butyl-1-methylxanthine (IDM), differentiated into mature adipocytes, laden with fat droplets, under normoxia (20% O2). However, adipocyte differentiation is completely inhibited under hypoxia (0.01% or 2% O2). Control group was not exposed to adipogenic induction factors (IDM). Cell death was similar among all groups. [29]

2.2.5 Biochemical regulators

Biochemical cues have long been studied as regulators of stem cell differentiation. Transmembrane proteins act as a cell's chemoreceptors; they bind signaling molecules from outside the cell and transmit information from outside chemical stimuli through sequences of molecular switches and signal transduction cascades to the nucleus. Primary cilia are also believed to be a cell's chemosensor (as well as a mechanosensor as mentioned previously) [78, 113]. Absence (often examined via knockout models) or altered expression of a solitary growth factor or matrix protein has the potential to lead to striking changes in differentiation during development or tissue regeneration. For example, *fibrodysplasia ossificans progressiva* (a disorder in which muscle and connective tissue is gradually ossified) occurs as a result of dysregulation of the BMP-4 signaling pathway [114]. Furthermore, introducing growth factors such as BMPs or TGF-β to a healing bone fracture has been demonstrated to enhance bone formation and decrease healing time [115, 116].

BMPs have also been commonly examined and have been shown to have roles in the initiation, promotion and maintenance of multiple differentiation

pathways, such as osteogenesis and chondrogenesis. It had been previously speculated that BMP-2 and BMP-4 were solely chondrogenic growth factors, produced by chondrocytes and stimulating chondrogenesis of MSCs [117]. BMP-2 and BMP-4 expression occurs within the first 24 hours post bone fracture, a time that correlates with the initiation of chondrogenesis of the MSCs within the callus [117]. More recently, Knippenberg *et al* [90] showed that BMP-2 induces an osteogenic phenotype in adipose derived MSCs. The same authors also demonstrated that BMP-7 induces a chondrogenic phenotype in adipose derived MSCs [90]. Treatment with BMP-2 upregulated the expression of runt-related transcription factor (runx-2), a key transcription factor associated with osteogenesis, and osteopontin, a known osteogenic marker while upregulation of BMP-7 increased the expression of aggrecan, an integral component of cartilaginous tissue matrix [90]. Other work has demonstrated that other factors (e.g. fibroblast growth factor 21 (FGF21)) can increase the osteogenic activity of BMP-2 via upregulation of the Smad signaling pathway [118]. BMP-2, along with BMP-4, was also detected in chondrogenic precursor cells in distraction osteogenesis in the same study [118]. This demonstrates that although BMPs play an important role in regulation of tissue differentiation, the role is complex.

There are many other growth factors which have been shown to influence MSC differentiation but to discuss them further would be exceeding the scope of this review. Geris *et al* [51] implemented a bioregulatory model of tissue differentiation and angiogenesis regulated solely by biochemical cues which was successful in predicting the stages of fracture healing (see Section 2.4.1 Stages of fracture healing and Section 2.5 Computational mechanobiology).

2.3 Angiogenesis

Angiogenesis refers to the development of new blood vessels. Angiogenesis is vital to the tissue regeneration process and is known to have an inherent effect on tissue differentiation during such events. As such, this part of the literature review will focus on reviewing current knowledge and experiments investigating regulation of angiogenesis. Accurate computational modelling of angiogenesis is key to many recent regulatory theories of MSC differentiation and this section will also look at how angiogenesis has been modelled *in silico.*

2.3.1 Environmental factors regulating angiogenesis

2.3.1.1 Biochemical factors

Vascular endothelial growth factor (VEGF) is a potent mitogen which has long been associated with stimulation of neovascularization. VEGF is secreted by cells to chemically stimulate the formation of new blood vessels. For example, hypertrophic chondrocyctes secrete VEGF during the ossification process in early skeletal development. Street *et al* [46] highlighted the importance of VEGF to bone repair. Treatment with a neutralizing VEGF receptor led to diminished angiogenesis and poor bone formation and progression of healing as a result. In a separate experiment as part of the same study, treatment with exogenous VEGF led to enhanced angiogenesis and progression of bone repair in both a rabbit radius gap defect model and a mouse femur fracture model.

Basic fibroblast growth factor (bFGF) is another regulator of endothelial cell behaviour [119]. bFGF stimulates angiogenesis as both an autocrine and paracrine factor inducing endothelial cell migration, proliferation and expression of growth factors, proteases and integrins involved in angiogenesis [120, 121]. bFGF activates a signalling cascade that mediates endothelial cell activity through binding to FGFR receptors [122, 123]. There are also many other biochemical factors secreted by cells to regulate angiogenesis such as BMPs, angiopoetins and RANKL but are beyond the scope of this review [119, 124]. A summary of such factors is shown in (Figure 2-16).

Chemotaxis is also observed as endothelial cells and blood vessels migrate toward regions of hypoxia. It has been demonstrated that a hypoxic tissue gradient is necessary for successful wound healing as capillary growth ceases upon removal of the gradient [47]. It has also been shown that hyperbaric oxygen stimulates vascularisation in bone defects [125]. Directed cell migration is enabled by cellular sensation of local concentration of chemical factors. Cells detect soluble factors (such as mentioned above) with specific membrane receptors. Next local excitation/global inhibition (LEGI) mechanisms detect local chemical gradients. This involves a local excitation signal inducing polarization whereas a local inhibitory chemical signal opposes it. This activation of chemotactic pathways leads the eventual accumulation of F-actin at the front of

the cell and P-Ten at the back and the eventual directed migration of a cell along a chemical gradient [126].

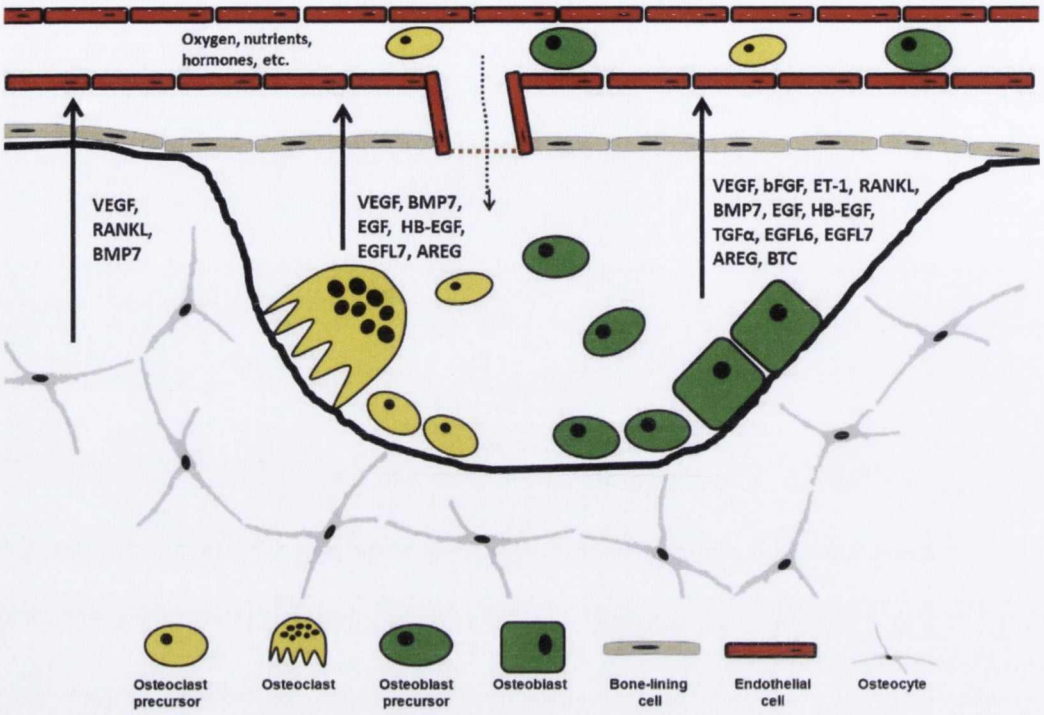

Figure 2-16. Secreted biochemical regulators of endothelial cell behaviour and angiogenesis [119]

2.3.1.2 Mechanics

Mechanics have also been shown to regulate angiogenesis. It has been demonstrated that excessive mechanical stimuli can prevent angiogenic progression *in vivo* [34-37], while *in vitro* studies have demonstrated that mechanical stretch can cause a decrease in endothelial cell (EC) proliferation [127]. However, it is also possible that mechanical stimuli in non-excessive magnitudes is beneficial for endothelial cell proliferation and migration, and hence, angiogenesis.

Studies undertaken found that applied cyclic strain promotes EC migration and tube formation [41] and stimulates EC and vascular smooth muscle cell (SMC) differentiation [45]. Boerckel *et al* [40] demonstrated that mechanical loading applied immediately post fracture repressed vascular progression into a fracture defect site. However, application of a mechanical stimulus 4 weeks post fracture stimulated vascular remodelling and increased bone formation as a result.

It could be assumed that the local mechanical stimulus experienced by ECs at the later time point would be significantly smaller in magnitude (due to a more stabilised callus) which could possibly explain the difference in response. Qiu *et al* [39] obtained similar findings demonstrating compressive stress to have both a stimulatory and inhibiting effect upon vascularisation during fracture healing depending upon the magnitude. Up to a threshold level compressive stress promoted vascularisation but beyond this level vascularisation was repressed. The expression level and absorbance of VEGF corresponded to the level of applied stress implicating the coupling of biochemical and mechanical cues in cellular response [39]. This is further evidenced by other studies. Yung *et al* [128] demonstrated that dynamic tension can initiate a cascade of autocrine and paracrine signalling between ECs and SMCs necessary for angiogenesis. The authors describe how secretion of angiopoietin (Ang)-2 is upregulated with the application of dynamic tension leading to increased EC migration and sprout formation. Endothelial cells have also been demonstrated to secrete other proangiogenic biochemical factors (such as BMP-2 and BMP-4) in response to mechanical stimuli [119].

Mechanics have been demonstrated to not only regulate the magnitude of an angiogenic response (or rate of blood vessel growth) but also to influence EC migration directionality (mechanotaxis) and hence vascular growth direction [42, 43, 129, 130]. Application of cyclic stretch has been demonstrated to align endothelial-cord-like structures perpendicular to the direction of applied stretch [131]. Matsumoto *et al* [42] observed that ECs preferentially aligned and migrated in a direction perpendicular to the direction of applied tensile strain in 2-D culture. Sprout-like structures formed predominantly in the direction perpendicular to applied strain in 3-D culture [42]. Moretti *et al* [132] showed that this reorientation can occur within a short period of time. Human umbilical vein endothelial cells (HUVEC) reoriented perpendicular to the direction of stretch within 4 hours of strain application. Yung *et al* [128] demonstrated that ECs upregulate Ang-2 and PDGF in response to strain application and subsequently have migration biased in the direction perpendicular to applied strain. SMCs increase PDGF receptors in response to applied strain but do not exhibit directional migration. It was found that straining SMCs in coculture with ECs

resulted in directed migration of SMCs toward ECs. As a result the authors proposed a dual sensory mechanism for blood vessel development whereby mechanics direct EC migration and chemical cues direct SMC migration toward ECs, a process which eventually leads to the development of blood vessel structures (Figure 2-17).

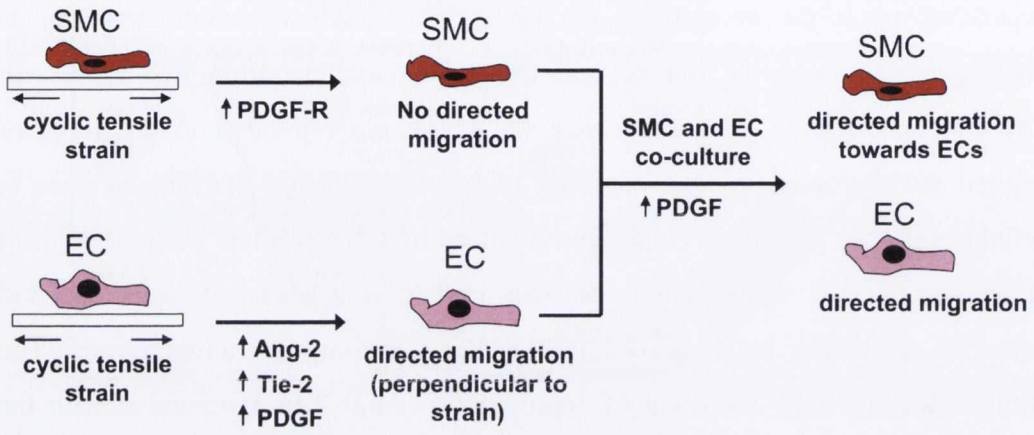

Figure 2-17. Potential mechanism by which strain regulates stages of angiogenesis. EC migration is directed by mechanics (in the direction perpendicular to strain) while SMC migration is towards ECs [128].

Cell alignment parallel to the direction of applied strain has also been observed [43]. It is possible that cell interaction with substrate topology via contact guidance can overrule the effect of reorientation. For example, Krishnan *et al* [43] found preferential EC migration parallel to the direction of applied strain. A possible explanation provided by the authors for this is that the underlying collagen matrix (of the collagen gels used in the study) prevents reorientation by the applied cyclic strain. It is also possible that the viscoelastic collagen gels may fail to maintain stress on the cells during strain application [43]. Tambe *et al* [133] found that cells migrate in order to maintain minimal local intercellular shear stress. This led the authors to hypothesize that migration orientation aligns itself with the orientation of maximum principal stress. This idea complements other physical principles such as Murray's law which postulates that vascular remodeling occurs so that flow is attained with the least possible energy. The influence of fluid flow upon EC migration has also been demonstrated [129, 130]. Fluid flow promotes directionally biased migration in the direction of flow. The magnitude of fluid flow stimulus is an important factor with a threshold needing to be surpassed in order to overcome the effects of

haptotaxis (ECs developed focal adhesions and migrated preferentially towards regions of higher surface density of collagen). Durotaxis is another observed mechanism of biased cell migration. Cells have been demonstrated to direct migration from softer matrix regions to stiffer matrix regions [134, 135].

Mechanotaxis can entail complex interplay between physical and chemical mechanisms in order to sense local gradients. A cell must detect differences in stimulus across the cell body, polarize in the appropriate direction and ultimately migrate along that direction. A force detection mechanism would typically involved force-induced conformational change in specific molecules which can alter enzyme or ion channel activity and initiate signalling cascades which lead to polarization [136]. For example, mechanical forces can unfold cryptic vincilin binding domains resulting in vincilin binding [137], which is actively involved in the mechanism of cell movement and spreading.

It is also plausible that mechanotaxis can occur independent of a chemical cascade to determine directionality. Physical forces do not require the mechanisms to sense and gradient as they already convey directional information. Variations in membrane tension which may accumulate directly from extrinsic mechanical signals may lead to cellular polarization and eventual directed migration. A homogeneous distribution of mechanosensors across the cell body is also conceivable. If such mechanosensors were proteins, they could stretch or unfold at differing rates at leading and trailing edges which could be transduced into soluble intracellular signals initiating polarization [126].

2.3.2 *In silico* models of angiogenesis

Early computational models of MSC differentiation during tissue regeneration did not consider angiogenesis [5, 7, 10, 49], in spite of experimental observations of its importance to MSC differentiation. Since then, models of angiogenesis of varying complexity have been developed with blood vessel activity regulated by either mechanical or biochemical cues.

Some models of angiogenesis were regulated by mechanics with inhibition of blood vessel growth in regions of a high mechanical stimulus. For example, Chen *et al* [52] used a diffusive model to predict angiogenesis during fracture repair. Vessel growth was inhibited in regions of high distortional strain. The

model also included a model of nutrient supply in order to make tissue differentiation predictions within the fracture callus. The study showed that, in the case of a large fracture gap, non-union may be induced by inadequate mechanical environment or by a deficiency in nutrient supply. Simon *et al* [138] used fuzzy logic modelling to incorporate blood perfusion into their model. Blood perfusion was decreased in regions of high distortional or dilatational strain. The model allowed investigation into stable and unstable cases. Slower revascularisation and slower healing in unstable fractures was successfully predicted by the model. Another interesting feature of the model was that healing in the less stable case was primarily limited by an inadequate mechanical environment, whereas the rate of angiogenic progression is the more dominant factor in the stable fracture.

Other models have included a blood vessel growth rate which is linearly related to a mechanical stimulus [50]. Checa and Prendergast [50] applied random walk theory [139] and a lattice approach to describe angiogenesis. A high mechanical stimulus (a combination of shear strain and fluid velocity) resulted in a blood vessel growth rate of zero but a lower mechanical stimulus resulted in a high blood vessel growth rate. Within the lattice approach, each finite element was discretised into lattice points. Each lattice point represented a potential position for a cell and its immediate extracellular matrix. Vessels were modelled as a sequence of adjoining lattice points filled with endothelial cells. This approach allowed explicit modelling of capillaries including branching and anastmosis as well as directionally biased blood vessel growth. Blood vessel growth directionality was biased in a chemotactic direction which was determined by the location of the highest concentration of hypertrophic chondrocytes (which were assumed to secrete VEGF). This model of angiogenesis has been used to explore a number of regenerative scenarios. Byrne *et al* [140] used this model of angiogenesis, combined with the tissue differentiation algorithim of Prendergast [8], to explore tissue growth within a scaffold. Sandino *et al* [21] used the same approach to examine tissue differentiation within a scaffold with irregular morphology. Khayerri *et al* [16] applied this model to investigate differentiation in the implanted bone chamber. Reina-Romo *et al* [141] added a similar model lattice model of angiogenesis to the tissue differentiation framework developed by

Gomez-Benito *et al* [23] to explore tissue differentiation during distraction osteogenesis.

Biochemical factors have also been assumed to regulate angiogenesis during *in silico* studies. Geris *et al* [51] progressed the modelling framework of Bailon-Plaza and van der Meulen [142] to include angiogenesis. Angiogenesis (and tissue differentiation for that matter) was regulated by biochemical cues, independent of mechanical effects, and was therefore a bio-regulatory model rather than a mechanoregulatory model. A series of differential equations was implemented to model angiogenesis. The study emphasised the importance of the formation of an adequate vascular network for successful fracture healing. This model has since been used to investigate fracture non-unions [143] and bone chamber experiments [53] with the incorporation of mechanics by making certain parameters dependent on mechanical stimuli, such as fluid flow and hydrostatic pressure. Pieffer *et al* [144] developed a model to include explicit modelling of individual vessels, a leading endothelial tip cell which controls vessel growth, vessel branching and anastomosis.

Other models of angiogenesis have been developed to include the molecular mechanisms of angiogenesis. Carlier *et al* [145] developed a multiscale model of sprouting angiogenesis which includes lateral inhibition of endothelial cells. The model can recreate the influence of molecular mechanisms of angiogenesis and successfully predicted many aspects of tip cell selection, excessive number of tip cells in regions of high VEGF concentration and due to loss of DII4 (a negative regulator of angiogenesis). Zheng *et al* [146] developed a continuous model of angiogenesis which includes initiation, sprout extension and vessel maturation. Regulating mechanisms of VEGF and angioproteins (Ang1 and Ang2) upon proliferation, migration and maturation are included and allow the model to reproduce experimentally observed aspects of corneal angiogenesis.

2.4 Fracture healing

Tissue differentiation has been commonly investigated via exploration of the bone healing process and as such is reviewed here. Fracture occurs when the strain limit of bone is exceeded, often by physical trauma. Repair of bone fracture normally involves repeatable spatial and temporal patterns of tissue differentiation

and, as a result, has often been considered as a model system to explore how environmental factors regulate stem cell differentiation *in vivo*. Specific hypotheses relating to how environmental factors impact stem cell differentiation can then be tested by attempting to simulate tissue differentiation patterns for each stage of fracture healing using computational models [7, 9, 10, 51, 138]. Some of these models will be reviewed in further detail later in this chapter (see Section 2.5 Computational mechanobiology).

2.4.1 Stages of fracture healing

Fracture repair can occur via either primary or secondary healing responses. Primary fracture healing entails a direct effort to re-establish an interrupted cortex via intramembranous ossification [147, 148]. A high degree of stability and anatomical reduction of the fracture ends is required for healing in this manner [149]. Inadequate stabilisation prevents the necessary fracture site vascularisation by rupturing any newly sprouted capillaries and secondary healing occurs [150]. Secondary fracture healing involves the formation of an external fracture callus and a slower revascularisation and healing process involving endochondral ossification [148]. Secondary healing is the dominant healing mechanism *in vivo* so this mode of healing shall be primarily discussed here.

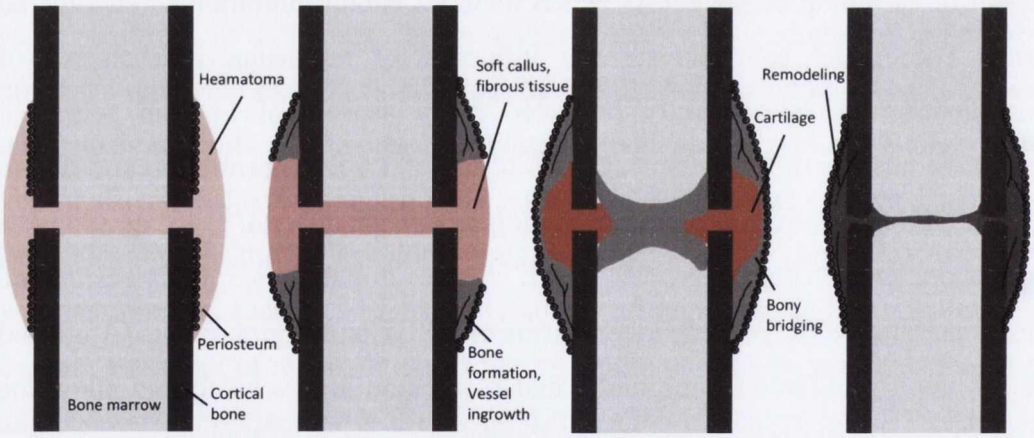

Figure 2-18. Schematic of a cross section of a healing long bone. Fracture healing progression: Inflammatory stage causes initial callus and hematoma formation. Intramembranous ossification occurs at the periosteal cortex distal to the fracture gap with cartilage formation in and adjacent to the fracture gap. Ossification continues via the endochondral route. The callus is remodelled to return the bone to its original geometry [151].

The standard classification of secondary fracture healing stages includes an inflammatory response followed rapidly by a reparative phase and, eventually,

a remodelling phase [147]. Fracture impact results in acute necrosis and damage of the adjacent marrow and bone [152]. The presence of much necrotic material instigates the formation of a hematoma and an intense inflammatory response (Figure 2-18). The region is invaded by inflammatory cytokines, growth factors, macrophages, leukocytes and other inflammatory cells. The hematoma is the source of these cells which have the ability to activate sequences of cellular events necessary for successful fracture healing [148, 153]. Migration of stem cells to the hematoma site from the endosteum, periosteum and surrounding muscle [148, 154] form a soft granulation tissue together with the aforementioned inflammatory cells, vessel cells and fibroblasts [153].

The formation of a fracture callus permits the reparative phase of fracture healing. Einhorn speculated that the most important event in fracture healing is early intramembranous ossification beneath the periosteum [155]. This leads to the lifting of the periosteum off the bone surface (Figure 2-19). With the lifting of the periosteum, comes the release of osteochondral progenitor cells which are now free to proliferate through the callus.

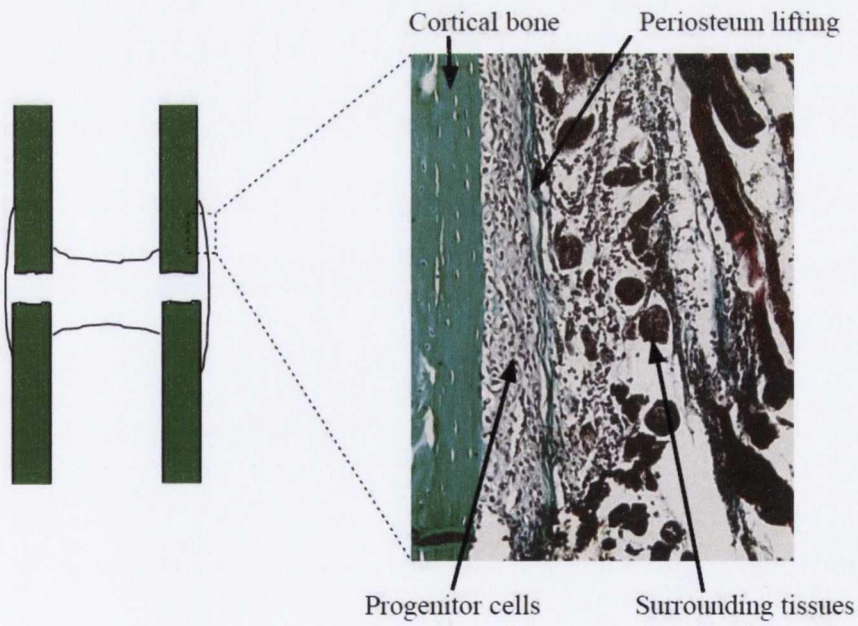

Figure 2-19. Periosteum lifting in the early reparative stage of fracture repair [156]

A front of bone formation proceeds from the periosteal and endosteal cortices towards the fracture gap via intramembranous ossification [7] (Figure 2-18 and Figure 2-20). High rates of proliferation allow chondrocytes to become

the dominant cell type in the external callus (Figure 2-21). Cartilage is generated and eventual cartilaginous bridging of the fracture gap occurs in the periosteal callus. The bone front now progresses via endochondral ossification (Figure 2-18). During this process, chondrocytes undergo hypertrophy. Hypertrophic chondrocytes are generally more prominent in close proximity to bone [157]. Hypertrophic chondrocytes direct the mineralization of their surrounding matrix [158], stiffening the tissue. The mineralised cartilage is subsequently invaded by blood capillaries allowing the ossification of the tissue and bone is formed. Bone formation continues until bony union is achieved and both the external and internal calluses are completely bone. This bridging creates a load transfer path through the outside of the callus (or alternatively through the internal callus in the case of endosteal healing) with the effect of minimizing strain in the fracture gap, leading to bone formation in the fracture gap. The callus is now almost completely bone [7].

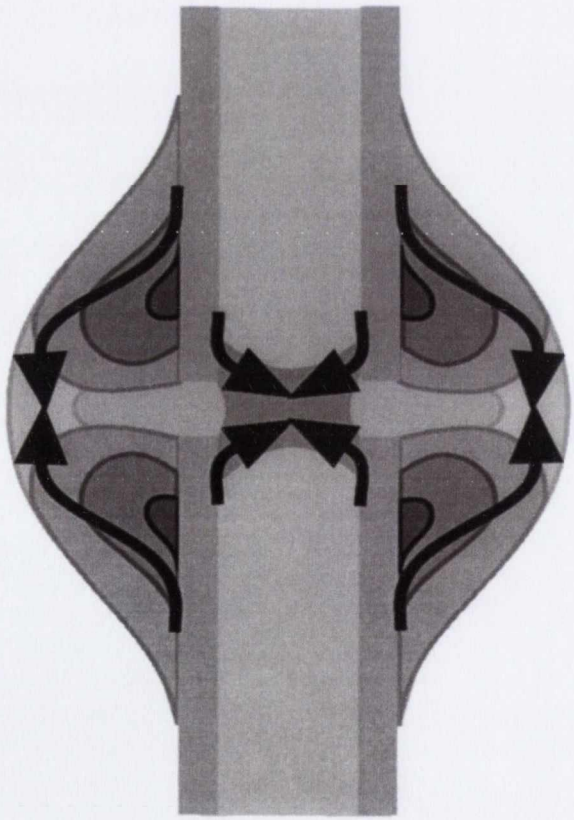

Figure 2-20. Bony progression during secondary bone repair [7]

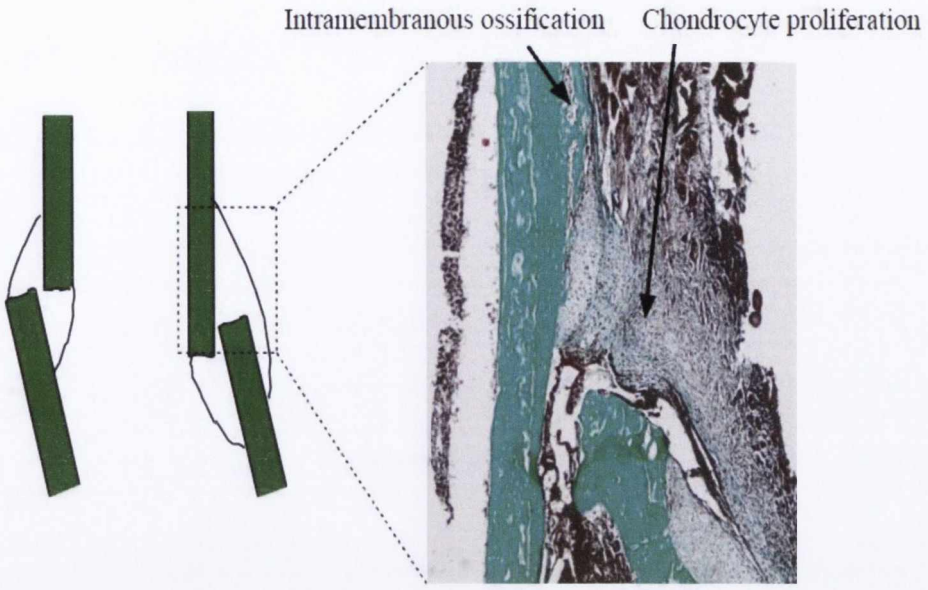

Figure 2-21. Chondrocyte proliferation during the reparative stage of fracture repair [156]

Once bony union is achieved, the load transfer path runs through the newly formed bone situated in the cortical gap. Strains are reduced in both periosteal and endosteal calluses. The bone there is "disused". In order to maintain metabolic efficiency, this bone is resorbed and the long bone's original shape is restored (Figure 2-18). In the endosteal callus, a medullarization process occurs whereby unneeded bone is resorbed and replaced by marrow in order to restore original bone architecture [159]. Bone modelling occurs over a long period of time (years) in order to restore the original lamellar bone structure [36].

An alternative classification of fracture healing stages was offered by Vetter *et al* [55]. Following an intensive study on fracture healing in sheep [160], it was found that substantial histological differences occur between individuals, even those harvested at the same time point and who had been subjected to the same mechanical fixation. A novel imaging analysis technique allowed the definition of 6 observed healing stages (Figure 2-22) according to topological criteria (Table 2-1) and independent of time. These images represent a qualitative description of average healing progression in the sheep model. Such images are potentially useful in a number of scenarios including the examination of

mechanobiological theories, the investigation of fracture repair progression with various mechanical fixation devices, intraspecies comparison etc.

Table 2-1 Definition of the criteria used to identify stages of fracture repair [55]

Healing Stage	Topological Criteria	Classification According to Healing Phases
Stage I	Remnants of hematoma still present in the callus	Late inflammatory phase
Stage II	No remnants of hematoma left, cartilage not yet formed	Early reparative phase
Stage III	Bridging via cartilage in the outer osteotomy zone, but no bony bridging of the osteotomy gap	Reparative phase
Stage IV	Formation of a periosteal bony bridge between the proximal and distal parts of the osteotomy callus	Late reparative phase
Stage V	Formation of an endosteal bony bridge between medial and lateral parts of the osteotomy callus	Early remodeling phase
Stage VI	Reduced size of the hard callus, resorption of the endosteal bony bridge	Remodeling phase

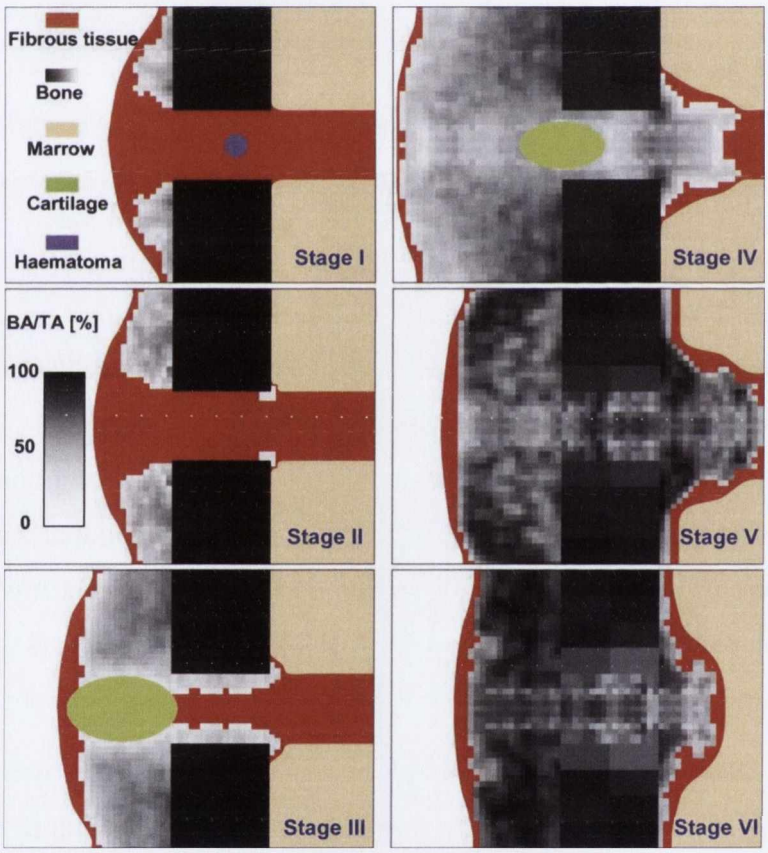

Figure 2-22. Vetter et al's classification of healing stages in fracture repair of sheep based upon averaged histological images [55]

2.4.2 Progenitor cell origin, migration and proliferation during fracture healing

During fracture healing, three sources of MSCs have been suggested: the bone marrow of the medullary cavity [161], the inner cambial layer of the periosteum

[147] or the surrounding soft tissues and lifted periosteum [162]. Bone marrow is known to contain a high density of stem cells with the ability to pursue any mesenchymic lineage [163]. Cells within the periosteum also play an important part in fracture repair [147]. The inner cambial layer is known to provide a source of progenitor cells to the callus followed the lifting of the periosteum during healing [147]. It is also speculated that the lifted periosteum is a third source of progenitor cells [162]. However, it is not known whether cells originate from surrounding muscle and soft tissues and invade the callus through the lifted periosteum or from the outer fibrous layer of the periosteum itself or from both sources. It has been suggested that these stem cells may not be uncommitted MSCs but osteoprogenitor cells with a predetermined commitment to bone formation through either endochondral or intramembranous modes of bone formation [161]. Leriche and Policard [162] even suggested that repair tissue was not generated from specialist cells but was in fact a consequence of activity from uncommitted fibroblasts which could develop osteogenic ability given specific environmental conditions. In other words, the reparative tissue does not originate from the bone itself but from the surrounding soft tissues [162]. Secreted factors such as BMPs (e.g. BMP-7) and tumuor necrosis factor-α (TNF-α) are believed to mediate the recruitment of necessary cells to the fracture site [164, 165]. The role of hypoxic gradients regulating stem cell trafficking by HIF-1 has also been suggested [166].

Stem cell origin was shown to have an important influence on fracture healing in an finite element study undertaken by Lacroix *et al* [167]. Upon investigation of the three aforementioned MSC origins, taken as sole cell sources, the rate of reduction of interfragmentary strain (IFS), a marker for recovery, was shown to be largest for cells originating from external tissue. Rate of recovery was 50% slower for cells originating from the inner cambial layer and if cells were solely sourced from the marrow, recovery could be as much as four times slower [167].

Cell proliferation is thought to increase rapidly during the inflammation phase of repair with cell division reaching a maximum rate as early as twenty-four hours after fracture [147]. This activity primarily occurs in the periosteum and in the tissues in the immediate vicinity of the periosteum and continues through the

length of the bone [147]. After a few days, this activity becomes restricted to the fracture gap and areas adjacent to the fracture gap where activity exceeds normal levels for a number of weeks [168].

2.4.3 Factors that vary healing

Fracture healing outcome can be affected by a number of factors. This next section will review the influence of mechanical stimulation, angiogenesis and oxygen on repair outcome.

2.4.3.1 Mechanical stimulation

Mechanical stimuli can alter the progression of fracture repair [68, 150, 160, 169]. Application of loading to healing fractures can be beneficial decreasing healing times and lessening the likelihood of delayed union [68, 169] . However, should loading be excessive, loading can be disadvantageous decreasing mechanical stability and prolonging healing time [150, 160, 169] . External loading and the nature of fracture fixation are important variables in determining the local mechanical environment and hence its influence upon healing within a fracture callus. Fixation which is highly unstable may lead to excessive mechanical stimuli and lead to delayed or non-union [160]. Some of this disparity may be explained by the timing of application of mechanical stimulation. Boerckel *et al* [40] found that while early loading was detrimental to healing, decreasing bone formation by up to 75%, loading applied 4 weeks post fracture was beneficial to healing increasing bone formation by 20%. It is probable that the strain environments are very different both time points (even if the magnitude of loading was similar) due to stiffer tissue existing at a more advanced stage of healing (4 weeks post fracture). This is just one example of the complex nature of the situation.

The type of mechanical stimulation is also important to healing progression. Axial loading (controlled micromovements, non-excessive in magnitude) has been demonstrated to enhance fracture repair progression and decrease healing time [68]. However, shear movements have been demonstrated as having poorer mechanical stability, delayed bone formation and longer healing times [169]. In contrast, there is also data available in the literature which proposes that shear stimulation is more beneficial than axial stimulation [70]. The

nature and magnitude of mechanical stimuli within a fracture healing environment is also influenced by a number of geometric factors such as fracture pattern and gap size. For example, smaller gaps heal quickly and more successfully than larger gap sizes where bone formation is significantly reduced [73]. In spite of extensive experimental investigations, the exact role of mechanical stimulation upon fracture healing progression is not fully understood. Technological advancements have led to the availability of computational tools to aid further investigation into these complex coupled relationships (See Section 2.5 Computational mechanobiology).

2.4.3.2 Angiogenesis and oxygen

In addition to a suitable mechanical environment, an adequate vascular supply is necessary for successful fracture repair [48]. Bone fracture causes severe blood vessel disruption and, usually, the formation of a hematoma. Interruption to the restoration of vascular function or development has been demonstrated to lead to delayed or non-union [35]. High levels of IFS have been linked to such delayed or non-union [34]. Nearly 40 years ago, Rhinelander [38] speculated that capillaries necessary for osseous growth were ruptured constantly due to high strains, delaying and/or preventing bone formation and hence, fracture healing.

The relationship between bone formation and blood supply has long been recognized [170, 171]. Bone is a highly vascularized tissue [150]. Blood vessels transport oxygen, nutrients and biological factors necessary for bone formation [171]. Hausman *et al* [172] showed that treatment of a fracture with TNP-470, a commonly used angiogenesis inhibitor, completely prevented fracture healing. The anti-angiogenic agent was shown to interrupt both endochondral and intramembranous modes of ossification [172]. Repression of angiogenic activities via other agents such as rapamycin has also been shown to delay fracture healing [92]. Evidence has also been provided that periosteal devascularisation of sheep culminates in decreased bone formation and delayed union [173]. Devascularisation of the surrounding muscle tissue in rabbits again showed delayed union [174]. A similar relationship exists between adipose tissue and blood supply [175]. Adipose is also a highly vascularized tissue with each

adipocyte nourished by an extensive capillary network [176] which supplies necessary nutrients, oxygen and biological factors.

Lu *et al* [177] found that chondrogenesis was not stimulated in an ischemic environment in spite of mechanical stability in fracture repair in mice. Instead there was an increase in formation of a fibrous fatty tissue [177]. Hausman *et al*, [172] found increased fibrous tissue formation in fractures where angiogenesis has been inhibited. Thrombospondin-2 (TSP2) is thought to be a negative regulator of angiogenesis [33, 178]. Fracture healing in mice which are null of this matricellular protein, heal via enhanced intramembranous (and diminished endochondral) ossification leading to quicker healing progression versus control mice with TSP2 present [33]. The same authors have also demonstrated that mice lacking TSP2 have accelerated ischemic healing displaying significant increases in bone regeneration [178]. This again supports the importance of angiogenesis in fracture healing progression supplying oxygen and other necessary factors for repair.

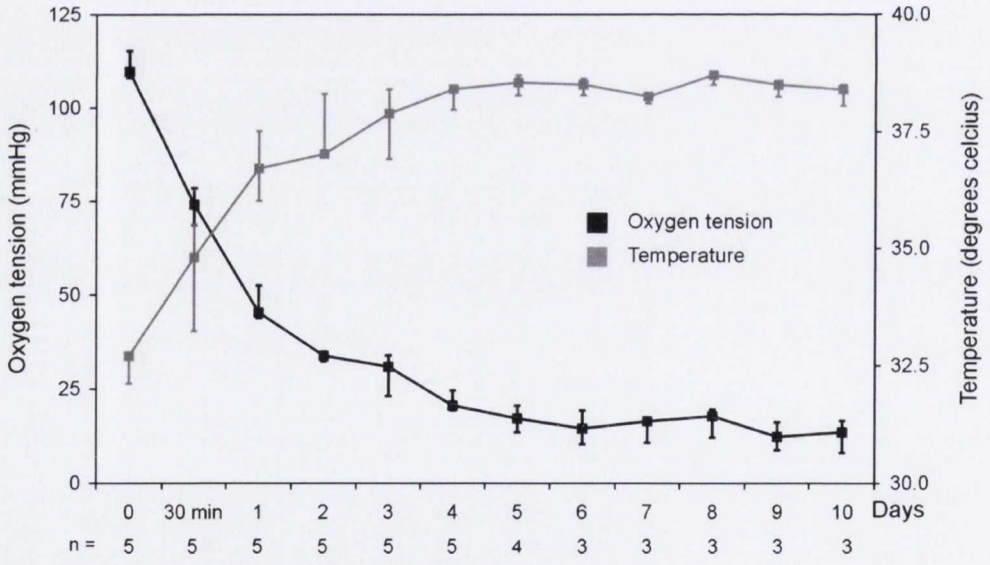

Figure 2-23. Fracture callus oxygen tension and temperature verus time post fracture [179]

Oxygen, an important regulator of stem cell differentiation (see Section 2.2.4 Oxygen availability) is a key component supplied by neovasculature in regenerative events such as fracture healing. A dramatic decrease in oxygen tension takes place over the first day post fracture [179] (Figure 2-23). Oxygen supply is severely diminished as vasculature is disrupted by the fracture trauma and oxygen tension drops to 0-2% in parts of the regenerative tissue [2]. Cellular

consumption of the existing oxygen (and some more temporarily provided by the blood pool created from injured vessels) causes this decrease. As neovasculature invades the callus during the early stages of repair, the decrease in oxygen levels slows and will eventually begin to increase towards being restored to pre-fracture levels. Lu *et al* [180] performed experiments investigating the effect of fracture healing in mice which breathed in hypoxic (13%), normoxic (21%) and hyperoxic (50%) conditions. Hyperoxia increased tissue vascularity and improved bone generation and healing time while hypoxia decreased tissue vascularity and diminished bone generation and increased healing time. Interestingly, there was no significant change in chondrogenesis or osteogenesis in either hypoxic nor hyperoxic conditions.

2.5 Computational mechanobiology

The original tissue differentiation hypothesis of Pauwels was based on logic and experimental observation. He did not have the facility to gauge tissue mechanical environment accurately. Technologic advancements have seen computer simulation employed more and more commonly to aid the search for scientific solution and has even been referred to as the "third method of science" [181] after experimentation and logic. Mechanobiology examines how mechanical stimulation regulates biological processes through cell signaling pathways (whereas biomechanics examines the mechanical behavior of biological systems) [4]. Computational mechanobiology uses computational tools to examine the coupling of mechanical signals with biological processes that are too complex to perform experimentally. For example, computational simulations can predict the relationship between global loads and local stresses and strains. The purpose of computational mechanobiology is to

"*determine quantitative rules that govern the effects of mechanical loading on tissue differentiation, growth, adaptation and maintenance by trial-and-error.*" [4]

More recent theories of mechano-regulation of tissue differentiation have been tested via computational mechanobiology. For this approach, an investigator would hypothesise a potential rule, input this rule into the computational framework and determine if the predicted outcome produces realistic tissue

structures and morphologies. Many tissue differentiation hypotheses have been incorporated into computational mechanobiological models in an attempt to simulate the time-course of fracture repair or other regenerative events [9, 138, 167]. A review of some of these hypotheses is included in this section.

Carter and co-workers proposed that intermittently applied stress determined the fate of mesenchymal tissue [5]. The mechanical stimuli proposed were hydrostatic stress and tensile strain or octahedral stress (Figure 2-24). Intramembranous ossification was predicted in regions with low mechanical stimulus. Compressive hydrostatic stress was a specific chondrogenic stimulus. Fibrous tissue was predicted by high levels of tensile strain or octahedral stress. High magnitudes of tensile strain or octahedral stress combined with high compressive hydrostatic stress predicted fibro-cartilage. And finally, cartilage was also predicted in an osteogenic mechanical environment which has low oxygen tension.

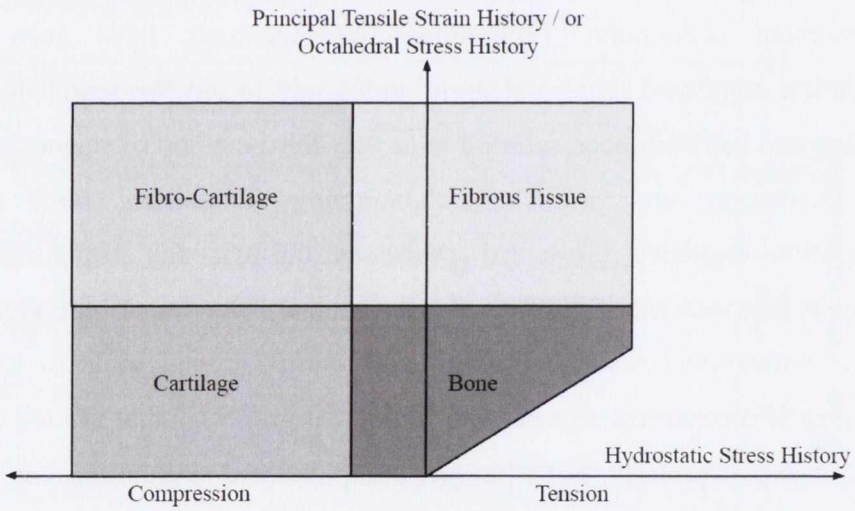

Figure 2-24. Tissue differentiation regulated by hydrostatic stress and tensile strain or octahedral stress [5]

Carter and co-workers initially varied axial and bending loads in two dimensional plane stress linear elastic finite element models to predict the octahedral shear stresses and hydrostatics stresses in a fracture callus [5]. It was concluded that intermittent hydrostatic stresses may play an important role in influencing tissue differentiation in the initial stage of fracture repair. A further study, found the role of hydrostatic stresses important for 3 stages of fracture repair [182]. These studies were successful in correlating tissue differentiation

patterns with mechanical stimuli but were not used to predict differentiation adaptively over time. This mechanobiological model has since been employed in studies of obliques fractures, psuedoarthrosis formation and distraction osteogenesis [49, 182, 183].

Claes and co-workers performed studies that combined data from *in vivo* and *in vitro* experiments with finite element analysis to assess how interfragmentary strain and gap size regulated tissue differentiation during fracture repair [73, 184]. The same authors then modelled 3 healing stages and compared the mechanical stimuli of radial strain, longitudinal strain and hydrostatic pressure to fracture repair histology [7]. The mechano-regulation algorithm they proposed is similar to the ideas of both Pauwels and Carter but contained quantified thresholds for the first time (Figure 2-25). Bone could not form in regions of high hydrostatic pressure or in regions of high strain. Connective tissue is predicted in regions of high tension. Endochondral ossification is predicted under compressive hydrostatic pressure. In addition, numerical values dividing tissue types are also proposed. This algorithm was further developed and combined with a "fuzzy logic" controller to examine trabecular fracture healing with a model system that could adapt iteratively [185, 186].

Soft tissues are predominantly made up of collagen and water and therefore, can be considered two phase tissues. For soft tissues, both liquid and solid phases interact to resist day-to-day loading. Viscoelastic effects associated with soft tissues can then be accounted for with the biphasic model proposed by Mow *et al* [187]. Prendergast [64] applied a biphasic model to implant interfaces in order to investigate the biophysical regulation of tissue differentiation. It was found that the biophysical stimuli, octahedral shear strain and relative fluid velocity, can be plotted as a mechano-regulatory pathway (Figure 2-26). A high stimulus (a combination of shear strain and fluid velocity) predicted fibrous tissue formation, a moderate stimulus predicted cartilage formation while a low stimulus predicted bone formation. This mechano-regulation algorithm could successfully predict tissue differentiation from granulation tissue to bone, cartilage or fibrous tissue. This was not possible with a linear model [188].

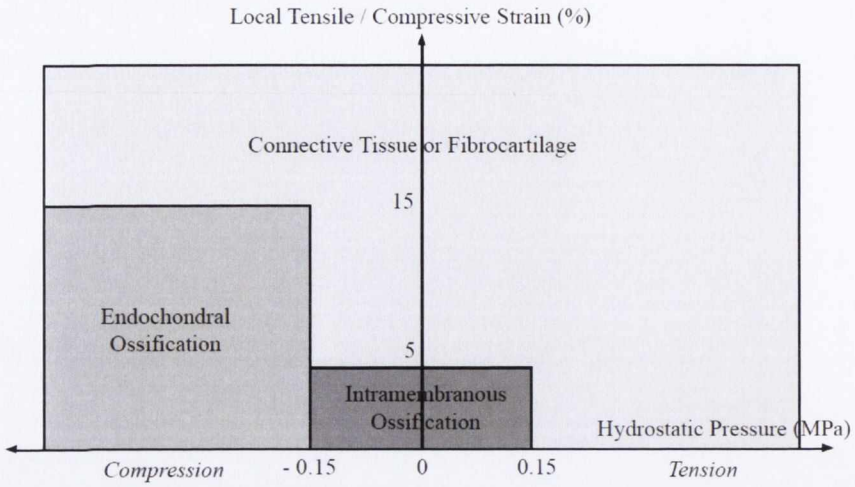

Figure 2-25. Claes and Heigele proposed regulation of tissue differentiation [7]

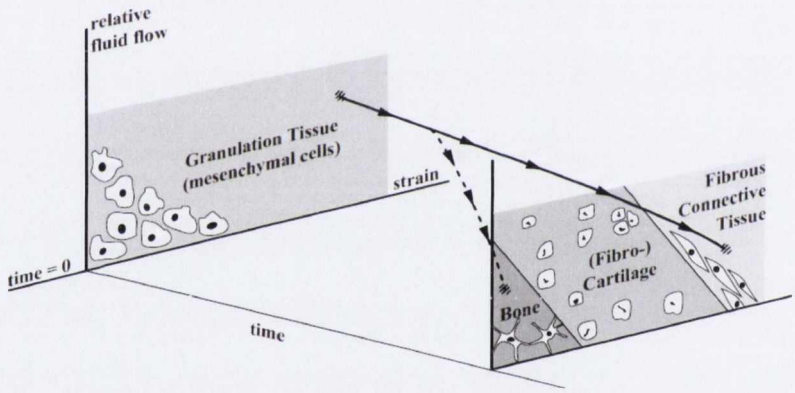

Figure 2-26. Tissue differentiation regulated by octahedral shear strain and fluid velocity [8]

Lacroix and Prendergast [10, 167] showed that tissue differentiation regulated by octahedral shear strain and fluid velocity could successfully predict the major events of fracture repair (including intramembranous ossification at the upper periosteal callus, cartilaginous bridging followed by bony bridging and finally remodelling of the callus). The model assumed axisymmetric geometry and biphasic material properties. The iterative procedure implemented allowed predictions of tissue phenotype distributions for all stages of fracture repair (Figure 2-27). This model was also used to successfully predict other regenerative events such as osteochondral defect repair [12, 13], distraction osteogenesis [14], neoarthrotis formation [18], osteotomized mandible [20], vertebral bodies [19] and the implanted bone chamber [15, 16].

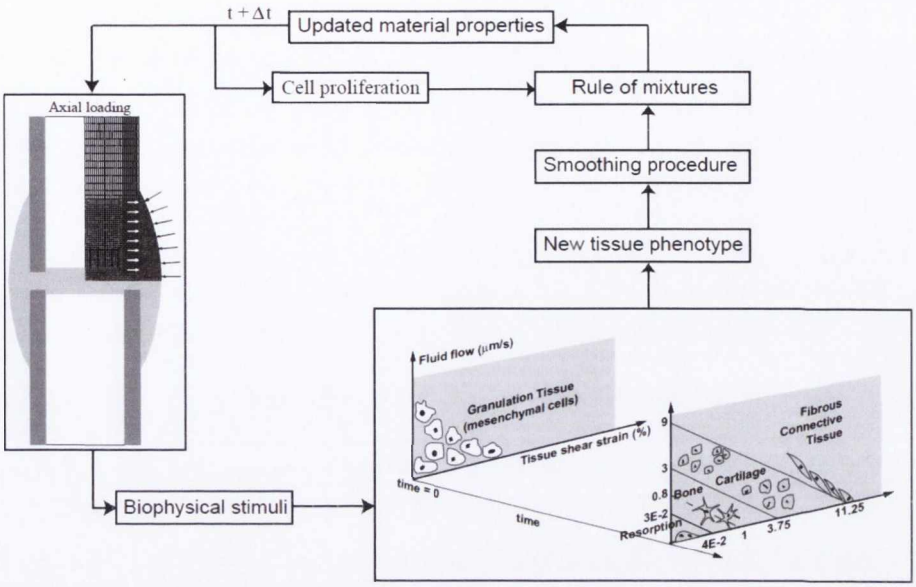

Figure 2-27. Iterative procedure implemented by Lacroix and Prendergast [10]

Isaksson *et al* [9] compared tissue differentiation theories of Claes and Heigele [7], Prendergast [8] and Carter *et al* [5], as well as differentiation regulated by single parameters such as deviatoric strain, fluid flow and pore pressure in a biphasic axisymmetric model of a fracture callus. The results of the study suggested that the most significant mechanical parameter guiding tissue differentiation may be deviatoric strain. Further investigation of the effects of torsional loads found that the combined stimulus of deviatoric strain and fluid velocity to be closest to experimental results, although none of the algorithms could fully predict the spatial and temporal patterns of healing under all loading conditions [189]. More recently, another study investigating various mechanical stimuli as regulators of tissue differentiation found volumetric strain to correlate the best with experimental data [22].

Callus geometry in all the aforementioned models was assumed to be constant with time but this is a limitation neglecting a potentially important factor. More recent models have included such callus volumetric growth. For example, Gomez-Benito *et al [23]* developed a model which included iteratively adaptive callus geometry based on the rate of tissue production, which was in turn regulated by mechanicals signals. With this model, the authors could successfully predict features of callus geometry such as increased size with increased

movement [23, 190]. Isaksson *et al* [14] successfully predicted temporal tissue differentiation patterns in a distraction osteogenesis model that used the tissue differentiation algorithm of Prendergast and co-workers, including an osmotic swelling model which allowed tissues to grow at individual rates. The model could also predict changes in differentiation that occurred due to varying the distraction rate and frequency.

Other regulatory models have been developed based upon biochemical factors rather than mechanical factors. Bailon-Plaza and van der Meulen developed a mathematical framework for the examination of the effects of growth factors upon fracture repair [142]. Geris *et al* [191] have shown that the mathematical model developed by Bailon-Plaza and van der Meulen [142], with differentiation regulated by growth factors, to be predictive of the semi-stabilized murine tibial fracture, corroborating the model for such a regenerative scenario. Geris *et al* [51] further developed this framework to include angiogenesis which was regulated by biological factors. This framework has since been successful in predicting compromised fracture healing scenarios [143, 144, 192]. The study concluded that the development of a sufficient vascular response is key to successful fracture healing. Some recent models have included stochastic processes. Perez and Prendergast [139] incorporated random walk theory into a lattice modelling approach to permit random cell movement. Finite elements were discretised into lattice points, with each lattice point representing a potential cell position. Using this method allows the explicit modelling of cells and random migration and proliferation of those cells. Simulation would predict a different result each time representative of some of the variability that exists in experimental studies. Khayyeri *et al* [15] also used such an approach to investigate the importance of cell activity rates showing that differences in mechano-sensitivity of cells could explain differences in tissue distributions in an implanted bone chamber. Other models of fracture repair have included a simulation of blood supply. Models of angiogenesis are discussed in Section 2.3.2 *In silico* models of angiogenesis.

2.6 Bone chamber experiments

The implanted bone chamber constitutes another suitable regenerative event for testing tissue differentiation hypotheses. It can provide a controlled mechanical environment through the application of known loads. Predetermined chamber geometry provides an advantage over investigation of tissue differentiation during other regenerative events. For example in fracture healing, heterogeneity in callus geometry is challenge when developing an FE model. This section will review bone chamber experiments and examine previous models of tissue differentiation which it have been applied to this regenerative scenario.

A titanium bone chamber was developed by Jacobsson *et al* [193] nearly 30 years ago to investigate the effects of irradiation upon bone, fat and blood vessel cells. Since then, other chambers were employed to investigate different aspects of tissue regeneration within the chamber including oxygen tension [194] and growth factor application [195]. In such experiments, load magnitudes within the chamber could not be varied with any accuracy and as such they were not suitable for testing of theories of mechano-regulation of tissue differentiation. A hydraulic bone chamber was developed by Guldberg *et al* [196] to examine the effect of loading upon bone tissue development within the chamber. The study demonstrated sensitivity and adaptation of bone tissue to *in vivo* mechanical stimulation.

Another bone chamber in which controlled loading of the tissue within the chamber could be achieved was developed by Tagil and Aspenberg [197]. In that study, spatial and temporal patterns of tissue distributions were assessed rendering it suitable for the testing of mechano-regulation hypotheses. The chamber consisted of a hollow screw with two ingrowth openings at the bottom (Figure 2-28). The chamber was surgically implanted into a rat tibia [197]. The two ingrowth openings lay in the bone marrow which allowed MSCs to penetrate and fill the chamber. Mechanical loading was applied via a piston, which exerted pressure on the developing ingrowth tissues.

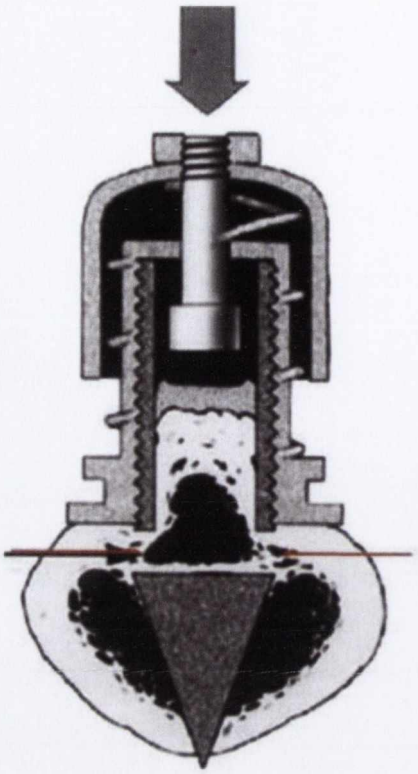

Figure 2-28. Cross section of the bone chamber [16]. The red arrows indicate the ingrowth openings. The grey arrow indicates the direction of loading applied by the piston.

The application of various loading regimes resulted in changes tissue differentiation patterns within the chamber [197, 198]. Unloaded groups presented with a well structured bone surface and a developed marrow cavity, while there was no formation of cartilage or necrotic tissue (Figure 2-29 (a)). Loaded groups (Figure 2-29 (b)) on the other hand included a layer of both cartilage and necrotic tissue on the bone surface. A subset of the loaded groups produced no cartilage and a poorly developed bone structure and marrow cavity. The reason behind this dichotomy was unclear. In a follow up study, it was found that persistent mechanical stimulation was required to maintain differentiated cartilage, but if mechanical stimulation was stopped, cartilage was replaced by bone. Continually loaded groups induced and maintained the presence of cartilage in the chamber [198]. Groups that were subjected to a period of loading, which induced cartilage differentiation, followed by a period of unloading, saw cartilage degenerate and be replaced by bone.

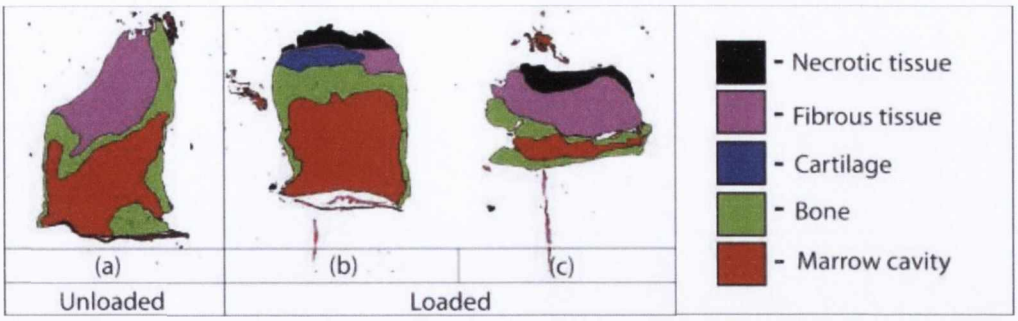

Figure 2-29. Simplified histology results [16]: (a) unloaded chamber (9 weeks) and (b) loaded chambers (9 weeks), including a developed marrow cavity, cartilage, and structured bone surface (c) loaded chamber (9 weeks), with an underdeveloped marrow cavity, no cartilage layer and poor bone structure

Khayyeri *et al* [15, 16] used the tissue differentiation model proposed by Prendergast and co-workers, in which differentiation is regulated by shear strain and fluid velocity to examine MSC differentiation in the implanted bone chamber. A 3 dimensional finite element model of the chamber was created. Simulations could successfully predict the load-dependency of tissue differentiation within the chamber and achieve qualitive agreement with histological data. A follow up study, identified alterations in the mechanosensitivity of MSCs as a possible explanation for the previously mentioned dichotomy in loaded results [15].

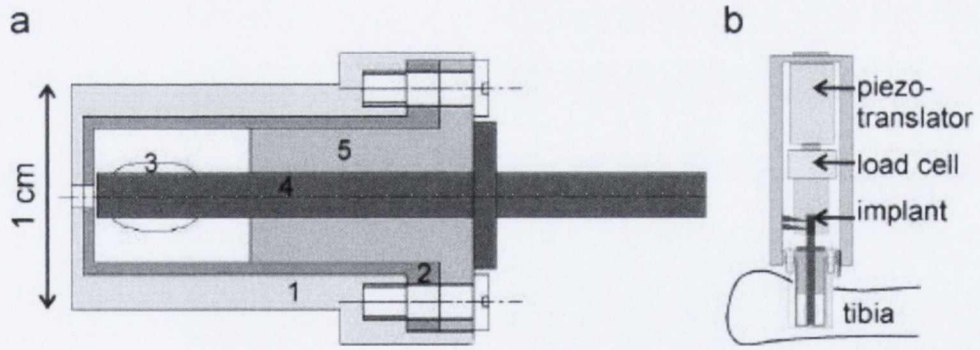

Figure 2-30. (a) Rabbit implanted bone chamber. (1) outer bone chamber, (2) inner bone chamber, (3) perforations, (4) implant, (5) Teflon bearing. (b) Complete bone chamber set up [199]

Geris and co-workers also performed computational mechanobiological investigations of a repeated sampling bone chamber [17, 53, 200-202]. The combined inner and outer chamber consisted of a perforated hollow cylinder which was implanted into the rabbit tibia. Controlled loading was achieved by an external loading device (Figure 2-30). An axisymmetric finite element model was

employed. Simulation predictions generated with tissue differentiation regulated by the hypothesis of Prendergast and co-workers [8] were successful in predicting essential aspects of tissue differentiation and bone regeneration under varying loading conditions within the chamber [17, 200]. The tissue differentiation hypotheses of Prendergast and co-workers [8] and Claes and Heigele and co-workers [7] to a rabbit implanted bone chamber case were also compared [201]. The study concluded, from the simulations generated, that while fluid flow was identified as an important regulator of tissue differentiation within the chamber, the authors were unable to separate the models in terms of their validity [201]. In a follow up study, it was found that existing mechanoregulatory theories of Carter and co-workers [5], Prendergast and co-workers [8] and Claes and Heigele and co-workers [7] were not fully predictive of tissue distributions within two different bone chamber geometries [199]. Computational simulations of the bone chamber experiment of Vandamme *et al* [202] provided support for the hypothesis that fluid flow influenced both angiogenesis and osteogenesis by regulating *in vivo* cell proliferation and differentiation [53].

2.7 Summary

Numerous different hypotheses for the mechano-regulation of tissue differentiation have been proposed. Despite, *in vitro* studies identifying both substrate stiffness and oxygen availability as regulators of MSC differentiation, these environmental cues have yet to be considered as regulators of MSC differentiation within such computational models. This work will develop a computational framework to test the hypothesis that tissue differentiation is regulated by substrate stiffness and oxygen availability *in vivo* during regenerative events such as fracture healing and the implanted bone chamber.

It is also clear from the literature that both mechanical signals and biochemical cues regulate EC physiology and in particular, bias EC migration and blood vessel growth directionality. Biochemical cues have been implemented as guiding stimuli in computational models of angiogenesis previously but the role of mechanical stimuli in directing such processes has yet to implemented and examined. The indirect effect of mechanical signals upon tissue differentiation will be investigated in this thesis through further examination of mechano-

regulation of angiogenesis. The computational framework will be further developed to incorporate mechano-regulated EC and blood vessel growth directionality and the validity of model predictions will be assessed via comparison to both *in vitro* and *in vivo* experimental observations.

Chapter3: Substrate stiffness and oxygen as regulators of stem cell differentiation during skeletal tissue regeneration: a mechanobiological model

(A modified version of this chapter has been published in PLoS One 7 (2013): e40737)

This chapter will describe the development of a computational framework capable of testing the hypothesis that substrate stiffness and oxygen availability regulate stem cell differentiation during fracture repair. Predictions of tissue distributions within a regenerating fracture callus generated by the model are compared to both histological assessments and to predictions from a well established tissue differentiation algorithm. Developing and testing this model framework is an important and necessary first step in tackling the global objective of this thesis.

3.1 Introduction

The analysis of regenerative events such as fracture healing in long bones has led to the development of a number of theories on how the local mechanical environment regulates stem cell differentiation. Over 50 years ago, Pauwels hypothesised that distortional shear stress is a specific stimulus for collagen fibres and that cartilage formation is induced by a compressive stress stimulus [3]. Bone formation, it was argued, could only occur after soft tissues had ensured sufficient stabilisation of the callus. Inspired by Pauwels' initial hypothesis, a number of investigators have proposed alternative mechanical stimuli as regulators of stem cell fate. Using computational tools such as finite element analysis, it has been possible to demonstrate a correlation between the local magnitudes of hydrostatic stress and tensile strain or octahedral stress and the appearance of specific tissue types within a fracture callus [5, 6]. A similar regulation mechanism using quantified limits for strain and hydrostatic pressure as stimuli for tissue differentiation has also been proposed [7]. An alternative theory suggests that tissue differentiation is regulated by a combined stimulus of octahedral shear strain and relative fluid velocity [8]. This model has been shown capable of predicting tissue differentiation during multiple regenerative events such as fracture healing [9, 10], osteochondral defect repair [12, 13], vertebral fracture repair [19], distraction osteogenesis [14, 20, 203], bone chamber ingrowth [16] and neoarthrosis formation [18, 204], providing strong corroboration for this hypothesis. In spite of this, understanding the relative importance and predictive ability of various biophysical cues as regulators of stem cell fate is challenging. For example, consideration of only a single mechanical stimulus such as deviatoric strain, volumetric strain or principal strain can lead to reasonably valid predictions of tissue differentiation during fracture repair [9, 22].

An inherent assumption of such hypotheses is that mechanical signals act directly on mesenchymal stem cells (MSCs) to regulate their differentiation pathway. In conjunction, or perhaps alternatively, the local mechanical environment could also act indirectly to regulate MSC differentiation by regulating angiogenesis and hence the supply of oxygen and other factors to the wound site. Inhibition of angiogenesis can lead to the development of hypoxic regions within a regenerating tissue, which may repress some differentiation

pathways while promoting others. *In vitro* studies have shown severe impairment of adipogenesis and osteogenesis at low oxygen tensions [27-29, 205], and a number of *in vivo* and *in silico* studies have highlighted the importance of angiogenesis for normal bone repair [50-53, 144, 150, 172]. On the other hand, chondrogenesis is enhanced under hypoxic conditions [30-32, 54, 205]. Furthermore, it has been found that cartilage formation is increased in more hypoxic fractures [33]. In addition to oxygen, other environmental cues are known to play a key role in regulating stem cell fate. It has been demonstrated that substrate stiffness directs stem cell differentiation [24, 60, 61]. Soft matrices that mimic the microenvironmental elasticity of brain tissue were shown to be neurogenic, stiffer matrices that mimic muscle tissue were found to be myogenic, while more rigid matrices that mimic collagenous bone were demonstrated to be osteogenic [24, 61].

The objective of this study was to test a new hypothesis for how environmental factors regulate stem cell differentiation during regenerative events such as fracture repair. Rather than assuming mechanical signals act directly on stem cells to determine their differentiation pathway, it was postulated that they act indirectly to regulate angiogenesis and hence partially determine the local oxygen environment within a regenerating tissue. Therefore, within the permissive environment of a fracture callus, which consists of a multitude of growth factors and cytokines, it was hypothesized that it is the stiffness of the adjacent substrate and the local oxygen availability that determines the differentiation pathway of MSCs that invade a fracture callus. This hypothesis has been motivated by *in vitro* observations reported in the literature of how these factors in isolation regulate stem cell differentiation, and will be tested by attempting to simulate the spatial and temporal formation of different tissue types during fracture healing using a computational model based on this hypothesis.

3.2 Methods

3.2.1 Model of stem cell differentiation

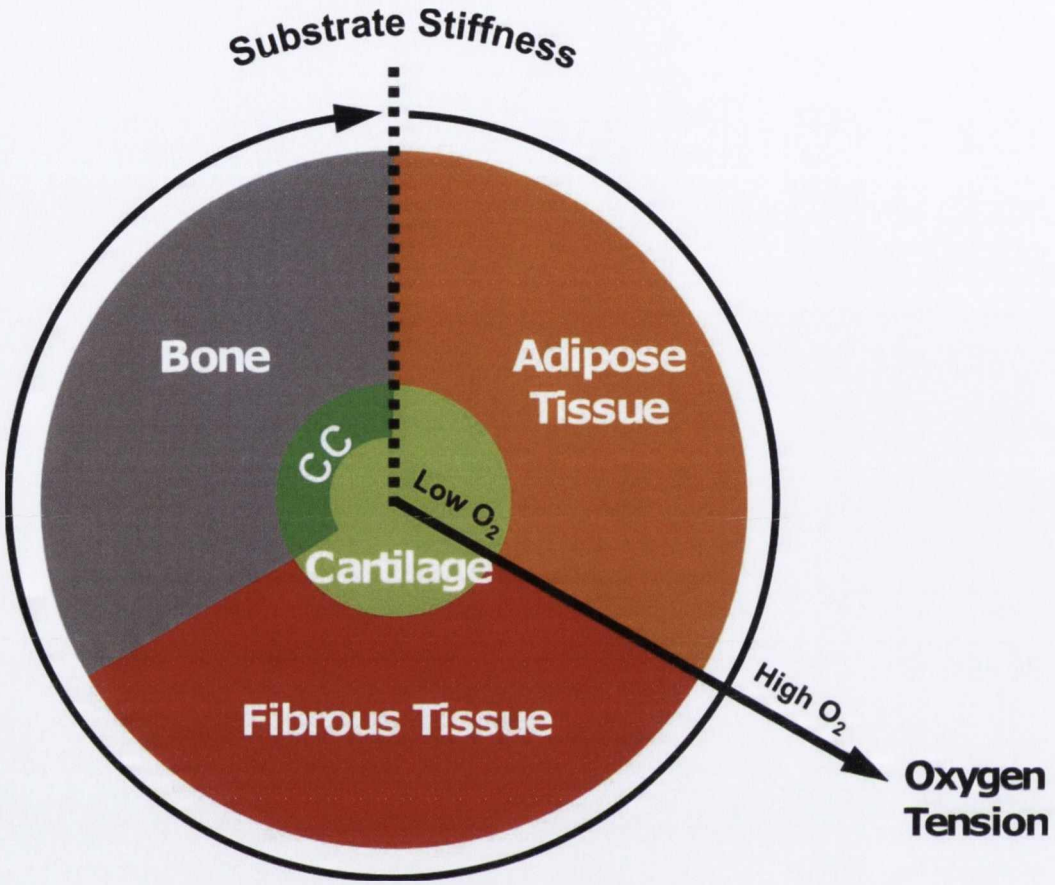

Figure 3-1. Tissue differentiation regulated by substrate stiffness and oxygen tension. The oxygen tension axis extends radially from the centre of the circle, low oxygen tension in the centre of the circle increasing towards the periphery. The substrate stiffness axis extends circumferentially in a clockwise direction from the right side of the dotted line at the top of the circle. The presence of a blood supply is also a prerequisite for formation of bone and marrow. (CC: Calcified cartilage)

The prominent tissue types involved in fracture repair are cartilage, marrow (which in the medullary cavity of long bones consists primarily of fatty yellow marrow), bone and fibrous connective tissue [55, 150]. For this study, an algorithm was developed whereby stem cell differentiation along either a chondrogenic, osteogenic or adipogenic lineage is regulated by the stiffness of the local substrate and the local oxygen tension (Figure 3-1).

The algorithm predictions can be described as follows:

1. **Chondrogenesis:** in regions of hypoxia
2. **Osteogenesis:** in regions with sufficient oxygen that are adjacent to bony tissue (i.e. a stiff substrate)
3. **Adipogenesis:** in regions with sufficient oxygen that are adjacent to marrow (i.e. a soft substrate)
4. **Fibrogenesis:** in all other regions

It has been shown that both osteogenesis and adipogenesis are repressed under hypoxic conditions [17-19]. It has also been shown that chondrogenesis is promoted under hypoxia [28-31]. Therefore, chondrogenesis was predicted by the algorithm when the local oxygen tension drops below a threshold value ($O_2^{cartilage}$), and was assumed to occur independent of the local substrate stiffness. The relationship between bone formation and blood supply has long been recognized [46, 171]. Blood vessels transport oxygen, nutrients and biological factors necessary for osteogenesis [171]. A similar relationship exists between blood supply and adipose tissue formation [175, 206, 207]. The presence of functional vascular supply was therefore a requirement for both adipogenesis and osteogenesis in this model. Should a sufficient blood supply, and hence oxygen supply, be present at a given point in the callus, the local substrate stiffness stimulus governs stem cell fate. *In vitro* studies have found that a stiff substrate can promote osteogenic differentiation while a soft substrate can promote adipogenic differentiation [24, 60]. Given that adipose tissue is a key component of marrow, the algorithm predicts adipogenesis and the reestablishment of the marrow cavity when the stiffness of the substrate is low. A stiff substrate led to the prediction of osteogenesis and the formation of bone. Should any of these conditions not be met, fibrogenesis and fibrous tissue formation was predicted (Figure 3-1).

The substrate stiffness stimulus at any point in the model was dependant upon the phenotype of surrounding elements (In this case 'element' refers to the discretized regions that make up the finite element model of the fractured bone and callus. This finite element (FE) model was used to predict the mechanical environment within the callus). Engler *et al* [24] refer to MSC differentiation

regulated by the "elasticity of the microenvironment" of the cell. For example, the stiffness of osteoid matrix produced by osteoblasts is approximately 30 kPa, however, the stiffness of woven bone itself is orders of magnitude higher (in the order of GPa). In this tissue differentiation model, osteogenesis occurred when stem cells were adjacent to newly formed bone and hence in contact with osteoid as a substrate (and similarly for adipogenesis). In this implementation, specific threshold values of stiffness were therefore not required. It takes time for an element to "fill" with a newly forming tissue (e.g. bone). This was accounted for in a tissue formation rate, *TFR*, which simulates the progression of "an osteogenic front" across the element (larger elements take longer to fill). This limiting rate was defined in units of volume (of new tissue formed) per surface area of suitable substrate (stiff or soft) available. Cells at the very edge of the element "sense" the required substrate, differentiate and produce "osteoid" (in the case of bone). Next, cells slightly further away from the edge of the element would sense the substrate. Therefore, it takes time for this bone front to cross an element and the next element cannot sense the osteogenic substrate until the adjoining element is full of bone. How "full" an element was of bone was recorded and carried forward from iteration to iteration. A number of subiterations (per day) were carried out so that this calculation is accurate. The incorporation of this *TFR* allowed the model to be independent of element size.

During endochondral ossification, hypertrophic chondrocytes are prominent in close proximity to bone [157, 208]. Hypertrophic chondrocytes are assumed to direct the mineralisation of their surrounding matrix [158]. This calcification stiffens the cartilage tissue [209]. In this algorithm, cartilage stiffened (by a factor of two) within close proximity to bone as a means to model this process of calcification. This calcified cartilage can be replaced by bone (endochondral ossification) assuming it can become adequately vascularized. Finally, during the remodelling phase of healing, bone resorption plays an important role in restoring the metabolic efficiency of the site by removing unnecessary bone. It has long been assumed that this resorption is strain related [210, 211]. Bone resorption occurred in this model when the octahedral shear strain in a bone element dropped below a threshold value ($\varepsilon^{resorption}$) (Table3-1). Mature bone was predicted following ten days of immature bone being predicted.

Table 3-1 Model parameters

Model Parameter	Symbol	Source	Unit	Value
*Angiogenesis Diffusion Coefficient	H	Estimated	mm^2/day	0.5
*Strain Threshold for Angiogenic Inhibition	ε^{angio}	[138]	%	6
Oxygen Diffusion Coefficient	G	[212]	m^2/s	2.2E-09
Oxygen Consumption Rate	Q	[213]	fmol/cell/hr	98
Maximum Cell Density	n^{max}	[51, 142]	$cells/mm^3$	5E03
Initial Oxygen Tension	$O_2^{initial}$	[179]	mmHg	74.1
*Maximum Tissue Formation Rate	TFR	Estimated	$mm^3/mm^2/day$	1
Bone Resorption Strain Limit	$\varepsilon^{resorption}$	[9]	%	0.005
Oxygen Tension Limit for Cartilage	$O_2^{cartilage}$	[27, 28]	%	3

*** The effect of varying these parameters was investigated (see Section 3.3 Results)**

3.2.2 Model of angiogenesis

Angiogenesis was modelled as a diffusive process [52]:

$$\frac{dA}{dt} = H\nabla^2 A \quad \begin{Bmatrix} H = 0.5, \varepsilon \le \varepsilon^{angio} \\ H = 0, \varepsilon > \varepsilon^{angio} \end{Bmatrix}$$

(Equation 3.1)

Where H is the angiogenic diffusion coefficient (which represents the speed at which new blood vessels progress through the callus), ε^{angio} is the threshold value of octahedral shear strain for inhibition of blood vessel progression (Table 3-1) and A is the blood vessel concentration. Blood vessels were assumed to invade the callus from the medullary cavity [159] and the periosteal cortex [154] (Figure 3-2 (b)). It is not clear in the literature whether vessels can also sprout from the lifted periosteum and surrounding muscle tissue (i.e. the external boundary of Figure

3-2 (b)). Simulations were performed with and without this boundary condition in order to investigate its effect on healing patterns. Locations in the model where it is assumed blood vessels originated were assigned a blood vessel concentration of 100%. Any element with greater than 90% concentration was considered as having a blood supply present. The presence of a blood supply was necessary for osteogenesis or adipogenesis. Angiogenic progression was inhibited in regions of high octahedral shear strain (ε). For the baseline simulation, 6 % octahedral shear strain was taken as this threshold value (ε^{angio}). This value was estimated from similar values taken by previous computational models described in the literature [138, 141]. However, given the uncertainty associated with this value, a parameter variation study was undertaken on its effect. As the rate at which blood vessels sprout and progress through a callus (represented by the diffusion coefficient *(H)* governing angiogenic progression), the tissue formation rate *(TFR)* and the threshold value of deviatoric strain for inhibition of blood vessel progression (ε^{angio}) have not been measured experimentally, the effect of changing these parameters was systematically investigated.

3.2.3 Model of oxygen transport

Oxygen (O_2) transport was described as a second diffusive process, the boundary conditions of which were dependant upon the state of the blood supply defined from the angiogenic model. Should an element have a blood supply present, the nodes of the element were assigned a fixed boundary condition equivalent to the initial or maximum oxygen concentration (see below). Oxygen consumption was considered a function of the local cell density [65]:

$$\frac{dO_2}{dt} = G\nabla^2 O_2 - Qn^{\max} n \qquad \text{(Equation 3.2)}$$

Where G is the oxygen diffusion coefficient, Q is the cellular oxygen consumption rate, O_2 is the current oxygen tension, n is the cell concentration (ranging from a minimum of 0 to a maximum of 1) and $n^{\max}$ is the maximum cell density. The local oxygen concentration at any point in the model was therefore dependant upon the initial oxygen state of the callus, the oxygen consumption rate (which in turn is dependant upon the local cell density) and proximity to a blood supply. MSC oxygen consumption rates vary within a range of values depending

on a number of factors [213]. For simplicity, the consumption rate, Q, was assumed to be constant. The oxygen diffusion coefficient, G, was taken to be that of oxygen in blood [212]. The initial oxygen concentration ($O_2^{initial}$) was taken to be 74.1mmHg [179] throughout the callus. The cell concentration, n, was obtained from the cell migration and proliferation model (see Appendix I). Maximum cell density (n^{max}) was an order of magnitude estimate similar to the range of values used elsewhere [51]. Values of all model parameters are available from Table 3-1. With these values, the predicted temporal changes in oxygen tension are presented and compared with experimental measurements in Section 3.3 Results.

3.2.4 Finite element model

An FE model was created similar to that used by Lacroix and Prendergast [10] to predict the biophysical stimuli within a fractured long bone (Figure 3-2 (a)). Axisymmetric geometry and biphasic material properties were assumed (Table 3-2). The cylindrical bone diaphysis had an internal diameter of 14mm, an external diameter of 20mm and an external callus diameter of 28mm. The fracture gap modelled spanned 3mm. A 300N axial ramp loading of 0.5s was applied at the top of the cortical shaft to simulate weight bearing on the fractured bone. The callus is assumed to be initially filled with granulation tissue. The described model was implemented into the commercial finite element software package MSC Marc (version 2008r1, MSC Software Corporation, Santa Ana (CA), USA).

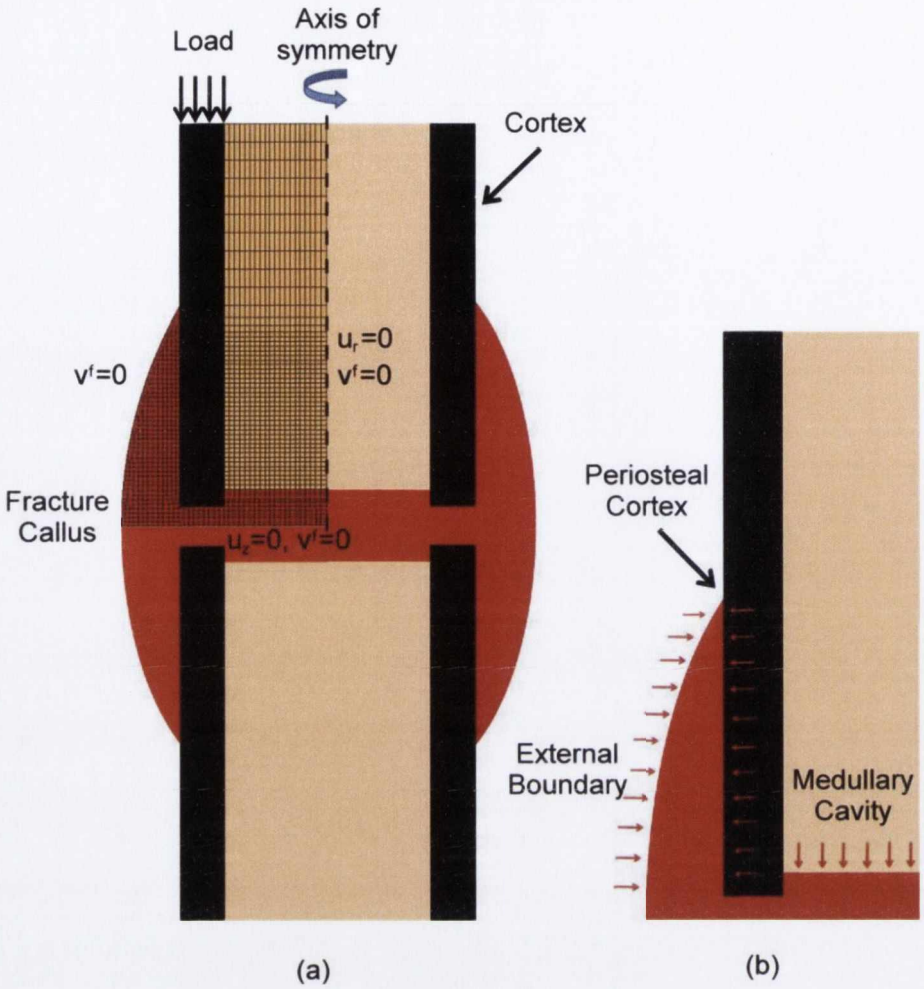

Figure 3-2. (a): Finite element model with loading and boundary conditions. (b): boundary conditions for angiogenic and cell models. Radial displacement, axial displacement and fluid velocity are shown as u_r, u_z, and v^f respectively

Table 3-2 Material properties

Material Property	Granulation Tissue	Fibrous Tissue	Cartilage*	Marrow	Immature Bone	Mature Bone	Cortical Bone
Young's Modulus (MPa)	0.2[a]	2[b]	10[a]	2[a]	1,000[a]	6,000[c]	20,000[c]
Permeability (mm2)	1E-11[a]	1E-11[b]	5E-15[d]	1E-14[a]	1E-13[a]	3.7E-13[e]	1E-17[f]
Poisson's Ratio	0.167[a]	0.167[a]	0.167[a]	0.167[a]	0.3[a]	0.3[a]	0.3[a]
Fluid Dynamic Viscosity (Ns/m2)	1E-9	1E-9	1E-9	1E-9	1E-9	1E-9	1E-9
Porosity	0.8[a]	0.8[a]	0.8[a]	0.8[a]	0.8[a]	0.8[a]	0.04[g]

a. Lacroix and Prendergast (2002) [10]; **b.** Hori and Lewis (1982) [214]; **c.** Claes and Heigele (1999) [7]; **d.** Armstrong and Mow (1982) [215]; **e.** Ochoa and Hillberry (1992) [216]; **f.** Cowin 1999 [217]; **g.** Schaffler and Burr (1988) [218]. * Calcified cartilage was assumed to have a Young's Modulus of 20 MPa. All other properties were identical to cartilage.

3.2.5 Iterative procedure

Tissue differentiation within the fracture callus was simulated via an iterative procedure similar to that described previously in the literature [10, 167] (Figure 3-3). Within each iteration, a prediction of mechanical stimuli, cell density, substrate stiffness, blood supply and oxygen availability was made in order to enable the local phenotype to be determined based on the tissue differentiation algorithm. Firstly, the finite element model of a fracture callus was used to predict the spatial patterns of mechanical stimuli within the callus. These mechanical stimuli influenced angiogenic progression, which was inhibited in regions of octahedral shear strain. The level of local oxygen availability was determined depending on the initial oxygen environment, local blood supply, cell consumption rate and cell density. Local phenotype predictions were then made according to the tissue differentiation algorithm. Cell proliferation and migration were modelled as a diffusive process (see Appendix I) [167]. Tissue material properties were influenced by cell density according to the rule of mixtures as previously described (see Appendix II) [10, 156, 167]. A temporal smoothing procedure was implemented to account for the delay between stimuli first acting on a cell and change of tissue type (see Appendix III) [10, 156, 167]. Updated material properties were input back into the FE model for the next iteration of the cycle. This iterative process is continued until a solution was converged upon.

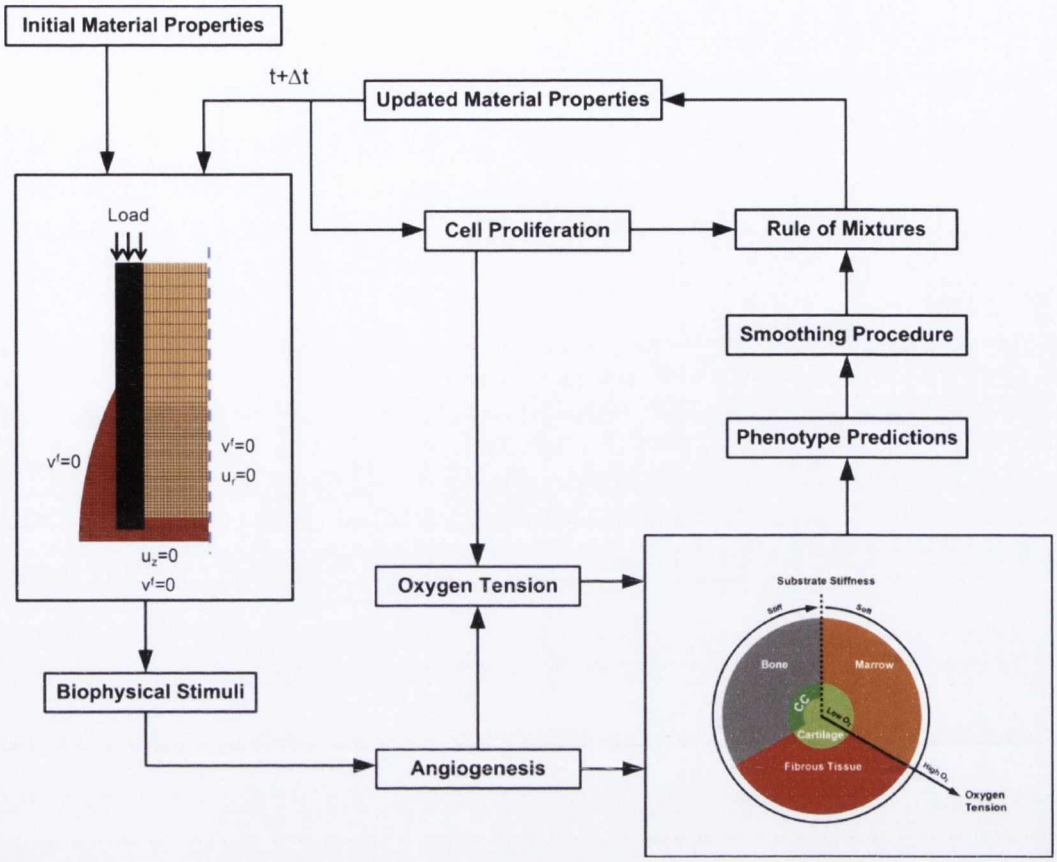

Figure 3-3. Iterative procedure for tissue differentiation hypothesis testing

For the purposes of comparison, the same iterative procedure was implemented with stem cell differentiation regulated by a well established algorithm in which stem cell fate was dictated by a combined stimulus of octahedral shear strain and fluid velocity [64]. When this stimulus was high, fibrous tissue was predicted, when the stimulus was moderate, cartilaginous tissue was predicted and a low stimulus results in the prediction of bone formation. Bone resorption was predicted when the stimulus fell below a very low threshold level.

3.3 Results

Model predictions of oxygen tension for the first ten days were compared to experimental measurements of oxygen tension in the periosteal region adjacent to the fracture gap [179] (Figure 3-4 (a)), demonstrating reasonably good agreement between the two. The temporal values of both oxygen tension and substrate stiffness varied throughout the facture callus, with different magnitudes predicted in the periosteal callus, fracture gap and endosteal callus (Figure 3-5). In the

endosteal callus (Figure 3-5 (a)), oxygen tension initially decreased but was restored to normal levels upon being vascularised early in the repair process. Fibrous tissue was initially predicted to form within this region of the callus (Figure 3-5 and Figure 3-6), hence the local substrate stiffness remained low. Eventually bone was predicted to form within the endosteal callus, initially at the stiff endosteal side of the cortex, and the substrate stiffness in this region of the model increased. This bone was eventually resorbed and replaced by marrow which progressed from the undamaged marrow body, resulting in a decrease in stiffness. In the fracture gap (Figure 3-5 (c)), the level of oxygen tension was predicted to decrease during the early stages of repair due to cellular consumption. Chondrogenesis proceeded, after initial fibrous tissue formation, followed by cartilage calcification, vascularisation and an increase in oxygen tension. In the upper periosteal callus (Figure 3-5 (b)), early vascularisation restored oxygen levels following initial decreases. Substrate stiffness in this region rapidly increased as bone, which was initially predicted to form on the stiff cortex, progressed into the lower cartilaginous periosteal callus. The hypoxic region that formed in the periosteal callus adjacent to the fracture gap early in healing later shifted towards the fracture gap (Figure 3-4 (b)). Cartilaginous tissue formation stabilised the callus and vascularisation eventually restored normal oxygen tension levels in the middle and latter stages of regeneration (Figure 3-4 (c)).

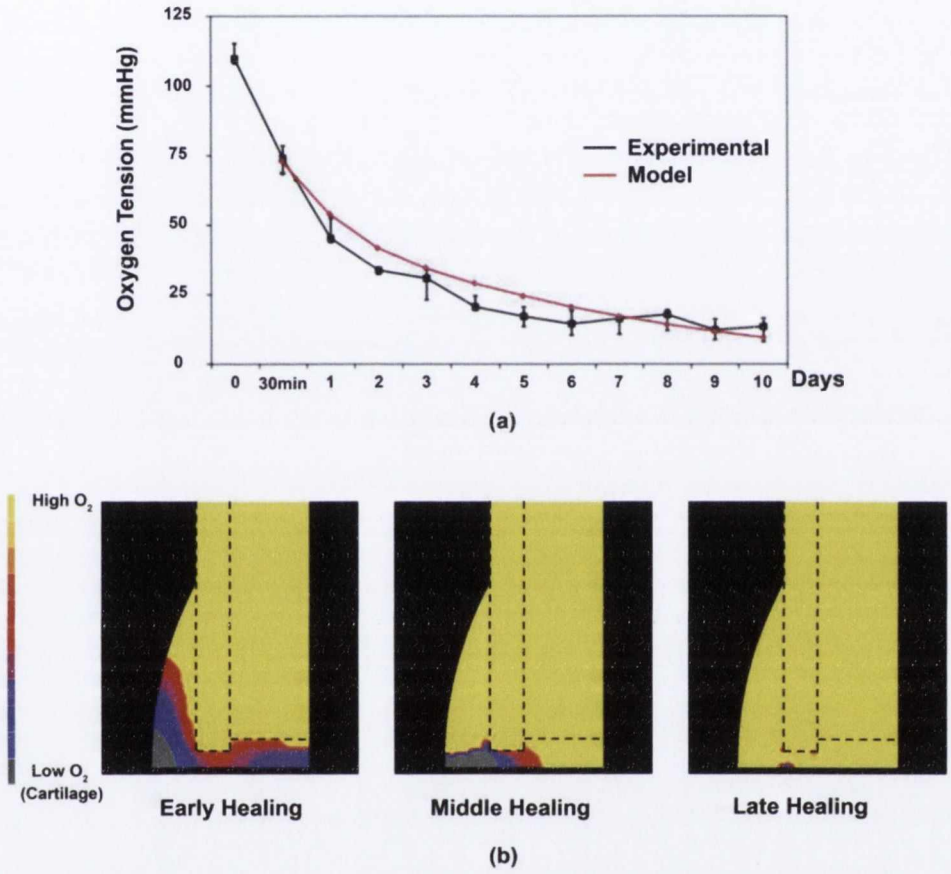

Figure 3-4. (a): Oxygen model predictions (from a representative element in the periosteal callus adjacent to the fracture gap) compared to experimental data for oxygen tension readings (Image adapted from Epari et al [179] with permission). (b): Predictions of oxygen tension in the callus at early (day 10), middle (day 20) and late (day 30) stages of healing.

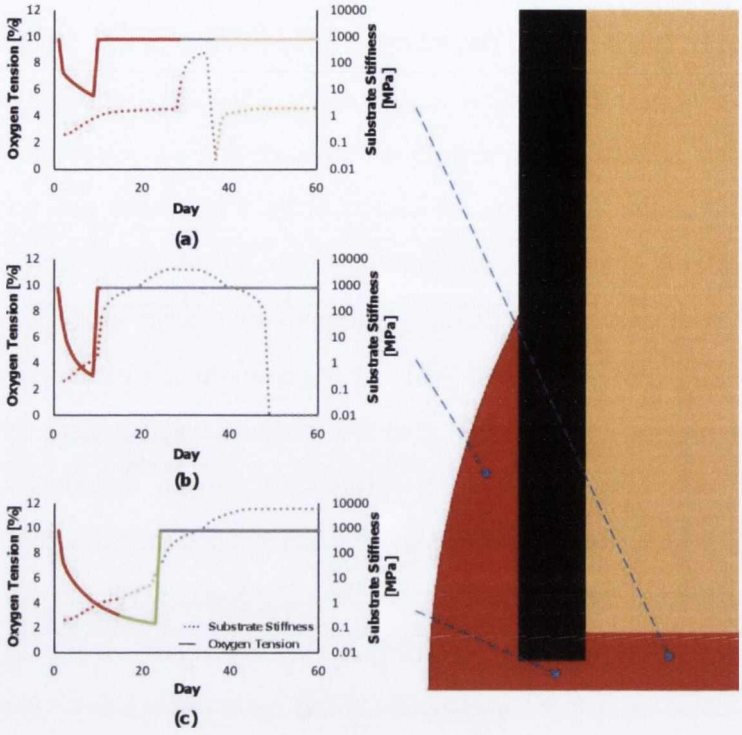

Figure 3-5. Model predictions for substrate stiffness and oxygen tension. Locations chosen as characteristic of the periosteal callus, fracture gap and endosteal callus respectively. It should be noted that substrate stiffness here refers to the macroscale stiffness of the regenerating tissue, where it is noted (as discussed in the manuscript) that the elasticity of the microenvironment of the cell is most likely different.

Predicted patterns of tissue differentiation were compared for the two models. In model A it is assumed that stem cell differentiation was regulated by substrate stiffness and oxygen availability, whereas in model B, differentiation was regulated by octahedral shear strain and relative fluid velocity [64]. The simulation results from both algorithms were compared to averaged histological images [55] for Stages III to VI of fracture healing (Figure 3-6). Both models predicted the major events of fracture repair (summarised here). Bone formation originates in the upper periosteal callus and proceeds towards the fracture gap (Stages I and II). Cartilage forms in the periosteal region adjacent the fracture gap to form a cartilaginous bridge (Stage III). This cartilage undergoes endochondral ossification and leads to periosteal bony bridging (Stage IV). Endosteal bony bridging follows and the fracture gap is now completely bone (Stage V). Periosteal bone is then remodelled to restore the original bone structure (Stage VI). Some differences between the two models are noticeable upon closer examination of the model predictions.

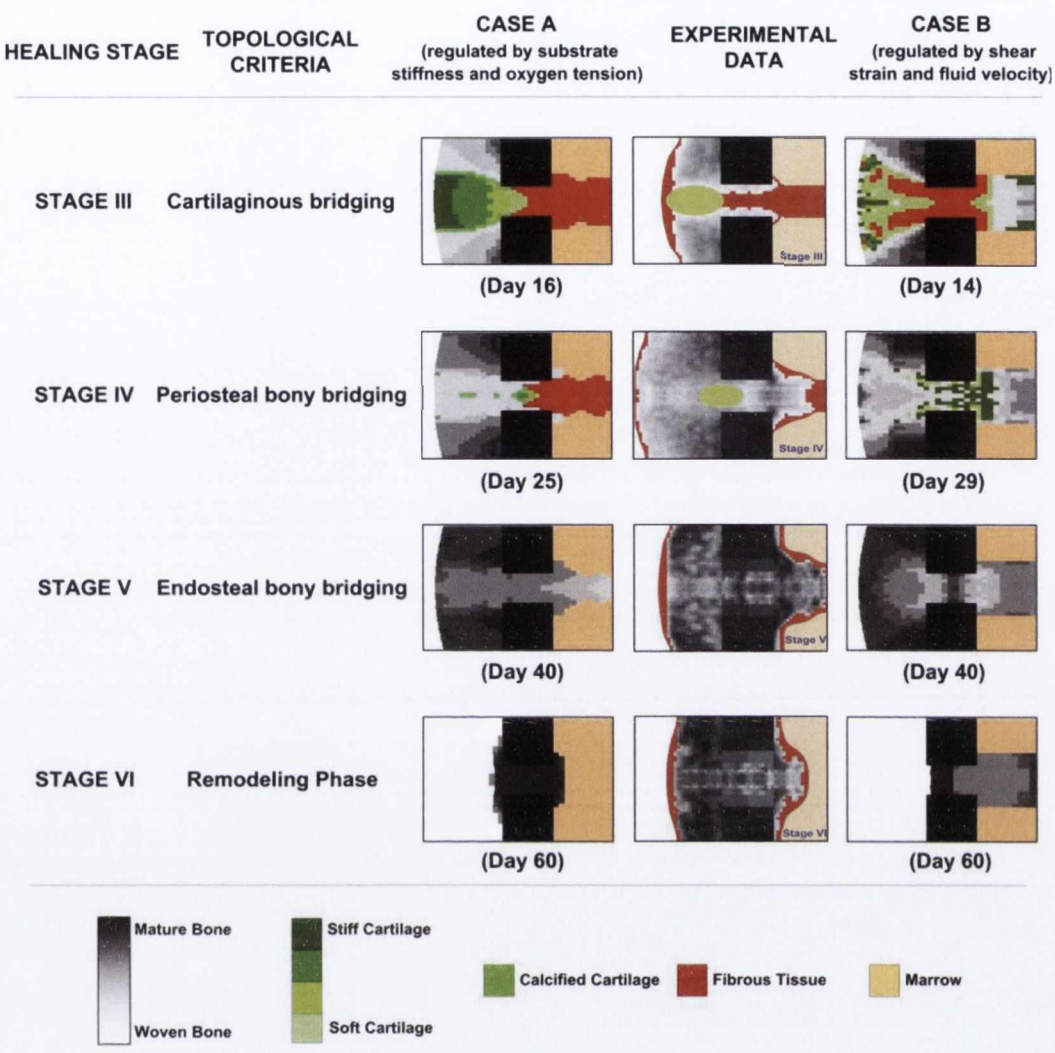

Figure 3-6. Model predictions versus experimental data. Model A: Model predictions for Stages III to VI of fracture healing when tissue differentiation is regulated by substrate stiffness and oxygen tension. Model B: Model predictions for Stages III to VI of fracture healing when tissue differentiation is regulated tissue shear strain and relative fluid velocity [9, 10]. Experimental Data: Averaged histological images obtained from an extensive study of fracture healing in sheep (Images adapted from Vetter et al [55] with permission)

For Stage III, model A (substrate stiffness and oxygen availability) predicted cartilaginous bridging of the periosteal callus and also less mature cartilage formation in the fracture gap. Bone formation progressed from the upper callus to fill the periosteal region above the fracture gap. Some marrow formation was evident endosteally at the existing marrow body. The rest of the internal callus remained as fibrous tissue. Model B (shear strain and fluid flow) predicted similar bone formation in the upper periosteal callus, cartilage formation in the outer periosteal callus and fibrous tissue in and adjacent to the fracture gap. Bone and cartilage were predicted to fill the remainder to the endosteal callus. For

Stage IV, model A predicted bony bridging in the periosteal callus adjacent to the fracture gap. Some bone formation was predicted to originate from the endosteal cortex. The endosteal callus remained predominantly fibrous tissue. Model B also predicted bony bridging in the outer periosteal callus. The fracture gap and adjacent regions were predominantly cartilage with some bony regions also. The remainder of the endosteal callus was full of bone. For Stage V, both algorithms predicted bone in the periosteal callus, endosteal callus and fracture gap. For Stage VI, model A predicted the resorption of the periosteal callus which was previously bone. The endosteal callus was also fully resorbed of bone which allows the recanalization and full restoration of the marrow of the medullary cavity. Model B also predicted full resorption of the periosteal callus but the endosteal callus remains full of bone.

A sensitivity analysis was performed to investigate the effect of modifying the angiogenic diffusion coefficient, H, the angiogenic strain threshold, ε^{angio}, and the tissue formation rate (TFR) (Figure 3-7). Models with the angiogenic threshold value increased to 8% strain predicted slightly less cartilage and more bone formation in the early stages of healing in comparison to the baseline simulation. Models with the threshold value reduced to 4% strain displayed slightly more cartilage and less bone formation in the early stages of healing in comparison to the baseline simulation. Healing, which was defined as when the fracture gap was full of bone, occurred earlier for an increased angiogenic inhibition threshold (8%) and occurred later for a decreased angiogenic inhibition threshold (4%) (3 days earlier and 6 days later respectively, see Figure 3-7 (c)). Decreasing the threshold for angiogenic inhibition to 2% strain resulted in a prediction of non-union (Figure 3-7 (a)). Halving the angiogenic diffusion coefficient (0.25) resulted in slower healing (9 days later). Doubling the angiogenic diffusion coefficient (1.0) was predicted to decrease the healing time by 1 day over the baseline simulation. Further increases in this coefficient appeared to cause simulations to converge upon a minimum healing time and had no additional effect. In this case, the bone formation rate becomes the limiting factor. Increasing the bone formation rate, while the angiogenic diffusion coefficient remained constant, had a similar convergence upon a minimum healing time (Figure 3-7 (b)).

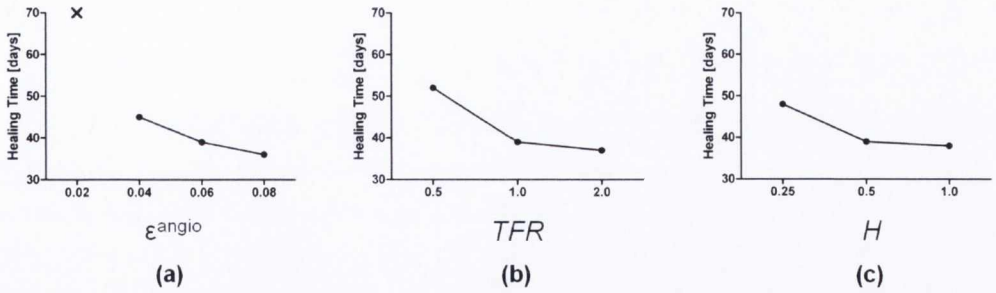

Figure 3-7. Effect on healing time of parameter variations. (a): Healing time versus angiogenic strain threshold, εangio (X signifies the prediction of non-union) (b): Healing time versus tissue formation rate, TFR. (c): Healing time versus angiogenic diffusion coefficient, H.

The addition of a third angiogenic boundary condition to simulate a blood vessel source from surrounding soft tissues resulted in a slightly faster healing time (one day less) but again led to a similar spatial pattern of healing. The removal of the angiogenic source from the marrow cavity resulted in no healing from the endosteal side until very late in healing and an increased healing time (7 days later). If both periosteal and external boundary blood supply sources were not included in the simulation, healing failed to occur with the marrow cavity as the sole angiogenic source. Further simulations (data not shown) demonstrated that increasing the applied load from 300N to values over 700N also leads to predictions of fracture non-union.

3.4 Discussion

A number of different hypotheses have been proposed for how extrinsic mechanical signals govern stem cell fate [5, 7, 8, 22, 189]. Support for these hypotheses has been provided by demonstrating that computational models based on such hypotheses can successfully predict aspects of tissue differentiation during regenerative events such as fracture healing. Despite *in vitro* studies identifying alternative environmental cues, such as substrate stiffness [24, 60, 61] and oxygen availability [28, 29, 31, 32, 205], as regulators of stem cell fate, little is known about what role these cues play in regulating tissue differentiation during regenerative events *in vivo*. In this study, it is demonstrated for the first time that the major events that occur during fracture healing can be predicted by a model that assumes substrate stiffness and oxygen availability regulate stem cell differentiation. In this model, mechanical factors act indirectly to regulate stem

cell fate by regulating angiogenesis and hence, in combination with cellular oxygen consumption, the local oxygen availability. The model predictions provide equally compelling data in support for this new hypothesis as previous studies [6, 7, 9, 10, 219] proposing that extrinsic mechanical signals act directly on stem cells to regulate their differentiation pathway.

A number of differences were observed between the model predictions based on substrate stiffness and oxygen availability (model A) and that of shear strain and fluid flow (model B) [8]. Endosteal cartilage is predicted by model B at both Stages III and IV of healing. This is due to high levels of fluid velocity contributing to the mechanical stimulus in the endosteal callus. Endosteal cartilage is not always observed histologically [55], and is not predicted by model A. In this model, the level of oxygen tension in the endosteal callus does not decrease sufficiently to induce cartilage formation as there is a close angiogenic supply which progresses from the existing marrow of the medullary cavity. Model B (shear strain and fluid flow) predicts endosteal bone formation originating from the centre of the medullary cavity. A low mechanical stimulus leads to this prediction. Observations from histological images typically show that endosteal bone tends to originate from the endosteal cortex and progress towards the centre of the cavity [7, 55]. This experimental observation is captured in model A, due to the requirement of a high substrate stiffness for osteogenesis. In addition, a high fluid velocity stimulus prevents bone resorption of the endosteal callus in model B. Resorption regulated by strain alone allows this endosteal bone to be resorbed in model A. This permits the subsequent recanalization and restoration of the marrow of the medullary cavity as occurs *in vivo* [55]. Both models predict resorption of the periosteal and endosteal calluses at a faster than physiological rate. It should also be noted that more recent models of tissue differentiation regulated by shear strain and fluid velocity also predict resorption of the endosteal callus [11].

In developing this model, a number of questions related to the endochondral pathway were considered. The underlying mechanism behind cartilage calcification and endochondral ossification is not fully understood but it is believed that hypertrophic chondrocytes play a role in directing cartilage mineralization [158]. What drives chondrocytes to become hypertrophic in the

first place is also not something that is fully understood. Proximity to a blood supply will undoubtedly increase oxygen levels in cartilage immediately adjacent to vascularised bone. The local oxygen tension is one factor which may regulate chondrocyte hypertrophy [32, 220], with emerging evidence suggesting that low oxygen conditions suppress the hypertrophic phenotype. In support of this, it has been demonstrated that chondrocyte maturation and subsequent bone formation is delayed by antiangiogenic treatment and that proangiogenic treatment induces the opposite effect (increased chondrocyte maturation and subsequent bone formation) [178, 221]. In the growing bone, a layer of hypertrophic chondrocytes is found in close proximity to existing bone [157, 208]. Calcified cartilage most commonly occurs at the interface with adjacent bone. Based on these observations it was assumed in this model that chondrocytes adjacent to bone undergo hypertrophy and direct the calcification of the surrounding cartilage tissue in this region. Other factors, such as mechanical cues [222-224], have also been shown to regulate chondrocyte hypertrophy. Future models could consider these potential regulators of chondrocyte hypertrophy.

In undertaking this approach, it has been assumed that mineralization precedes vascularisation, stiffening the tissue before vessel ingrowth. This stiffening provides some protection to blood vessels from possible shearing due to high strains at the interface. Only in the case where the stability provided by the calcified cartilage is not sufficient to facilitate progression of vascularisation will the calcified cartilaginous tissue not be replaced by bone. The alternative, vascularisation of the cartilaginous template preceding mineralization, is also possible. Further investigation is required to attempt to answer this question more affirmatively.

The implementation of the substrate stiffness stimulus in this model could also be interpreted in a slightly different way, where the driving stimuli are oxygen tension and 'proximity to' bone (for osteogenesis) and 'proximity to' adipose tissue (for adipogenesis) (Figure 3-8). For example, in the presence of a blood supply (and hence sufficient oxygen), the osteogenic stimulus is pre-existing bone. One key factor associated with 'proximity' to a tissue is the local substrate stiffness or elasticity which it provides a cell and which is clearly a key environmental factor regulating MSC fate decisions. However, it is also

recognised that tissues themselves may be a source of growth factors, and hence proximity to a bone, for example, may also mean proximity to higher concentrations of growth factors or other biochemical cues necessary for osteogenesis. In either interpretation, the implementation is as performed in this study.

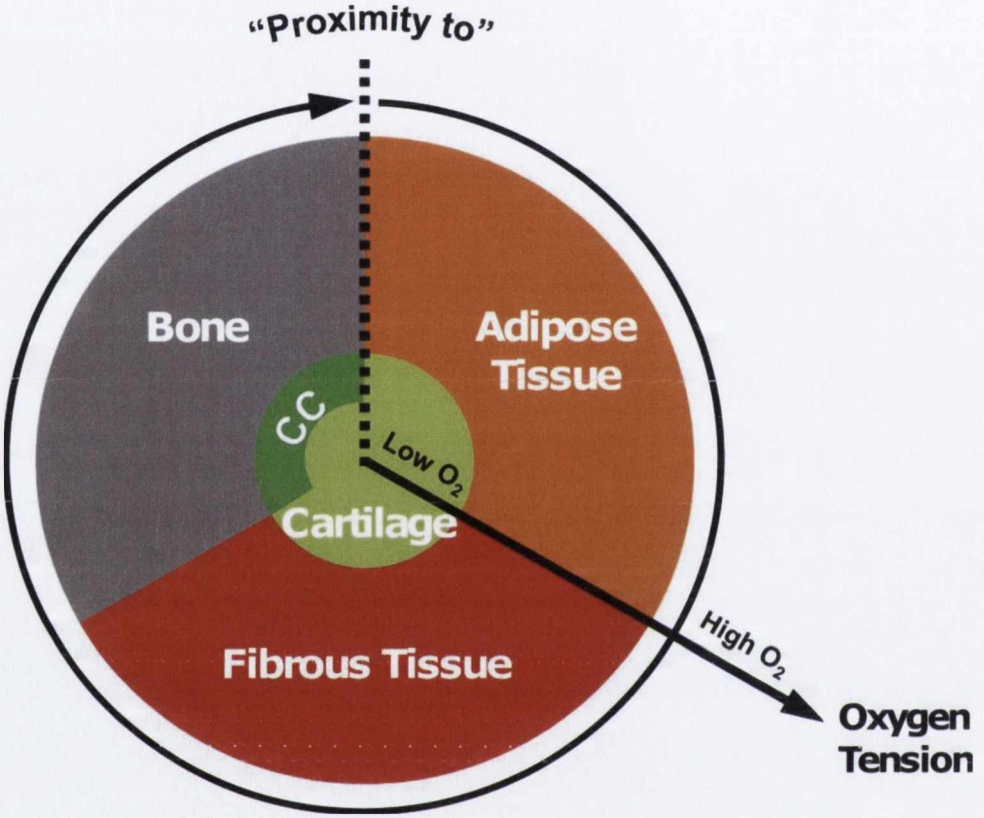

Figure 3-8. Tissue differentiation regulated by proximity and oxygen tension. The oxygen tension axis extends radially from the centre of the circle, low oxygen tension in the centre of the circle increasing towards the periphery. Bone and adipose tissue formation occur when there is sufficient oxygen tension "in proximity" to existing adipose tissue or bone fronts. The presence of a blood supply is also a prerequisite for formation of bone and adipose tissue. (CC: Calcified cartilage)

There are some limitations associated with this model. Firstly, an axisymmetric geometry is adopted. It is assumed that the axisymmetric model will still provide a reasonable prediction of the environment within such a callus. Only axial loading is considered, implying that the model is most representative of well fixed fractures. Cell proliferation/migration and angiogenesis, modelled as diffusive processes, are simplified representations of complex *in vivo* processes. More complex models have been implemented [11, 16, 50, 51, 144] but I do not believe that implementing such models would significantly alter the model predictions and, hence, the corroboration of the underlying model hypothesis.

Inhibition of angiogenesis in this study is assumed to be as a result of a high shear strain stimulus but there is also the possibility that lower concentrations of blood vessels demonstrated in unstabilised fractures [37, 40, 150] may simply be due to the formation of avascular tissue (i.e. cartilage) itself. The oxygen model implemented in this study assumes a constant cell oxygen consumption rate. It has been shown that this is not the case [213]. Convection of regulatory factors is not considered. Again, the objective in this study was not to create a perfect model of oxygen transport and consumption, but merely to implement a model with sufficient predictive ability to allow us to test the hypothesis proposed in this thesis. It should also be noted that a simplified model of bone marrow reestablishment has been implemented in this study. It is recognized that the marrow of the medullary cavity of long bones contains not only the marrow stroma and adipose tissue predicted by this algorithm, but also hematopoietic and lymphatic cells. Again, these simplifications were implemented to enable to test hypothesis of the study to be tested without introducing additional complexity. A specific stimulus for fibrous tissue formation is not offered by this tissue differentiation model. There is evidence that a mechanical stimulus can induce fibrous tissue formation [5] and this warrants further investigation. Fracture callus growth and size are also key factors not considered in this study [23, 190]. It should be noted that gradients in growth factors that may also regulate tissue differentiation [51, 142] were not considered. It is acknowledged that the presence of such factors may be critical to initiate stem cell differentiation. For example, it has recently been demonstrated that even well vascularised bone defects may not fully regenerate, which has been associated with a decreased expression of key regulatory factors such as BMP-2 and BMP-4 [225]. Only by explicitly including such factors into the model (as demonstrated, for example, by Geris *et al* [192]) can complex cases of non-union be simulated. Finally the model does not consider a role for substrate stiffness in regulating chondrogenesis, rather assuming it is regulated entirely by oxygen availability which is most likely a simplification.

In spite of these limitations this model, which assumes that stem cell fate is regulated by substrate stiffness and oxygen tension, can successfully predict all the major events of fracture repair. In doing so it has been demonstrated how

disparate environmental cues, which have been shown to independently regulate stem cell fate *in vitro*, are potentially integrated by MSCs *in vivo* to drive differentiation during regenerative events such as fracture healing. Of course, the results of these simulations only provide preliminary support for the underlying model hypothesis, and should not be used to conclude one hypothesis (e.g. differentiation regulated by substrate stiffness and oxygen) is more valid than another (e.g. differentiation regulated by shear strain and fluid flow). All that can definitively be stated is that one cannot reject either hypothesis tested as part of this computational mechanobiological analysis. Furthermore, model predictions should not be used to support the idea that substrate stiffness and oxygen tension alone entirely determine stem cell differentiation. Other biochemical cues are also most likely required. If the fracture callus is viewed as a permissive environment, where multiple growth factors and cytokines are present that will allow MSCs to differentiate down multiple different pathways, this study provides support for the hypothesis that the oxygen tension and substrate stiffness play a key role in determining cell fate in such a permissive environment. Whether these factors act alone, or in combination with extrinsic biophysical signals such as hydrostatic pressure, strain and fluid flow, to regulate MSC differentiation is a critical question. Mounting experimental data from *in vitro* studies suggests all of these factors are important [101, 226]. Decoupling the relative importance of these various cues is challenging using computational models alone, but may in the future be possible by integrating computational models with appropriately designed *in vitro* and *in vivo* studies of stem cell differentiation.

Chapter4: The role of oxygen as a regulator of stem cell differentiation during fracture repair in TSP2-null mice

(A modified version of this chapter has been published in J Orthop Res. 2013 (10):1585-96. doi: 10.1002/jor.22396)

The previous chapter concluded that both tissue differentiation algorithms regulated by mechanical signals (octahedral shear strain and relative fluid velocity) and regulated by substrate stiffness and oxygen availability successfully predicted the stages of fracture healing. Corroboration was provided for both algorithms in that case. However, there are cases in the literature where significant changes in tissue differentiation are observed while the mechanical environment is not changed and hence, tissue differentiation hypotheses regulated solely by mechanics could not predict such differences in tissue differentiation. Fractures in TSP2-null mice heal via enhanced intramembranous and reduced endochondral ossification versus wild type controls.

This chapter describes a systematic investigation of a number of potential mechanisms causing such changes using the previously developed tissue differentiation model framework. Should the model be predictive of both cases, further support is provided for the hypothesis that stem cell differentiation is regulated by substrate stiffness and oxygen tension during fracture repair.

4.1 Introduction

Numerous environmental factors have been implicated as regulators of mesenchymal stem cell (MSC) fate during regenerative events such as fracture healing. The local mechanical environment within a fracture callus is believed to play a key role in regulating tissue differentiation [5, 7, 8], with corroboration for such hypotheses often provided by computational mechanobiological models [6, 10, 189]. In such simulations, the validity of the underlying hypothesis is tested based on the ability of the model to predict realistic temporal and spatial patterns of stem cell differentiation during tissue regeneration [12, 16, 18]. In addition to extrinsic mechanical cues, *in vitro* experiments have highlighted other factors such as local substrate stiffness [24, 60] and oxygen tension [31, 32] as important regulators of MSC differentiation. Furthermore, it has been demonstrated that a computational mechanobiological model that assumes MSC differentiation is regulated by local substrate stiffness and oxygen availability can predict typical patterns of tissue differentiation observed experimentally during fracture healing [227]. The finding that similar modelling frameworks [189] can be used to corroborate different hypotheses points to a limitation of simulation, in isolation, as a method to test hypotheses related to MSC differentiation. One possible reason for this relates to the coupled nature of environmental factors that are believed to regulate stem cell fate *in vivo*. For example, during regenerative events such as fracture healing MSCs might directly sense extrinsic mechanical cues which in turn might direct their differentiation pathway, however the same mechanical factors will also act to regulate neovascularisation and hence oxygen levels within the fracture callus, another important determinant of differentiation. The task of elucidating relative roles of coupled environmental factors such as mechanical signals and oxygen as regulators of stem cell fate would be greatly facilitated by *in vivo* studies where one factor is constant while the other is varied. Genetically modified mice can provide such model systems whereby at least some of the variables regulating MSC differentiation can be manipulated while others are kept constant (e.g. by eliminating a protein involved in vascularisation). Therefore, integrating *in vivo* murine studies with computational mechanobiological models could provide a novel platform to explore the role of

specific environmental cues in regulating stem cell differentiation during tissue regeneration.

Thrombospondin-2 (TSP2) is a matricellular protein that is highly expressed in developing and healing tissues. The absence of this protein following genetic disruption (knockout) has been shown to affect MSC differentiation during fracture repair [33]. TSP2-null mice heal via a less cartilaginous callus with enhanced intramembranous bone formation. Ten days post fracture, TSP2-null mice show 30% more bone and 40% less cartilage than wild type (WT) controls [33]; thus, TSP2-null mice demonstrate reduced endochondral ossification and enhanced appositional bone formation. This occurs despite the fact that the mechanical environment during the initial stage of regeneration is similar in both genetic backgrounds. The dominant hypothesis for this phenotype is that there is a shift in fracture MSC fate resulting in TSP2-null MSCs becoming osteoblasts to a greater level than WT MSCs. Furthermore, it is hypothesized that this differentiation shift develops because of altered vascularization and tissue oxygenation. TSP2 is known to directly inhibit endothelial cell growth [228, 229] with mice lacking TSP2 exhibiting greater callus vascularity than WT controls [33]. The increased vascularity in the fracture callus is hypothesised to lead to increased oxygen levels, with this enhanced oxemia promoting differentiation to a direct osteoblastic lineage. However, providing definitive support for this hypothesis is confounded by the fact TSP2 is multifunctional and can regulate other aspects of MSC function such as proliferation [33, 230]. TSP2-null mice exhibit increased rates of cell proliferation with levels of apoptosis remaining equivalent to WT controls [33]. It is possible that increased cell proliferation could also influence the regenerative pathway and explain the differences in MSC fate observed. Another explanation offered is that stem cells within the callus of TSP2-null mice are metabolically different than cells of WT mice, which could in turn alter the spatial availability of regulatory cues such as oxygen.

The objective of this study was to provide further support for the hypothesis that changes in oxygen availability within the callus of TSP2-null mice are responsible for the differences in tissue differentiation during fracture repair. The hypothesis was be tested by applying the previously developed computational model of tissue differentiation [227], in which substrate stiffness and oxygen

tension regulate stem cell differentiation, to mouse long bone fracture healing and exploring if altering the rate of angiogenesis within the model is predictive of the changes in tissue differentiation observed in TSP2-null mice. The possibility that alternative effects of TSP2 deletion are driving experimentally observed changes in MSC differentiation was also investigated. The effect of increased cell proliferation, increased stem cell number originating from the marrow, decreased cell oxygen consumption rate and a stiffened TSP2-null callus upon predicted patterns of differentiation is also examined. Corroboration for a given hypotheses can be provided where implementing such changes within the model (e.g. increased angiogenesis, increased MSC proliferation *etc*) results in realistic predictions of stem cell differentiation during fracture repair in TSP2-null mice.

4.2 Methods

4.2.1 Experimental setup

The full experimental details are available elsewhere [33], a summary of which is included here. Mice that had a targeted disruption of the *Thbs2* gene (TSP2-null group) were subjected to the following procedures and compared to WT controls. Closed transverse fractures were created in tibiae of 9 to 10 week-old mice. A hole in the cortex of the medial aspect of the tibial tuberosity was bored using a hypodermic needle into which a sterile 0.009-in-diameter, stainless steel pin was inserted. The pin was inserted the full length of the tibia until resistance was felt. This pin provided stability to the fracture site. Tape "splints" provided initial rotational stability for the first 48 hours. At harvest, right tibias were dissected, intramedullary pins removed and tissues stored for subsequent histological analysis. Left tibias were treated similarly and examined via μCT scanning and torsional mechanical testing. μCT analysis facilitated calculation of the callus volume, bone volume and bone mineral density. Histological sections stained with Safranin-O were used to differentiate between the total callus area, cartilaginous area and woven bone area.

4.2.2 Immunohistochemistry for hypoxia

(the work in this section was performed by Dishowitz M, Sweetwyne M, Miedel E)

WT and TSP2-null mice were fractured, and five days post fracture injected intraperitoneally with 1.5 mg hypoxyprobe reagent (Hypoxyprobe™-1 Plus Kit, Hypoxyprobe, Inc, Burlington MA, USA). Six minutes post-injection the mice were euthanized and fractured tibia rapidly fixed in 4% paraformaldehyde and then decalcified and embedded in paraffin and longitudinally sectioned at 7 micron thickness. Pimonidazole adducts were detected using anti-pimonidazole adduct antibody and a goat anti-rabbit secondary antibody conjugated to Tetramethylrhodamine isothiocyanate (TRITC), as directed using the Hypoxyprobe™-1 kit. A rabbit IgG was used as a control for the anti-pimonidazole antibody. Sections were counter stained with DAPI to stain nuclei. The area of TRITC staining was quantified by collecting images at 100X magnification using an Olympus BX51 fluorescence microscope with a filter for TRITC fluorescence. Images were acquired with a Spot RT32 megapixel camera at constant exposure. Callus area and area of TRITC positivity were determined using ImageJ, and data is presented as a percentage of the TRITC positive areas relative to total evaluated area with the % of TRITC positive areas in the IgG control subtracted. Cell number per callus area was calculated by acquiring images at 400X using a DAPI fluorescence filter. These images were then analysed using ImageJ to calculate cellularity. Each DAPI stained nuclei was counted as a cell per field area to determine cell density.

4.2.3 Finite element model

A finite element (FE) model of a mouse fracture callus was created in order to predict the biophysical stimuli within the fractured bone (Figure 4-1). Axisymmetric geometry and biphasic material properties were assumed (Table 4-1). Dimensions for the model were obtained from experimental geometrical measurements (Table 4-2). An axial ramp load was applied in 0.5s at the top of the cortical shaft in order to simulate weight bearing. Maximum axial loading of the intact mouse tibia has been approximated at 1.2N [231]. The callus is assumed to be initially filled with granulation tissue. The described model was implemented into the commercial finite element software package MSC Marc (version 2008r1, MSC Software Corporation, Santa Ana, CA, USA).

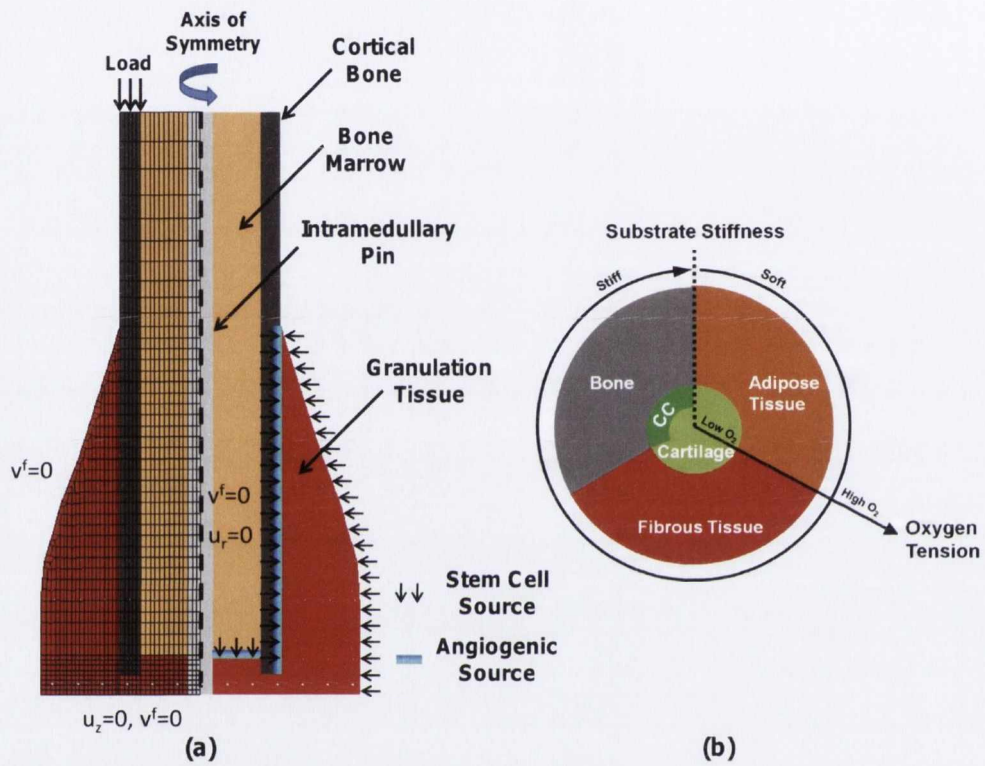

Figure 4-1. (a) FE model with loading and boundary conditions for angiogenic and cell models. Radial displacement, axial displacement and fluid velocity are shown as u_r, u_z, and v^f respectively. (b) Tissue differentiation model regulated by substrate stiffness and oxygen tension. Oxygen tension is low in the centre of the circle increasing towards the periphery. The substrate stiffness axis extends circumferentially increasing in a clockwise direction from the right side of the dotted line at the top of the circle. The presence of a blood supply is also a prerequisite for formation of bone and marrow. (CC: Calcified cartilage)

Table 4-1 Material properties

Material property	Granulation Tissue	Fibrous Tissue	Cartilage*	Marrow	Immature Bone	Mature Bone	Cortical Bone
Young's Modulus(MPa)	0.2[a]	2[b]	10[a]	2[a]	1,000[a]	6,000[c]	20,000[c]
Permeability(mm^2)	1E-11[a]	1E-11[b]	5E-15[d]	1E-14[a]	1E-13[a]	3.7E-13[e]	1E-17[f]
Poisson's Ratio	0.167[a]	0.167[a]	0.167[a]	0.167[a]	0.3[a]	0.3[a]	0.3[a]
Fluid Dynamic Viscosity(Ns/m^2)	1E-9	1E-9	1E-9	1E-9	1E-9	1E-9	1E-9
Porosity	0.8[a]	0.8[a]	0.8[a]	0.8[a]	0.8[a]	0.8[a]	0.04[g]

a. Lacroix and Prendergast (2002) [10]; **b.** Hori and Lewis (1982) [214]; **c.** Claes and Heigele (1999) [7]; **d.** Armstrong and Mow (1982) [187]; **e.** Ochoa and Hillberry (1992) [216]; **f.** Cowin 1999 [217]; **g.** Schaffler and Burr (1988) [218]. * Calcified cartilage was assumed to have a Young's Modulus of 20 MPa. All other properties are identical to cartilage. ** Pin was modelled as a linear elastic stainless steel with a Young's Modulus of 200 GPa and Poisson's Ratio of 0.3.

Table 4-2 Geometrical measurements for finite element model

Dimension	Measurement
Callus Length	6.33 mm
Callus Max Radius	1.365 mm
Cortex Radius**	0.68 mm
Cortex Width	0.17 mm
Pin Radius	0.11 mm
Fracture Gap	0.17 mm

** Distance laterally from centreline of medullary cavity to outer surface of cortical bone.

4.2.4 Tissue differentiation model

The previously developed tissue differentiation model whereby stem cell fate along either a chondrogenic, osteogenic or adipogenic lineage is regulated by stiffness of the local substrate and local oxygen tension was applied to the mouse fracture model (Figure 4-1 (b)) [227]. Briefly, both osteogenesis and adipogenesis were assumed to be repressed under hypoxic conditions [27-29], with chondrogenesis instead supported in such a low oxygen environment [30-32, 54]. To implement this rule, chondrogenesis was predicted in regions of the callus where the local oxygen tension fell below a threshold value ($O_2^{cartilage}$) (Table 4-3). In regions where a sufficient oxygen supply existed the substrate stiffness stimulus regulates stem cell differentiation. A stiff substrate supported osteogenic differentiation whereas a soft substrate supported adipogenesis. Fibrogenesis was predicted in regions of the callus where none of these conditions were met.

Table 4-3 Model parameters

Model Parameter	Symbol	Source	Unit	Value
Angiogenesis Diffusion Coefficient	H	Estimated	mm^2/day	0.01-0.08
Strain Threshold for Angiogenic Inhibition	ε^{angio}	[227]	%	6
Oxygen Diffusion Coefficient	G	[212]	m^2/s	2.2E-09
Oxygen Consumption Rate	Q	Estimated	fmol/cell/hr	98
Maximum Cell Density	n^{max}	[51, 142]	$cells/mm^3$	5 E03
Initial Oxygen Tension	$O_2^{initial}$	[179]	mmHg	74.1
Maximum Tissue Formation Rate	TFR	[227]	$mm^3/mm^2/day$	1
Bone Resorption Strain Limit	$\varepsilon^{esorption}$	[9]	%	0.005
Oxygen Tension Limit for Cartilage	$O_2^{cartilage}$	[27, 28]	%	3
Cell Diffusion Coefficient	D	[227]	mm^2/day	0.34-0.68

Models of the callus mechanical environment, angiogenesis, oxygen availability and cell migration were all incorporated into an iterative procedure to generate phenotype predictions for all regions of the callus with regulation of tissue differentiation as described in the preceding paragraph (see Section 3.2.5 Iterative procedure for more details). Firstly, the local mechanical environment for all regions of the callus was predicted using the FE model. A diffusive model was used to simulate angiogenic progression. Blood vessels were assumed to invade the callus from the medullary cavity [159] and the periosteal cortex [154] (Figure 4-1 (a)). It was also possible that new vessels could sprout from the surrounding soft tissues. Simulations were performed with and without this boundary condition in order to investigate its effect on healing pattern. The level of local octahedral shear strain was assumed to regulate the progression of blood vessels, with angiogenesis inhibited in regions of the callus where a threshold strain was exceeded. Previous models of angiogenesis have assumed a similar

process whereby high levels of shear strain and fluid flow prevent blood vessel progression [50]. Oxygen transport was also modelled as a diffusive process, with boundary conditions for this model dependent upon the local blood supply. Oxygen tension was initially assumed to be high throughout the callus [179]. As the simulation progressed oxygen diffused in from new blood vessels and was consumed at a rate dependent upon cell density. Cell density was determined from a diffusive model which estimates cell migration and proliferation throughout the callus. MSCs differentiated into either osteoblasts, chondrocytes, adipocytes or fibroblasts according to the tissue differentiation algorithm. Material properties for all elements in the mesh were updated and the finite element model computed the mechanical environment again. This iterative loop continued until convergence upon a solution was achieved. Each iteration represented one day.

4.2.5 Baseline simulation of fracture repair in wild type (WT) mice

In order to investigate the potential effect of deleting TSP2 on stem cell differentiation during fracture healing, it was first explored whether the proposed model could successfully predict patterns of repair in the WT animal. The effect of perturbing this model in different ways could then be used to help identify the underlying mechanisms driving the changes in tissue differentiation in TSP2-null mice. Given the difficulty in determining the proportion of the axial load bore by the medullary pin, simulations were first performed with axial loads of 20%, 50% and 80% of normal tibial loading. The rate of angiogenic progression, as determined by the diffusion coefficient (D_{angio}), was also varied. Simulations were performed with rates of angiogenic progression of 0.01, 0.025, and 0.04. The closest prediction to quantitative experimental data (a combination of a spatial mapping coefficient and tissue area fraction (Table 4-4) for the 10 days post fracture time point from this set of 9 simulations (3 different loading conditions and 3 different rates of angiogenic progression)) was chosen as representative of the WT case. The *spatial mapping coefficient* is a ratio of the area in the model with correctly predicted tissue phenotype to the total area of differentiating tissue within the callus. The model was deemed to be correct in its prediction of the tissue phenotype (bone, cartilage or other) in a particular element if the phenotype is the same as the corresponding region in an identical mesh mapped onto a representative histological section of the callus at 10dpf (Figure 4-2).

Table 4-4 Prediction of the percentage area of the callus filled with cartilage and bone and the spatial mapping coefficients for 10dpf as a result of parameter variations for modelling the WT case

Cartilage

Load \ D_{angio}	0.01	0.025	0.04
20%	43.44	38.17	33.20
50%	44.31	40.20	35.21
80%	46.03	45.44	43.63

*WT cartilage was 42.17 % experimentally

Bone

Load \ D_{angio}	0.01	0.025	0.04
20%	23.49	41.71	53.05
50%	19.01	31.79	40.46
80%	14.17	23.46	26.25

*WT bone was 27.90 % experimentally

Spatial Mapping Coefficient

Load \ D_{angio}	0.025	0.04
20%	0.712	0.791	0.705
50%	0.711	0.805	0.750
80%	0.666	0.763	0.730

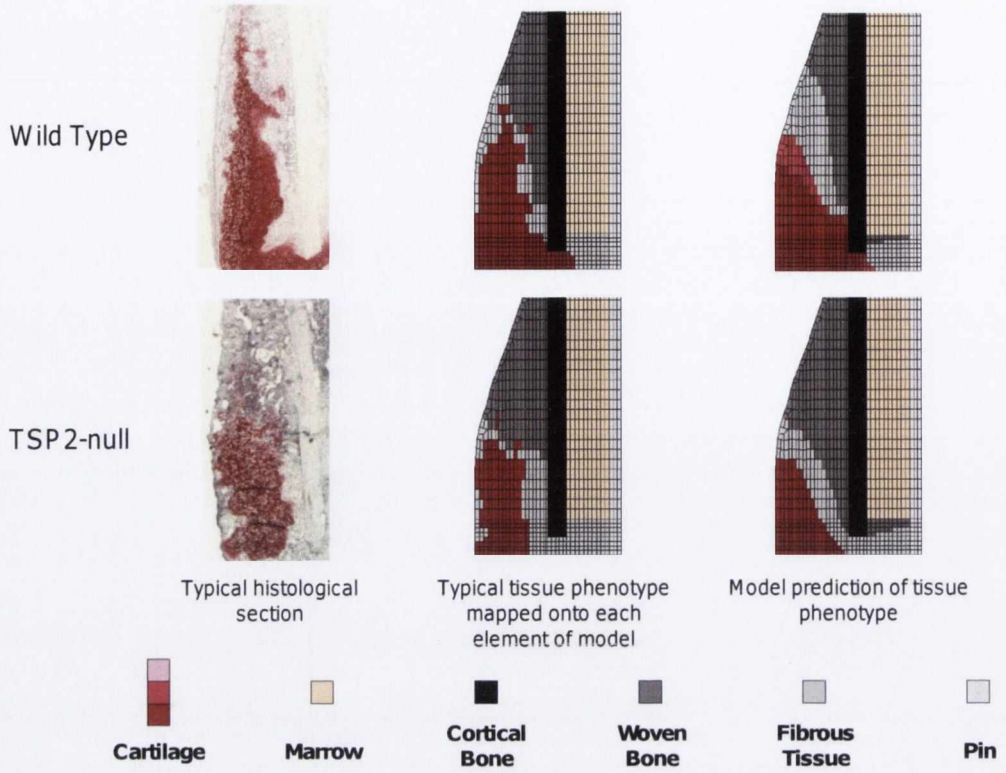

Figure 4-2. Left - Typical histological sections for the 10 dpf time point (Safranin-O staining). Centre - Tissue phenotypes from typical histological section mapped onto a mesh of callus identical in geometry to the FE mesh. Right - Model predictions of tissue phenotype. The examples shown in this figure are for WT and TSP2-null (bottom) (case A).

4.2.6 Simulation of fracture repair in TSP2-null mice

Once experimental patterns of tissue differentiation in the WT case were successfully predicted, the model was perturbed in order to investigate the potential mechanisms that may be driving the dramatic differences in tissue differentiation observed in TSP2-null mice. Five cases were investigated:

Case A- Increased angiogenic progression rate: Experimental observations showed an increased blood vessel density of approximately 67% by day 5 for TSP2-null mice versus WT counterparts [33]. In order to model this, the baseline WT simulation rate of angiogenic progression was increased until approximately 67% more vessels existed (by area) 5 days post fracture (dpf). The angiogenic diffusion coefficient was increased from 0.025 to 0.08 in order to achieve this.

Case B- Increased cell proliferation rate: TSP2 has also been shown to regulate MSC proliferation. The effect of increasing the cell proliferation rate by a factor of 2 was also investigated.

Case C- Increased cell source from the Marrow: It has been suggested that marrow could make a greater contribution to healing in TSP2-null mice than in WT counterparts as an increase in marrow CFU-F has been observed. The density of the stem cell source at the marrow was increased by a factor of 2 to investigate this possibility.

Case D- Decreased cellular oxygen consumption rate: Another potential impact of TSP2 deletion is to alter the oxygen consumption rate of MSCs. It is conceivable that a decreased consumption rate (and hence greater oxygen availability) would result in a less cartilaginous callus. While I am not aware of any experimental data to support this hypothesis, a simulation was performed with an oxygen consumption rate half that of the baseline model in order to investigate its effect on the predicted patterns of differentiation.

Case E- Increased callus stiffness: Another potential mechanism which may be driving the differences in stem cell fate observed in the TSP2-null case is a stiffened callus. This was modelled as a doubling of the granulation tissue stiffness to 0.4 MPa. The alternative hypothesis, namely that the callus of TSP2-null mice is softer would intuitively lead to a prediction higher callus strains and hence less angiogenesis (i.e. the opposite of what is observed *in vivo*), and hence was not considered here as a potential mechanism.

These five cases were compared to quantitative experimental data for TSP2-null mice to assess the validity of simulation predictions.

4.3 Results

4.3.1 Fractures of TSP2-null mice show reduced hypoxia

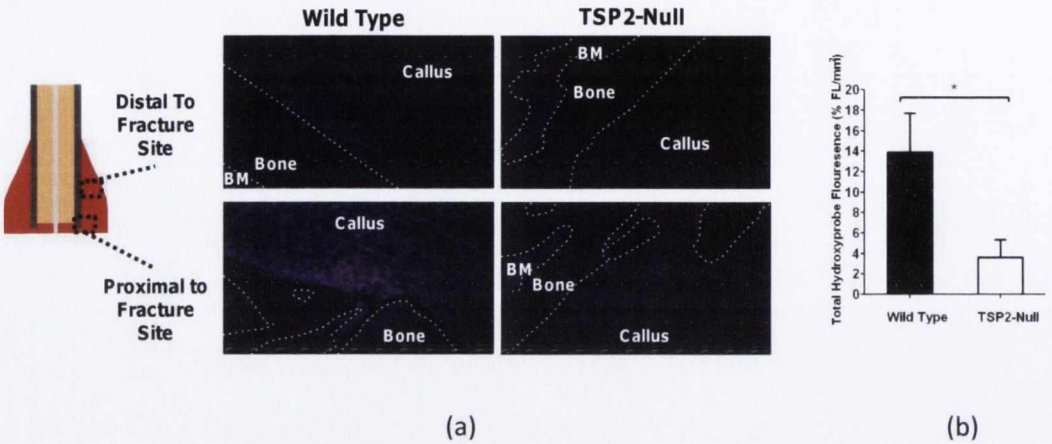

Figure 4-3. (a) Staining for hypoxia 5 days post fracture in WT (left) and TSP2-null mice (Top row: at fracture site. Bottom row: distal to fracture site). Reddish-puple indicates areas of pimonidazole adduct detection indicative of hypoxia. Blue staining is DAPI for nuclei. (b) Total Flourescence per square millimetre for WT and TSP2-null mice. (WT = 4460 ± 638.26 cells/mm2, TSP2-null = 3834 ± 195.14 cells/mm2. Difference is not statistically significant).

5 days post fracture, pimonidazole adducts were detected intensely around the fracture site indicating a significant hypoxic region developing within WT mice (Figure 4-3 (a)). Much less staining occurred for the TSP2-null mouse in close proximity to the fracture site, indicating greater oxygen availability. Only very light staining occurred distal to the fracture site for both the WT and TSP2-null animals, indicative of normoxic conditions in these regions of the repair tissue. The staining results are strongly supported when hypoxyprobe fluorescence per unit area is compared for TSP2-null versus WT mice. WT mice exhibited approximately four times more fluorescence area indicative of a significantly more hypoxic callus in the WT case (Figure 4-3 (b)).

4.3.2 Wild type model

The model case with 50% of the axial load being supported by the cortex and the angiogenic rate at 0.025 mm^2/day was chosen as model predictions of tissue differentiation during fracture repair given that this prediction was closest to that observed experimentally in the WT case (assessed via a combination of the spatial mapping coefficient and the prediction of the total area of the callus filled with either cartilage or bone- see Table 4-4). The model predicted hypoxic conditions

in the periosteal region close to the fracture site and within the fracture gap itself 5dpf. Near normoxic conditions were predicted distal to the fracture site in the upper periosteal callus and in the inner endosteal callus (Figure 4-4).

The main stages of fracture healing were successfully predicted including periosteal cartilaginous bridging, both periosteal and endosteal bony bridging followed by eventual bone remodelling (Figure 4-5). Ten days post fracture, the model predicted woven bone formation in the upper periosteal callus, extending down along the periosteal cortex ten days post fracture. Cartilage was predicted in the fracture gap and periosteal callus, extending higher up into the periosteal callus further from the cortex. Negligible cartilage was predicted in the endosteal callus. Qualitatively spatial predictions of tissue differentiation were similar to that observed histologically and the predictions of total bone and cartilage formation are also similar to the quantitative measures made in the experiments (Figure 4-6). Quantitative measurements of bone and cartilage formation were also similar to model predictions (Figure 4-7(a)). The addition of a blood supply source from the surrounding soft tissues led to a prediction of higher levels of oxygen availability for the oxygen consumption rates assumed in the model. As model predictions with only 2 sources of new blood vessels were more predictive of experimental findings, the surrounding soft tissue as an angiogenic source was excluded from the remaining simulations.

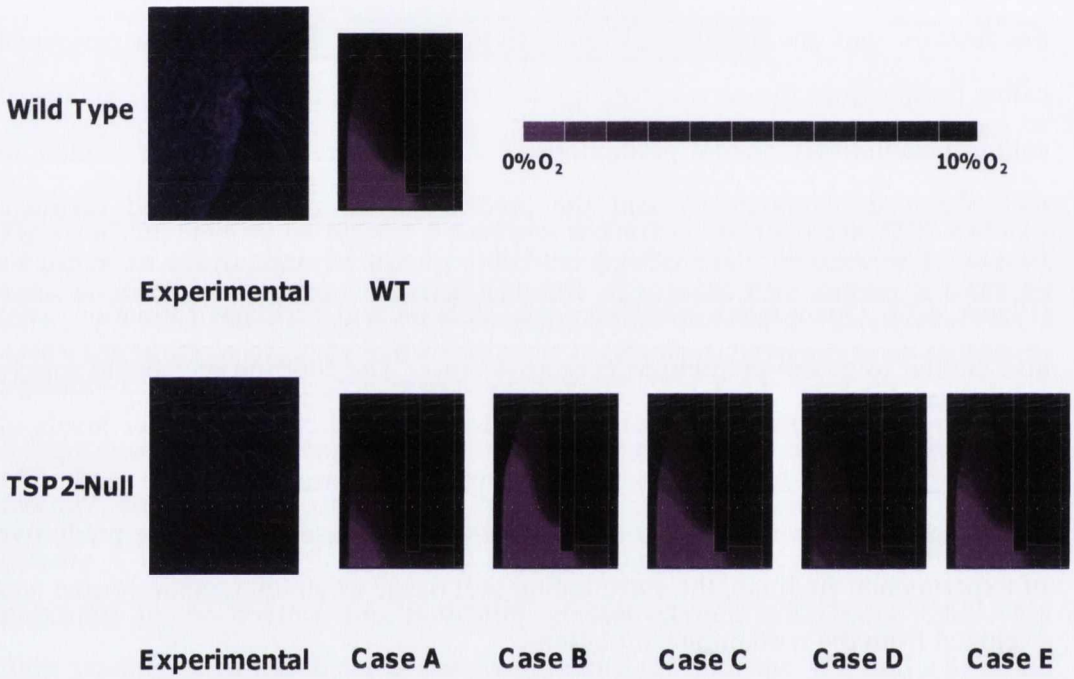

Figure 4-4. Model predictions of the state of the oxygen environment in the callus 5 days post fracture for the WT case and the four possible TSP2-null case predictions compared with hypoxyprobe stains for the region adjacent to the fracture gap.

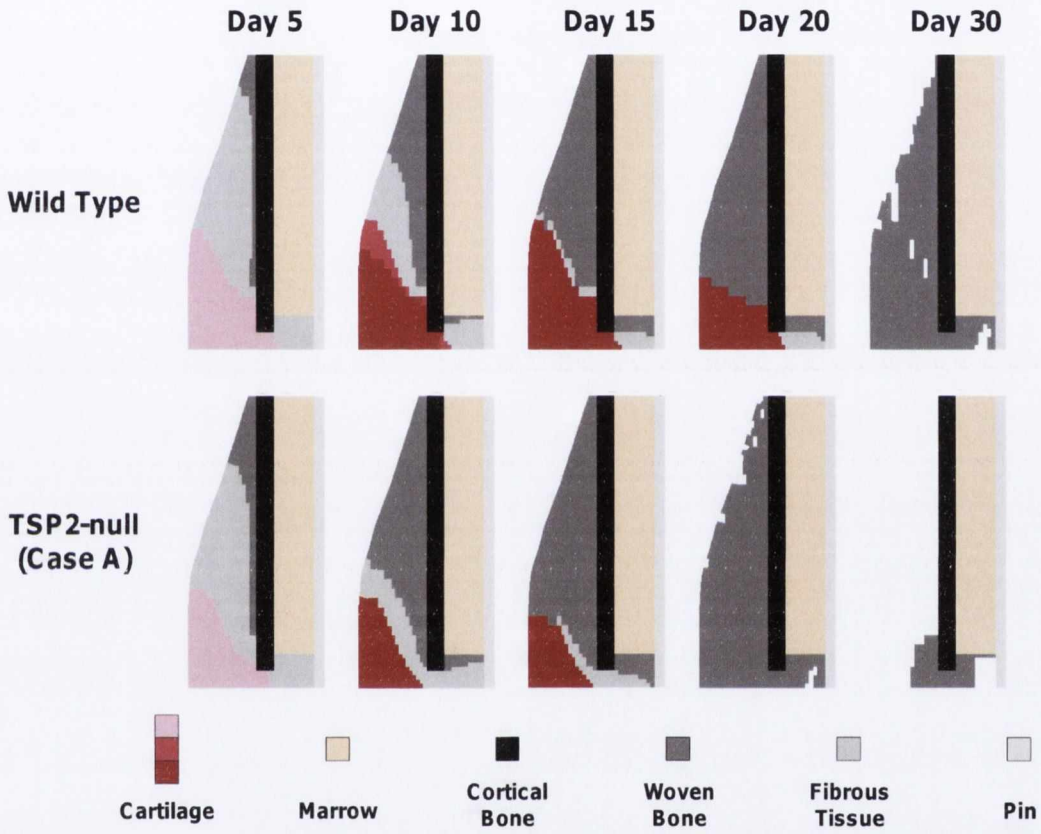

Figure 4-5. Model predictions of tissue differentiation pattern for the TSP2-null (case A) and WT case at day 5, 10, 15, 20 and 30.

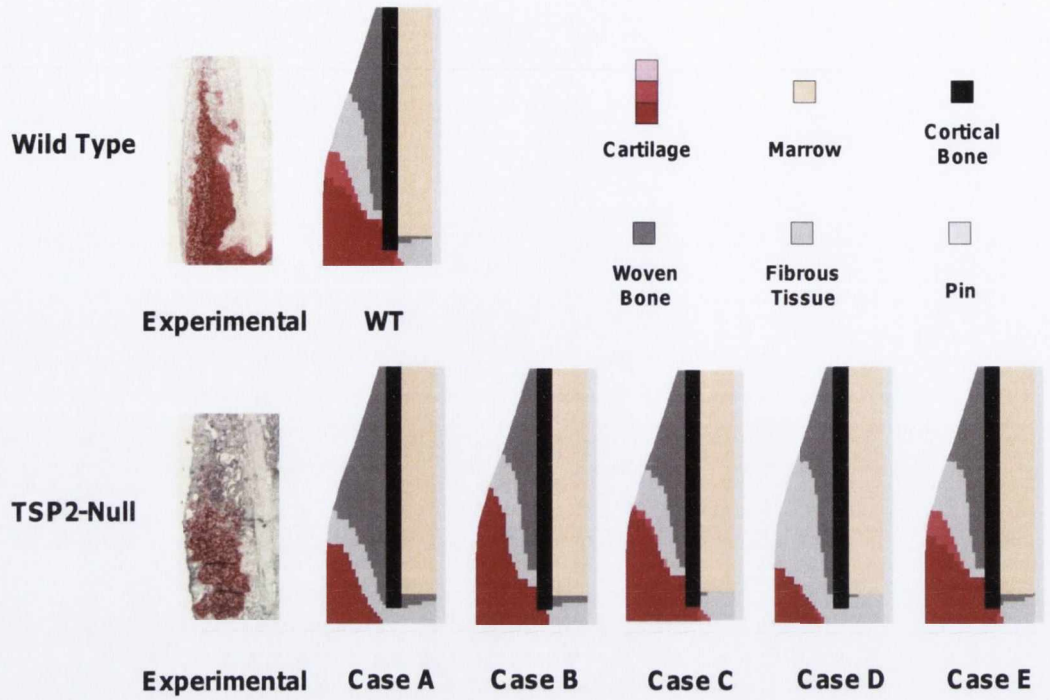

Figure 4-6. Safranin-O staining (red) 10 days post fracture for the WT and TSP2-null case is compared to model predictions for cartilage and bone formation for the WT case and the five possible TSP2-null cases.

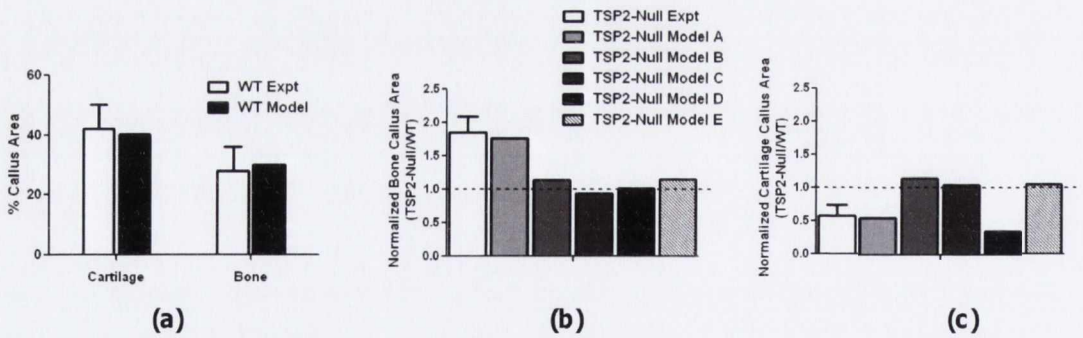

Figure 4-7. (a) Area of callus occupied by bone and cartilage formation for WT compared to predictions using the model. % Change in (b) bone and (c) cartilage formation (WT versus TSP2-null) observed experimentally (TSP2-null Expt) and predicted by the model (model TSP2-null cases A, B, C and D versus model WT case).

4.3.3 Case A: increased angiogenic rate

A significantly smaller hypoxic region was predicted to form by increasing the angiogenic progression rate in the model (Figure 4-4). Oxygen tension was

predicted to be lowest in the periosteal callus at the level of the fracture gap. Cartilage tissue formation after 10 days was predicted to decrease by approximately 45% and was confined more to the area immediately around the fracture. New bone tissue was predicted to extend further down the callus and fills more of the periosteal callus when compared to WT predictions at this time point (Figure 4-6). Quantitatively bone formation was predicted to increase by approximately 77% 10 days post-fracture (Figure 4-7 (b)). The spatial mapping coefficient for this case was 0.785.

4.3.4 Case B: increased cell proliferation

Increasing cell proliferation was predicted to increase the size of the hypoxic region within the callus (Figure 4-4). The hypoxic region extended distally and proximally in the periosteal callus and slightly more toward the endosteal side of the fracture site. Cartilage formation increased by approximately 14% and filled more of the distal periosteal callus away from the fracture site (Figure 4-6). There was little change in bone formation in comparison to WT predictions (Figure 4-7). The spatial mapping coefficient for this case was 0.645.

4.3.5 Case C: increased cell infiltration from the marrow

Increasing stem cell number originating from the marrow decreased oxygen tension slightly in the endosteal callus. There was a small increase in cartilage on the endosteal side of the fracture site but overall there were no significant changes different from the WT case (Figure 4-4). Quantitatively, cartilage and bone formation remained similar to WT predictions (Figure 4-6and Figure 4-7). The spatial mapping coefficient for this case was 0.656.

4.3.6 Case D: decreased oxygen consumption

Decreasing the oxygen consumption rate resulted in a prediction of a significantly smaller hypoxic region in the outer periosteal callus (Figure 4-4). Cartilage formation is decreased and was confined to the periosteal callus. No cartilage was predicted within the fracture gap (Figure 4-6). Bone formation remained similar to the WT case (Figure 4-7). The spatial mapping coefficient for this case was 0.599.

4.3.7 Case E: stiffened callus

A stiffened granulation tissue did not significantly change the predicted levels of oxygen availability within the callus (Figure 4-4). Cartilage and bone formation also remained similar to WT predictions (Figure 4-6and Figure 4-7). The spatial mapping coefficient for this case was 0.644.

4.4 Discussion

MSC differentiation during regenerative events such as fracture healing is known to be modulated by extrinsic mechanical signals [5, 7, 8]. Recently, *in vitro* experiments have also highlighted other environmental factors (e.g. substrate stiffness [24, 60] and oxygen availability [31, 32]) as regulators of MSC differentiation. Computational mechanobiological models have also provided support for the hypothesis that such cues can drive differentiation *in vivo* [227] (see Chapter 3). In order to decouple the relative importance of specific regulatory factors on stem cell fate an attempt was made to simulate fracture repair in different scenarios where the mechanical environment was believed to be comparable but where bone regeneration occurred *via* different pathways.

Fracture repair in TSP2-null mice utilizes greater intramembranous bone formation as opposed to the typical endochondral pathway, in spite of the fact that the mechanical environment in the early stages of repair in both animals is presumed similar. Therefore differences in MSC fate in TSP2-null mice are unlikely due to changes in the mechanical environment within the early callus of these animals. The objective of this study was to explore the role of oxygen as a regulator of stem cell fate in TSP2-null mice. The results of this study provide further support for the hypothesis that by enhancing vascularisation within the callus, deletion of TSP2 increases oxygen availability and that this in turn supports a more osteogenic phenotype.

To confirm that deletion of TSP2 leads to the development of a less hypoxic callus, immunohistochemistry was used to identify hypoxic regions within the calluses of WT and TSP2-null mice. Intense staining of pimonidazole adducts that develop with hypoxia close to the fracture site indicated a considerable hypoxic region in WT mice. In contrast, less staining occurred in TSP2-null mice, indicative of enhanced oxygenation. Similar differences in the

spatial development of hypoxia within the callus were also predicted by the model.

In order to examine potential mechanisms driving experimentally observed changes in MSC differentiation within TSP2-null mice, a model was first created to simulate tissue differentiation in the WT case. 5 days post fracture, hypoxia was predicted in the periosteal callus close to the fracture site and in the fracture gap itself but not distal to the fracture site. This is consistent with the regions of hypoxia observed with hypoxyprobe staining (Figure 4-3). 10 days post-fracture, the predicted patterns of tissue differentiation are also consistent with histological observations (Figure 4-6). Bone was predicted to fill the upper periosteal callus extending further down the periosteal cortex. Cartilage was predicted by the model in the in the lower periosteal callus and also in the fracture gap. Cartilage was not predicted adjacent to the endosteal cortex. Bone formed adjacent to the endosteum via intramembranous ossification. This is consistent with other experimental findings that the endosteum does not form cartilage even when stimulated by BMPs [66]. Quantitatively, model predictions were very close to experimental results, as evident by both the prediction of the percentage of the total callus area filled by either cartilage or bone (Figure 4-7) and the spatial predictions of phenotype (Table 4-4), further confirming the predictive capability of a tissue differentiation model regulated by substrate stiffness and oxygen availability.

Once successful prediction of fracture repair in the WT case was achieved, this model was perturbed in order to help elucidate the underlying mechanisms leading to changes in the spatial and temporal patterns of stem cell differentiation in the TSP2-null mice. Five possible impacts of disruption of the TSP2 gene and an absence of TSP2 protein were considered: firstly increasing the rate of angiogenic progression (case A), secondly increasing the rate of cell proliferation (case B), thirdly increasing stem cell source from the marrow (case C), fourthly decreasing cellular oxygen consumption (case D) and lastly increasing callus stiffness (case E). Increasing granulation tissue stiffness (case E) by a factor of 2 had very little effect upon predicted oxygen environment 5 days post fracture or tissue differentiation pattern 10 days post fracture. Only a slight increase in bone formation was predicted. Even if the absence of TSP2 made the callus twice as

stiff as normal (and there is no reason to believe that such stiffening occurs upon deletion of TSP2), the extrinsic mechanical environment can still slow the formation and progression of new blood vessels. As such, angiogenic progression was only slightly increased compared to the WT case and the oxygen environment, and hence tissue differentiation, was predicted to remain similar to that of the WT case. 64.4% of the total area was predicted to have the correct tissue type. For these reasons, the model does not provide support for the hypothesis that changes in MSC fate in TSP2-null mice are explained by an increase in callus stiffness.

Decreased cellular oxygen consumption (case D) was predicted to lead to increases in callus oxygen levels and to the development of a smaller hypoxic region at day 5. Less cartilage formation was predicted as a result of this increased oxygen availability. Predicted levels of bone formation were relatively unaffected as a blood supply still remained a prerequisite for bone formation. The blood supply at day 10 was very similar to the WT case and therefore the increased bone formation observed in the TSP2-null case could not be predicted. Only 59.9% of the total area was predicted to have the correct tissue type which is the lowest of all cases. For this reason, the model does not provide support for the hypothesis that changes in MSC fate in TSP2-null mice can be explained by a decreased cellular oxygen consumption rate.

Increasing cellular infiltration from the marrow (case C) by a factor of 2 again had very little effect upon predicted oxygen environment 5 days post fracture. In this case, there were more cells in the endosteal callus which consume more oxygen. However, these cells were in close proximity to an oxygen source (marrow cavity) which limited the effect of increased consumption on oxygen levels in the region. Overall, predictions remained similar to WT case and were not predictive of dramatic changes observed experimentally. 65.6% of the total area was predicted to have the correct tissue type which is notably lower than for case A. For these reasons, the model does not provide support for the hypothesis that changes in MSC fate in TSP2-null mice can be explained by an increase in progenitor cell availability from the bone marrow.

Implementing a higher proliferative rate in the model (case B) increased the cell density within all regions of the callus, thereby increasing overall levels

of oxygen consumption resulting in the formation of a larger hypoxic region 5 days post facture. This resulted in a prediction of greater cartilage formation, while bone formation also increased very slightly. A greater number of MSCs meant more tissue was produced and a stiffer callus. This contrasts to the decrease in cartilage formation observed experimentally. 64.5% of the total area was predicted to have the correct tissue type which is again lower than for case A. For these reasons, the model does not provide support for the hypothesis that changes in MSC fate in TSP2-null mice can be explained by an increase in cell proliferation rate.

Increasing the rate of angiogenic progression (case A) was the only simulation capable of successfully predicting the smaller hypoxic region at the fracture site, decreased cartilage formation and increased bone formation as observed experimentally. A faster rate of angiogenic progression increased oxygen levels within the callus leading to lower levels of chondrogenesis. Overall, healing in this model was predicted to progress at a faster rate than the WT case. By day 30 (Figure 4-5), remodelling of the callus was at a late stage for the TSP2-null (case A) whereas only preliminary remodelling had occurred in the same time period for the WT case. Healing was predicted to occur more substantially through intramembranous ossification and less through endochondral ossification in this simulation of fracture repair in TSP2-null mice (case A). 78.5% of the total area was predicted to have the correct tissue type which is the greatest of all cases. These model predictions mimic experimental observations and provide support for the hypothesis that changes in MSC fate in TSP2-null mice can be explained by an increase in the angiogenesis.

Changes in tissue differentiation in TSP2-null mice occurred in spite of an initially similar mechanical environment. As a result, the mechanical environment alone cannot explain these changes in differentiation pattern. Other studies investigating tissue differentiation in transgenic mice have also found differences in lineage specification within what would appear to be (initially at least) a similar mechanical environment. Colnot *et al* [232] demonstrated increased and persistent cartilage generation in the callus of MMP9 deficient mice. Kosaki *et al* [233] also showed persistent cartilage and significantly delayed repair in mice deficient in MMP13. The lack of such MMPs has been implicated to diminish angiogenic

activity (e.g. impaired vascular invasion of hypertrophic cartilage) which in turn may be responsible for the changes in tissue differentiation observed in these studies. In support of this, it has been shown that hypoxia may suppress chondrocyte hypertrophy [220]. Such studies again highlight the role of factors other than mechanics, such as oxygen supply, in the regulation of tissue differentiation. However, there are also studies that point to a more complicated relationship between oxygen availability and tissue differentiation. For example, it has been demonstrated that neither chondrogenesis nor osteogenesis was dramatically altered during early fracture healing in mice exposed to hypoxic or hyperoxic external environmental conditions [180].

The model in this study does have some limitations. Axisymmetric geometry was adopted assuming medial and lateral sides of the callus are identical. This is not the case but it was assumed that the model still provided a reasonable prediction of the mouse fracture callus environment. Only axial loading was considered, which assumed that complete lateral stability was provided by the intramedullary pin and torsional stability was provided by the applied splints. As the magnitude of the axial load is unknown, this model parameter was varied. Some progenitor cells may have restricted phenotypes during fracture healing [234]. In this model, cell differentiation capacity was not restricted which is a limitation of the study. A specific stimulus for fibrous tissue formation is not offered by this tissue differentiation model. There is however evidence that mechanical cues can promote fibrous tissue formation [5] and this warrants further investigation. It is acknowledged that other factors supplied by blood vessels, such as growth factors [235] and not just oxygenation, may be important to initiate and direct stem cell differentiation. It is possible that the cell populations present are not equivalent (ie the WT could have more inflammatory cells relative to the TSP2-null etc). This model does not account for this possibility. In a similar study of tissue differentiation during fracture healing [22], a more complex spatial mapping analysis was performed to assess the validity of each simulation prediction. It was felt that the simpler techniques adopted here were sufficient to meet the specific objectives of this study. Diffusive processes were employed to model cell proliferation/migration, angiogenesis and oxygen transport. These were simplified representations of

complex *in vivo* processes. More complex models have been implemented [11, 16, 50, 51, 144], however, I do not believe that the implementation of such models would dramatically alter model predictions and, hence, corroboration of underlying hypotheses. This study assumed biphasic material properties which accounted for certain flow dependent viscoelastic phenomena but ignored the inherent flow independent viscoelasticity of regenerating soft tissues. Finally, this study investigated five potential mechanisms individually as sole drivers for changes in MSC fate in TSP2-null mice. It is possible that two or more of these mechanisms are in fact occurring *in vivo* but the purpose of this study was to decouple the relative importance of each effect in explaining experimental observations.

In spite of these limitations, this study provided corroboration for the hypothesis that increased vascularization, and hence oxygen supply is the dominant factor which leads to a less cartilaginous callus and enhanced intramembranous bone formation in TSP2-null mice. Four other potential mechanisms were unable to predict changes in the size of the hypoxic region in the callus as well as the increased intramembranous ossification and decreased cartilage formation that is observed experimentally. This may have proven difficult, costly and even impossible to investigate with experimental techniques alone and highlights the benefits of integrating computational models with studies of genetically modified mice as has been performed herein to better understand how genetic and environmental factors interact to regulate stem cell fate *in vivo*. Future work will focus on further decoupling the roles of mechanical stimuli, oxygen availability and substrate stiffness in the regulation of MSC differentiation in other regenerative scenarios.

Chapter5: Substrate stiffness and oxygen availability as regulators of mesenchymal stem cell differentiation within a mechanically loaded bone chamber

(A modified version of this chapter is currently under review for publication)

The previous two chapters of this thesis have provided support for the hypothesis that substrate stiffness and oxygen availability regulate stem cell differentiation during tissue regeneration in two different cases of fracture repair following corroboration of the hypothesis after valid tissue distribution patterns were predicted by the tissue differentiation model.

However, a robust test of a hypothesis requires undertaking multiple experiments attempting to falsify the hypothesis. In the context of testing tissue differentiation hypotheses within an *in silico* framework, the greater the number of scenarios in which the underlying model hypothesis is subjected to attempted falsifiability, but ultimately corroborated, the stronger the hypothesis becomes. This chapter will apply test the hypothesis that substrate stiffness and oxygen availability regulate stem cell differentiation in a different regenerative event, the *in vivo* bone chamber.

5.1 Introduction

While it is well established that soluble factors, such as transforming growth factor beta (TGF-β) [115] and bone morphogenetic proteins (BMPs) [117], regulate mesenchymal stem cell (MSC) differentiation during tissue regeneration, it is becoming increasingly clear that mechanical cues also play a key role in determining the fate of such cells. Extrinsic mechanical stimuli such as tissue deformation, fluid flow and hydrostatic pressure are often implicated as regulators of tissue differentiation *in vivo* [5, 7, 8]. In addition, *in vitro* studies have identified several other environmental stimuli as key regulators of MSC differentiation. For example, the stiffness of the local matrix elasticity has been shown to be intimately linked to MSC differentiation, where an osteogenic phenotype is promoted by a stiff substrate, while adipogenesis is enhanced by exposure to a soft substrate [24, 26, 60]. Oxygen availability is another known regulator of MSC differentiation [27-32]. Both adipogenesis and osteogenesis have been shown to be diminished under low oxygen conditions [27-29], whereas chondrogenesis is promoted by hypoxia [30-32].

One of the main challenges associated with *in vivo* studies of stem cell fate is to accurately isolate and relate specific environmental stimuli to the temporal and spatial patterns of differentiation that occur during development or tissue regeneration. *In silico* studies can be used to predict the state of the local environment experienced by stem cells during complex developmental or regenerative events. As such, hypotheses for how MSC differentiation is regulated *in vivo* can be either corroborated or rejected based on the ability of *in silico* models to accurately predict spatial and temporal patterns of tissue differentiation observed experimentally [5, 7, 8, 10, 12, 16, 49, 201]. For example, fracture repair, having been studied experimentally for decades, is probably the most extensively employed regenerative event for testing hypotheses for how various environmental factors regulate MSC differentiation. Hypotheses where tissue differentiation is regulated by mechanical stimuli [5, 7, 8, 10, 23, 189], biochemical factors [51, 143, 144] or a combination of oxygen availability and substrate stiffness (Chapter 3 and Chapter 4) [227, 236] have all been at least partially corroborated by comparing model predictions of fracture repair to experimental observations. However, a robust test of a given hypothesis requires

undertaking multiple experiments attempting to falsify the hypothesis. In the context of testing such tissue differentiation hypotheses within an *in silico* framework, the greater the number of scenarios in which the underlying model hypothesis is subjected to attempted falsifiability [1], but ultimately corroborated, the stronger the hypothesis becomes [56].

It has been previously demonstrated that is it possible to simulate the temporal and spatial patterns of tissue differentiation during facture repair using a computational model where MSC differentiation is regulated by local oxygen availability and the stiffness of the surrounding substrate [227, 236]. To further test this bioregulatory theory, it is necessary to investigate if such a model could be used to successfully predict MSC differentiation during other regenerative events. The mechanically loaded bone chamber, as described by Tagil and Aspenberg [197], provides a well-defined mechanical environment and has previously been shown suitable for testing the validity of tissue differentiation hypotheses [15, 16, 53]. To enable the accurate simulation of the regenerative process inside the bone chamber, it was first sought to develop a model that could adequately describe the process of angiogenesis such that the local levels of oxygen within the bone chamber could be predicted. To this end a lattice-based model of angiogenesis capable of simulating blood vessel growth in both mechanically loaded and unloaded conditions was developed. This was coupled this with the previous theory of tissue differentiation [227] in a combined lattice and finite element based computational framework to test the hypothesis that substrate stiffness and oxygen availability regulate stem cell differentiation *in vivo* within an implanted bone chamber.

5.2 Methods

5.2.1 Bone chamber experiment

In the experimental study performed by Tagil and Aspenberg [197], a threaded titanium chamber was formed from two semi-cylinders held in place by a hexagonal closed screw cap. The bottom end of the chamber was surgically screwed into the tibia of male Sprague-Dawley rats. Two openings at the implanted end allowed tissue ingrowth into the front of the chamber (Figure 5-1 (A)). A mechanical stimulus was provided by a manually loaded piston (loaded

group). The loaded group wasn't subjected to any mechanical stimulus for the first 3 weeks of the study, followed by 6 consecutive weeks of loading. The unloaded group was not subjected to any loading for the duration of the 9 weeks. Full experimental details are available elsewhere [197].

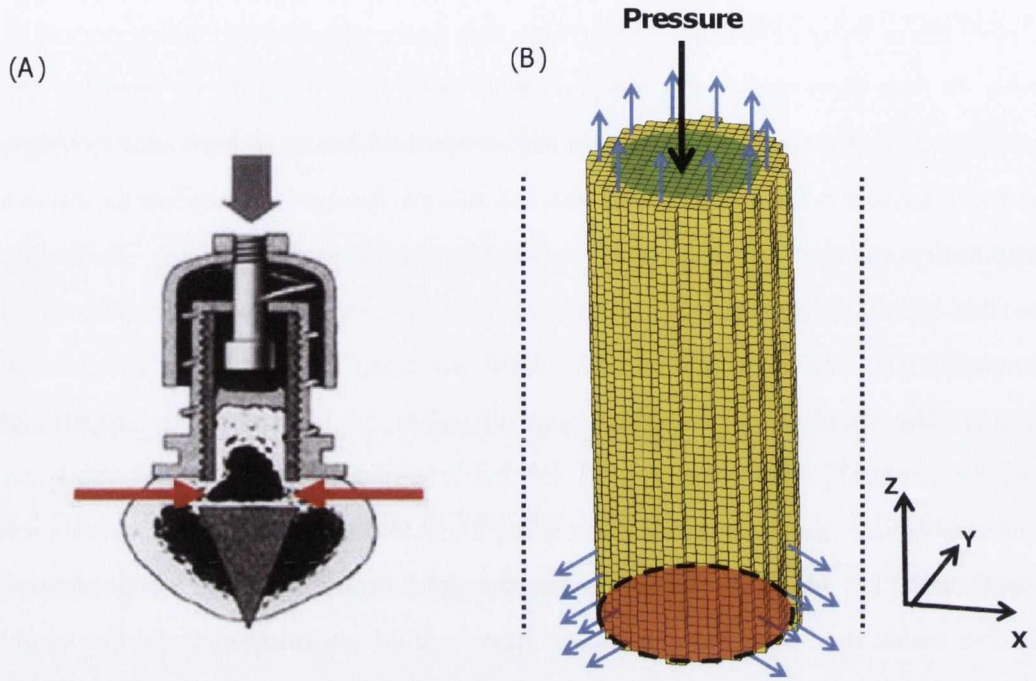

Figure 5-1. (A) Cross section of the implanted bone chamber. Red arrows point to the ingrowth openings and the grey arrow indicates the direction of applied pressure (Adapted from [198] with permission). (B) Finite element model of the implanted bone chamber. The displacement in outer chamber was constrained in the x and y directions (thin dotted line). Displacement at the base of the chamber was constrained in x, y and z directions (thicker dotted line). Free fluid flow boundary conditions were applied at the top of the chamber (to represent the gap between piston and chamber wall) and at the ingrowth holes (blue arrows).

5.2.2 Bone chamber finite element model

A 3-dimensional finite element (FE) model consisting of 14,200 finite elements was created to predict the mechanical environment within the inner bone chamber [16, 197] (Figure 5-1 (B)). Biphasic material properties were adopted (Table5-1). The applied boundary conditions (Figure 5-1 (B)) allowed fluid flow from ingrowth openings and also from the small area between the piston and the wall at the top (distal region) of the chamber, constrained radial displacements along the chamber walls and axial displacement at the chamber base. The described model was implemented into the commercial finite element software package MSC Marc (version 2008r1, MSC Software Corporation, Santa Ana, CA).

Table 5-1. Material properties

Material Property	Granulation Tissue	Fibrous Tissue	Cartilage	Marrow	Bone	Mature Bone
Young's Modulus (MPa)	0.2[a]	2[b]	10[a]	2[a]	1,000[a]	6,000[c]
Permeability (mm2)	1E-11[a]	1E-11[b]	5E-15[d]	1E-14[a]	1E-13[a]	3.7E-13[e]
Poisson's Ratio	0.167[a]	0.167[a]	0.167[a]	0.167[a]	0.3[a]	0.3[a]
Fluid Dynamic Viscosity (Ns/m2)	1E-9	1E-9	1E-9	1E-9	1E-9	1E-9
Porosity	0.8[a]	0.8[a]	0.8[a]	0.8[a]	0.8[a]	0.8[a]

a. Lacroix and Prendergast (2002) [10]; **b.** Hori and Lewis (1982) [214]; **c.** Claes and Heigele (1999) [7]; **d.** Armstrong and Mow (1982) [215]; **e.** Ochoa and Hillberry (1992) [216]; **f.** Cowin 1999 [217]; **g.** Schaffler and Burr (1988) [218]

5.2.3 Cell migration and proliferation

Models of cell migration and proliferation were implemented using a lattice based approach. Within this approach, each finite element was discretised into a 3 dimensional lattice consisting of 1000 lattice points (10 points in each dimension) (Figure 5-2). Each lattice point represented a potential position for a cell and its immediate extracellular matrix. All finite elements were cubic with side length of 0.1mm giving each lattice point a spacing of 10 μm. Cell migration was implemented as a stochastic process by filling the allotted new cell position and vacating the previously filled position using random walk theory [11, 139]. Each cell attempted to migrate randomly into one of the adjoining lattice positions. Should the adjoining cell position be occupied, the cell remains in its original position. Cell proliferation was implemented in a similar fashion by filling the allotted new cell position (with a "daughter" cell) while the previously filled position remained filled (with the "parent" cell). Migration/proliferation was limited only if the adjoining cell position is occupied. Phenotype specific migration (M) and proliferation (P) rates (Table 5-2) determined the number of attempted migration or proliferation actions per 12h iteration (see Section 0

Tissue differentiation for more information on iterative procedure). 30% of cells positions in the ingrowth holes where initially filled with MSCs [16]. 5% of all other cell positions up to the height of the ingrowth holes were also randomly filled with MSCs. MSCs could only differentiate once the minimum age for differentiation (Age_{diff}) was reached [16] (Table5-3).

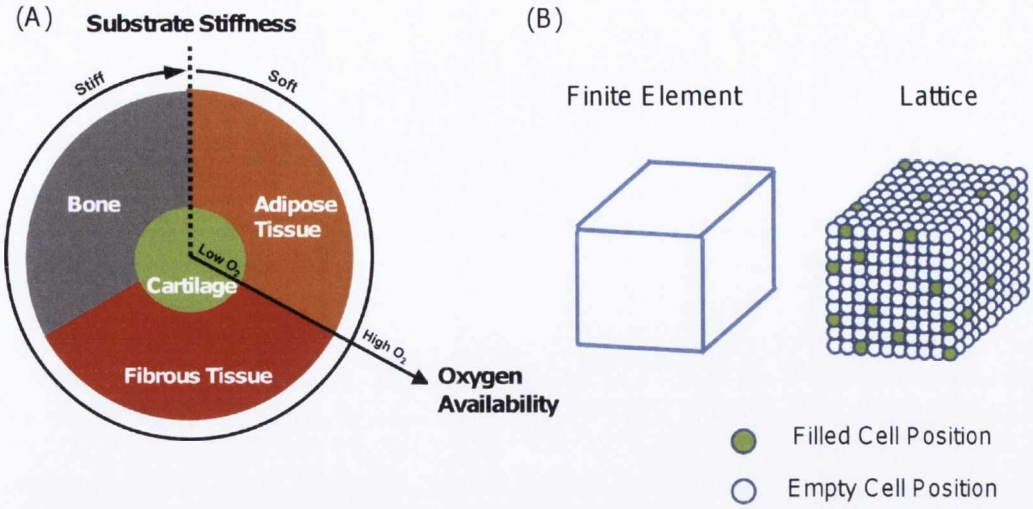

Figure 5-2. (A) Tissue differentiation regulated by substrate stiffness and oxygen availability. The oxygen availability axis extends radially from the centre of the circle, low oxygen in the centre of the circle increasing towards the periphery. The substrate stiffness axis extends circumferentially in a clockwise direction from the right side of the dotted line at the top of the circle. The presence of a blood supply is also a prerequisite for formation of bone and marrow. (B) A 3 dimensional finite element with corresponding lattice. Each lattice point represents a potential location for a cell and its immediate extracellular matrix.

Table 5-2 Cell model parameters

Model Parameter	Fibroblasts	Chondrocytes	Adipocytes	Osteoblasts	MSCs
Proliferation Rate $(1/2day)^{-1}$	0.27 [a]	0.1 [a]	0.2	0.15 [a]	0.3 [a]
Migration Rate (μm/h)	26.6 [b]	N/A	26.6	N/A	26.6 [b]
Degradation Rate $(1/2day)^{-1}$	0.025 [a]	0.05 [a]	0.05	0.08 [a]	0.025 [a]
Differentiation Rate $(1/2day)^{-1}$	N/A	N/A	N/A	N/A	0.15 [a]

a. Isaksson et al (2008) [237] ; **b.** Appeddu and Shur (1994) [238].

Table 5-3 Tissue differentiation model parameters

Model Parameter	Symbol	Source	Unit	Value
Strain Threshold for Angiogenic Inhibition	ε^{angio}	[227]	%	6
Blood Vessel Growth Rate	V	Estimated	$\mu m(1/2day)^{-1}$	40
Minimum Length Branching	L_{min}	[50]	μm	100
Maximum Length (without) Branching	L_{max}	[239]	μm	300
Minimum Age for Differentiation	Age_{diff}	[16]	days	6
Oxygen Diffusion Coefficient	G	[212, 227]	m^2/s	2.2E-09
Oxygen Consumption Rate	Q	[213, 227]	fmol/cell/h	98
Initial Oxygen Tension	$O_2^{initial}$	[179, 227]	mmHg	74.1
Oxygen Tension Limit for Cartilage	$O_2^{cartilage}$	[27, 28, 227]	%	3

5.2.4 Angiogenesis and oxygen transport

Angiogenesis was also modelled using a lattice based approach, similar to Checa and Prendergast (2009) [50], where capillaries were modelled as a consecutive sequence of lattice points filled with endothelial cells (EC) [240]. Vessel growth occurred at a constant rate (V) (Table 5-3) and could occur in either a random direction or the previous direction of growth with equal probability. EC death occurred where the local octahedral shear strain exceeded a threshold value (ε^{angio}) (Table 5-3). Capillaries were permitted to branch and form new vessels, the probability of which occurring was a function of the length of the vessel. L_{min} represents the minimum length for a sprout to branch, while L_{max} represents the maximum length for a non-branching sprout (Table 5-3). Should two capillaries meet, anastmosis (fusion) occurred. Cell position in the ingrowth holes were initially filled with 30% ECs as the initial source of blood vessels. Oxygen transport was simulated as a diffusive process, the boundary conditions of which were dependent upon the state of the blood supply [227, 236]. Similar to studies

of other tissue regenerative events [227, 236] and consistent with oxygen tension measurements inside a similar bone chamber experiment [194], oxygen availability was initially assumed to be high in the chamber. As the simulation progressed, oxygen (O_2) diffused from blood vessels and was consumed at a rate calculated as the product of a cellular consumption rate (Q) and cell density (n) (see Equation 5.1 below) (parameters used in the model of oxygen transport are available in Table 5-3). Cell density was determined from the number of filled lattice points at a given location.

$$\frac{dO_2}{dt} = G\nabla^2 O_2 - Qn^{\max} n \qquad \text{(Equation 5.1)}$$

5.2.5 Tissue differentiation

In this study, the process of MSC differentiation was regulated by substrate stiffness and oxygen availability [227] (Figure 5-2 (A)). In brief, this theory proposed that osteogenesis and adipogenesis were inhibited in regions of hypoxia, while chondrogenesis was promoted is such a low oxygen environment (defined as regions in which the local oxygen drops below a threshold value ($O_2^{cartilage}$) (Table 5-3). Where a sufficient oxygen supply existed, differentiation was regulated by the stiffness of the local substrate. A high substrate stiffness promoted osteogenesis, whereas low substrate stiffness promoted adipogenesis (It was further assumed that adipogenesis would further support the establishment of bone marrow). Fibrogenesis was predicted in regions of the chamber where none of these conditions were upheld. The substrate stiffness stimulus at any point in the model was dependent upon the phenotype of surrounding lattice points. Engler *et al* refer to MSC differentiation regulated by the ''elasticity of the microenvironment'' of the cell [24]. For example, the stiffness of osteoid matrix produced by osteoblasts is approximately 30 kPa, however, the stiffness of woven bone itself is orders of magnitude higher (in the order of GPa). In this tissue differentiation model, osteogenesis occurs when stem cells are adjacent to newly formed bone and hence in contact with osteoid as a substrate (and similarly for adipogenesis). In this implementation, specific threshold values of stiffness are therefore not required.

Tissue differentiation within the bone chamber was simulated via an iterative procedure (Figure 5-3). Within each iteration, a prediction of mechanical stimuli, cell phenotypes and densities, blood supply and oxygen availability is generated in order to enable the local phenotype predictions to be determined. Each iteration was 12 hours. In the computational model, a soft substrate stimulus was assumed along the base of the chamber which sits in the host marrow. The chamber walls were assumed to provide a stiff stimulus. Differentiated adipose tissue was also assumed to provide a soft substrate stimulus for further adipogenesis, while extracellular osteoid from differentiated osteoblasts was assumed to provide a stiff substrate stimulus for further osteogenesis. The process of endochondral ossification occurred in the model when a chondrocyte experienced a stiff (osteogenic) stimulus and the region was invaded by blood vessels. These (would-be hypertrophic) chondrocytes were removed through apoptosis to be replaced by the osteoblasts of the oncoming bone front. Fibroblasts subjected to an osteogenic stimulus also underwent apoptosis and new bone replaced the existing fibrous tissue (a process similar to intramembranous ossification where ossification initiates on a fibrous connective tissue membrane). Apoptosis occurred at a rate D which determined the proportion of existing cells undergoing apoptosis in that particular iteration (Table 5-2). Different cell types synthesizing matrix of drastically different properties could exist within a single element, therefore a rule of mixtures was implemented to determine the properties of each element [140]. To prevent unphysiologically rapid changes in material properties, values were averaged over the last 10 iterations [10]. Also, should a finite element become dominated by one cell type (defined as at least 50% of the cell positions in an element which has a minimum of 100 cell positions occupied), other cell types within the element were also assumed to undergo apoptosis.

5.2.6 Simulations

As per experimental protocol [197], tissue differentiation predictions in loaded and unloaded conditions were compared. Loading was simulated in the FE model via the application of a pressure of 2MPa [16] on the top surface of the ingrowing tissues. The pressure was applied via a linear ramp from 0 to 2 MPa in 0.3s followed by holding at 2 MPa for a further 2.7s [16]. The time-course of both groups was computed in a series of 12 hour iterations (Figure 5-3). The bone

chamber was initially assumed to be filled with granulation tissue. In each iteration, the progression of angiogenesis was simulated based on the prevailing local biophysical stimulus. Cells migrated, proliferated and depending on the calculated oxygen availability and substrate stiffness, the MSCs differentiated into different cell phenotypes. At the end of each iteration, the material properties of the bone chamber FE model were updated (Figure 5-3). The time-dependent tissue differentiation process inside the bone chamber was simulated for 9 weeks, following Tagil and Aspenberg's experimental protocol [197].

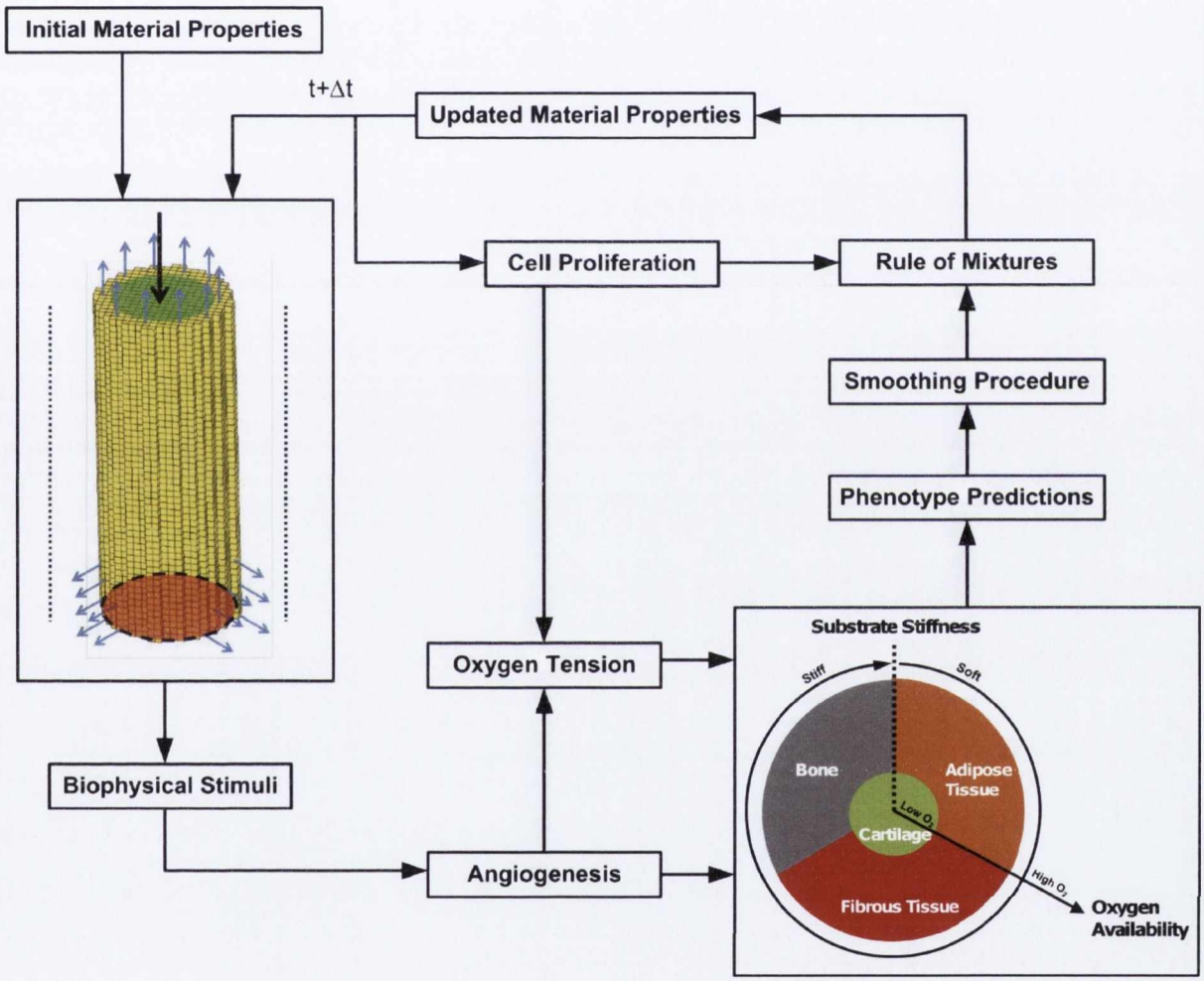

Figure 5-3. Iterative procedure for generating temporal and spatial predictions of tissue differentiation.

The authors of the bone chamber experiments reported that a dichotomous result was observed histologically for the loaded case [197]. In approximately half the loaded cases, cartilage was not observed. Additional simulations were performed with altered model parameters to investigate several possible explanations for such a dichotomy. It is possible that MSC density may be

different in the marrow of different animals. It is also possible that as pressure was applied manually through the experiments, variability in the magnitude of this stimulus may have occurred. As a result, simulations were performed with altered MSC density (20%, 30%, 50%) and varied magnitude of applied pressure at the top of the cortex (1MPa, 2MPa, 3MPa) to investigate such potential mechanisms. It was assumed in the experiment that the ingrowth holes lay fully in the marrow cavity, but it may be possible that the upper cortex restricts MSC access to the chamber (that normally occurs via the ingrowth holes). Therefore, a simulation with partially blocked ingrowth holes was also performed (where the upper 1/3 of ingrowth holes were blocked to simulate potential inconsistent implant positioning during surgery).

5.3 Results

Predominately fibroblastic differentiation was predicted within the bone chamber during the first three weeks of the study when no external mechanical loading was applied (Figure 5-4 and Figure 5-5). Osteogenic and adipogenic differentiation was initially predicted to be confined to areas immediately adjacent to the chamber holes, with increased adipogenesis by week 3. Early osteogenic differentiation was predicted to occur primarily along the chamber walls, firstly in the regions around the ingrowth holes at the front of the chamber and then progressing toward the back region of the chamber. Adipogenesis were predicted more homogeneously along the proximal (bottom) region of the chamber but again began at the front of the chamber progressing towards the back (Figure 5-6). Blood vessels progressed in a random fashion from the ingrowth holes to fill the majority of the proximal region of the chamber by the end of week 3, with the exception being a region at the back of the chamber which remained unserved by vessels. As no mechanical loading was applied for the first three weeks, similar predictions were made for the loaded and unloaded cases during this time period.

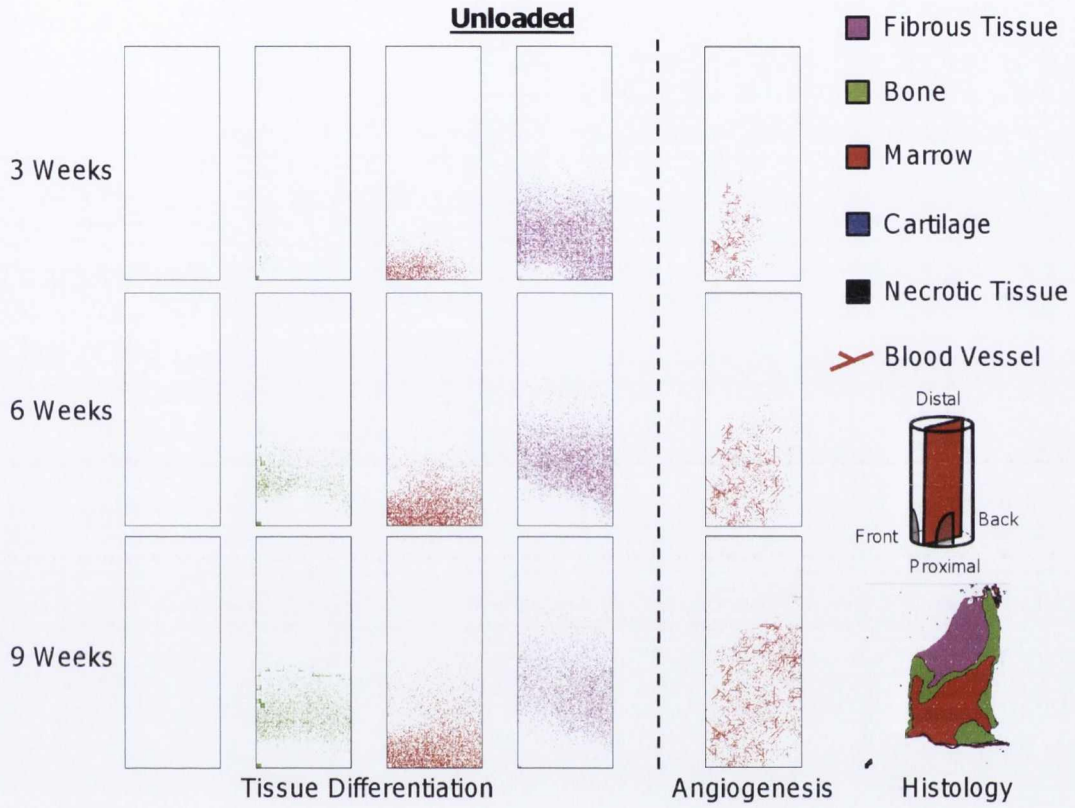

Figure 5-4. Unloaded case tissue differentiation predictions for 3, 6 and 9 week time points (side elevation view). Results are presented as a cross section from front to back of chamber (see red slice of schematic on right of figure). Bottom right: simplified histology results from experimental study [197] (Adapted from [16] with permission).

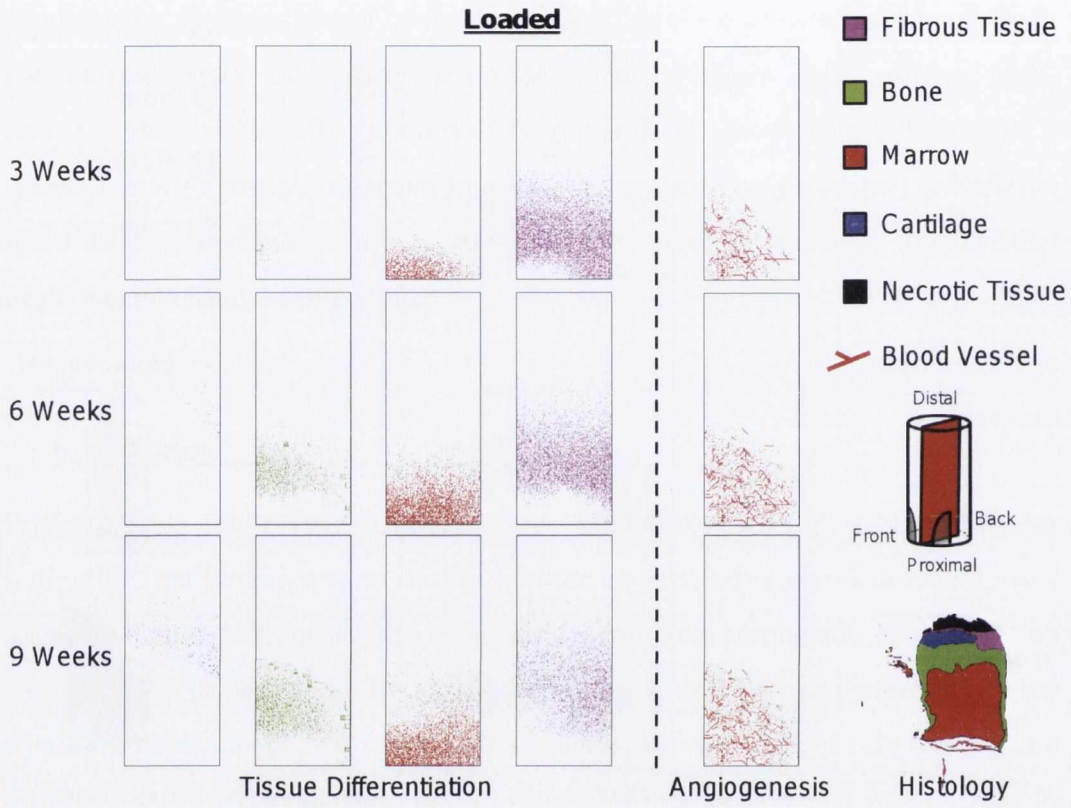

Figure 5-5. Loaded case tissue differentiation predictions for 3, 6 and 9 week time points (side elevation view). Results are presented as a cross section from front to back of chamber (see red slice of schematic on right of figure). Bottom right: simplified histology results from experimental study [197] (Adapted from [16] with permission).

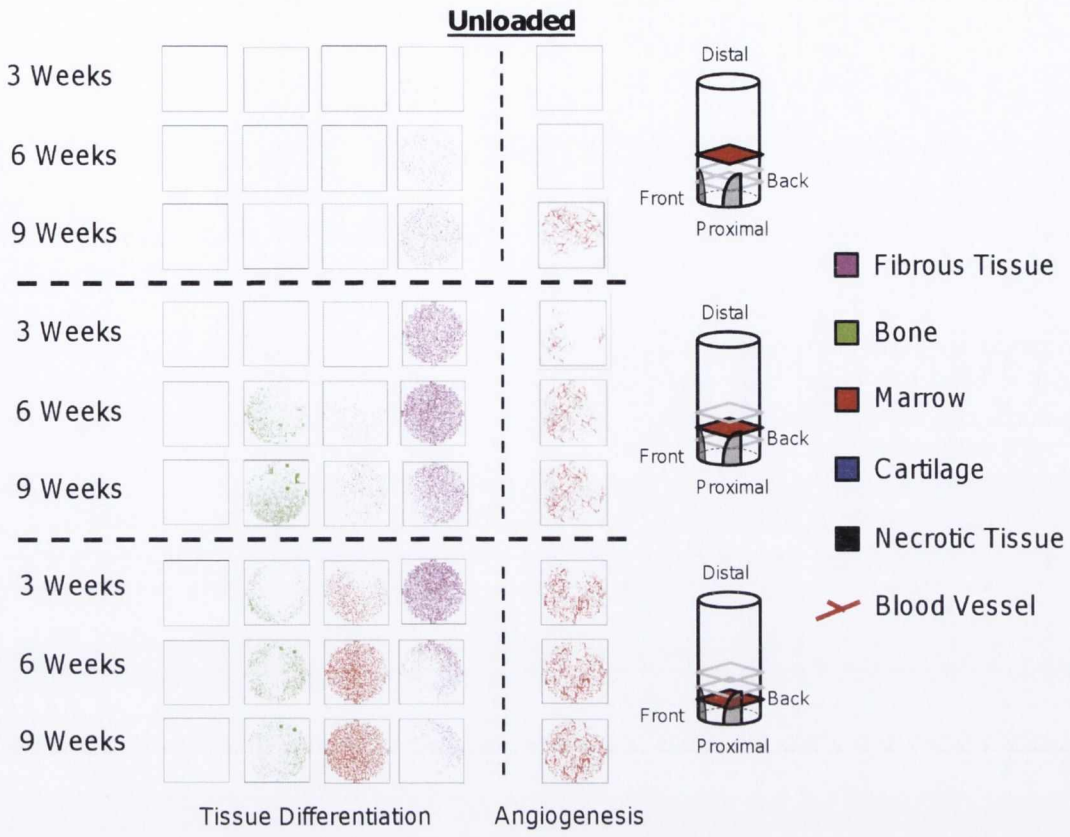

Figure 5-6. Unloaded case tissue differentiation predictions for 3, 6 and 9 week time points (plan view). Results are presented for heights of 2.5mm, 1.5mm (middle) and 2.5mm (bottom) (see red slice of schematics on right of figure).

From week 3 to week 6, new osteoblasts and adipocytes were predicted to occupy a larger part of the unloaded bone chamber (Figure 5-4 and Figure 5-6). Osteoblasts were predicted to spread radially inwards from the walls towards the centre of the chamber (Figure 5-5 and Figure 5-7). Osteoblastic differentiation was also predicted in more distal regions of the chamber, but bone was still more prominent closer to the ingrowth holes than the back of the chamber (Figure 5-4 and Figure 5-6). Homogenous adipogenic differentiation was predicted in the proximal region of the chamber. An increase in fibroblastic differentiation was predicted in the distal region of the chamber, with apoptosis of fibroblasts predicted in the proximal region of the chamber. All of this was similar for both loaded and unloaded cases. A small number of MSCs were predicted to differentiate into chondrocytes in the upper (distal) regions of the chamber for the loaded case. Such chondrogenesis was not predicted in the unloaded case. In the unloaded case, blood vessels were predicted to fill the remaining empty regions at the back of the chamber and to also progress further up the chamber. In the loaded

case, this progression into the back and distal regions of the chamber was predicted to be much slower.

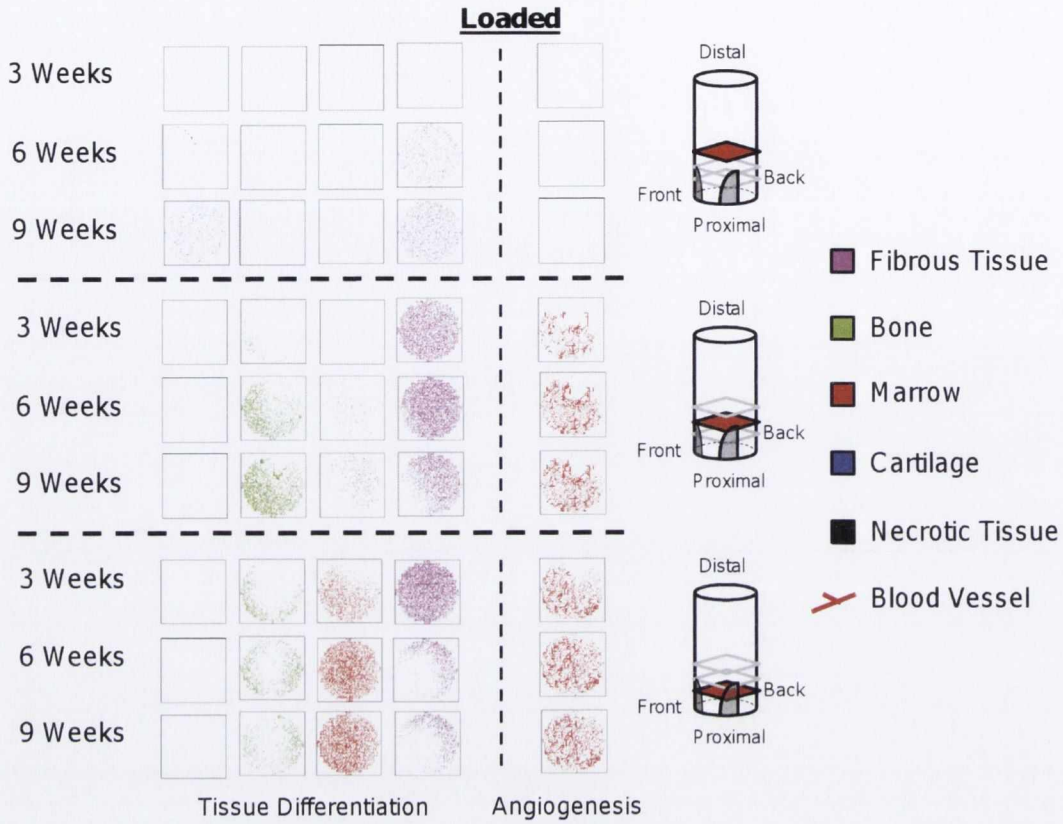

Figure 5-7. Loaded case tissue differentiation predictions for 3, 6 and 9 week time points (plan view). Results are presented for heights of 2.5mm, 1.5mm (middle) and 2.5mm (bottom) (see red slice of schematics on right of figure).

At the end of the 9 week simulated period, osteoblasts were predicted to bridge across the centre of the chamber. In the lower chamber osteoblasts primarily existed along the chamber walls (Figure 5-4 and Figure 5-5). At the end of the 9 week simulation, the total amounts of each tissue type within the chamber were computed (Figure 5-8). There was slightly more bone predicted to form in the unloaded case (32.4% versus 27.6%), with osteoblastic differentiation predicted further up the chamber also. By week 9, adipogenesis was predicted almost homogeneously across the proximal region of the chamber, with new marrow tissue making up 34.8% and 33.2% of the neo-tissue within the chamber for the unloaded and loaded cases respectively (Figure 5-8 and Table 5-4). Fibroblasts were predicted to persist in the distal regions of the chamber, but underwent apoptosis and were replaced by osteoblasts and adipocytes in lower regions of the chamber for both loaded and unloaded cases (Figure 5-6 and Figure

5-7). Blood vessels approached the distal region in the loaded case, but in the unloaded case extend further up into the chamber. Greater levels of chondrogenesis were predicted in the distal regions of the loaded chamber, with cartilage making up approx 2.5% of total tissue content by at week 9 (Figure 5-8 and Table 5-4). No cartilage was predicted in the unloaded case.

Table 5-4. Tissue fractions from experimental analysis (14; 196) and model predictions

	Bone (%)	Cartilage (%)	Marrow (%)	Fibrous Tissue (%)	Necrotic Tissue (%)
Experiment					
Unloaded	31.0 ± 11.7	0.0 ± 0.0	38.6 ± 5.7	30.4 ± 9.8	0.0 ± 0.0
Loaded	23.5 ± 12.7	3.3 ± 3.3	30.6 ± 23.1	35.0 ± 32.7	7.4 ± 5.3
Model Predictions					
Unloaded	32.4	0.0	34.8	32.8	0.0
Loaded	27.6	2.5	33.2	36.7	0.0

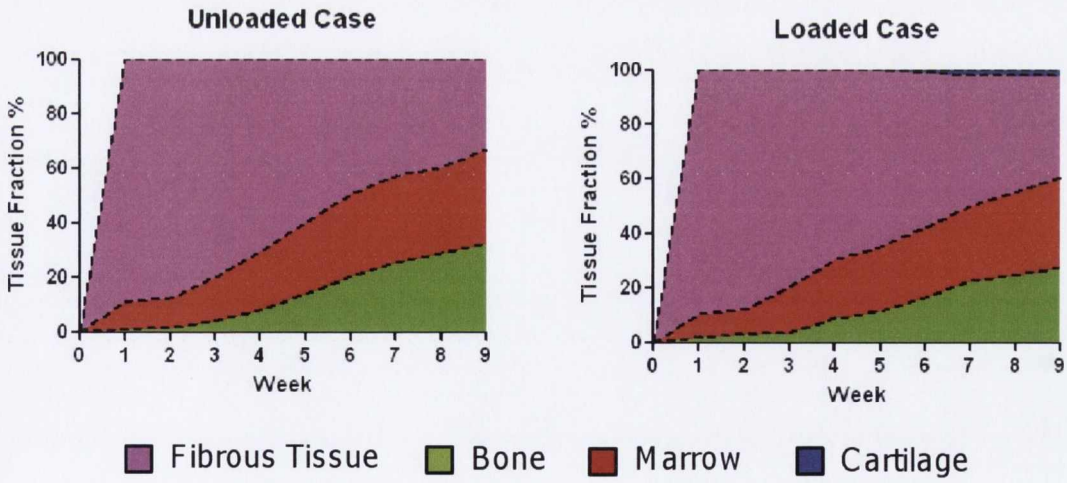

Figure 5-8. Temporal tissue phenotype fractions for unloaded and loaded cases.

The effect of parameter variations theorised as possible explanations for the dichotomous result observed experimentally [16, 197] in the loaded case is summarised here (data not shown). Decreasing the magnitude of applied pressure to 1MPa from 2MPa for the loaded case resulted in very little change in

differentiation because a similar sized region of high strain suppressing angiogenesis was still predicted. Increasing the magnitude from 2MPa to 3MPa led to slightly more blood vessel inhibition in the distal regions of the chamber and hence a small increase in the number of chondrocytes and a small decrease in the number of osteoblasts predicted. Altered implant positioning resulted in all tissues forming lower down in the chamber. Partially blocking the holes in the proximal end of the chamber was predicted to increase adipogenic differentiation and reduce fibrogenic differentiation. Chondrogenic differentiation was still predicted in a similar quantity to the baseline simulation. Increased initial MSC density (from 30% to 50%) results in increased chondrogenic differentiation as a result of higher cellular oxygen consumption. Other tissue type predictions remained similar in terms of both positioning and tissue fraction percentage. Decreased initial MSC density (from 30% to 20%) predicts delayed and decreased chondrogenic differentiation with all other tissue fractions remaining similar. Also, the majority of tissue formation occurred more towards the proximal end of the chamber.

5.4 Discussion

In vitro studies have identified biochemical cues [57, 90], extrinsic mechanical signals such as pressure and deformation [84, 87], as well as substrate stiffness [24, 60] and oxygen availability [27-32] as regulators of MSC differentiation. Identifying relationships between such stimuli and temporal and spatial patterns of tissue differentiation using *in vivo* experiment alone is complex, expensive and often impractical. *In silico* studies provide a mechanism for testing a given tissue differentiation hypotheses by means of 'trial and error' [4], whereby a given hypothesis is either corroborated or rejected based on its ability to successfully predict patterns of tissue differentiation during regenerative events. The implanted bone chamber provides a suitable regenerative event for attempted corroboration of tissue differentiation theories using such *in silico* approaches. This study employed a computational framework in which tissue differentiation is regulated by substrate stiffness and oxygen availability [227], in an attempt to predict MSC fate *in vivo* within an implanted bone chamber [197]. Predictions from the model provide corroboration for the hypothesis that tissue differentiation during such regenerative events is indeed regulated by substrate stiffness and oxygen

availability, providing further support for the key role that such stimuli play in regulating MSC fate *in vivo*.

During the early stages of regeneration, the model predicted only small amounts of osteogenic differentiation (Figure 5-4 and Figure 5-5). Osteogenesis was predicted predominantly along the chamber walls, which provide the required stiff substrate for differentiation to proceed along this pathway. Such osteogenic differentiation along the chamber walls is also observed histologically [16, 197]. Higher levels of adipogenesis than osteogenesis were predicted in the early stages of the simulation, with expansion of the existing host marrow into the proximal region of the chamber. As both adipogenesis and osteogenesis were assumed to depend on the existence of a blood supply, differentiation of MSCs towards adipocytes and osteocytes was initially predicted in greater numbers in regions adjacent to the ingrowth holes, advancing towards the back regions of the chamber as vessels progressed. A large number of fibroblasts were predicted in the chamber during the early stages of the study as the level of oxygen did not drop sufficiently to provide the hypoxic conditions necessary for chondrogenesis. (These predictions were similar for both loaded and unloaded cases as loading only begins 3 weeks post-implantation. The stochastic nature of cell migration and proliferation as well as blood vessel growth directionality results in every simulation being slightly different).

Six weeks post-implantation, a relatively small number of chondrocytes were predicted above the bony layer for the loaded case. This was due to mechanical loading causing high strains in the distal part of the chamber, which delays or prevents blood vessel progression into this region of the chamber (Figure 5-5 and Figure 5-7). The presence of large numbers of cells in a region not served by blood vessels resulted in the development of hypoxic conditions locally within the bone chamber, which in turn promoted chondrogenesis. In the unloaded case, no such mechanical inhibition of blood vessel growth occurred and hence blood vessels filled more of the distal region of the chamber (Figure 5-4 and Figure 5-6). Such vessels provided enough oxygen to prevent the development of a hypoxic region and hence chondrogenic differentiation did not occur.

After the full nine week term, chondrogenic differentiation increased in the loaded case due to continued blood vessel disruption (and hence the development of larger hypoxic regions) caused by the excessive strains in the distal regions of the chamber (Figure 5-5 and Figure 5-7). There was again no vessel disruption in the unloaded case, allowing vessels to progress further up the chamber and thereby preventing the development of hypoxic regions and subsequent chondrogenesis (Figure 5-4 and Figure 5-6). This is in agreement with experimental observations of cartilage formation in the loaded case and none in the unloaded case [197]. The cartilage in the loaded case was also predicted to form in the correct spatial location above the bone layer, and in similar amounts to that observed experimentally (3.3% observed experimentally compared to 2.5% predicted by the model, see Table 5-4). Less osteogenic differentiation was predicted in the loaded case due to inhibition of blood vessel growth. This is also in agreement with experimental observations (Figure 5-8 and Table 5-4). Experimentally there was less marrow formation observed in the loaded case, however the simulations only predicted a small difference. Fibroblastic differentiation was predicted in the distal region of the chamber above a layer of bone, which again agrees with histology for both the loaded and unloaded cases.

Partial corroboration for an alternative tissue differentiation model where MSC fate is regulated by octahedral shear strain and relative fluid velocity has previously been provided by attempting to simulate the time course of tissue formation within the same implanted bone chamber modelled in this study [16]. In that case, simulations were not completely predictive of the unloaded experiment. For example, a chamber filled with bone was predicted after 9 weeks, with prediction of little or no fibrous tissue formation. This occurred because fibrous tissue formation could only occur under the direct application of load in that model. The tissue differentiation model in question [8] does not include a specific stimulus for adipogenesis and therefore does not enable prediction of experimentally observed adipose cells in the marrow cavity under either loading conditions. In contrast, the model governed by substrate stiffness and oxygen availability includes adipogenesis and fibrous tissue formation without the direct influence of mechanical loading, and was thus able to predict fibrous tissue

formation above the bony region as well as adipose cells beneath the bony bridge (Figure 5-4 and Figure 5-6).

The mechano-regulation model based on strain and fluid velocity was predictive of the spatial and temporal patterns of cartilage formation in the loaded case [16], which was also successfully predicted by the model regulated by substrate stiffness and oxygen availability. However, differences do occur between the model predictions in terms of the primary method of bone formation within the loaded chambers. Both models predicted bone formation in the unloaded phase by intramembranous ossification. Differences were predicted upon the application of loading after 3 weeks. The model in this study predicts endothelial cell necrosis upon loading, leading to a decrease in progression of bone up the chamber. Osteogenesis was predicted to slow but with continued formation via intramembranous ossification with only small amounts of endochondral bone formation. This is contrary to the previous model [8] (regulated by shear strain and fluid velocity) which predicted apoptosis of the intramembranous bone upon load application. New bone then formed primarily via the endochondral ossification process (differentiation of MSCs into chondrocytes before they are replaced with osteoblasts) rather than through the intramembranous route observed in this study. Without extra experimental data on spatial tissue distributions from earlier time points, it is impossible to distinguish which model is more accurate in its predictions of the mechanisms of bone formation *in vivo*. The fact that neither underlying hypothesis for MSC differentiation can be fully falsified by simulating this particular experiment points to the need for further work to elucidate the specific roles of particular environmental cues in regulating stem cell fate *in vivo*.

There are some limitations associated with the model. Firstly, a dichotomy was observed in the experimental results, with cartilage only being observed in approximately half the cases where mechanical loading was applied, but not being observed in the other cases. Changes in MSC density, loading magnitude or partially blocked ingrowth holes did not lead to a simulation prediction of no cartilage for the loaded case. However, decreased initial MSC density predicted delayed and decreased chondrogenic differentiation, suggesting that this may play a role in explaining the dichotomous result observed experimentally. This

dichotomy in the loaded case may also be at least partially explained by variable mechanosensitivity among animals. This was posed as a possible explanation by Khayyeri *et al* following a study which could predict aspects of both sides of the dichotomy by varying model parameters referring to mechanosensitivity [15]. There are also some other limitations associated with the present study. The model of angiogenesis employed in this study does not consider chemotaxis which can bias blood vessel growth directionality towards a source of VEGF for example [46]. Chemotaxis has been implemented in similar lattice models of angiogenesis [50, 141] with blood vessel directionality biased towards VEGF which was assumed to be secreted by hypertrophic chondrocytes. It is unlikely that such an addition would significantly influence simulation predictions as chondrocytes are small in number and are predicted in regions where blood vessels are likely to be inhibited by high shear strains. Blood vessel growth rate was assumed constant and independent of strain which is another simplification of the model of angiogenesis. The model contains many parameters obtained from the literature and includes some simplifications of complex biological processes such as cellular migration and proliferation which may result in deviations in model predictions from experimental observations. All cell sizes are assumed to be exactly that of a lattice position which is not representative of the biological reality. Furthermore, the generation of necrotic tissue is not considered in the model but is observed experimentally. Finally, the process of bone resorption is not accounted for in the model.

In conclusion, previous studies have postulated a direct role for mechanics in regulating MSC differentiation during tissue regeneration. This work points to the indirect role that mechanics may play in regulating MSC fate by inhibiting (mechano-regulated) blood vessel progression and hence disrupting oxygen availability within regenerating tissues. The study therefore provides further support for the hypothesis that substrate stiffness and oxygen availability regulate stem cell differentiation *in vivo*. This tissue differentiation hypothesis has therefore been further corroborated by simulating multiple different regenerative events [227, 236] thereby strengthening its validity.

Chapter6: A mechanobiological model of endothelial cell migration and proliferation

(A modified version of this chapter is currently under review for publication)

Up to this point, this thesis has examined the hypothesis that substrate stiffness and oxygen availability regulated stem cell differentiation in three regenerative scenarios (two cases of fracture repair and one case of an implanted bone chamber). At the heart of this hypothesis is that mechanical stimuli act indirectly, rather than directly, to influence differentiation. One important mechanism of this indirect influence is the mechano-regulation of angiogenesis and endothelial cell behaviour.

Applied mechanical strain has been demonstrated to influence multiple aspects of endothelial cell (EC) physiology *in vitro*. This next chapter employs a novel lattice based approach to decouple how aspects of endothelial cell behaviour altered by mechanical stimuli may explain the results of an *in vitro* study which found significant changes in EC migration, proliferation rates and directionality.

6.1 Introduction

The formation of neovasculature is central to many instances of tissue regeneration. For example, successful wound healing has been shown to be dependent upon adequate angiogenesis [241], while bone repair is delayed or fails altogether upon an ischemic insult [177]. Infiltration of vasculature is also essential for successful integration of engineered tissues [242]. Blood vessels supply nutrients, growth factors (e.g. BMP-2) and oxygen to the site of regeneration [235], all of which are essential for a tissue to successfully regenerate and/or integrate. There is also a strong direct influence of angiogenesis on tissue differentiation. For example, the presence of blood vessels is a prerequisite for bone formation [46]. Blood vessels can also indirectly influence tissue differentiation by determining the local oxygen environment [2, 171, 236]. It has been demonstrated in vitro that low oxygen availability favours cartilage formation whereas high oxygen availability (typically supplied by blood vessels) is more favourable to osteogenesis and bone formation [27, 28, 30-32, 220]. In spite of the importance and influence of vasculature in these areas and others, how angiogenesis is regulated by local environmental cues is still not fully understood.

To date, it has been established that angiogenesis is regulated by growth factors such as vascular endothelial growth factor (VEGF) [46, 243, 244]. Recent data also suggests that mechanical signals can play a role in regulating angiogenesis and endothelial cell (EC) behaviour [41-45]. For example, it has been demonstrated that the application of mechanical stretch can regulate neovessel sprouting, orientation and elongation, affecting both characteristics of neovessel growth and network morphometry [43]. Mechanical cues have also been shown to alter vascular development within contracting wounds, where tissue tension directed translocation of the vasculature in the repairing tissue [44]. *In vitro* studies suggest that such changes in angiogenesis could be mediated, at least in part, by alterations in EC behaviour in response to mechanical cues [42-44]. Elucidating the exact role that mechanics might play in regulating angiogenesis using experimentation alone is complicated by the fact that biophysical cues could impact upon multiple aspects of cellular behaviour such as the rate and/or directionality of EC migration as well as proliferation. Hence

novel methods are required to probe how mechanics might impact upon different aspects of EC physiology.

Coupling *in silico* studies with experimental observations offers an efficient and often effective means of exploring cellular mechanobiology [4, 10, 142, 143, 227]. Such computational models have recently been used to begin to investigate how mechanical cues might impact upon angiogenesis during tissue regeneration [50, 53, 141, 143, 144], providing support for the hypothesis that EC proliferation during such processes is indeed mechano-regulated. However, in vitro studies suggest that other aspects of EC physiology, such as the rate and directionality of migration, are also in some way mechano-regulated [41-45]. To explore this *in silico* requires the development of modelling frameworks that can describe such cellular processes. A lattice-based modelling approach has previously been used to model stem cell proliferation, migration and also for modelling blood vessel growth [16, 21, 50, 139, 140, 239, 245], however this approach has yet to be applied to the explicit modelling of altered EC migration and proliferation in response to mechanical cues. The objective of this study was to develop a computational model (specifically a lattice based model) capable of describing changes in EC migration and proliferation in response to alterations in its mechanical environment. This model was then used to test a number of hypotheses for how mechanical cues might regulate EC migration and proliferation. Specifically, this study attempted to use the computational model to simulate experimentally observed changes in EC behaviour observed in response to mechanical stretch [42]. The experimental study in question [42] observed that mechanical strain regulated the spatial location and proliferation of ECs seeded onto silicone membranes. The computational model was used to test the hypothesis such changes in EC behaviour could be explained by either increased EC migration, increased EC proliferation or directionality biased EC migration in response to loading or a combination of these factors.

6.2 Methods

6.2.1 Description of experiment to be modelled

The modelling framework described below was used to simulate a previously published experimental study of EC proliferation and migration in response to

applied mechanical stretch [42]. The full experimental details of this study are available elsewhere [42], only a summary of which is included here. 2000 human umbilical vein endothelial cells (HUVECs) were seeded (in 2mm circular adhesive regions) onto gelatin-coated silicone sheets. These cells were cultured for 12 hours so that adhesion occurs before applying cyclic strain. A custom made mechanical strain device was used to apply 7% cyclic strain to the silicone sheets (in the x-direction, see Figure 6-1). Cell proliferation at specific spatial locations was analysed at various time points post strain initiation. To determine EC proliferation spatially in the culture, a line perpendicular to the direction of strain (i.e. in the y- direction), that bisected the cell region, was used. Cells within 200μm of this line were analysed to determine cell proliferation as a function of the distance along the y-axis (Figure 6-1 (D)). Image analysis software also enabled tracking of individual cell movements and measurement of the length and width of the entire cell populated region.

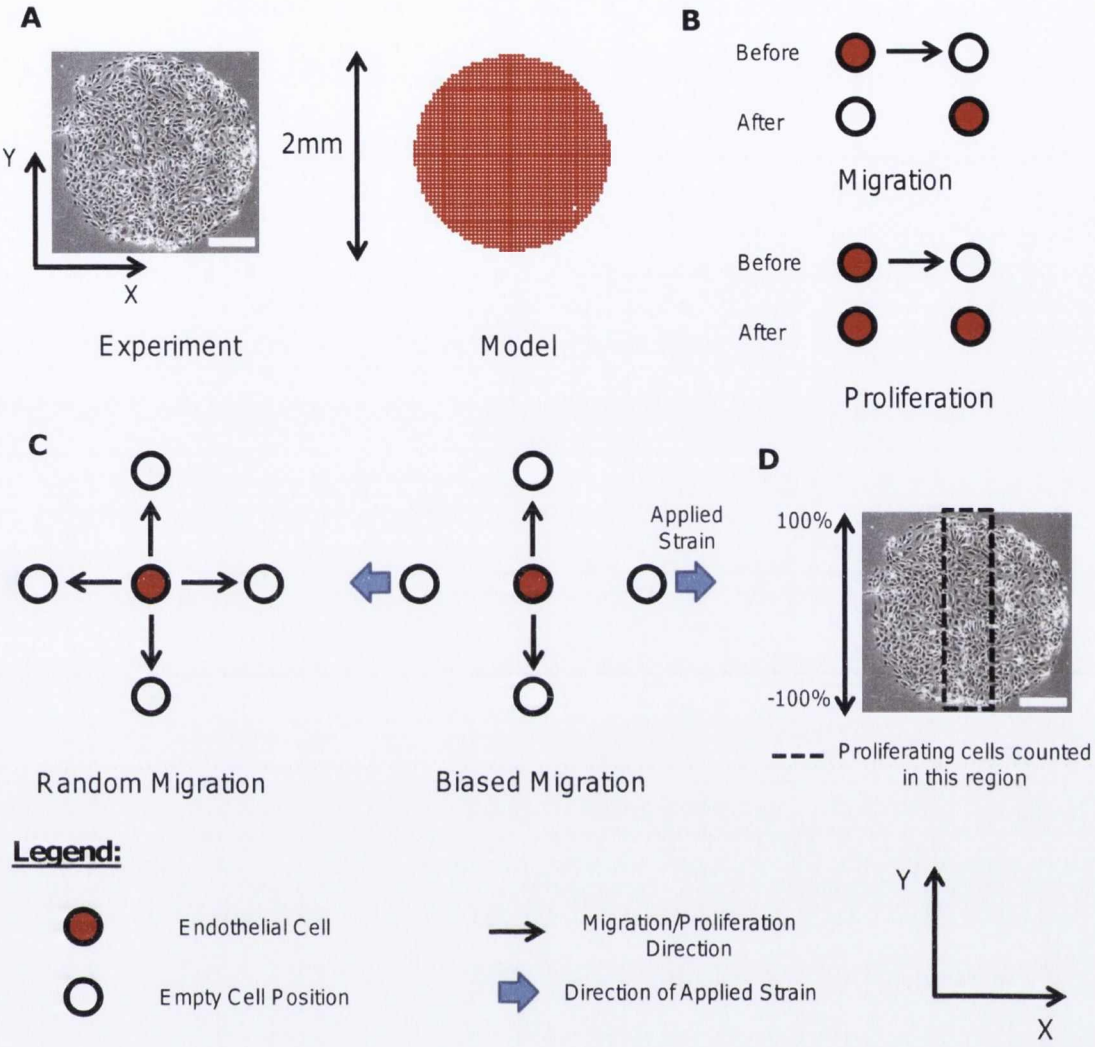

Figure 6-1. (A) Circular region of endothelial cells in both experimental and model setups. (B) Lattice model interpretation of the processes of cell migration and proliferation. (C) Lattice model interpretation of biased migration (cell can move in two possible directions perpendicular to direction of applied strain) and random migration (cell can move in all four possible directions). (D) Area of cellular region used for counting number of proliferating cells. Radial distance is calculated as a percentage in the positive and negative directions from the centre to the top and bottom edges of the region respectively.

6.2.2 Model setup

The lattice model used in this study was based on that described elsewhere in the literature (25). A square region of 200 by 200 lattice points (representing a square region of 8 mm by 8 mm) was created. Each lattice point represented a potential cell position. A circular region of 2mm diameter was filled with 2000 ECs (Figure 6-1 (A)). Therefore, the spacing between the centres of each cell was assumed to be approximately 40 μm. EC migration was implemented by filling the allotted

new cell position and vacating the previously filled position (Figure 6-1 (B)). In 2D space (as implemented in this study), each EC attempts to migrate randomly into one of the four adjoining lattice points (Figure 1C). Should the adjoining cell position be occupied, the EC remained in its original position. The migration rate (M) determined the number of attempted migration actions per iteration (1 hour). (The order of attempted migration was randomized to prevent artificially created patterns of biased migration).

EC proliferation was implemented by filling the allotted new cell position with a "daughter" cell while the previously filled position remains filled with the "parent" cell (Figure 6-1 (B)). Cells proliferated randomly into one of the four adjoining lattice points. Should the adjoining cell position into which an EC was attempting to proliferate into be occupied, contact inhibition occurred and the EC remained in its original position and did not proliferate. During each iteration (1 hour), a proportion of randomly chosen ECs attempted to proliferate based upon a proliferation rate (P).

Both the migration and proliferation rate were varied until the model accurately predicted EC migration and proliferation in the unloaded case (P = 0.02, M = 1). 3 potential drivers of altered EC migration and proliferation in response to mechanical stimulation were then explored. Firstly, increased cell migration (case A) was investigated by increasing the cell migration rate M (by a factor of four) to 4 attempted migrations per hour. Secondly, increased cell proliferation (case B) was investigated by increasing the cell proliferation rate (P) by a factor of two to 0.04 attempted proliferations per hour. Thirdly, biased migration (case C) was investigated by permitting EC cells to migrate into only one of 2 cells positions located in the direction perpendicular to the applied strain (Figure 6-1 (C)). Finally, All 3 potential drivers (case D) were included together. (Models where only 2 different drivers were combined were also performed and the results of these simulations are available as supplementary material, see Appendix IV).

6.3 Results and discussion

A summary of the results of the experimental study reported by Matsumoto *et al* [42] is first provided, where the effect of cyclic uniaxial strain on EC dynamics

was investigated in a 2D culture system. In the unloaded case, it was found that ECs that initially were seeded in circular patterns (Figure 6-1 (A)) migrated randomly to form a larger circular region (Figure 6-2 (A)). Cell numbers (initially 2000) remained approximately constant during the culture period (Figure 6-2 (B)). The diameter of the region of cells increased approximately linearly, with a similar rate in both X and Y directions (Figure 6-2 (C)). It was also found that proliferation was restricted to the peripheral regions of the seeded circular area up to at least the 24 hour time point (Figure 6-2 (D)).

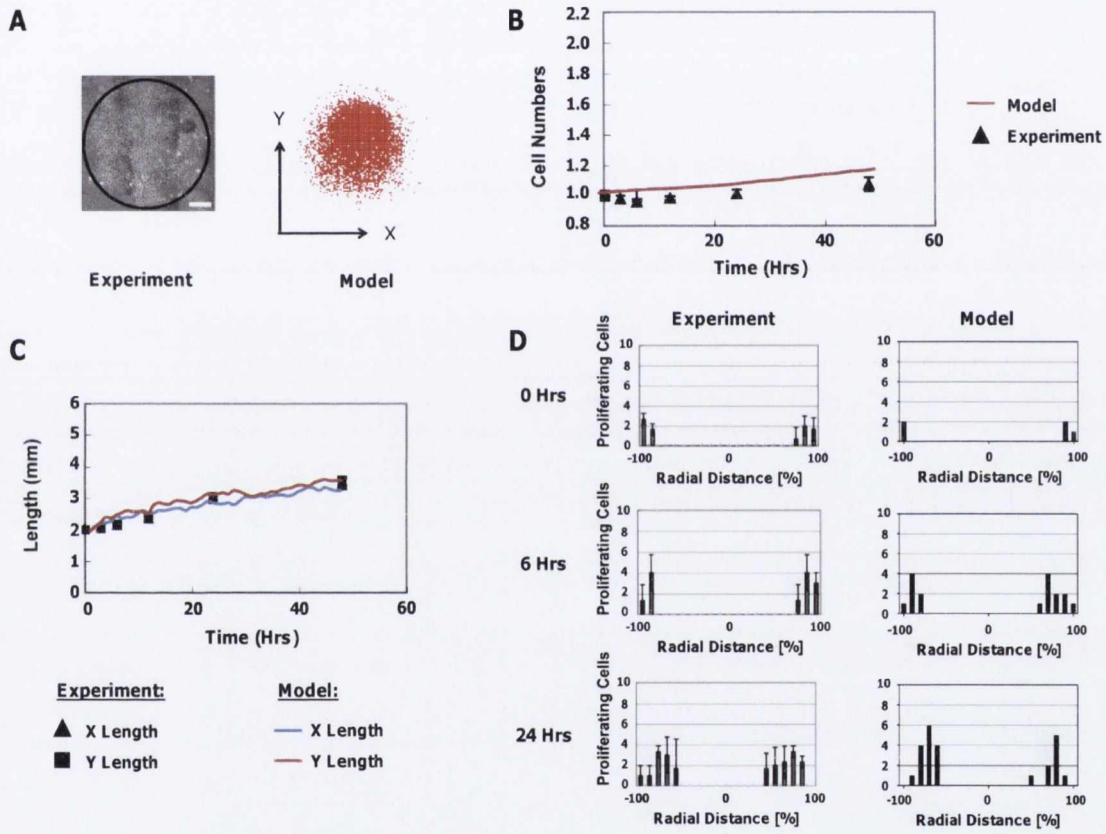

Figure 6-2. Model predictions – unstrained case. (A) Model prediction of the final distribution of the endothelial cell population compared to that observed experimentally. (B) Model prediction of the change in the total cell number over time compared to that observed experimentally. (C) Model prediction of the variation in the X and Y lengths of the endothelial cell region over time compared to that observed experimentally. (D) Model predictions of the number of proliferating cells at various radial distances (Y direction) from the centre ('0') of the EC population at the 0 hour, 6 hour and 24 hour time points compared to that observed experimentally.

Upon application of cyclic uniaxial strain, the region of ECs became elongated in the direction perpendicular to the applied strain (Figure 6-3 (A)). Overall, cell numbers increased by approximately 70% by the 48 hour time point (Figure 6-3 (B)). The diameter of the initially circular EC region (2mm initial diameter) increased approximately linearly with time to form an elliptical shape, with dimensions of approximately 2.4 and 3.3 mm in the X and Y direction respectively (Figure 6-3 (C)). Proliferation was initially restricted to the peripheral regions of the cell population but did occur in central regions at the 24 hour time point (Figure 6-3 (D)).

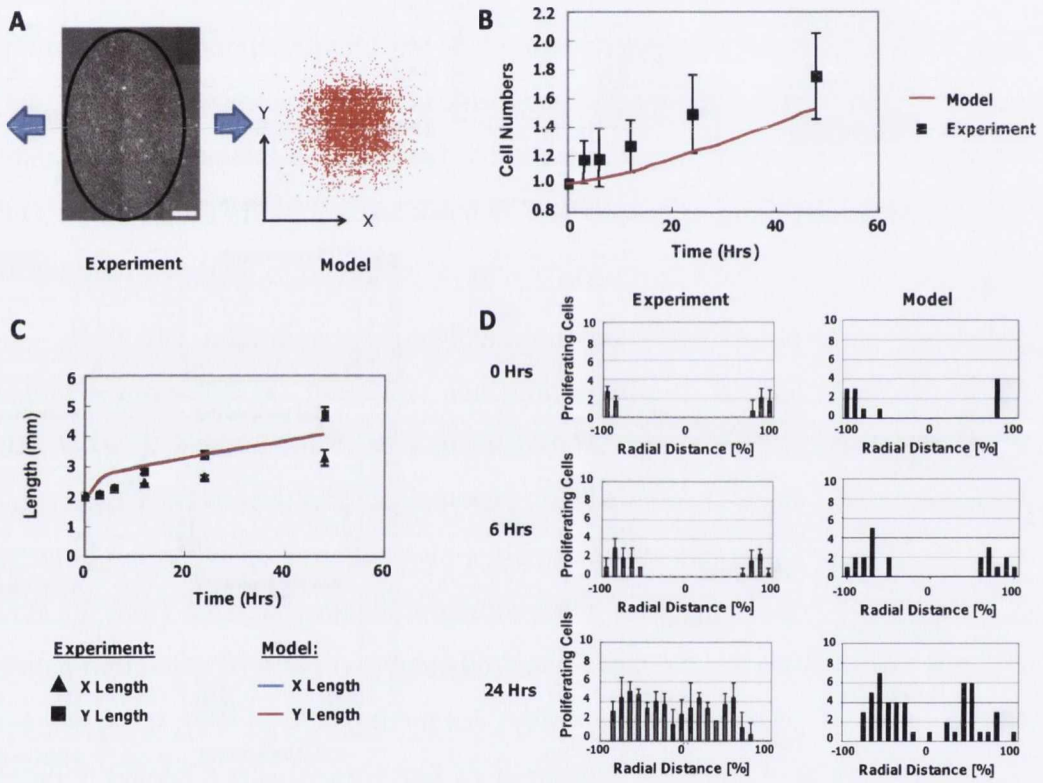

Figure 6-3. Model Predictions – case A: Increased EC migration due to application of strain. (A) Model prediction of the final distribution of the endothelial cell population compared to that observed experimentally. (B) Model prediction of the change in the total cell number over time compared to that observed experimentally. (C) Model prediction of the variation in the X and Y lengths of the endothelial cell region over time compared to that observed experimentally. (D) Model predictions of the number of proliferating cells at various radial distances (Y direction) from the centre ('0') of the EC population at the 0 hour, 6 hour and 24 hour time points compared to that observed experimentally.

6.3.1 Model predictions- unstrained case

In order to perform a successful investigation into the mechanisms of EC behaviour, it was first necessary to create a model with sufficient predictive power to accurately simulate the unloaded experiment. To this end, a parameter variation study was performed where the speed of EC migration and proliferation was varied. A circular pattern of ECs of similar width to that found in the *in vitro* experiment was predicted (Figure 6-2 (A)). Total cell number was predicted to increase approximately linearly with time by ~10% by the 48 hour time point, although no significant increase was observed experimentally (Figure 6-2 (B)). One possible explanation for this is that cell death (apoptosis) was not modelled which may have occurred to a limited extent experimentally. The width of the cell region in the X and Y directions was predicted to increase approximately linearly with time to 3.25 and 3.40 mm respectively (Figure 6-2 (C)). Proliferation was predicted to be limited to the outer region of the circular area of cells for each of the 0, 6 and 24 hour time points, which correlates well with the *in vitro* findings (Figure 6-2 (D)). Contact inhibition in the central region prevents proliferation from occurring in this region within the model. Overall, the model adequately predicts all of the experimental observations of the unloaded case.

Once the unloaded case was successfully predicted by the model, it was possible to test if particular aspects of EC physiology, such as alterations in their rate of proliferation or migration, are involved in their response to dynamic strain. This was achieved by perturbing these parameters in the model and testing if such changes were predictive of the changes in EC behaviour observed experimentally.

6.3.2 Model predictions – case A: increased EC migration due to the application of strain

Increasing the rate of EC migration (case A) was unable to predict the oval shape adopted by the cell population following the application of dynamic stretch. Instead, cells migrated in random directions creating an approximately circular region of cells (Figure 6-3 (A)). Cell number increased by 55% (Figure 6-3 (B)) during the course of the simulation, which approaches that observed experimentally. This large increase in cell number compared to the unloaded case can be explained as follows. Increased migration of ECs creates more open cell

positions within the lattice model, thereby reducing the effect that contact inhibition has on EC proliferation, particularly in central regions of the cell seeded silicone sheets. EC proliferation during the first 6 hours of the simulation was predicted solely in the peripheral regions of the cell seeded area (Figure 6-3 (D)). A small amount of EC proliferation was predicted to occur in the central region after 24 hours, similar to that observed experimentally. This was again due to the creation of more open cell positions in the central regions of the seeded area allowing EC proliferation to occur. As would be expected, this simulation was unable to predict anisotropic EC migration as cells migrate randomly but approximately equally in all directions (width in the X and Y directions of 3.97mm and 3.98mm respectively) (Figure 6-3 (C)). Therefore overall, increasing the rate of migration alone could not predict all experimental observations.

6.3.3 Model predictions – case B: increased EC proliferation due to the application of strain

Increasing the rate of EC proliferation (case B) was unable to predict the oval shape adopted by the EC population following the application of dynamic stretch. Instead, cells were predicted to migrate in random directions, again creating an approximately circular region of cells (Figure 6-4 (A)). Cell number increased by 60% (Figure 6-4 (B)) compared to the 0 hour time point, which again approaches the experimental result. This simulation was unable to predict anisotropic EC migration as cells migrate randomly but approximately equally in all directions (Width in the X and Y directions of 3.35mm and 3.38mm respectively) (Figure 6-4 (C)). Early proliferation was predicted solely in peripheral regions but this model perturbation cannot predict proliferation occurring in central regions at the 24 hour time point (Figure 6-4 (D)). Contact inhibition prevented this. Overall, increasing the rate of proliferation alone could not predict all experimental observations.

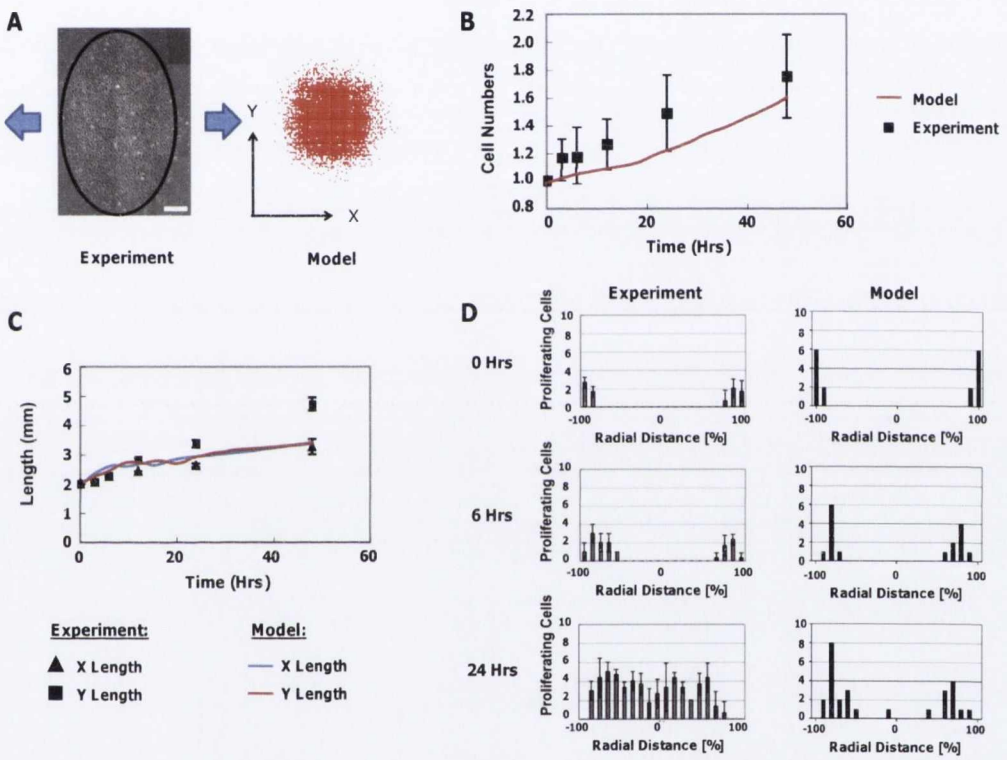

Figure 6-4. Model Predictions – case B: Increased EC proliferation due to application of strain. (A) Model prediction of the final distribution of the endothelial cell population compared to that observed experimentally. (B) Model prediction of the change in the total cell number over time compared to that observed experimentally. (C) Model prediction of the variation in the X and Y lengths of the endothelial cell region over time compared to that observed experimentally. (D) Model predictions of the number of proliferating cells at various radial distances (Y direction) from the centre ('0') of the EC population at the 0 hour, 6 hour and 24 hour time points compared to that observed experimentally.

6.3.4 Model predictions – case C: biased EC migration in the direction perpendicular to applied strain

Having cells preferentially migrate in the direction perpendicular to the applied strain (case C) successfully predicted the oval shape adopted by the EC population in the dynamically loaded group (Figure 6-5 (A)). This simulation predicted a small increase in cell number of 24%, which was less than that observed experimentally (Figure 6-5 (B)). The model successfully predicted the divergence in width of the initially circular cell region, with a greater final width in the Y direction than in the X direction (width of 3.29 mm in the Y direction versus 2.45 mm in the X direction) (Figure 6-5 (C)). This was due to directionally biased EC migration. Finally, this model perturbation predicted EC proliferation in peripheral regions at early time points, but cannot predict proliferation in central regions of the seeded area at the 24 hour time point (Figure 6-5 (D)). Contact inhibition in the central regions again prevented this. Therefore, biasing migration directionality alone could not predict all experimental observations.

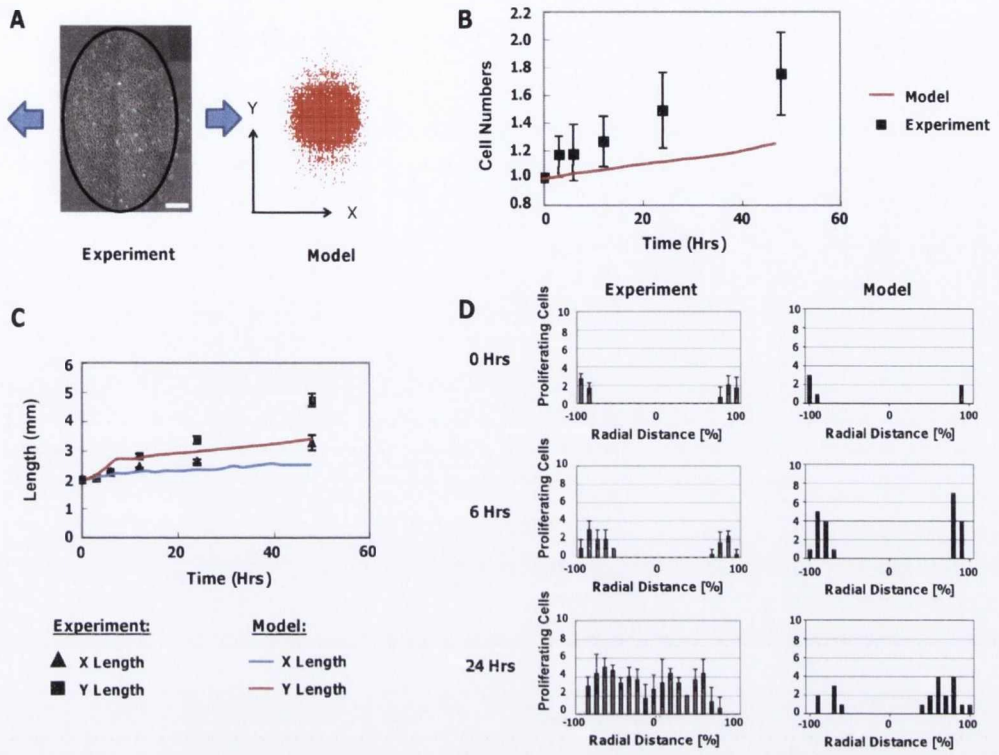

Figure 6-5. Model Predictions – case C: Biased EC migration in the direction perpendicular to applied strain. (A) Model prediction of the final distribution of the endothelial cell population compared to that observed experimentally. (B) Model prediction of the change in the total cell number over time compared to that observed experimentally. (C) Model prediction of the variation in the X and Y lengths of the endothelial cell region over time compared to that observed experimentally. (D) Model predictions of the number of proliferating cells at various radial distances (Y direction) from the centre ('0') of the EC population at the 0 hour, 6 hour and 24 hour time points compared to that observed experimentally.

6.3.5 Model predictions – case D: strain increases the rate of EC migration and proliferation and leads to directionally biased migration

The model implementing all 3 perturbations simultaneously (case D) successfully predicted the oval shape adopted by the EC population in the dynamically loaded group (Figure 6-6 (A)). This case predicted an increase in cell numbers of 94%, slightly higher than that observed experimentally. This increase was due to a combination of increased migration lowering the likelihood of contact inhibition and a faster rate of EC proliferation (Figure 6-6 (B)). The divergence in width of the circular cellular region, with a greater final width in the Y direction was successfully predicted (width of 5.12mm in the Y direction versus 3.15mm in the

X direction) (Figure 6-6 (C)). Finally, this case predicted early proliferation solely in peripheral regions and can also predict proliferation occurring in the central region after 24 hours as viewed experimentally (Figure 6-6 (D)). This was again predominantly due to the creation of more open cell positions allowing proliferation to occur and the greater proliferation rate allowing a larger increase in cell number in the central region at the 24 h time point. Implementing the combination of increased migration, increased proliferation and biased migration in response to loading was the only case which was fully predictive of experimental observations. The results of combining any two perturbations from case A, B or C together are provided as supplementary data (see Appendix IV).

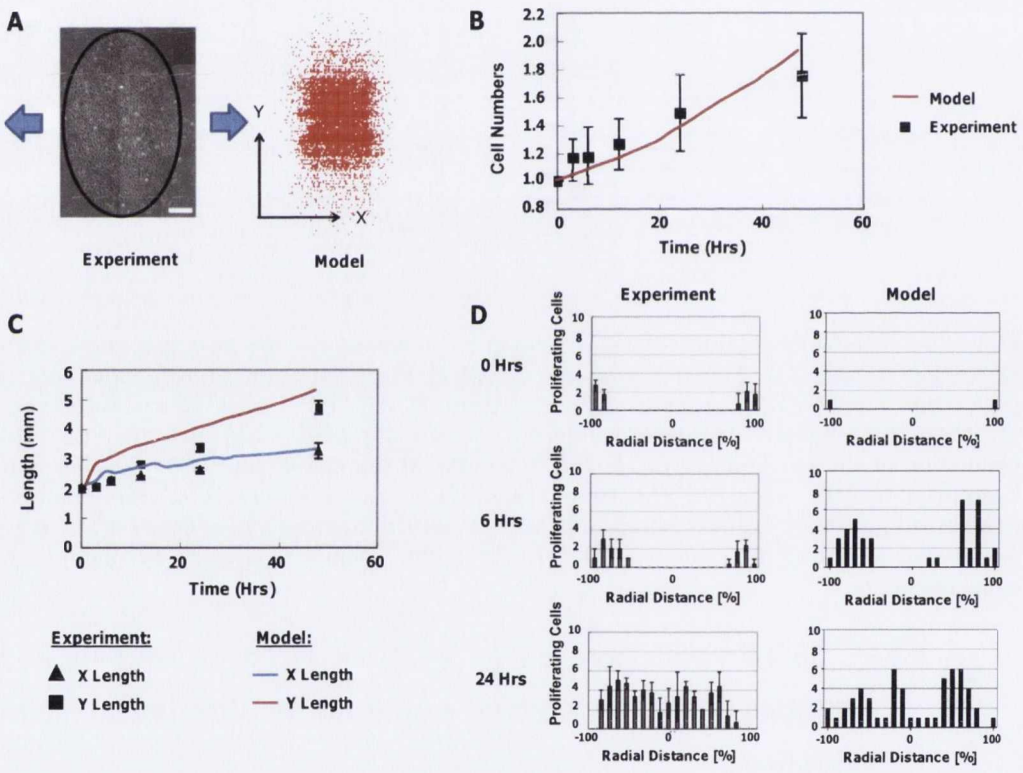

Figure 6-6. Model Predictions – case D: Strain increases the rate of EC migration and proliferation and leads to directionally biased migration. (A) Model prediction of the final distribution of the endothelial cell population compared to that observed experimentally. (B) Model prediction of the change in the total cell number over time compared to that observed experimentally. (C) Model prediction of the variation in the X and Y lengths of the endothelial cell region over time compared to that observed experimentally. (D) Model predictions of the number of proliferating cells at various radial distances (Y direction) from the centre ('0') of the EC population at the 0 hour, 6 hour and 24 hour time points compared to that observed experimentally.

6.3.6 Model limitations

There are some limitations associated with this study. Firstly, the lattice approach assumes all cells are identical in cell shape and size which is not the case in reality. Cell positioning is also limited to the exact spacing of the lattice and cells cannot exist in between these spacings which again is a limitation of the approach. Cell reorientation in the direction perpendicular to applied strain (as assumed here) has been observed in several studies [42, 128, 131, 132]. However, cell alignment parallel to the direction of applied strain has also been observed [43]. A possible explanation for this is that the underlying collagen matrix (of the collagen gels used in the study) prevents reorientation by the applied cyclic strain. In spite of the model limitations, this study demonstrates that in order to replicate all experimental observations [42], increased migration, increased proliferation and directionality biased migration in response to loading are all needed to be included in the model. This would suggest that the application of dynamic loading to ECs results in increased EC migration, increased EC proliferation and biased EC migration in the direction perpendicular to applied strain. Such findings have important implications for understanding how mechanics may regulate angiogenesis. While specific changes were made to the rate of EC migration and proliferation in this model, the general conclusions for how mechanics regulate EC behaviour may be applicable for how mechanical cues regulate angiogenesis *in vivo*. Future studies will test this concept by attempting to simulate regenerative events *in vivo* by extrapolating the rules (in terms of biased migration etc) that apply here for ECs *in vitro* to blood vessels *in vivo*.

6.4 Conclusions

Understanding how mechanics regulate ECs and angiogenesis is essential for research into the areas of wound healing, tissue engineering, bone repair etc. While *in vitro* studies clearly demonstrate that mechanical cues regulate EC behaviour, it is often difficult to decouple how such signals impact specific aspects of cellular behaviour using experimental techniques alone. *In silico* approaches offer an inexpensive and often efficient method for performing such investigations which would be complex to perform experimentally. This study used a computational lattice model to simulate an experimental study which

revealed differences in EC distribution and number due to the application of cyclic strain [42]. The predictions of this computational model provide support for the hypothesis that dynamic strain increases both EC migration and proliferation, and that EC migration directionality is biased in the direction perpendicular to applied strain, as only by incorporating all such phenomena into the model was it capable of predicting all experimentally observed outcomes. In this study, EC migration was biased in the direction perpendicular to applied strain. However, in 3 dimensions there are an infinite number of perpendicular directions (like the spokes on the wheel of a bike). The direction perpendicular to the applied strain also represents the direction of minimum principal strain and the minimum absolute strain, either of which could be a potential guiding stimulus for biased EC migration in this (or other) studies. Alternatively, instead of biased migration in the direction perpendicular to the applied strain (or some variant as described above), it may be that ECs tend not to migrate in the direction of applied strain (or in this case the direction of the 1st principal strain). Such a rule would be implemented in the model in exactly the same way as biased migration perpendicular to the applied strain and would therefore result in the same simulation outcomes as presented here. Future studies will explore alternative *in vitro* and *in vivo* regenerative events using *in silico* models to address these questions.

Chapter7: A mechano-regulation model of angiogenesis during large bone defect regeneration

The previous chapter of the thesis examined how the application of mechanical strain affects endothelial cell (EC) physiology *in vitro*. A major conclusion is that EC migration is biased in a direction perpendicular to the applied strain. However, there are a number of mechanical descriptions of this 2-D result.

The next chapter of the thesis will investigate whether a similar phenomenon might occur *in vivo* in 3 dimensions. The lattice model of angiogenesis developed in Chapter 5 will be adapted to include biased blood vessel growth directionality. The hypothesis that blood vessel growth directionality *in vivo* is regulated by the local mechanical environment will be tested by attempting to simulate angiogenesis during the regeneration of stabilized and unstabilized large bone defects. In addition, the hypothesis that a tissue differentiation model regulated by substrate stiffness and oxygen availability can predict MSC fate within such large bone defects will be subsequently tested, where the local oxygen levels are determined using this new mechano-regulation model of angiogenesis.

7.1 Introduction

A number of computational mechanobiological models have been developed which provide support for the hypothesis that tissue differentiation during regenerative events such as fracture healing is directly regulated by extrinsic mechanical stimuli [5, 7, 8]. MSC fate and tissue regeneration are also known to be strongly affected by angiogenesis and oxygen availability [46, 171, 220, 235] . In the context of bone repair, a vascular supply and the associated delivery of oxygen and nutrients is known to play a role in the regulation of both intramembranous and endochondral ossification [46, 171]. Neovascularization during tissue regeneration is known to be influenced by the local mechanical environment [41-43, 45]. For example, angiogenic progression may be inhibited in regions of high mechanical stimulus [38, 150], where capillaries are "sheared" off in regions of high mechanical strain [38]. In addition, vessel directionality may also be influenced by mechanics [42-44]. This raises the possibility that tissue differentiation during regenerative events such as fracture healing is not directly regulated by the local mechanical environment, but is indirectly regulated by such cues due to the impact they have on angiogenesis and the associated delivery of regulatory factors such as oxygen. Such questions can potentially be addressed using *in silico* approaches, however it requires the development of computational models that can describe the impact of mechanics on angiogenesis during tissue regeneration.

Previous computational models of tissue differentiation during regenerative events have highlighted the importance of including an accurate model of angiogenesis [50, 51, 53, 141, 227, 236]. In particular, *in silico* techniques have been employed previously to help elucidate the role of biochemical in regulating the directionality of blood vessel growth [50, 51]. However, computational tools have yet to be employed to examine the effects of mechanics in regulating the directionality of neovascularization *in vivo*. This is despite the fact that there is strong evidence to suggest that neovascular formation *in vivo* is mechano-regulated [37, 150], with the application of early mechanical loading shown to inhibit vascular invasion into large bone defects [40]. The previous chapter of this thesis developed a mechano-regulation model of EC migration *in vitro*. By postulating that ECs are biased to migrate in a direction

perpendicular to the applied strain, the model was capable of accurately predicting experimentally observed patterns of cell migration on 2 dimensional strips subjected to tensile strain [42], suggesting that such mechanical cues could similarly direct angiogenesis *in vivo*. (It should be noted that a direction perpendicular to applied tensile strain in 2 dimensions may correspond to several directions in 3 dimensions. For example, it can be described as the direction of minimum principal strain or as a direction perpendicular to the maximum principal strain). It has also been suggested that EC migration aligns with the orientation of the maximal principal stress [133]. These diverse findings demonstrate that the understanding of the mechanobiology of neovascular formation remains poorly understood.

The objective of this study was to develop a computational mechanobiological model to investigate the influence of mechanics upon the directionality of blood vessel growth during tissue regeneration in mechanically stabilized and unstabilized large bone defects. Simulation of blood vessel growth directionality regulated by several mechanical guiding stimuli (direction of minimum principal strain, direction of maximum principal strain and any direction perpendicular to the maximum principal strain) were compared to μCT angiography results for neovascular network formation in stabilized and unstabilized large bone defects [40]. Having developed an accurate simulation of mechano-regulated angiogenesis, the model was then used to test the hypothesis that MSC differentiation is indirectly regulated by the local mechanical environment due to its effect on neovascular formation and hence the local levels of oxygen within the regenerating tissue. To this end, I attempted to simulate the temporal and spatial patterns of tissue differentiation within stabilized and unstabilized large bone defects based on the hypothesis that MSC fate is regulated by the local substrate stiffness and oxygen availability.

7.2 Methods

7.2.1 Details of experimental study to be modeled

Full details of the experimental study under investigation are available elsewhere [40], but elements important to creation of the tissue differentiation model are described here. 8mm bilateral critically sized rat femur defects were surgically

created [246, 247]. Two groups were examined. Either stiff or compliant fixation plates stabilized the fractures. Fixators allowed some compressive load along the bone axis but bending and torsional loads were minimized. MicroCT angiography was used to quantify vascular structures within the callus 3 weeks after the creation of the defects. A defect volume of interest [248] [248] was defined as a 6.3 mm long, 5 mm diameter cylinder which contained only the region of the bone defect [40]. A total VOI was also defined as a 7mm diameter cylinder of the same length which included the region of the bone defect and immediate surrounding soft tissues and callus (Figure 7-1 (A)). Tissue differentiation was histologically assessed allowing comparisons of cartilage and bone formation for the different groups.

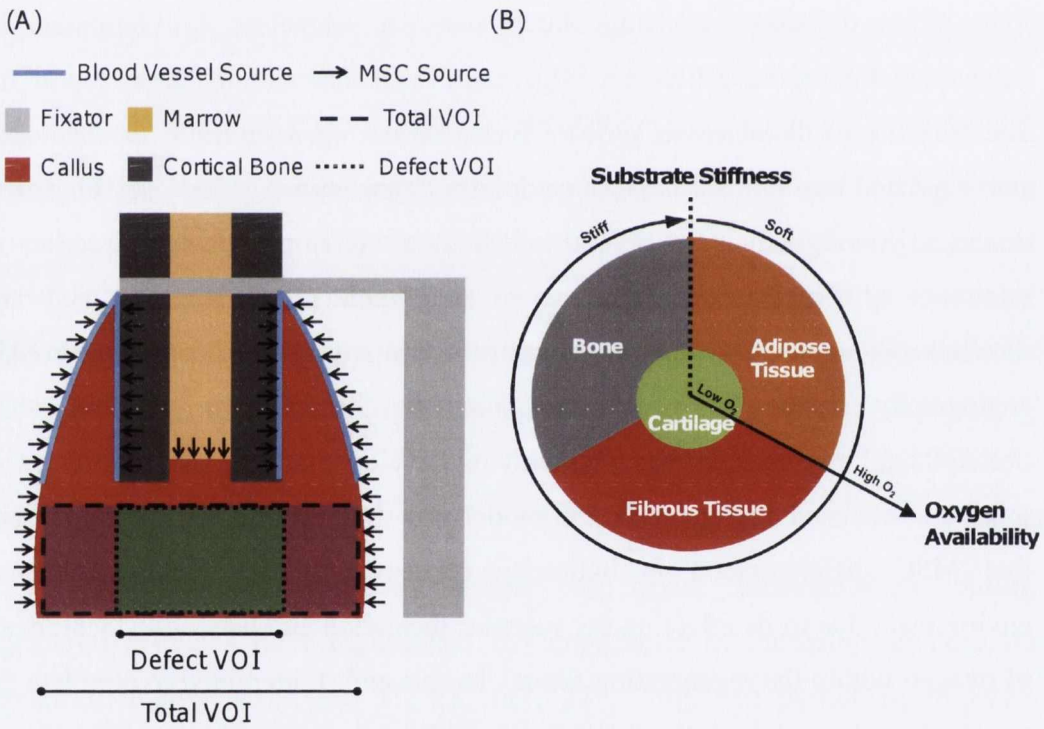

Figure 7-1. (A) Geometry of large bone defect under investigation, including the presence of an external fixator. The figures illustrates the MSC and blood vessel sources as well as the defect VOI and total VOIs. (B) Tissue differentiation regulated by substrate stiffness and oxygen availability. The oxygen availability axis extends radially from the centre of the circle, low oxygen in the centre of the circle increasing towards the periphery. The substrate stiffness axis extends circumferentially in a clockwise direction from the right side of the dotted line at the top of the circle. The presence of a blood supply is also a prerequisite for formation of bone and marrow

7.2.2 Finite element model

A finite element (FE) model consisting of 8259 elements was created to predict the mechanical environment within the fracture callus (Figure 7-2 (A)). The

fixator was modeled as rectangular. Biphasic material properties were adopted for all tissues except the pin and fixator (Table 7-1). The pin and fixator were modeled as linear elastic materials with a Poisson's ratio of 0.3. The Young's Modulus of the fixator was determined via parameter convergence to the total system stiffness value obtained in the experimental study (compliant fixation 8.4N/mm, stiff fixation 214.3N/mm) [40]. These values were obtained from mechanical tests of stiff and complaint plates (which were affixed to excised femurs) in the experiment. Equivalent system stiffness was achieved with a stiffness of the fixator of 40 MPa for the compliant configuration and 5 GPa for the stiff configuration. The Young's Modulus of the pin was taken to be 200 GPa in both cases. An axial load of 10N was applied to the top of the bone. This magnitude was an estimation taken from a similar FE model of the rat femur reported in the literature [249]. The described model was implemented into the commercial finite element software package MSC Marc (version 2008r1, MSC Software Corporation, Santa Ana, CA).

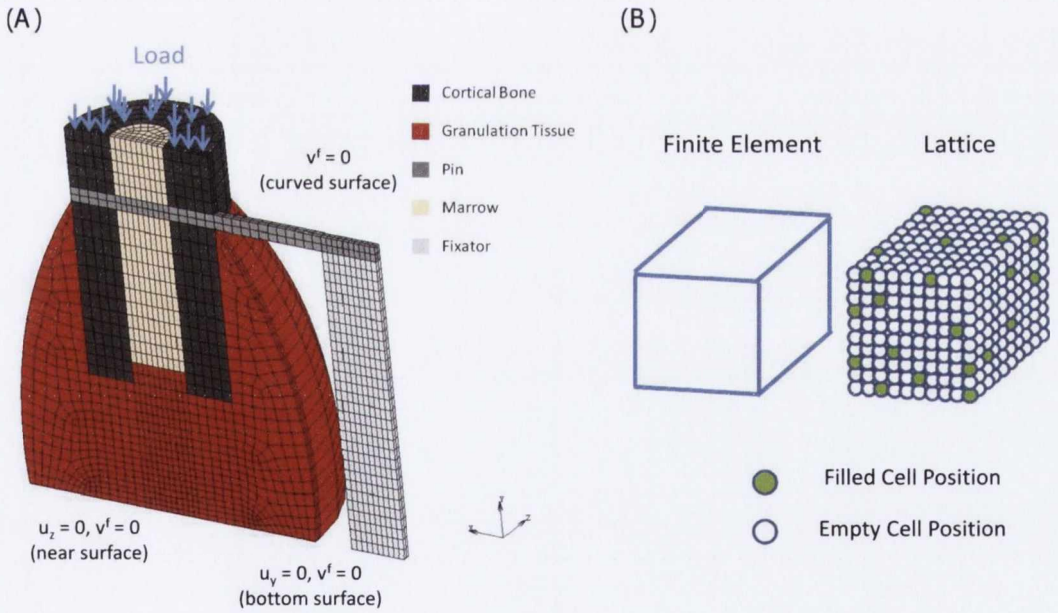

Figure 7-2. (A) FE Model of the fracture callus and fixator. Loading is applied on the top of the cortex. Radial displacement, axial displacement and fluid velocity boundary conditions are shown as u_z, u_y, and v^f respectively. (B) A 3 dimensional finite element with corresponding lattice. Each lattice point represents a potential location for a cell and its immediate extracellular matrix.

Table 7-1 Material properties

Material Property	Granulation Tissue	Fibrous Tissue	Cartilage	Marrow	Immature Bone	Mature Bone	Cortical Bone
Young's Modulus (MPa)	0.2[a]	2[b]	10[a]	2[a]	1,000[a]	6,000[c]	20,000[c]
Permeability (mm2)	1E-11[a]	1E-11[b]	5E-15[d]	1E-14[a]	1E-13[a]	3.7E-13[e]	1E-17[f]
Poisson's Ratio	0.167[a]	0.167[a]	0.167[a]	0.167[a]	0.3[a]	0.3[a]	0.3[a]
Fluid Dynamic Viscosity (Ns/m2)	1E-9	1E-9	1E-9	1E-9	1E-9	1E-9	1E-9
Porosity	0.8[a]	0.8[a]	0.8[a]	0.8[a]	0.8[a]	0.8[a]	0.04[g]

a. Lacroix and Prendergast (2002) [10]; **b.** Hori and Lewis (1982) [214]; **c.** Claes and Heigele (1999) [7]; **d.** Armstrong and Mow (1982) [215]; **e.** Ochoa and Hillberry (1992) [216]; **f.** Cowin 1999 [217]; **g.** Schaffler and Burr (1988) [218].

7.2.3 Angiogenesis

Simulation of blood vessel growth was implemented using a lattice based approach. Within this approach, each finite element was discretised into lattice points [50, 139] (Figure 7-1 (B)). Each lattice point represented a potential position for a cell and its immediate extracellular matrix. Spacing between each lattice point was 10 μm. Vessels were modelled as a sequence of adjoining lattice points filled with endothelial cells [240]. EC death occurred where the local octahedral shear strain exceeded a threshold value (ε^{angio}) (Table 7-2). Capillaries were permitted to branch and form new vessels, the probability of which occurring was a function of the length of the vessel. L_{min} represents the minimum length for a sprout to branch, while L_{max} represents the maximum length for a non-branching sprout value (Table 7-2). Anastmosis (fusion of capillaries) occurred should two vessels meet. As element size and shape were irregular, the element in which a lattice point was located was determined via calculation of the equation of the plane for each side of an element (Appendix V).

Table 7-2 Tissue differentiation model parameters

Model Parameter	Symbol	Source	Unit	Value
Strain Threshold for Angiogenic Inhibition	ε^{angio}	Estimated	%	18
Blood Vessel Growth Rate	V	Estimated	μm.(1/2day)$^{-1}$	200
Minimum Length Branching	L_{min}	[50]	mm	100
Maximum Length (without) Branching	L_{max}	[239]	mm	300
Minimum Age for Differentiation	Age_{diff}	[16]	days	6
Oxygen Diffusion Coefficient	G	[212, 227]	m^2/s	2.2E-09
Oxygen Consumption Rate	Q	[213, 227]	fmol/cell/hr	98
Initial Oxygen Tension	$O_2^{initial}$	[179, 227]	mmHg	74.1
Oxygen Tension Limit for Cartilage	$O_2^{cartilage}$	[27, 28]	%	3

It was assumed that vessels would either move in a random direction, in the same direction as it was previously moving in or in a direction determined by a guiding mechanical stimulus (mechanotaxis). The probability of vessels growing in the same direction as previously (P_{prev}) was taken as 0.4, similar to previous studies employing such a lattice model of angiogenesis [16, 50, 141]. The sum of the probability of a vessel moving in a random direction (P_{rand}) and in a direction determined by a mechanical stimulus (P_{mech}) was taken as 0.6 ($P_{rand} + P_{mech} = 0.6$). The values of P_{rand} and P_{mech} were assumed dependent upon the magnitude of mechanical stimulation (Figure 7-3).

It was assumed that vessels could invade the callus from the periosteal cortex [154] and from the surrounding muscle tissues of the upper callus. Vessel progression from the marrow cavity was omitted for two reasons. Firstly, vessel activity has been observed to be significantly delayed from the inner callus due to the haemotoma formation at that site[52]. Secondly, μCT images of angiography from the experimental study [40] showed very few vessels progressing from this central region. ECs were positioned at the blood vessel source boundary conditions at the outer callus and periosteal cortex with 10% and 30% of cell positions filled respectively. This represented the dominant vascular response from the periosteal cortex [15]. Results from these simulations were compared to experimental data for local blood vessel concentration.

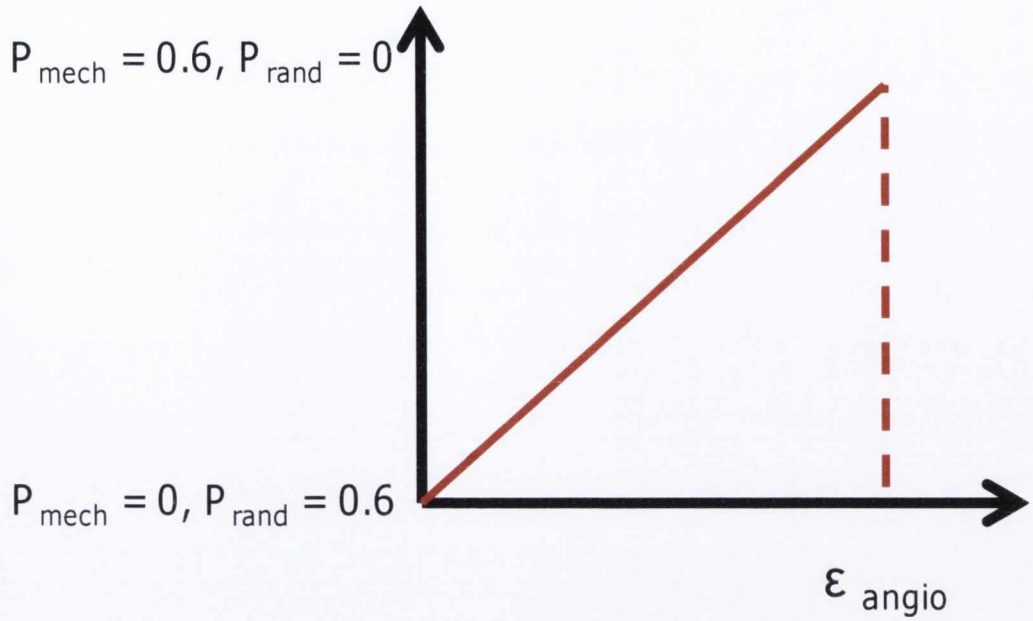

Figure 7-3. Hypothesized relationship between the magnitude of strain and the probability of vessel directionality being determined by a mechanical stimulus (P_{prev} = 0.4, P_{mech} + P_{rand} = 0.6). The greater the magnitude of strain, the greater the influence of mechano-regulated blood vessel directionality. Beyond ε_{angio} vessel death occurs.

7.2.4 Cell migration, cell proliferation and oxygen transport

Models of cell (MSCs, osteoblasts, adipocytes, chondrocytes and fibroblasts) migration and proliferation were implemented as stochastic processes using a similar lattice based approach as adopted for blood vessel growth simulation [50, 139]. Cell migration was implemented by filling the allotted new cell position and vacating the previously filled position using random walk theory [25]. Each cell attempted to migrate randomly into one of the adjoining lattice positions. Should the adjoining cell position be occupied, the cell remains in its original position. Cell proliferation was implemented in a similar fashion by filling the allotted new cell position (with a "daughter" cell) while the previously filled position remained filled (with the "parent" cell). Migration/proliferation was limited only if the adjoining cell position is occupied. The migration rate (M) and proliferation rate (P) (Table 7-3) determined the number of attempted migration or proliferation actions per unit time. 30% of cells positions along the assigned boundary conditions (Figure 7-1 (A)) where initially filled with MSCs [16]. 5% of all other cell positions were also randomly filled with MSCs. MSCs could only differentiate once the minimum age for differentiation (Age_{diff}) was reached [16] (Table 7-2). Should an element become dominated by one cell type (defined as at

least 50% of the cell positions in an element which has a minimum of 10% of total element cell positions occupied), other cell types within the element were assumed to undergo apoptosis.

Table 7-3 Cell model parameters

Model Parameter	Fibroblast	Chondrocyte	Adipocyte	Osteoblast	MSC
Proliferation Rate ($1/2day^{-1}$)	0.27 [a]	0.1 [a]	0.2	0.15 [a]	0.3 [a]
Migration Rate (μm/h)	26.6[b]	N/A	26.6 [b]	N/A	26.6 [b]
Differentiation Rate ($1/2day^{-1}$)	N/A	N/A	N/A	N/A	0.15 [a]

a. Isaksson et al (2008) [237] ; **b.** Appeddu and Shur (1994) [238].

Oxygen transport was simulated as a diffusive process, the boundary conditions of which were dependent upon the state of the blood supply determined from the model of angiogenesis [227]. Similar to previous studies of other tissue regenerative events, oxygen availability was initially assumed to be high throughout the callus [179, 227]. As the simulation progressed, oxygen (O_2) diffused from blood vessels and was consumed at a rate calculated as the product of a cellular consumption rate (Q) and cell density (see Equation 7.1 below and Table 7-2). Cell density (n) was determined from the number of filled lattice points at a given location.

$$\frac{dO_2}{dt} = G\nabla^2 O_2 - Qn^{\max} n \qquad \text{(Equation 7.1)}$$

7.2.5 MSC differentiation

The previously developed tissue differentiation model where MSC differentiation was determined by the stiffness of the local substrate elasticity and oxygen availability was applied to the callus (Figure 7-2 (B)). Osteogenesis and adipogenesis were repressed in regions of hypoxia (defined as regions in which the local oxygen drops below a threshold value ($O_2^{cartilage}$) (Table 7-2), while chondrogenesis was promoted in such regions. Where oxygen availability was sufficient, MSC fate was regulated by the stiffness of the local substrate. A high substrate stiffness promoted osteogenesis, whereas a low substrate stiffness

promoted adipogenesis. Fibrogenesis was predicted in regions of the callus where none of these conditions are upheld. The substrate stiffness stimulus at any point in the model is dependent upon the phenotype of surrounding lattice points. Engler *et al* refer to MSC differentiation regulated by the ''elasticity of the microenvironment'' of the cell [24]. For example, the stiffness of osteoid matrix produced by osteoblasts is approximately 30 kPa, however, the stiffness of woven bone itself is orders of magnitude higher (in the order of GPa). In this tissue differentiation model, osteogenesis occurs when stem cells are adjacent to newly formed bone and hence in contact with osteoid as a substrate (and similarly for adipogenesis). In this implementation, specific threshold values of stiffness are therefore not required. Tissue differentiation within the bone defect was simulated via an iterative procedure. Within each iteration, a prediction of mechanical stimuli, cell phenotypes and densities, blood supply and oxygen availability is generated in order to enable the local phenotype predictions to be determined. Each iteration was 12 hours.

7.2.6 Simulations

Simulations were performed for four cases (random vessel growth or 3 cases of mechanotaxis, see below) for each of stiff and compliant fixation conditions. The simulated period lasted for 3 weeks in order to compare with experimental data for vessel volume in the defect VOI and total VOI as well as with observations of tissue differentiation within the defect. The first simulation (case A) did not include a mechanical guiding stimulus driving biased blood vessel growth directionality. Vessels could either grow in a random direction ($P_{rand} = 0.6$) or in the previous direction ($P_{prev} = 0.4$). The next 3 cases included 3 different mechanical guiding stimuli, namely the direction of minimum principal strain (case B), the direction of maximum principal strain (case C) and the third case was any perpendicular direction to the maximum principal strain (case D). Simulations performed with $\varepsilon_{angio} = 0.06$ predicted non-union (which which did not agree with the experiment). Therefore a larger threshold of $\varepsilon_{angio} = 0.18$ was employed instead.

7.3 Results

7.3.1 Case A- random

Simulations without a mechanical guiding stimulus (with P_{rand} = 0.6 irrespective of strain level) predicted blood vessels to quickly fill the upper periosteal callus in both stiff and compliant cases (Figure 7-4 and Figure 7-5). Vessels proceeded in a stochastic manner and partially filled the lower regions of the periosteal and endosteal calluses as well as the fracture gap region. In stiff case, there was a greater number of vessels present in both the total VOI and defect VOI compared to the compliant case due to lower levels of EC death (Figure 7-6).

In terms of tissue differentiation, similar patterns of repair are observed in both the stiff and compliant cases (Figure 7-4 and Figure 7-5). The upper callus quickly filled with osteoblasts while chondrocytes filled the lower periosteal callus, fracture gap and endosteal callus for both stiff and complaint fixation conditions. As healing continued, bone formation progressed to fill more of the outer periosteal callus. At the 3 week time point, bony bridging had yet to occur for both cases. Similar quantities of bone and cartilage were predicted for the stiff and the compliant cases (Figure 7-7).

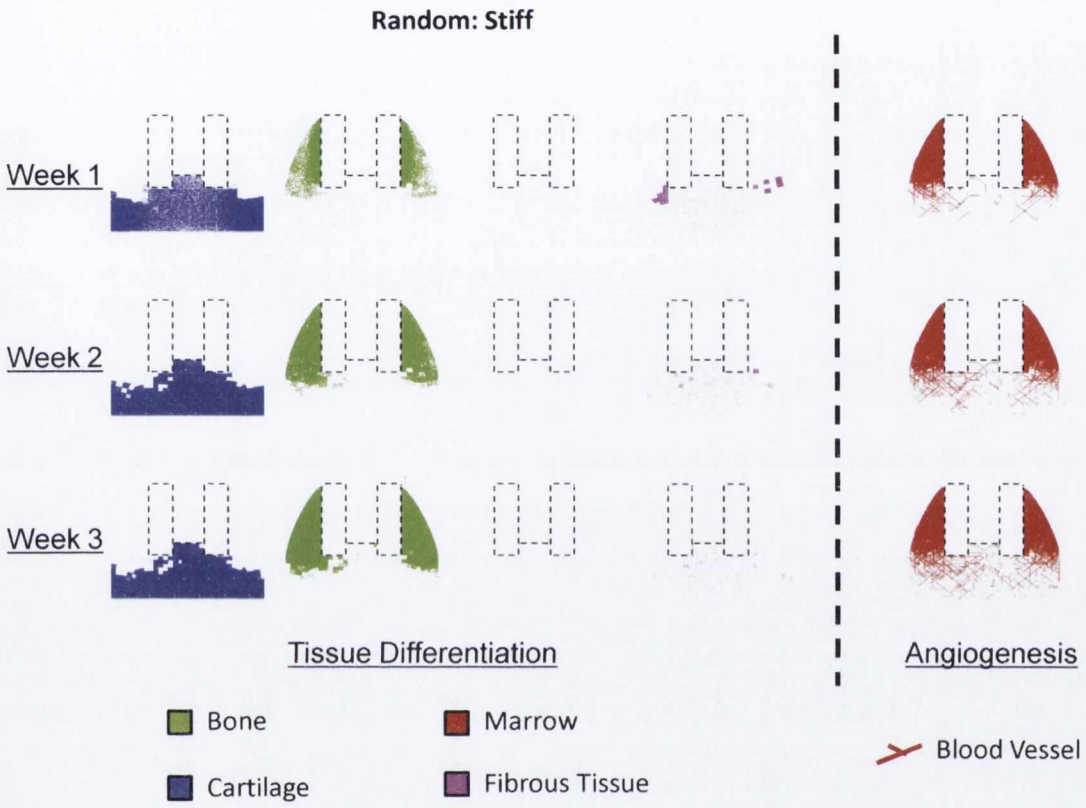

Figure 7-4. Tissue differentiation and angiogenesis predictions for case A under stiff fixation

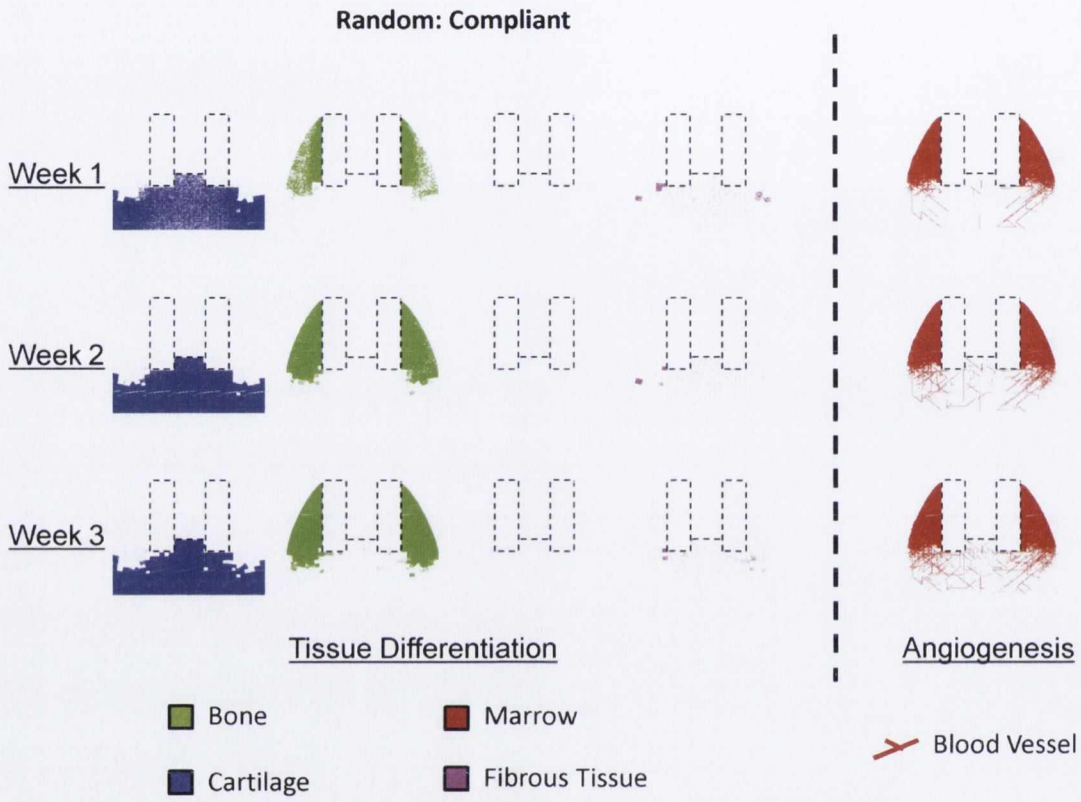

Figure 7-5. Tissue differentiation and angiogenesis predictions for case A under compliant fixation

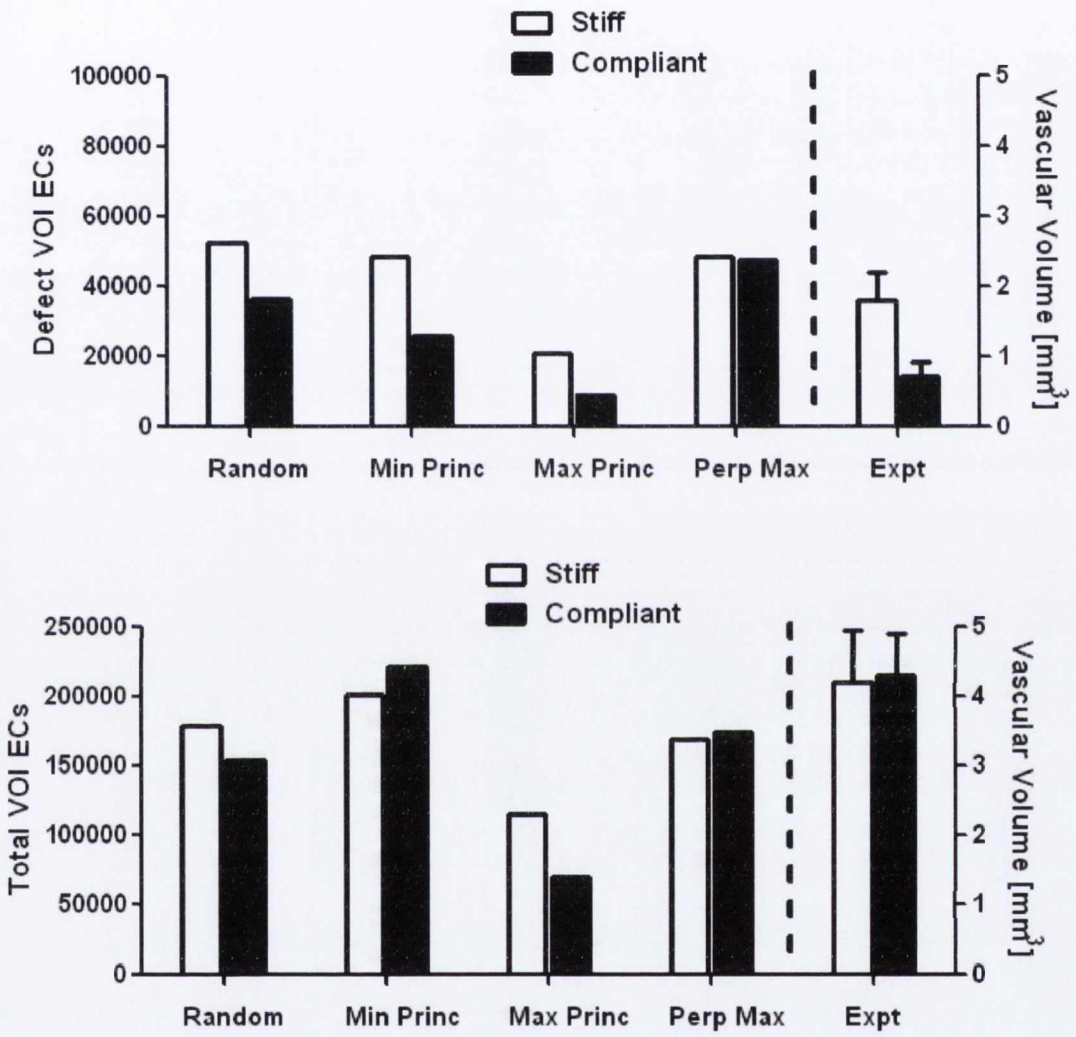

Figure 7-6. Predicted quantities of ECs present in both defect and total VOIs for all cases are compared experimental values for vascular volume [40] (2.5μg BMP-2).

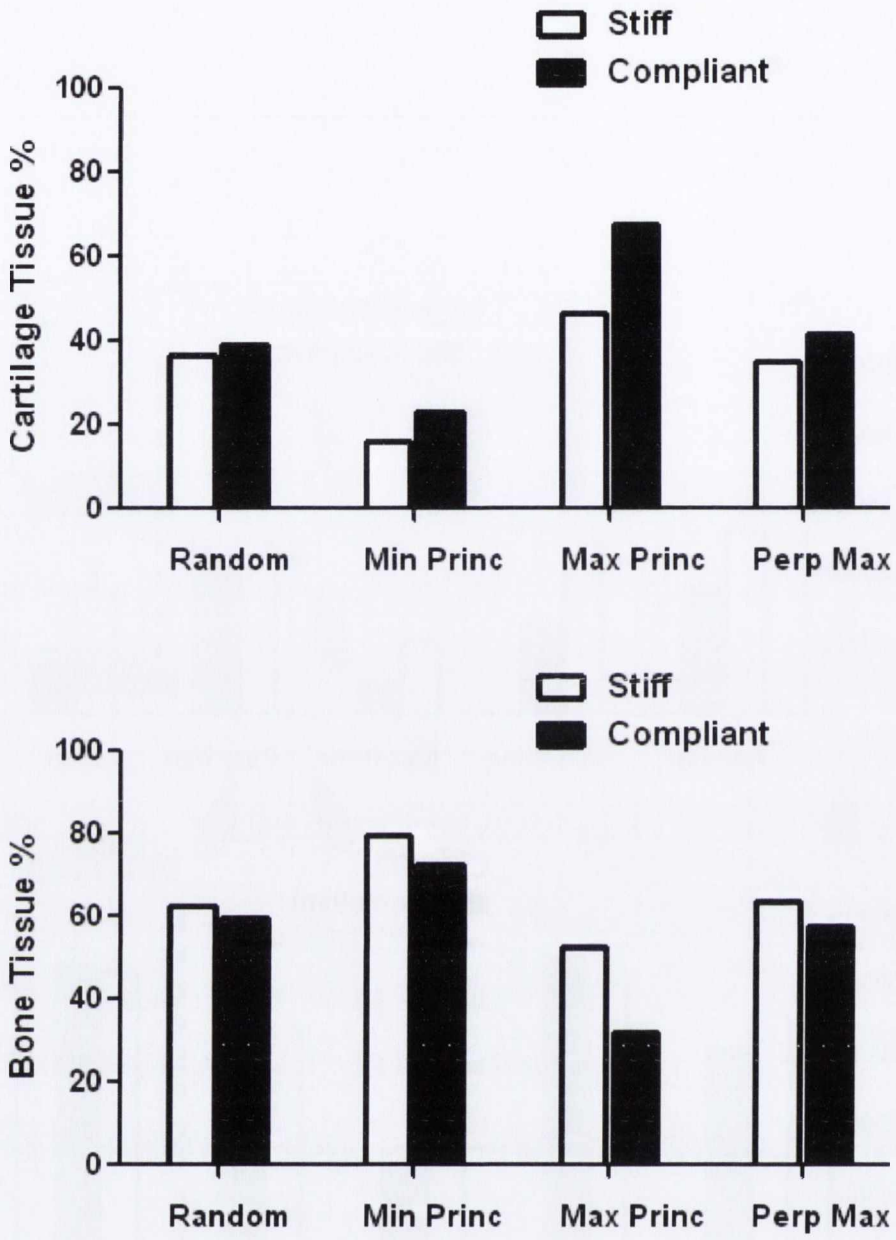

Figure 7-7. Predicted tissue fraction percentages for cartilage [250] and bone (bottom) for all cases

7.3.2 Case B- direction of minimum principal strain

Implementing minimum principal strain as a guiding stimulus for blood vessel growth directionality in the model also lead to a prediction of vessels quickly filling the upper periosteal callus in both stiff and compliant cases (Figure 7-8 and Figure 7-9). Vessels were biased to grow towards the lower outer periosteal callus with the minimum principal strain mechanical guiding stimulus. This bias was more prominent in the compliant case (particularly at the week 1 time point), with vessels heading more directly towards the lower outer periosteal callus, whereas

vessels proceeded in a more random fashion in the stiff case (Figure 7-8 and Figure 7-9). After 3 weeks, similar levels of angiogenesis within the total VOI was predicted for both stiff and compliant fixation conditions (Figure 7-6). In the defect VOI, higher levels of angiogenesis were predicted for the stiff case.

In terms of tissue differentiation, the upper callus was predicted to quickly fill with osteoblasts, with chondrocytes filling the lower periosteal callus, fracture gap and endosteal callus for both stiff and complaint fixations (Figure 7-8 and Figure 7-9). As healing continued, bone formation progressed to fill the outer periosteal callus. In the stiff case, the bone front progressed to fill the outer periosteal callus and fracture gap simultaneously as the bone front progressed down the callus. In contrast, for the compliant case blood vessels and the bone front were both predicted to progress towards the outer periosteal callus, with very little bone formation in the fracture gap itself. As a result bony bridging was achieved in the compliant case at the 3 week time point, while in the stiff case the bone ends were on the verge of bridging. Greater bone and less cartilage were predicted in the stiff case compared to the compliant case (Figure 7-7).

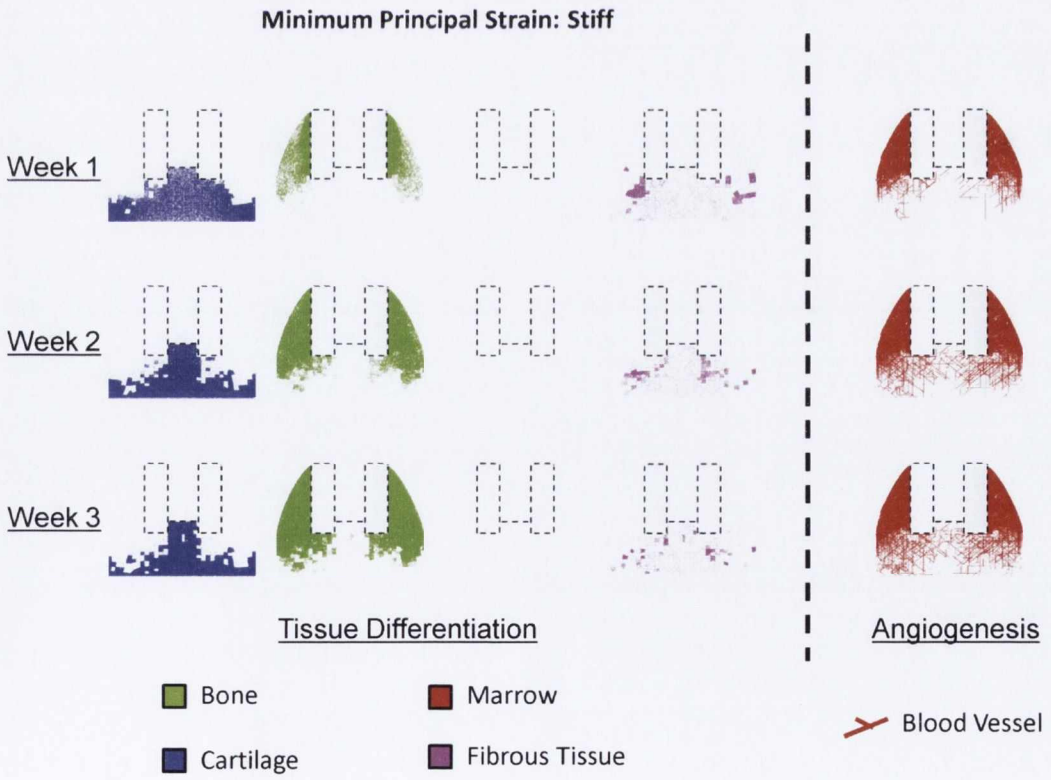

Figure 7-8. Tissue differentiation and angiogenesis predictions for case B under stiff fixation

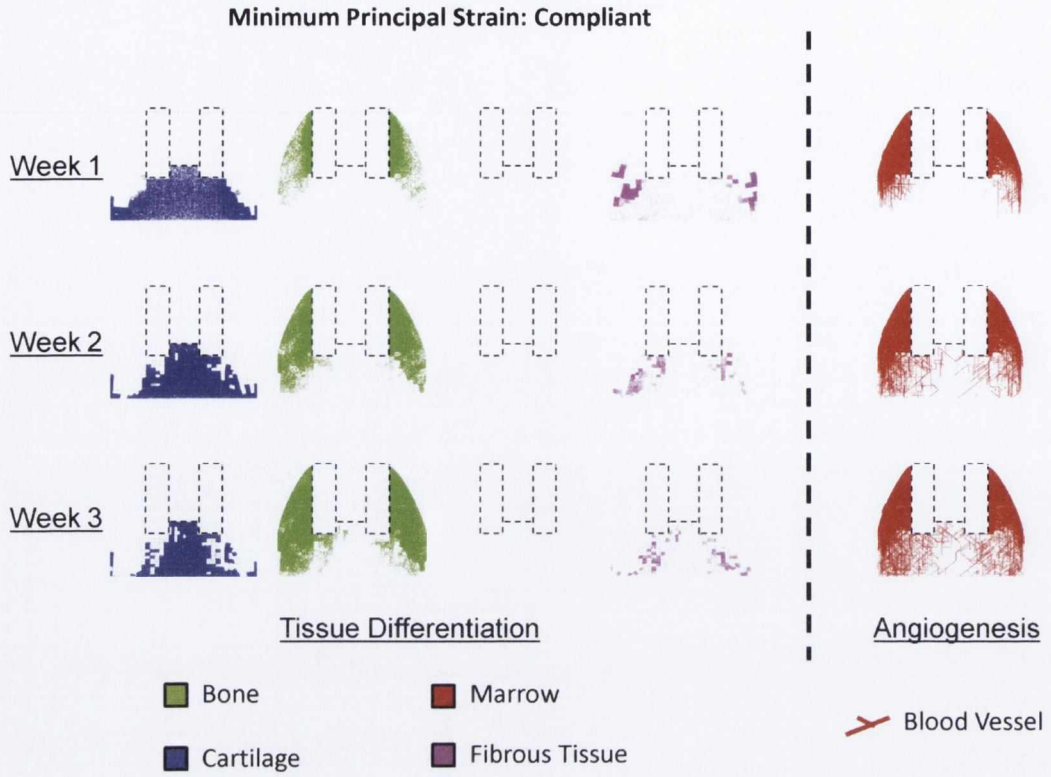

Figure 7-9. Tissue differentiation and angiogenesis predictions for case B under compliant fixation

7.3.3 Case C- direction of maximum principal strain

Vessels were also predicted to quickly fill the upper callus when implementing maximum principal strain as a guiding stimulus for blood vessel growth directionality (Figure 7-10 and Figure 7-11). However, vessels were biased to grow in a circumferential direction around the callus (or in z-direction (Figure 7-1 (A)) (i.e. into the page in the case of the 2 dimensional images presented). This bias was more prominent in the compliant case, with a lower number of vessels growing in a stochastic direction leading to a prediction of less vessels in both the total VOI and defect VOI compared to the stiff case. A significantly smaller number of vessels was predicted in both the total VOI and defect VOI in comparison to the first 2 cases presented (case A and case B) (Figure 7-6).

The major stages of healing were similar to that described for the first 2 cases, but healing was predicted to proceed at a slower pace (Figure 7-10 and Figure 7-11). Cartilage formation was predicted to be greater and to fill all regions below the fracture gap. Bone filled the upper callus rapidly but progression down the callus was significantly slower due to the slow progression

of blood vessels into the lower regions of the callus. This effect was even more prominent in the compliant case. No bony bridging was predicted for either the stiff of the compliant case at the 3 week time point. Greater bone and less cartilage were predicted for the stiff case compared to the compliant case (Figure 7-7).

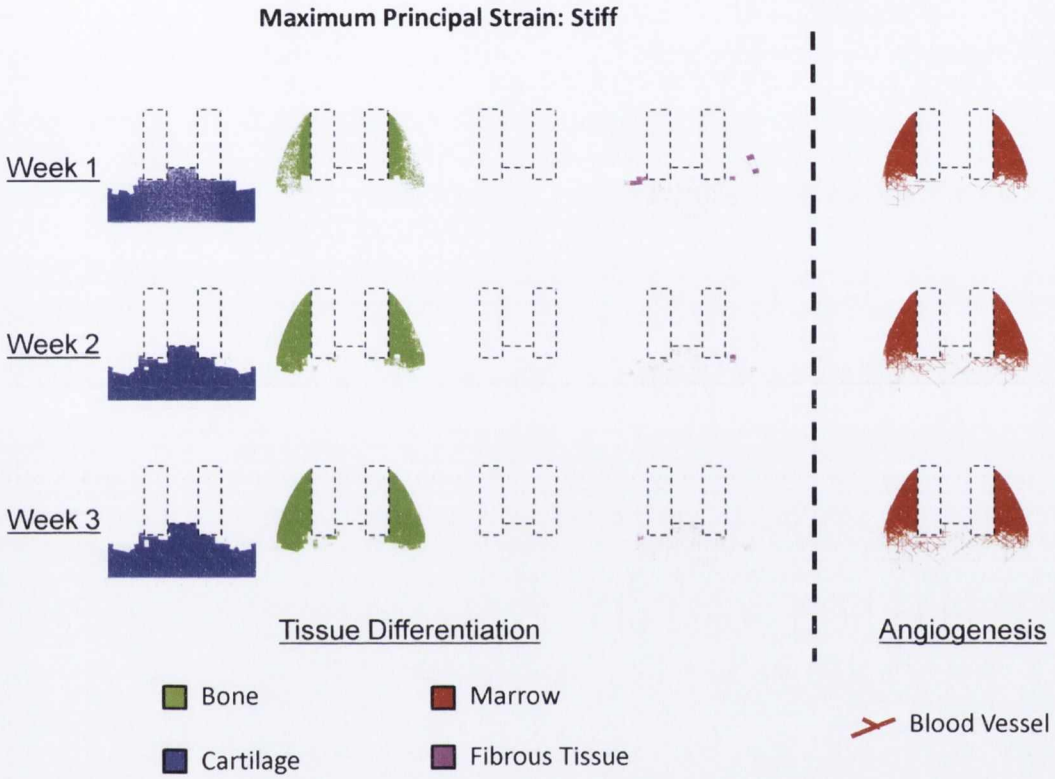

Figure 7-10. Tissue differentiation and angiogenesis predictions for case C under stiff fixation

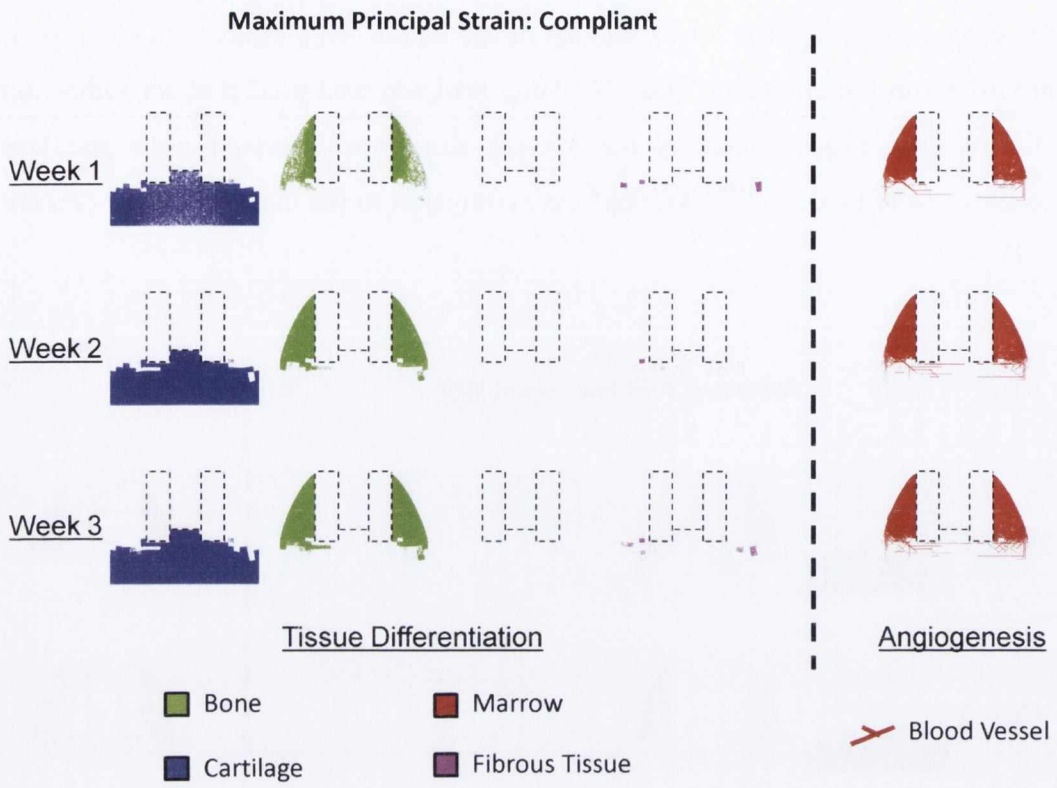

Figure 7-11. Tissue differentiation and angiogenesis predictions for case C under stiff fixation

7.3.4 Case D- perpendicular to maximum principal strain

In this case, vessels were again predicted to quickly fill the upper callus. Vessels slowly proceeded towards regions of the callus below the fracture gap (Figure 7-12 and Figure 7-13). A lower number of vessels was predicted in both the defect VOI and total VOI compared to case A and case B. Similar numbers of ECs were predicted in defect VOI and total VOIs under both compliant and stiff fixation conditions (Figure 7-6). Healing was predicted to proceed in a similar fashion to case C above. Greater bone and less cartilage were predicted in the stiff case compared to the compliant case (Figure 7-7).

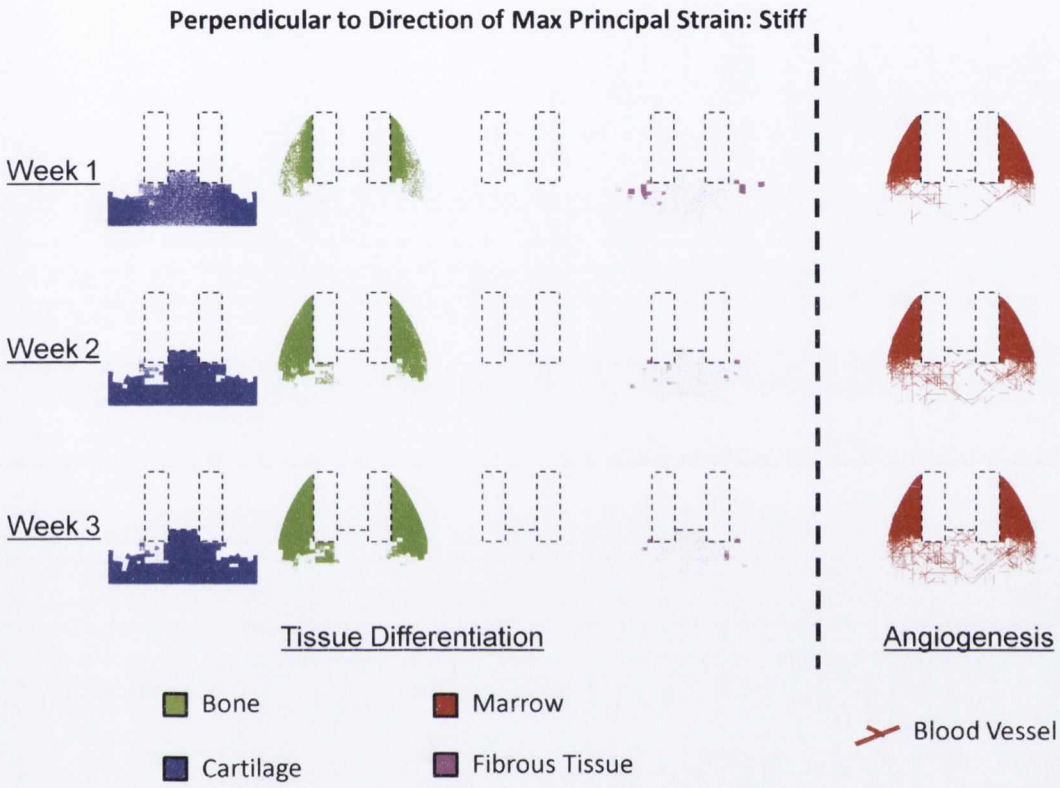

Figure 7-12. Tissue differentiation and angiogenesis predictions for case D under stiff fixation

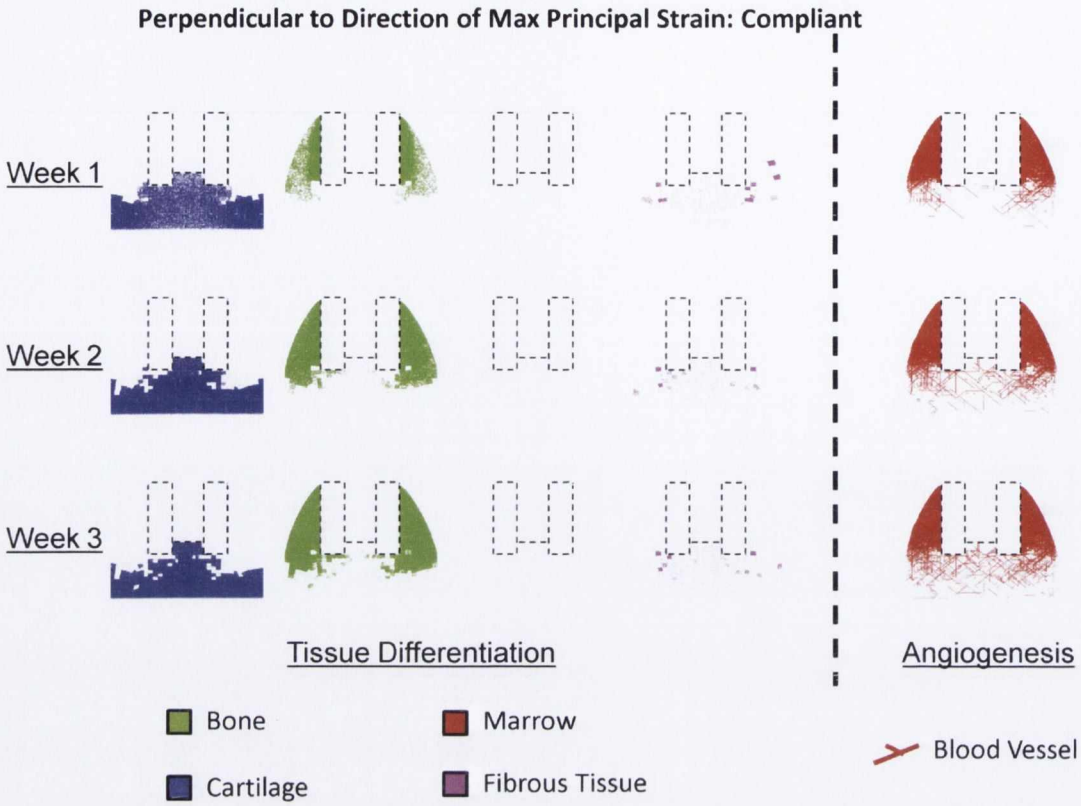

Figure 7-13. Tissue differentiation and angiogenesis predictions for case D under stiff fixation

7.4 Discussion

Angiogenesis is a vital process for nearly all tissue regeneration scenarios. Biochemical factors have long been implicated to regulate this process [46, 119], although it is increasingly recognized that mechanics may also be a key regulator of neovascularization [38, 41-43, 45, 150]. To date, a clear picture of how angiogenesis is mechano-regulated *in vivo* has yet to emerge. *In silico* studies can provide a framework for the investigation of scenarios that are often impractical to investigate using traditional *in vitro* or *in vivo* approaches. The objective of this study was to test the hypothesis that mechanical cues guide blood vessel directionality during tissue regeneration *in vivo*. This hypothesis was motivated by *in vitro* observations of the effect of mechanical strain on EC migration [42]. The hypothesis was tested by comparing simulation predictions with blood vessel growth direction regulated by various mechanical stimuli (direction of minimum principal strain, direction of maximum principal strain and any perpendicular direction to the direction of maximum principal strain) to the results of an

experimental study [40] which assessed the spatial patterns of neovascular formation in stabilized and unstabilized large bone defects.

Simulations with minimum principal strain guiding blood vessel growth directionality (case B) was the only case that lead to a prediction of a similar quantity of total VOI vascularization under both fixation conditions and a lesser amount of defect VOI vascularization under compliant fixation (Figure 7-6). This matches with experiential observations of angiogenesis. Under compliant fixation conditions, greater vessel death was predicted due to higher levels of strain within the callus, which reduced the number of vessels within the total VOI. However, this effect was compensated for through greater biased blood vessel migration towards the lower callus in the compliant case, where vessels aligned with the direction of minimum principal strain. This same effect lead to biased migration of blood vessels towards the outer periosteal callus in the complaint case (a region included in the total VOI but not in the defect VOI), hence the prediction of a lower vascularization in the defect VOI.

The random simulation (case A), with no mechano-regulation of blood vessel directionality (but with EC death in regions where the strain exceeded the threshold for viability), predicted a small decrease in the levels of vascularity in both the total VOI and defect VOI, which did not fully comply with what was observed experimentally (Figure 7-6). Greater vessel death occurred in both total and defect VOIs for the complaint case, and as there was no bias in blood vessel growth directionality, there was no compensatory effect (as in case A above), leading to decreases in angiogenesis within both VOIs. Dramatically lower number of vessels were predicted in both VOIs for the compliant model in case C (mechanical guiding stimulus in the direction of maximum principal strain), which again did not fully comply with what was observed experimentally (Figure 7-6). Greater bias in the direction of maximum principal strain led to vessels primarily being guided away from both VOIs in a circumferential direction. No significant differences in vascularity between compliant and stiff fixations were predicted for case D (mechanical guiding stimulus in a perpendicular direction to the maximum principal strain) which did not comply with the experimental data (Figure 7-6). In all cases (A-D) an increase in bone tissue fraction was predicted in the stiff case, with a corresponding decrease in cartilage tissue formation,

which complied with experimental findings Figure 7-7). This difference was greatest in the simulation with maximum principal strain directing blood vessel growth (case C), but only a very small difference was predicted in case D (blood vessel directionality biased in a direction perpendicular to the direction of maximum principal strain).

For case A (minimum principal strain direction), different patterns of bone formation were predicted for the compliant and stiff defects (Figure 7-4 and Figure 7-5). With a stiff fixator, the ossification front was predicted to move parallel to the fracture line towards the centre of the fracture. In the compliant case, the bone front initially bridges the external callus (due to the high strain magnitude guiding vessels to that location). The callus is then stabilized allowing more random vessel progression and bone formation in a direction perpendicular to the fracture line from the external callus towards the fracture gap and internal callus. Both patterns of bone regeneration have been described in the literature [7, 55, 151, 156, 251, 252], with the results of this study suggesting that differences in defect stability may be leading to changes in blood vessel growth directionality and hence, bone formation. The prediction of primarily soft tissues in the fracture gap under compliant fixation but some bone tissue under stiff fixation is also consistent with experimental observations [40].

The mechanism hypothesized in this study may also potentially explain, or partially explain, the potential beneficial effect of loading upon vascularization, and hence bone healing, observed in some cases in the literature. Low magnitude loading has been shown to be beneficial for blood vessel progression, whereas excessive loading has been shown to be inhibitory to angiogenesis [39]. It is speculated that mechanical loading, in magnitudes which do not cause vessel shearing, may preferentially direct vessels within the regenerating tissue in a more efficient manner than simple random vessel migration and hence may be beneficial to healing. In the case of secondary fracture healing, vessels could be guided towards the external periosteal callus during the early stages of loading. This would allow swift bony bridging of the external callus, stabilizing the fracture. Lower strains would then allow more random vessel progression with vessels penetrating the fracture gap and bone formation eventually filling in between the fracture ends.

There are a number of limitations associated with this study. Firstly, simplified callus and fixator geometry was assumed in this study. Secondly, the model contains many parameters obtained from the literature and includes some simplifications of complex biological processes such as cellular migration and proliferation which may result in some deviations in model predictions from experimental observations. All cell sizes are assumed to be exactly that of a lattice position which is not representative of the biological reality. The blood vessel growth rate was assumed to be constant which is potentially another simplification. Thirdly, the implanted hydrogel and the influence of BMP-2, which was included in the experimental study, and other growth factors was omitted in this study. Restricted MSC fate potential of precursor cells in this region and the influence of biochemical cues, which are not included in this model, are possible explanations for this deviation. It should also be noted that the values presented for tissue phenotype are fraction and angiogenesis are likely sensitive to the thresholds used in the angiogenesis model. For example, a lower probability of random blood vessel migration would likely cause greater deviations in predictions between compliant and stiff fixation conditions.

In spite of these limitations, this study provides evidence in favour of the hypothesis that blood vessel migration is biased in the direction of minimum principal strain *in vivo* during tissue regeneration. This was the only simulation set that could successfully predict experimentally measured differences in vascular volume between the stabilized and unstablilized defects. A model with inhibition alone (i.e. random vessel migration) could not fully predict these differences, strengthening the case for the alternative mechano-regulatory hypothesis proposed in this study. As such, the simulations demonstrate for the first time how angiogenesis might be mechano-regulated in a manner other than vessel inhibition or regulation of vessel growth rate. This study also subsequently, through successful prediction of the stages of fracture healing, provides support for the hypothesis that mechanical cues act indirectly (rather than directly) to regulate MSC differentiation through the mechano-regulation of blood vessel growth and hence oxygen supply in the regenerating tissue. Of course, the results of these simulations only provide preliminary support for the underlying model hypotheses. Future work will attempt further falsification of the hypothesis that

blood vessel growth directionality is biased in the direction of minimum principal strain. Spatial and temporal data describing vessel density will be required to attempt to validate model predictions.

Chapter8: Discussion

The primary objective of this thesis was to test the hypothesis that substrate stiffness and oxygen availability regulate stem cell differentiation during tissue regeneration. This was achieved by developing a computational framework capable of testing this hypothesis during multiple cases of tissue regeneration and by employing the principles of computational mechanobiology. An inherent assumption of this hypothesis is that mechanical signals act indirectly, rather than directly, to regulate MSC differentiation. Specifically, mechanics are assumed to regulate angiogenesis and hence the supply of oxygen and other nutrients to a regenerative site. As this thesis progressed, the computational framework was developed to more accurately depict mechano-regulated angiogenesis and mechanically guided blood vessel directionality in particular.

This chapter will firstly discuss the major findings of and methods employed during this thesis, both in terms of the global objective of this work and then in light of the sub objectives of the individual studies which were undertaken as part of this thesis. The tissue differentiation model is then discussed and compared with other well established regulatory hypotheses. Next, the limitations of the modeling framework as well as possible improvements and additions will be discussed. The chapter will conclude by highlighting the significance of the research undertaken as part of this thesis.

8.1 Major findings of this thesis

The first major challenge of this work was to develop the necessary computational tools to test the hypothesis that tissue differentiation is regulated by substrate stiffness and oxygen availability. A suitable regenerative scenario for attempted corroboration of this hypothesis also needed to be decided upon. Fracture healing was chosen as a first regenerative event for attempted corroboration of this hypothesis for a number of reasons. During fracture healing, MSCs may pursue multiple different phenotypes (e.g chondrocytes, fibroblasts, osteoblasts, adipocytes etc), with their fate regulated by local environmental cues. Fracture healing is an extensively studied regenerative event, with well established repeatable spatial and temporal patterns of tissue differentiation. For such reasons, it is commonly used to test *in silico* tissue differentiation hypotheses [6, 7, 9, 10, 22, 51]. As such, many aspects of model framework development were based upon previous mechanobiological frameworks. A diffusive model of cell migration and proliferation, a similar axisymmetric finite element model of a fracture callus, biphasic material properties and rule of mixtures were based on previous works [10, 167]. However, it was necessary to develop and integrate new models of angiogenesis and oxygen supply into the framework. It was also necessary to determine a set of quantitative rules for tissue differentiation based upon the substrate stiffness and oxygen stimuli.

Predictions of the computational model compared favorably with averaged histological images [55] for the different stages of fracture repair. Intramembranous ossification in the upper periosteal callus followed by progression of the bone front towards the fracture gap, cartilaginous bridging preceeding bony bridging, restoration of the marrow of the medullary cavity and final bone remodeling to restore bone to its original geometry were all successfully predicted by the model providing corroboration for the hypothesis that substrate stiffness and oxygen availability regulate MSC differentiation during fracture healing. However, predictions with tissue differentiation regulated by a shear strain and fluid velocity were also successful in predicting the major stages of fracture healing, demonstrating that multiple regulatory hypotheses can be corroborated for the fracture repair regenerative scenario. This motivated the

examination of a regenerative case where changes in tissue distribution occur without a change in the mechanical environment.

One example is fracture healing in Thrombonspondin-2 (TSP2)-null mice. Significant changes in healing pattern occur upon knockout of the TSP2 matricellular protein despite similar mechanical conditions to control animals. This represented an ideal regenerative case to test whether a tissue differentiation hypothesis regulated by substrate stiffness and oxygen availability could be predictive of such changes given a simple thought experiment could conclude that a solely mechanoregulatory tissue differentiation hypothesis could not predict these differences. As the *in vivo* effects of TSP2 deletion (which were possibly multiple and of a coupled nature) were unclear, a systematic investigation of five potential drivers of the changes in tissue differentiation was undertaken. The same model framework developed in the first study was applied to fracture repair in the mouse model and successfully predicted MSC differentiation patterns in the wild type (WT) case. Altering model parameters to coincide with the previously mentioned potential drivers generated five sets of model predictions, only one of which successfully predicted the experimentally observed changes in tissue differentiation upon TSP2 knockdown. The model identified increased angiogenic progression as a result of TSP2 deletion as the key driver of the altered healing pattern. Such a conclusion could not have been reached by employing a tissue differentiation hypothesis regulated solely by mechanical stimuli, providing greater support for the role of substrate stiffness and oxygen in the regulation of MSC differentiation. This study was the second case of fracture repair that the model was capable of predicting, providing further support for the underlying hypothesis. However, a robust test of a tissue differentiation hypothesis involves attempted falsification across multiple regenerative events. In the context of testing such tissue differentiation hypotheses with an *in silico* framework, the greater the number of regenerative scenarios in which the underlying model hypothesis is subjected to attempted falsifiability but ultimately corroborated, the stronger the hypothesis becomes.

The next study of this thesis tested the hypothesis that substrate stiffness and oxygen availability could predict MSC differentiation *in vivo* in a different regenerative event, the implanted bone chamber. The *in vivo* bone chamber was a

suitable regenerative scenario for testing the predictive capacity of the model a number of reasons. Advantageous properties included constant known geometry, known loading conditions and quantifiable spatial and temporal patterns of tissue differentiation [197]. The *in vivo* bone chamber has also been used previously for attempted falsification of other tissue differentiation hypotheses [15, 16] allowing comparison of model predictions to predictions with MSC fate regulated directly by mechanical stimuli. For this study, a lattice modeling approach replaced diffusive models of blood vessel growth and cell migration and proliferation. This approach allowed explicit and more accurate modeling of cells, cellular behavior and individual blood vessels. The addition of stochastic elements of such behaviours [139] was also enabled as a result of such an approach being adopted. Corroboration was achieved for both loaded and unloaded cases, including elements which could were not predicted by a well established tissue differentiation hypothesis regulated by shear strain and fluid velocity [16], such as prediction of marrow in both loading conditions and of fibrous tissue in unloaded conditions.

Having successfully corroborated the tissue differentiation model across 3 cases and 2 regenerative events, the indirect effects of mechanics on regulation of differentiation were further probed. The mechanical environment is known to alter tissue distribution patterns during *in vivo* regenerative events and this thesis hypothesizes that this is primarily due to mechano-regulation of angiogenesis (rather than a direct effect on differentiation) which in turn regulates the oxygen availability at a regenerating site. As such, the next study undertaken in this thesis investigated the effects of mechanical stimuli upon endothelial cell (EC) behavior in an *in vitro* study [42]. A lattice model was again adopted and employed in a novel way to explicitly model EC migration and proliferation. Model predictions provided a set of rules to describe EC behavior following the application of loading to a circular region of cells. Only predictions that included all 3 rules (increased migration and proliferation rates as well as biased migration perpendicular to applied strain) were predictive of the experimental data. These findings for how mechanics may regulate EC behaviour *in vitro* provided an insight into how mechanics might be regulating angiogenesis *in vivo*.

The final study of this thesis investigated the hypothesis that angiogenesis *in vivo* is directionally biased upon the application of mechanical strain. Chapter 6 of the thesis provided support for the hypothesis of biased endothelial cell migration in a direction "perpendicular" to the direction of applied strain in vitro in two dimensions, but this may have many possible meanings in the context of angiogenesis in three dimensions. Chapter 7 of the thesis explored the hypothesis that a specific mechanical stimulus is guiding blood vessel directionality *in vivo*. Simulations were performed with 3 potential mechanical guiding stimuli guiding regulating blood vessel growth directionality. Angiogenesis in the direction of minimum principal strain was the only guiding stimuli to successfully predict spatial blood vessel progression during large bone defect healing. This study, therefore, provided support for the hypothesis that blood vessel growth directionality is biased in the direction of minimum principal strain during tissue regeneration in the healing of stabilized and unstabilized fractures. It was thus demonstrated for the first time how mechano-regulation of angiogenesis, by a manner other than just vessel inhibition, can be incorporated into an *in silico* tissue differentiation framework to successfully predict *in vivo* quantative spatial blood vessel information for stable and unstable fracture repair. This updated modelling framework was also successful in accurately predicting the progression of healing in stabilized and unstabilized fracture repair. By doing so, this study also provided further support for the indirect role of mechanical signals in regulating MSC fate, in this case through the mechano-regulation of blood vessel growth directionality.

8.2 Comparisons to previous mechano-regulation models

8.2.1 Tissue differentiation model

The next section of the discussion will compare the tissue differentiation model framework developed and tested in this thesis to other well established models of tissue differentiation. As previously mentioned, within the context of testing tissue differentiation hypotheses with an *in silico* framework, the larger the number of scenarios in which the underlying model hypothesis is subjected to attempted falsifiability but ultimately corroborated, the stronger the hypothesis becomes. This work provides corroboration for the tissue differentiation model

regulated by substrate stiffness and oxygen availability for 4 cases across 2 regenerative events (fracture repair and the *in vivo* bone chamber), during both loaded and unloaded conditions providing strong initial support for this hypothesis. However, some well established algorithms have had corroboration provided across many more events. For example, the model of Prendergast and co-workers, in which differentiation is regulated by shear strain and fluid velocity, has been corroborated for a much greater number of regenerative events including fracture healing [9-11], osteochondral defect repair [12, 13], distraction osteogenesis [14], implanted bone chamber [15-17], neoarthrotis formation [18] and others [19-21]. The mechano-regulated theories of Carter and co workers and Claes and Heigele and co-workers have also been corroborated across multiple regenerative events including multiple cases of fracture repair, distraction osteogenesis and the implanted bone chamber [5, 7, 49, 182, 183, 185, 186, 189, 201]. Geris *et al* [191] have shown the mathematical model of by Bailon-Plaza and van der Meulen [142] could be further developed to be predictive of the semi-stabilized murine tibial fracture model corroborating the model, with differentiation regulated by growth factors, for the fracture healing regenerative scenario. Angiogenesis was further added to this bioregulatory model with successful prediction of compromised fracture healing situations [51, 144, 192]. There have also been cases where existing mechano-regulatory models were not predictive of experimental results.

The underlying model hypothesis developed in this thesis still has to be tested to the same extent as other well established models, but initial results are positive. The only direct comparison this model has had is with the model of Prendergast and co-workers, where differentiation is regulated by shear strain and fluid velocity, and in both cases (fracture healing and the bone chamber) the model has performed positively. In those regenerative cases, the model successfully predicted phenomena that the mechano-regulatory algorithm did not; including the prediction of fibrous tissue in the bone chamber or re-establishment of the marrow of the medullary cavity during fracture repair. In addition, no solely mechano-regulatory algorithm is capable of predicting the changes in tissue distribution upon deletion of the TSP2 matricellular protein in the murine model. Future work still remains to further test the hypothesis that substrate stiffness and

oxygen availability regulate MSC differentiation during tissue regeneration but strong initial support has been provided in this work.

8.2.2 Model of angiogenesis

One part of the modeling framework which was further investigated was the model of angiogenesis. With oxygen one of the key stimuli driving differentiation, the necessity for an accurate model of angiogenesis is obvious. Previous models of angiogenesis have been regulated by both biochemical growth factor stimuli [50, 51, 144, 146, 253] and also by mechanics [50, 53, 144]. Both blood vessel growth rate (including EC necrosis) and directionality have been influenced in such models. The initial model of angiogenesis included in the modeling framework developed at the beginning of this thesis was influenced only by inhibition of blood vessel growth in regions of high shear strain. Upon parameter variation investigations, it was found that predictions were best when this threshold was set at 6%. However it remains unclear as to whether angiogenesis is negatively affected by such low levels of strain [42, 43, 73, 128]. This motivated the hypothesis that possibly mechanics were affecting blood vessel growth through a second mechanism. This led to the development and ultimate corroboration of the hypothesis that blood vessel growth directionality is biased in the direction of minimum principal strain.

There is substantial evidence that biochemical effects also regulate blood vessel progression [46, 119-121, 123]. This work does however highlight a novel mechanism which plausibly regulates blood vessel growth directionality. However, this mechanism needs to be subjected to further investigation in order to provide greater corroboration and evidence in its favour. This work provides initial support in favour of the hypothesis that the direction of minimum principal strain acts as a mechanical guiding stimulus for directionality of neovascularization.

8.3 Model limitations

As with any computational modeling framework (or any study for that matter) there are limitations associated with the approaches taken and assumptions made.

There is also always potential for future improvement. This section discusses some to these limitations and possible improvements.

Firstly, the tissue differentiation modeling framework developed in this thesis does not include an explicit stimulus for fibrous tissue. It is possible that rather than fibrous tissue being a "default" tissue phenotype, fibrogenesis might occur in regions of low oxygen availability but where insufficient chondrogenic growth factors exist or in regions with a very high mechanical stimulus [5, 87]. It may be necessary to add a specific stimulus for fibrogenesis for future computational investigations of other regenerative scenarios such as MSC differentiation within osteochondral defect repair. Secondly, the model ignores the direct influence of mechanical stimuli upon differentiation. There is abundant *in vitro* [84, 87, 91] and *in silico* [5, 7, 8, 143, 192] evidence to support this direct influence. Mechanics is also believed to regulate processes such as chondrocyte hypertrophy and endochondral ossification [222, 254]. It is therefore likely that mechanics do influence differentiation directly, to some degree at least, but whether it's the dominant driver of differentiation is a question raised by the results of this thesis. This work also assumes that marrow formation occurs following a prediction of adipogenesis which is an oversimplification as bone marrow is a very complex tissue. It is recognized that the marrow of the medullary cavity of long bones contains not only the adipose tissue predicted by the tissue differentiation algorithm, but also hematopoietic and lymphatic cells among others. Such a simplification was implemented to enable to the testing of the hypothesis of the study without introducing additional complexity. The influences of biochemical cues such as growth factors are not included in the modeling framework in spite of numerous studies demonstrating the influence of such factors on both differentiation and angiogenesis [46, 51, 114-116]. The model of oxygen transport implemented in this study assumes a constant cellular oxygen consumption rate which has been shown not to be the case [213]. More complex models have been implemented [255, 256], however the objective of this work was to not to create a perfect model of oxygen transport and consumption but to implement a model with sufficient predictive abilities to allow us to examine the hypothesis at hand. In the current framework, cell migration and proliferation rates are constant. It is possible that such rates are dependent on

environmental factors such as oxygen availability [257], growth factors [258] and mechanical stimuli [11, 239].

8.4 Summary

In spite of such limitations, the results of this work provide strong evidence to support the hypothesis that stem cell differentiation is regulated by substrates stiffness and oxygen availability *in vivo.* It is extremely difficult to design and perform *in vivo* studies to accurately isolate and relate specific stimuli, such as those identified in previously mentioned *in vitro* studies, to the temporal and spatial patterns of tissue differentiation that occur during regenerative events. *In silico* studies such as those performed in this thesis, however, can be used to predict the state of the local environment experienced by MSCs during complex regenerative scenarios. As such, hypotheses for how MSC differentiation is regulated *in vivo* can be either corroborated or rejected based on the ability of *in silico* models to accurately predict spatial and temporal patterns of tissue differentiation observed experimentally [5, 7, 8, 10, 12, 16, 49, 201]. Such corroboration and/or rejection provide improved understanding of the regulation of MSC physiology. The therapeutic potential of MSCs is substantial. MSCs therapies could provide potential treatment opportunities for osteoarthritis, chondral defects, fracture repair, bone and cartilage tissue engineering. The model developed in this work thesis enhances current knowledge and understanding of MSC behaviour. The model could also be used to provide valuable predictions of how potential treatment options (such as the addition of MSCs to a fracture site which may be susceptible to delayed or non-union in different quantities and at different stages of healing) may alter healing. Research such as this will bring us closer to exploiting the full potential of MSC therapies in regenerative medicine.

Chapter9: Conclusions and future directions

9.1 Conclusions

The primary objective of this thesis was to test the hypothesis that substrate stiffness and oxygen availability regulate stem cell differentiation during tissue regeneration. At the heart of this hypothesis, mechanical stimuli (which have long been implicated as having a direct role in the regulation of MSC differentiation [5, 7, 8]) were assumed to have only an indirect role in directing stem cell fate through the mechano-regulation of angiogenesis. As part of this thesis, a number of studies were designed to test this hypothesis leading to the following conclusions:

- A novel bioregulatory computational framework was successfully developed to test the hypothesis that MSC differentiation is regulated by substrate stiffness and oxygen availability
- This model was initially corroborated by successfully predicting the temporal and spatial patterns of tissue differentiation during fracture repair
- The model identified increased angiogenic progression as the key driver of significant changes in tissue phenotype observed upon the deletion of the Thromospondin-2 (TSP2) protein in mice
- The previously simplified diffusive models of angiogenesis and cell migration and proliferation were replaced by lattice modeling techniques which allowed explicit modeling of individual cells and aspects of cell physiology as well as explicit modeling of individual blood vessels and vessel network morphology
- The model was further corroborated by successfully predicting the major tissue structures and morphologies under both loaded and unloaded conditions in an implanted bone chamber.
- Predictions from a computational model, which employed lattice techniques in a novel way to explicity model endothelial cell (EC) physiology, provided support for the hypothesis that dynamic strain

increases both EC migration and proliferation, and that EC migration directionality is biased in the direction perpendicular to applied strain

- Further development of the model of angiogenesis allowed the hypothesis that a mechanical stimulus regulates blood vessel growth directionality *in vivo* to be tested in stabilized and unstablized fracture repair
- Corroboration was provided for the hypothesis that minimum principal strain regulated blood vessel growth directionality during stabilized and unstabilized fracture repair

9.2 Future Directions

The modeling framework developed in this thesis provides strong initial support for the hypothesis that MSC differentiation during tissue regeneration is regulated by substrate stiffness and oxygen availability. This work also provides support for the hypothesis that mechanical stimulation primarily influences stem cell fate indirectly via the mechanoregulation of neovascularization. However, there are more studies that may be undertaken in order to further probe such hypotheses:

- Distraction osteogenesis is a suitable regenerative event for the testing of the bioregulatory model developed in this thesis. Temporal and spatial experimental data of tissue differentiation patterns is available for assessment of validation of *in silico* predictions. Multiple mechanoregulatory models have already been corroborated for this regenerative situation [14, 141]. Comparisons of the predictive capabilities of different regulatory models provide valuable information which can be used to decipher the key drivers of MSC differentiation *in vivo*
- Another suitable regenerative event for attempted corroboration of the existing hypothesis is tissue differentiation within osteochondral defect repair. The well established tissue differentiation model of Prendergast and co-workers has successfully been corroborated for this event [12]. The application of the existing model to such a regenerative event could provide valuable further insights into its predictive ability and provide comparison to a model regulated by direct mechanical stimuli

- There is experimental data available that demonstrates changes in tissue distributions in fractures of different gap sizes, even if the interfragmentary strain (IFS) remains similar [73]. This is an interesting finding and another suitable regenerative scenario for attempted falsification of the hypothesis at hand. The application of the existing tissue differentiation model to such a regenerative event could provide another assessment of its predictive power
- There are also many other specific cases of regenerative events which are suitable for investigation of the tissue differentiation hypothesis presented in this thesis via computational mechano-biological approaches. Different cases of the implanted bone chamber [17, 53], cases of non-union in fracture healing [192], torsionally loaded fractures [189] and healing of oblique fractures [49] are examples of cases which have been used in the testing of other regulatory theories
- Further attempted falsification of the hypothesis that blood vessel growth directionality is biased in the direction of minimum principal strain can be undertaken by applying the existing model to other regenerative scenarios. Spatial and temporal data describing vessel density would be required to compare with model predictions
- The modeling framework itself could be enhanced to include aspects of cell physiology not included in the current simulations. Potential inclusions are the effect on cell proliferation and migration rates of oxygen availability [257] or mechanical stimulation [12]. Other potential inclusions are cell apoptosis in regions where zero oxygen is predicted and cell specific oxygen consumption rates. The model currently allows cell doublings which has been shown to be untrue (This is potentially an important factor in atrophic non-union). As previously mentioned in Section 8.3, a specific stimulus for fibrous tissue is also a potential inclusion to the model
- Further studies could be performed to potentially investigate the role of factors other than mechanics, such as VEGF [46] or hypoxia [243], in regulating blood vessel growth rates and directionality

- The model could be expanded to investigate other important aspects of cell differentiation, such as hypertrophy. Cases where differences in rates of chondrocyte hypertrophy are observed and suspected to ultimately influence differentiation patterns [178]. Potential stimuli which may regulate hypertrophy such as oxygen availability [220] could be investigated

Bibliography

1. Popper, K., *Conjectures and Refutations, London: Routledge and Keagan Paul, 1963, pp. 33-39.* Reading in the Philosophy Science, ed. T. Schick. 2000, Mountain View: CA: Mayfield Publishing Company. 2000, pp. 9-13.

2. Heppenstall, R.B., G. Grislis, and T.K. Hunt, *Tissue gas tensions and oxygen consumption in healing bone defects.* Clinical Orthopaedics and Related Research, 1975(106): p. 357-65.

3. Pauwels, F., *[A new theory on the influence of mechanical stimuli on the differentiation of supporting tissue. The tenth contribution to the functional anatomy and causal morphology of the supporting structure].* Z Anat Entwicklungsgesch, 1960. **121**: p. 478-515.

4. van der Meulen, M.C. and R. Huiskes, *Why mechanobiology? A survey article.* Journal of Biomechanics, 2002. **35**(4): p. 401-14.

5. Carter, D.R., P.R. Blenman, and G.S. Beaupre, *Correlations between mechanical stress history and tissue differentiation in initial fracture healing.* J Orthop Res, 1988. **6**(5): p. 736-48.

6. Carter, D.R., G.S. Beaupre, N.J. Giori, and J.A. Helms, *Mechanobiology of skeletal regeneration.* Clin Orthop Relat Res, 1998(355 Suppl): p. S41-55.

7. Claes, L.E. and C.A. Heigele, *Magnitudes of local stress and strain along bony surfaces predict the course and type of fracture healing.* J Biomech, 1999. **32**(3): p. 255-66.

8. Prendergast, P.J., R. Huiskes, and K. Soballe, *ESB Research Award 1996. Biophysical stimuli on cells during tissue differentiation at implant interfaces.* J Biomech, 1997. **30**(6): p. 539-48.

9. Isaksson, H., W. Wilson, C.C. van Donkelaar, R. Huiskes, and K. Ito, *Comparison of biophysical stimuli for mechano-regulation of tissue differentiation during fracture healing.* J Biomech, 2006. **39**(8): p. 1507-16.

10. Lacroix, D. and P.J. Prendergast, *A mechano-regulation model for tissue differentiation during fracture healing: analysis of gap size and loading.* J Biomech, 2002. **35**(9): p. 1163-71.

11. Byrne, D.P., D. Lacroix, and P.J. Prendergast, *Simulation of fracture healing in the tibia: Mechanoregulation of cell activity using a lattice modeling approach.* J Orthop Res, 2011.

12. Kelly, D.J. and P.J. Prendergast, *Mechano-regulation of stem cell differentiation and tissue regeneration in osteochondral defects.* Journal of Biomechanics, 2005. **38**(7): p. 1413-1422.

13. Kelly, D.J. and P.J. Prendergast, *Prediction of the optimal mechanical properties for a scaffold used in osteochondral defect repair.* Tissue Engineering, 2006. **12**(9): p. 2509-2519.

14. Isaksson, H., O. Comas, C.C. van Donkelaar, J. Mediavilla, W. Wilson, R. Huiskes, and K. Ito, *Bone regeneration during distraction osteogenesis: mechano-regulation by shear strain and fluid velocity.* Journal of Biomechanics, 2007. **40**(9): p. 2002-11.

15. Khayyeri, H., S. Checa, M. Tagil, P. Aspenberg, and P.J. Prendergast, *Variability observed in mechano-regulated in vivo tissue differentiation can be explained by variation in cell mechano-sensitivity.* Journal of Biomechanics, 2011. **44**(6): p. 1051-8.

16. Khayyeri, H., S. Checa, M. Tagil, and P.J. Prendergast, *Corroboration of mechanobiological simulations of tissue differentiation in an in vivo bone chamber using a lattice-modeling approach.* J Orthop Res, 2009. **27**(12): p. 1659-66.

17. Geris, L., A. Andreykiv, H. Van Oosterwyck, J.V. Sloten, F. van Keulen, J. Duyck, and I. Naert, *Numerical simulation of tissue differentiation around loaded titanium implants in a bone chamber.* Journal of Biomechanics, 2004. **37**(5): p. 763-9.

18. Nagel, T. and D.J. Kelly, *Mechano-regulation of mesenchymal stem cell differentiation and collagen organisation during skeletal tissue repair.* Biomech Model Mechanobiol, 2010. **9**(3): p. 359-72.

19. Boccaccio, A., D.J. Kelly, and C. Pappalettere, *A mechano-regulation model of fracture repair in vertebral bodies.* J Orthop Res, 2011. **29**(3): p. 433-43.

20. Boccaccio, A., P.J. Prendergast, C. Pappalettere, and D.J. Kelly, *Tissue differentiation and bone regeneration in an osteotomized mandible: A computational analysis of the latency period.* Medical and Biological Engineering and Computing, 2008. **46**(3): p. 283-298.

21. Sandino, C., S. Checa, P.J. Prendergast, and D. Lacroix, *Simulation of angiogenesis and cell differentiation in a CaP scaffold subjected to compressive strains using a lattice modeling approach.* Biomaterials, 2010. **31**(8): p. 2446-52.

22. Vetter, A., F. Witt, O. Sander, G.N. Duda, and R. Weinkamer, *The spatio-temporal arrangement of different tissues during bone healing as a result of simple mechanobiological rules.* Biomech Model Mechanobiol, 2011.

23. Gomez-Benito, M.J., J.M. Garcia-Aznar, J.H. Kuiper, and M. Doblare, *Influence of fracture gap size on the pattern of long bone healing: a computational study.* J Theor Biol, 2005. **235**(1): p. 105-19.

24. Engler, A.J., S. Sen, H.L. Sweeney, and D.E. Discher, *Matrix Elasticity Directs Stem Cell Lineage Specification.* Cell, 2006. **126**(4): p. 677-689.

25. Guvendiren, M. and J.A. Burdick, *Stiffening hydrogels to probe short- and long-term cellular responses to dynamic mechanics.* Nature communications, 2012. **3**: p. 792.

26. Dupont, S., L. Morsut, M. Aragona, E. Enzo, S. Giulitti, M. Cordenonsi, F. Zanconato, J. Le Digabel, M. Forcato, S. Bicciato, et al., *Role of YAP/TAZ in mechanotransduction.* Nature, 2011. **474**(7350): p. 179-83.

27. Holzwarth, C., M. Vaegler, F. Gieseke, S.M. Pfister, R. Handgretinger, G. Kerst, and I. Muller, *Low physiologic oxygen tensions reduce proliferation and differentiation of human multipotent mesenchymal stromal cells.* BMC Cell Biol, 2010. **11**: p. 11.

28. Fehrer, C., R. Brunauer, G. Laschober, H. Unterluggauer, S. Reitinger, F. Kloss, C. Gully, R. Gassner, and G. Lepperdinger, *Reduced oxygen tension*

attenuates differentiation capacity of human mesenchymal stem cells and prolongs their lifespan. Aging Cell, 2007. **6**(6): p. 745-57.

29. Yun, Z., H.L. Maecker, R.S. Johnson, and A.J. Giaccia, *Inhibition of PPAR[gamma]2 Gene Expression by the HIF-1-Regulated Gene DEC1/Stra13: A Mechanism for Regulation of Adipogenesis by Hypoxia.* Developmental Cell, 2002. **2**(3): p. 331-341.

30. Kanichai, M., D. Ferguson, P.J. Prendergast, and V.A. Campbell, *Hypoxia promotes chondrogenesis in rat mesenchymal stem cells: a role for AKT and hypoxia-inducible factor (HIF)-1alpha.* J Cell Physiol, 2008. **216**(3): p. 708-15.

31. Meyer, E.G., C.T. Buckley, S.D. Thorpe, and D.J. Kelly, *Low oxygen tension is a more potent promoter of chondrogenic differentiation than dynamic compression.* J Biomech, 2010. **43**(13): p. 2516-23.

32. Hirao, M., N. Tamai, N. Tsumaki, H. Yoshikawa, and A. Myoui, *Oxygen tension regulates chondrocyte differentiation and function during endochondral ossification.* J Biol Chem, 2006. **281**(41): p. 31079-92.

33. Taylor, D.K., J.A. Meganck, S. Terkhorn, R. Rajani, A. Naik, R.J. O'Keefe, S.A. Goldstein, and K.D. Hankenson, *Thrombospondin-2 influences the proportion of cartilage and bone during fracture healing.* J Bone Miner Res, 2009. **24**(6): p. 1043-54.

34. Hente, R., B. Fuchtmeier, U. Schlegel, A. Ernstberger, and S.M. Perren, *The influence of cyclic compression and distraction on the healing of experimental tibial fractures.* J Orthop Res, 2004. **22**(4): p. 709-15.

35. Weitzel, P.P. and J.L. Esterhai, Jr., eds. *Delayed union, nonunion and synovial pseudarthrosis*. Bone Formation and Repair, ed. C.T. Brighton, G.E. Friedlaender, and J.M. Lane. 1994, AAOS: Rosmount, IL. 505-527.

36. Rhinelander, F.W., *The normal microcirculation of diaphyseal cortex and its response to fracture.* J Bone Joint Surg Am, 1968. **50**(4): p. 784-800.

37. Lienau, J., H. Schell, G.N. Duda, P. Seebeck, S. Muchow, and H.J. Bail, *Initial vascularization and tissue differentiation are influenced by fixation stability.* J Orthop Res, 2005. **23**(3): p. 639-45.

38. Rhinelander, F.W., *Tibial blood supply in relation to fracture healing.* Clin Orthop Relat Res, 1974(105): p. 34-81.

39. Qiu, J., Chen, H-B., Chu, T-W., Zhang L., *Different compressive stress and the expression of local vascularization factor in fracture healing.* Chinese Journal of clinical rehabilitation, 2006. **10**(5): p. 56-58.

40. Boerckel, J.D., B.A. Uhrig, N.J. Willett, N. Huebsch, and R.E. Guldberg, *Mechanical regulation of vascular growth and tissue regeneration in vivo.* Proc Natl Acad Sci U S A, 2011. **108**(37): p. E674-80.

41. Von Offenberg Sweeney, N., P.M. Cummins, E.J. Cotter, P.A. Fitzpatrick, Y.A. Birney, E.M. Redmond, and P.A. Cahill, *Cyclic strain-mediated regulation of vascular endothelial cell migration and tube formation.* Biochemical and Biophysical Research Communications, 2005. **329**(2): p. 573-82.

42. Matsumoto, T., Y.C. Yung, C. Fischbach, H.J. Kong, R. Nakaoka, and D.J. Mooney, *Mechanical strain regulates endothelial cell patterning in vitro.* Tissue Engineering, 2007. **13**(1): p. 207-17.

43. Krishnan, L., C.J. Underwood, S. Maas, B.J. Ellis, T.C. Kode, J.B. Hoying, and J.A. Weiss, *Effect of mechanical boundary conditions on orientation of angiogenic microvessels.* Cardiovascular research, 2008. **78**(2): p. 324-32.

44. Kilarski, W.W., B. Samolov, L. Petersson, A. Kvanta, and P. Gerwins, *Biomechanical regulation of blood vessel growth during tissue vascularization.* Nature medicine, 2009. **15**(6): p. 657-64.

45. Yan, Z.Q., Y.Q. Li, B.B. Cheng, Q.P. Yao, L.Z. Gao, Q.C. Gao, X.B. Gong, Y.X. Qi, and Z.L. Jiang, *Effects of stretched vascular endothelial cells and smooth muscle cells on differentiation of endothelial progenitor cellss.* Journal of Mechanics in Medicine and Biology, 2013. **13**(2).

46. Street, J., M. Bao, L. deGuzman, S. Bunting, F.V. Peale, Jr., N. Ferrara, H. Steinmetz, J. Hoeffel, J.L. Cleland, A. Daugherty, et al., *Vascular endothelial growth factor stimulates bone repair by promoting angiogenesis and bone turnover.* Proc Natl Acad Sci U S A, 2002. **99**(15): p. 9656-61.

47. Knighton, D.R., Silver, I.A., Hunt, T.K., *Regulation of wound-healing angiogenesis- Effect of oxygen gradients and inspired oxygen concentration.* Surgery, 1981. **90**(2): p. 262-270.

48. Hulth, A., *Current concepts of fracture healing.* Clin Orthop Relat Res, 1989(249): p. 265-84.

49. Loboa, E.G., G.S. Beaupre, and D.R. Carter, *Mechanobiology of initial pseudarthrosis formation with oblique fractures.* Journal of orthopaedic research : official publication of the Orthopaedic Research Society, 2001. **19**(6): p. 1067-72.

50. Checa, S. and P.J. Prendergast, *A mechanobiological model for tissue differentiation that includes angiogenesis: a lattice-based modeling approach.* Ann Biomed Eng, 2009. **37**(1): p. 129-45.

51. Geris, L., A. Gerisch, J.V. Sloten, R. Weiner, and H.V. Oosterwyck, *Angiogenesis in bone fracture healing: a bioregulatory model.* J Theor Biol, 2008. **251**(1): p. 137-58.

52. Chen, G., F. Niemeyer, T. Wehner, U. Simon, M.A. Schuetz, M.J. Pearcy, and L.E. Claes, *Simulation of the nutrient supply in fracture healing.* J Biomech, 2009. **42**(15): p. 2575-83.

53. Geris, L., K. Vandamme, I. Naert, J. Vander Sloten, H. Van Oosterwyck, and J. Duyck, *Mechanical loading affects angiogenesis and osteogenesis in an in vivo bone chamber: a modeling study.* Tissue Eng Part A, 2010. **16**(11): p. 3353-61.

54. Buckley, C.T., T. Vinardell, and D.J. Kelly, *Oxygen tension differentially regulates the functional properties of cartilaginous tissues engineered from infrapatellar fat pad derived MSCs and articular chondrocytes.* Osteoarthritis and Cartilage, 2010. **18**(10): p. 1345-1354.

55. Vetter, A., D.R. Epari, R. Seidel, H. Schell, P. Fratzl, G.N. Duda, and R. Weinkamer, *Temporal tissue patterns in bone healing of sheep.* J Orthop Res, 2010. **28**(11): p. 1440-7.

56. Khayyeri, H., H. Isaksson, and P.J. Prendergast, *Corroboration of computational models for mechanoregulated stem cell differentiation.* Computer methods in biomechanics and biomedical engineering, 2013.

57. Pittenger, M.F., A.M. Mackay, S.C. Beck, R.K. Jaiswal, R. Douglas, J.D. Mosca, M.A. Moorman, D.W. Simonetti, S. Craig, and D.R. Marshak, *Multilineage Potential of Adult Human Mesenchymal Stem Cells.* Science, 1999. **284**(5411): p. 143-147.

58. Friedenstein, A.J., U.F. Deriglasova, N.N. Kulagina, A.F. Panasuk, S.F. Rudakowa, E.A. Luria, and I.A. Ruadkow, *Precursors for fibroblasts in different populations of hematopoietic cells as detected by the in vitro colony assay method.* Exp Hematol, 1974. **2**(2): p. 83-92.

59. Caplan, A.I., *The mesengenic process.* Clin Plast Surg, 1994. **21**(3): p. 429-35.

60. Park, J.S., J.S. Chu, A.D. Tsou, R. Diop, Z. Tang, A. Wang, and S. Li, *The effect of matrix stiffness on the differentiation of mesenchymal stem cells in response to TGF-beta.* Biomaterials, 2011. **32**(16): p. 3921-30.

61. Pek, Y.S., A.C. Wan, and J.Y. Ying, *The effect of matrix stiffness on mesenchymal stem cell differentiation in a 3D thixotropic gel.* Biomaterials, 2010. **31**(3): p. 385-91.

62. McBeath, R., D.M. Pirone, C.M. Nelson, K. Bhadriraju, and C.S. Chen, *Cell shape, cytoskeletal tension, and RhoA regulate stem cell lineage commitment.* Dev Cell, 2004. **6**(4): p. 483-95.

63. Caplan, A.I., *Mesenchymal stem cells.* J Orthop Res, 1991. **9**(5): p. 641-50.

64. Prendergast, P.J., *Finite element models in tissue mechanics and orthopaedic implant design.* Clin Biomech (Bristol, Avon), 1997. **12**(6): p. 343-366.

65. Krinner, A., M. Zscharnack, A. Bader, D. Drasdo, and J. Galle, *Impact of oxygen environment on mesenchymal stem cell expansion and chondrogenic differentiation.* Cell Prolif, 2009. **42**(4): p. 471-84.

66. Yu, Y.Y., S. Lieu, C. Lu, and C. Colnot, *Bone morphogenetic protein 2 stimulates endochondral ossification by regulating periosteal cell fate during bone repair.* Bone, 2010. **47**(1): p. 65-73.

67. Panjabi, M.M., A.A. White, 3rd, and J.W. Wolf, Jr., *A biomechanical comparison of the effects of constant and cyclic compression on fracture healing in rabbit long bones.* Acta orthopaedica Scandinavica, 1979. **50**(6 Pt 1): p. 653-61.

68. Goodship, A.E. and J. Kenwright, *The influence of induced micromovement upon the healing of experimental tibial fractures.* The Journal of bone and joint surgery. British volume, 1985. **67**(4): p. 650-5.

69. Augat, P., K. Margevicius, J. Simon, S. Wolf, G. Suger, and L. Claes, *Local tissue properties in bone healing: influence of size and stability of the osteotomy gap.* J Orthop Res, 1998. **16**(4): p. 475-81.

70. Park, S.H., K. O'Connor, H. McKellop, and A. Sarmiento, *The influence of active shear or compressive motion on fracture-healing.* The Journal of bone and joint surgery. American volume, 1998. **80**(6): p. 868-78.

71. Weinans, H. and P.J. Prendergast, *Tissue adaptation as a dynamical process far from equilibrium.* Bone, 1996. **19**(2): p. 143-9.

72. Perren, S.M., *Physical and biological aspects of fracture healing with special reference to internal fixation.* Clin Orthop Relat Res, 1979(138): p. 175-96.

73. Claes, L., P. Augat, G. Suger, and H.J. Wilke, *Influence of size and stability of the osteotomy gap on the success of fracture healing.* J Orthop Res, 1997. **15**(4): p. 577-84.

74. Ingber, D.E., *Integrins, tensegrity, and mechanotransduction.* Gravitational and space biology bulletin : publication of the American Society for Gravitational and Space Biology, 1997. **10**(2): p. 49-55.

75. Huebsch, N., P.R. Arany, A.S. Mao, D. Shvartsman, O.A. Ali, S.A. Bencherif, J. Rivera-Feliciano, and D.J. Mooney, *Harnessing traction-mediated manipulation of the cell/matrix interface to control stem-cell fate.* Nature materials, 2010. **9**(6): p. 518-26.

76. Ingber, D.E., *Cellular mechanotransduction: putting all the pieces together again.* FASEB journal : official publication of the Federation of American Societies for Experimental Biology, 2006. **20**(7): p. 811-27.

77. Hoey, D.A., M.E. Downs, and C.R. Jacobs, *The mechanics of the primary cilium: an intricate structure with complex function.* Journal of Biomechanics, 2012. **45**(1): p. 17-26.

78. Muhammad, H., Y. Rais, N. Miosge, and E.M. Ornan, *The primary cilium as a dual sensor of mechanochemical signals in chondrocytes.* Cellular and molecular life sciences : CMLS, 2012. **69**(13): p. 2101-7.

79. Hoey, D.A., S. Tormey, S. Ramcharan, F.J. O'Brien, and C.R. Jacobs, *Primary cilia-mediated mechanotransduction in human mesenchymal stem cells.* STEM CELLS, 2012. **30**(11): p. 2561-70.

80. Donahue, H.J., *Gap junctions and biophysical regulation of bone cell differentiation.* Bone, 2000. **26**(5): p. 417-22.

81. Hirschi, K.K., J.M. Burt, K.D. Hirschi, and C. Dai, *Gap junction communication mediates transforming growth factor-beta activation and endothelial-induced mural cell differentiation.* Circulation research, 2003. **93**(5): p. 429-37.

82. Jiang, J.X., A.J. Siller-Jackson, and S. Burra, *Roles of gap junctions and hemichannels in bone cell functions and in signal transmission of mechanical stress.* Frontiers in bioscience : a journal and virtual library, 2007. **12**: p. 1450-62.

83. Janssen, D.A., J.G. Hoenderop, K.C. Jansen, A.W. Kemp, J.P. Heesakkers, and J.A. Schalken, *The mechanoreceptor TRPV4 is localized in adherence junctions of the human bladder urothelium: a morphological study.* The Journal of urology, 2011. **186**(3): p. 1121-7.

84. Takahashi, I., G.H. Nuckolls, K. Takahashi, O. Tanaka, I. Semba, R. Dashner, L. Shum, and H.C. Slavkin, *Compressive force promotes sox9, type II collagen and aggrecan and inhibits IL-1beta expression resulting in chondrogenesis in mouse embryonic limb bud mesenchymal cells.* J Cell Sci, 1998. **111 (Pt 14)**: p. 2067-76.

85. Campbell, J.J., D.A. Lee, and D.L. Bader, *Dynamic compressive strain influences chondrogenic gene expression in human mesenchymal stem cells.* Biorheology, 2006. **43**(3-4): p. 455-70.

86. Mouw, J.K., J.T. Connelly, C.G. Wilson, K.E. Michael, and M.E. Levenston, *Dynamic compression regulates the expression and synthesis of chondrocyte-specific matrix molecules in bone marrow stromal cells.* STEM CELLS, 2007. **25**(3): p. 655-63.

87. Haudenschild, A.K., A.H. Hsieh, S. Kapila, and J.C. Lotz, *Pressure and distortion regulate human mesenchymal stem cell gene expression.* Ann Biomed Eng, 2009. **37**(3): p. 492-502.

88. Day, T.F., X. Guo, L. Garrett-Beal, and Y. Yang, *Wnt/beta-catenin signaling in mesenchymal progenitors controls osteoblast and chondrocyte differentiation during vertebrate skeletogenesis.* Developmental Cell, 2005. **8**(5): p. 739-50.

89. Sumanasinghe, R.D., S.H. Bernacki, and E.G. Loboa, *Osteogenic differentiation of human mesenchymal stem cells in collagen matrices: effect of uniaxial cyclic tensile strain on bone morphogenetic protein (BMP-2) mRNA expression.* Tissue Engineering, 2006. **12**(12): p. 3459-65.

90. Knippenberg, M., M.N. Helder, B. Zandieh Doulabi, P.I. Wuisman, and J. Klein-Nulend, *Osteogenesis versus chondrogenesis by BMP-2 and BMP-7 in adipose stem cells.* Biochemical and Biophysical Research Communications, 2006. **342**(3): p. 902-8.

91. Li, Y.J., N.N. Batra, L. You, S.C. Meier, I.A. Coe, C.E. Yellowley, and C.R. Jacobs, *Oscillatory fluid flow affects human marrow stromal cell proliferation and differentiation.* Journal of orthopaedic research : official publication of the Orthopaedic Research Society, 2004. **22**(6): p. 1283-9.

92. Arnsdorf, E.J., P. Tummala, R.Y. Kwon, and C.R. Jacobs, *Mechanically induced osteogenic differentiation--the role of RhoA, ROCKII and cytoskeletal dynamics.* Journal of cell science, 2009. **122**(Pt 4): p. 546-53.

93. Woods, A., G. Wang, and F. Beier, *RhoA/ROCK signaling regulates Sox9 expression and actin organization during chondrogenesis.* The Journal of biological chemistry, 2005. **280**(12): p. 11626-34.

94. Arnsdorf, E.J., P. Tummala, and C.R. Jacobs, *Non-canonical Wnt signaling and N-cadherin related beta-catenin signaling play a role in mechanically induced osteogenic cell fate.* PLoS One, 2009. **4**(4): p. e5388.

95. Day, T.F. and Y. Yang, *Wnt and hedgehog signaling pathways in bone development.* The Journal of bone and joint surgery. American volume, 2008. **90 Suppl 1**: p. 19-24.

96. Angele, P., J.U. Yoo, C. Smith, J. Mansour, K.J. Jepsen, M. Nerlich, and B. Johnstone, *Cyclic hydrostatic pressure enhances the chondrogenic phenotype of human mesenchymal progenitor cells differentiated in vitro.* J Orthop Res, 2003. **21**(3): p. 451-7.

97. Miyanishi, K., M.C. Trindade, D.P. Lindsey, G.S. Beaupre, D.R. Carter, S.B. Goodman, D.J. Schurman, and R.L. Smith, *Dose- and time-dependent effects of cyclic hydrostatic pressure on transforming growth factor-beta3-induced chondrogenesis by adult human mesenchymal stem cells in vitro.* Tissue Engineering, 2006. **12**(8): p. 2253-62.

98. Zeiter, S., P. Lezuo, and K. Ito, *Effect of TGF beta1, BMP-2 and hydraulic pressure on chondrogenic differentiation of bovine bone marrow mesenchymal stromal cells.* Biorheology, 2009. **46**(1): p. 45-55.

99. Finger, A.R., C.Y. Sargent, K.O. Dulaney, S.H. Bernacki, and E.G. Loboa, *Differential effects on messenger ribonucleic acid expression by bone marrow-derived human mesenchymal stem cells seeded in agarose constructs due to ramped and steady applications of cyclic hydrostatic pressure.* Tissue Engineering, 2007. **13**(6): p. 1151-8.

100. Zhang, Z., J. Messana, N.S. Hwang, and J.H. Elisseeff, *Reorganization of actin filaments enhances chondrogenic differentiation of cells derived from murine embryonic stem cells.* Biochemical and Biophysical Research Communications, 2006. **348**(2): p. 421-7.

101. Kelly, D.J. and C.R. Jacobs, *The role of mechanical signals in regulating chondrogenesis and osteogenesis of mesenchymal stem cells.* Birth Defects Research Part C - Embryo Today: Reviews, 2010. **90**(1): p. 75-85.

102. Wang, N., J.P. Butler, and D.E. Ingber, *Mechanotransduction across the cell surface and through the cytoskeleton.* Science, 1993. **260**(5111): p. 1124-7.

103. Wang, N., I.M. Tolic-Norrelykke, J. Chen, S.M. Mijailovich, J.P. Butler, J.J. Fredberg, and D. Stamenovic, *Cell prestress. I. Stiffness and prestress are closely associated in adherent contractile cells.* Am J Physiol Cell Physiol, 2002. **282**(3): p. C606-16.

104. Nicolaije, C., J. van de Peppel, and J.P. van Leeuwen, *Oxygen-induced transcriptional dynamics in human osteoblasts are most prominent at the onset of mineralization.* Journal of cellular physiology, 2013. **228**(9): p. 1863-72.

105. Sahai, S., A. Williams, M.L. Skiles, and J.O. Blanchette, *Osteogenic differentiation of adipose-derived stem cells is hypoxia-inducible factor-1 independent.* Tissue engineering. Part A, 2013. **19**(13-14): p. 1583-91.

106. Salim, A., R.P. Nacamuli, E.F. Morgan, A.J. Giaccia, and M.T. Longaker, *Transient changes in oxygen tension inhibit osteogenic differentiation and Runx2 expression in osteoblasts.* The Journal of biological chemistry, 2004. **279**(38): p. 40007-16.

107. Ducy, P., R. Zhang, V. Geoffroy, A.L. Ridall, and G. Karsenty, *Osf2/Cbfa1: a transcriptional activator of osteoblast differentiation.* Cell, 1997. **89**(5): p. 747-54.

108. Karsenty, G., P. Ducy, M. Starbuck, M. Priemel, J. Shen, V. Geoffroy, and M. Amling, *Cbfa1 as a regulator of osteoblast differentiation and function.* Bone, 1999. **25**(1): p. 107-8.

109. Semenza, G.L., *HIF-1: mediator of physiological and pathophysiological responses to hypoxia.* Journal of applied physiology, 2000. **88**(4): p. 1474-80.

110. Duval, E., S. Leclercq, J.M. Elissalde, M. Demoor, P. Galera, and K. Boumediene, *Hypoxia-inducible factor 1alpha inhibits the fibroblast-like markers type I and type III collagen during hypoxia-induced chondrocyte redifferentiation: hypoxia not only induces type II collagen and aggrecan, but it also inhibits type I and type III collagen in the hypoxia-inducible factor 1alpha-dependent redifferentiation of chondrocytes.* Arthritis and rheumatism, 2009. **60**(10): p. 3038-48.

111. Duval, E., C. Bauge, R. Andriamanalijaona, H. Benateau, S. Leclercq, S. Dutoit, L. Poulain, P. Galera, and K. Boumediene, *Molecular mechanism of hypoxia-induced chondrogenesis and its application in in vivo cartilage tissue engineering.* Biomaterials, 2012. **33**(26): p. 6042-51.

112. Hsu, S.H., C.T. Chen, and Y.H. Wei, *Inhibitory Effects of Hypoxia on Metabolic Switch and Osteogenic Differentiation of Human Mesenchymal Stem Cells.* STEM CELLS, 2013.

113. Bodle, J.C., C.D. Rubenstein, M.E. Phillips, S.H. Bernacki, J. Qi, A.J. Banes, and E.G. Loboa, *Primary cilia: the chemical antenna regulating human adipose-derived stem cell osteogenesis.* PLoS One, 2013. **8**(5): p. e62554.

114. Kaplan, F.S., J. Fiori, D.L.P. LS, J. Ahn, P.C. Billings, and E.M. Shore, *Dysregulation of the BMP-4 signaling pathway in fibrodysplasia ossificans progressiva.* Annals of the New York Academy of Sciences, 2006. **1068**: p. 54-65.

115. Joyce, M.E., A.B. Roberts, M.B. Sporn, and M.E. Bolander, *Transforming growth factor-beta and the initiation of chondrogenesis and osteogenesis in the rat femur.* The Journal of cell biology, 1990. **110**(6): p. 2195-207.

116. Linkhart, T.A., S. Mohan, and D.J. Baylink, *Growth factors for bone growth and repair: IGF, TGF beta and BMP.* Bone, 1996. **19**(1 Suppl): p. 1S-12S.

117. Bostrom, M.P., J.M. Lane, W.S. Berberian, A.A. Missri, E. Tomin, A. Weiland, S.B. Doty, D. Glaser, and V.M. Rosen, *Immunolocalization and expression of bone morphogenetic proteins 2 and 4 in fracture healing.* Journal of orthopaedic research : official publication of the Orthopaedic Research Society, 1995. **13**(3): p. 357-67.

118. Sato, M., T. Ochi, T. Nakase, S. Hirota, Y. Kitamura, S. Nomura, and N. Yasui, *Mechanical tension-stress induces expression of bone morphogenetic protein (BMP)-2 and BMP-4, but not BMP-6, BMP-7, and GDF-5 mRNA, during distraction osteogenesis.* Journal of bone and mineral research : the official journal of the American Society for Bone and Mineral Research, 1999. **14**(7): p. 1084-95.

119. Chim, S.M., J. Tickner, S.T. Chow, V. Kuek, B. Guo, G. Zhang, V. Rosen, W. Erber, and J. Xu, *Angiogenic factors in bone local environment.* Cytokine & growth factor reviews, 2013.

120. Seghezzi, G., S. Patel, C.J. Ren, A. Gualandris, G. Pintucci, E.S. Robbins, R.L. Shapiro, A.C. Galloway, D.B. Rifkin, and P. Mignatti, *Fibroblast growth factor-2 (FGF-2) induces vascular endothelial growth factor (VEGF) expression in the endothelial cells of forming capillaries: an autocrine mechanism contributing to angiogenesis.* The Journal of cell biology, 1998. **141**(7): p. 1659-73.

121. Klein, S., F.G. Giancotti, M. Presta, S.M. Albelda, C.A. Buck, and D.B. Rifkin, *Basic fibroblast growth factor modulates integrin expression in microvascular endothelial cells.* Molecular biology of the cell, 1993. **4**(10): p. 973-82.

122. Turner, N. and R. Grose, *Fibroblast growth factor signalling: from development to cancer.* Nature reviews. Cancer, 2010. **10**(2): p. 116-29.

123. Ornitz, D.M., J. Xu, J.S. Colvin, D.G. McEwen, C.A. MacArthur, F. Coulier, G. Gao, and M. Goldfarb, *Receptor specificity of the fibroblast growth factor family.* The Journal of biological chemistry, 1996. **271**(25): p. 15292-7.

124. Tsiridis, E., N. Upadhyay, and P. Giannoudis, *Molecular aspects of fracture healing: which are the important molecules?* Injury, 2007. **38 Suppl 1**: p. S11-25.

125. Pedersen, T.O., Z. Xing, A. Finne-Wistrand, S. Hellem, and K. Mustafa, *Hyperbaric oxygen stimulates vascularization and bone formation in rat calvarial defects.* International journal of oral and maxillofacial surgery, 2013. **42**(7): p. 907-14.

126. Roca-Cusachs, P., R. Sunyer, and X. Trepat, *Mechanical guidance of cell migration: lessons from chemotaxis.* Current opinion in cell biology, 2013.

127. Woodell, J.E., M. LaBerge, E.M. Langan, 3rd, and R.H. Hilderman, *In vitro strain-induced endothelial cell dysfunction determined by DNA synthesis.* Proceedings of the Institution of Mechanical Engineers. Part H, Journal of engineering in medicine, 2003. **217**(1): p. 13-20.

128. Yung, Y.C., J. Chae, M.J. Buehler, C.P. Hunter, and D.J. Mooney, *Cyclic tensile strain triggers a sequence of autocrine and paracrine signaling to regulate angiogenic sprouting in human vascular cells.* Proceedings of the National Academy of Sciences of the United States of America, 2009. **106**(36): p. 15279-84.

129. Hsu, S., R. Thakar, D. Liepmann, and S. Li, *Effects of shear stress on endothelial cell haptotaxis on micropatterned surfaces.* Biochemical and Biophysical Research Communications, 2005. **337**(1): p. 401-9.

130. Uttayarat, P., M. Chen, M. Li, F.D. Allen, R.J. Composto, and P.I. Lelkes, *Microtopography and flow modulate the direction of endothelial cell migration.* American journal of physiology. Heart and circulatory physiology, 2008. **294**(2): p. H1027-35.

131. Joung, I.S., M.N. Iwamoto, Y.T. Shiu, and C.T. Quam, *Cyclic strain modulates tubulogenesis of endothelial cells in a 3D tissue culture model.* Microvascular research, 2006. **71**(1): p. 1-11.

132. Moretti, M., A. Prina-Mello, A.J. Reid, V. Barron, and P.J. Prendergast, *Endothelial cell alignment on cyclically-stretched silicone surfaces.* Journal of materials science. Materials in medicine, 2004. **15**(10): p. 1159-64.

133. Tambe, D.T., C.C. Hardin, T.E. Angelini, K. Rajendran, C.Y. Park, X. Serra-Picamal, E.H. Zhou, M.H. Zaman, J.P. Butler, D.A. Weitz, et al., *Collective cell guidance by cooperative intercellular forces.* Nature materials, 2011. **10**(6): p. 469-75.

134. Lo, C.M., H.B. Wang, M. Dembo, and Y.L. Wang, *Cell movement is guided by the rigidity of the substrate.* Biophysical journal, 2000. **79**(1): p. 144-52.

135. Choi, Y.S., L.G. Vincent, A.R. Lee, K.C. Kretchmer, S. Chirasatitsin, M.K. Dobke, and A.J. Engler, *The alignment and fusion assembly of adipose-derived stem cells on mechanically patterned matrices.* Biomaterials, 2012. **33**(29): p. 6943-51.

136. Roca-Cusachs, P., T. Iskratsch, and M.P. Sheetz, *Finding the weakest link: exploring integrin-mediated mechanical molecular pathways.* Journal of cell science, 2012. **125**(Pt 13): p. 3025-38.

137. del Rio, A., R. Perez-Jimenez, R. Liu, P. Roca-Cusachs, J.M. Fernandez, and M.P. Sheetz, *Stretching single talin rod molecules activates vinculin binding.* Science, 2009. **323**(5914): p. 638-41.

138. Simon, U., P. Augat, M. Utz, and L. Claes, *A numerical model of the fracture healing process that describes tissue development and revascularisation.* Comput Methods Biomech Biomed Engin, 2011. **14**(1): p. 79-93.

139. Perez, M.A. and P.J. Prendergast, *Random-walk models of cell dispersal included in mechanobiological simulations of tissue differentiation.* Journal of Biomechanics, 2007. **40**(10): p. 2244-53.

140. Byrne, D.P., D. Lacroix, J.A. Planell, D.J. Kelly, and P.J. Prendergast, *Simulation of tissue differentiation in a scaffold as a function of porosity, Young's modulus and dissolution rate: application of mechanobiological models in tissue engineering.* Biomaterials, 2007. **28**(36): p. 5544-54.

141. Reina-Romo, E., M.J. Gomez-Benito, J. Dominguez, and J.M. Garcia-Aznar, *A lattice-based approach to model distraction osteogenesis.* Journal of Biomechanics, 2012. **45**(16): p. 2736-42.

142. Bailon-Plaza, A. and M.C. van der Meulen, *A mathematical framework to study the effects of growth factor influences on fracture healing.* J Theor Biol, 2001. **212**(2): p. 191-209.

143. Geris, L., J.V. Sloten, and H. Van Oosterwyck, *Connecting biology and mechanics in fracture healing: an integrated mathematical modeling framework for the study of nonunions.* Biomechanics and Modeling in Mechanobiology, 2010. **9**(6): p. 713-24.

144. Peiffer, V., A. Gerisch, D. Vandepitte, H. Van Oosterwyck, and L. Geris, *A hybrid bioregulatory model of angiogenesis during bone fracture healing.* Biomech Model Mechanobiol, 2011. **10**(3): p. 383-95.

145. Carlier, A., L. Geris, K. Bentley, G. Carmeliet, P. Carmeliet, and H. Van Oosterwyck, *MOSAIC: a multiscale model of osteogenesis and sprouting*

angiogenesis with lateral inhibition of endothelial cells. PLoS computational biology, 2012. **8**(10): p. e1002724.

146. Zheng, X., Koh, G. Y., Jackson, T., *A continuous model of angiogenesis: initiation, extension, and maturation of new blood vessels modulated by vascular endothelial growth factor, angioproteins, platelet-derived growth factor-b, and pericytes.* Discrete and continuous dynamical systems, series B, 2013. **18**(4): p. 1109-1154.

147. McKibbin, B., *The biology of fracture healing in long bones.* J Bone Joint Surg Br, 1978. **60-B**(2): p. 150-62.

148. Einhorn, T.A., *The cell and molecular biology of fracture healing.* Clin Orthop Relat Res, 1998(355 Suppl): p. S7-21.

149. Marsell, R. and T.A. Einhorn, *The biology of fracture healing.* Injury, 2011. **42**(6): p. 551-5.

150. Claes, L., K. Eckert-Hubner, and P. Augat, *The effect of mechanical stability on local vascularization and tissue differentiation in callus healing.* J Orthop Res, 2002. **20**(5): p. 1099-105.

151. Isaksson, H., *Recent advances in mechanobiological modelling of bone regeneration.* Mechanics Research Communications, 2012. **42**: p. 22-31.

152. Perren, S.M., *Fracture healing. The evolution of our understanding.* Acta Chir Orthop Traumatol Cech, 2008. **75**(4): p. 241-6.

153. Frost, H.M., *The biology of fracture healing. An overview for clinicians. Part I.* Clin Orthop Relat Res, 1989(248): p. 283-93.

154. Gerstenfeld, L.C., D.M. Cullinane, G.L. Barnes, D.T. Graves, and T.A. Einhorn, *Fracture healing as a post-natal developmental process: molecular, spatial, and temporal aspects of its regulation.* J Cell Biochem, 2003. **88**(5): p. 873-84.

155. Einhorn, T.A., *Enhancement of fracture-healing.* J Bone Joint Surg Am, 1995. **77**(6): p. 940-56.

156. Lacroix, D., *Simulation of tissue differentiation during fracture healing*, in *Dept. of Mechanical Engineering*,2000, Trinity College Dublin: Dublin.

157. Mackie, E.J., Y.A. Ahmed, L. Tatarczuch, K.S. Chen, and M. Mirams, *Endochondral ossification: how cartilage is converted into bone in the developing skeleton.* Int J Biochem Cell Biol, 2008. **40**(1): p. 46-62.

158. Kronenberg, H.M., *Developmental regulation of the growth plate.* Nature, 2003. **423**(6937): p. 332-6.

159. Brueton, R.N., M. Brookes, and F.W. Heatley, *The vascular repair of an experimental osteotomy held in an external fixator.* Clinical Orthopaedics and Related Research, 1990(257): p. 286-304.

160. Epari, D.R., H. Schell, H.J. Bail, and G.N. Duda, *Instability prolongs the chondral phase during bone healing in sheep.* Bone, 2006. **38**(6): p. 864-70.

161. Owen, M., *The origin of bone cells.* Int Rev Cytol, 1970. **28**: p. 213-38.

162. Leriche, R. and A. Policard, eds. *The Normal and Pathological Physiology of Bone, Its Problems.*, ed. S. Moore and J.A. Key. 1928, C. V. Mosby Co.: St Louis.

163. Bianco, P., M. Riminucci, S. Gronthos, and P.G. Robey, *Bone Marrow Stromal Stem Cells: Nature, Biology, and Potential Applications.* STEM CELLS, 2001. **19**(3): p. 180-192.

164. Kon, T., T.J. Cho, T. Aizawa, M. Yamazaki, N. Nooh, D. Graves, L.C. Gerstenfeld, and T.A. Einhorn, *Expression of osteoprotegerin, receptor activator of NF-kappaB ligand (osteoprotegerin ligand) and related proinflammatory cytokines during fracture healing.* Journal of bone and mineral research : the official journal of the American Society for Bone and Mineral Research, 2001. **16**(6): p. 1004-14.

165. Bais, M.V., N. Wigner, M. Young, R. Toholka, D.T. Graves, E.F. Morgan, L.C. Gerstenfeld, and T.A. Einhorn, *BMP2 is essential for post natal osteogenesis but not for recruitment of osteogenic stem cells.* Bone, 2009. **45**(2): p. 254-66.

166. Ceradini, D.J., A.R. Kulkarni, M.J. Callaghan, O.M. Tepper, N. Bastidas, M.E. Kleinman, J.M. Capla, R.D. Galiano, J.P. Levine, and G.C. Gurtner, *Progenitor cell trafficking is regulated by hypoxic gradients through HIF-1 induction of SDF-1.* Nature medicine, 2004. **10**(8): p. 858-64.

167. Lacroix, D., P.J. Prendergast, G. Li, and D. Marsh, *Biomechanical model to simulate tissue differentiation and bone regeneration: application to fracture healing.* Med Biol Eng Comput, 2002. **40**(1): p. 14-21.

168. Tonna, E.A. and E.P. Cronkite, *Cellular Response to Fracture Studied with Tritiated Thymidine.* J Bone Joint Surg Am, 1961. **43**: p. 352-362.

169. Augat, P., J. Burger, S. Schorlemmer, T. Henke, M. Peraus, and L. Claes, *Shear movement at the fracture site delays healing in a diaphyseal fracture model.* Journal of orthopaedic research : official publication of the Orthopaedic Research Society, 2003. **21**(6): p. 1011-7.

170. Hulth, A. and S. Olerud, *Early Fracture Callus in Normal and Cortisone Treated Rats. A Study by a Combination of Tetracycline Labelling, Microangiography and Microradiography.* Acta Orthop Scand, 1964. **34**: p. 1-23.

171. Cenni, E., *ANGIOGENESIS AND BONE REGENERATION.* J Bone Joint Surg Br, 2005. **87-B**(SUPP_I): p. 58-.

172. Hausman, M.R., M.B. Schaffler, and R.J. Majeska, *Prevention of fracture healing in rats by an inhibitor of angiogenesis.* Bone, 2001. **29**(6): p. 560-4.

173. Wallace, A.L., E.R. Draper, R.K. Strachan, I.D. McCarthy, and S.P. Hughes, *The effect of devascularisation upon early bone healing in dynamic external fixation.* J Bone Joint Surg Br, 1991. **73**(5): p. 819-25.

174. Holden, C.E., *The role of blood supply to soft tissue in the healing of diaphyseal fractures. An experimental study.* J Bone Joint Surg Am, 1972. **54**(5): p. 993-1000.

175. Hausman, G.J. and R.L. Richardson, *Adipose tissue angiogenesis.* J Anim Sci, 2004. **82**(3): p. 925-34.

176. Bouloumie, A., K. Lolmede, C. Sengenes, J. Galitzky, and M. Lafontan, *Angiogenesis in adipose tissue.* Ann Endocrinol (Paris), 2002. **63**(2 Pt 1): p. 91-5.

177. Lu, C., T. Miclau, D. Hu, and R.S. Marcucio, *Ischemia leads to delayed union during fracture healing: a mouse model.* J Orthop Res, 2007. **25**(1): p. 51-61.

178. Miedel, E., M.I. Dishowitz, M.H. Myers, D. Dopkin, Y.Y. Yu, T.S. Miclau, R. Marcucio, J. Ahn, and K.D. Hankenson, *Disruption of thrombospondin-2 accelerates ischemic fracture healing.* Journal of orthopaedic research : official publication of the Orthopaedic Research Society, 2013. **31**(6): p. 935-43.

179. Epari, D.R., J. Lienau, H. Schell, F. Witt, and G.N. Duda, *Pressure, oxygen tension and temperature in the periosteal callus during bone healing--an in vivo study in sheep.* Bone, 2008. **43**(4): p. 734-9.

180. Lu, C., N. Saless, X. Wang, A. Sinha, S. Decker, G. Kazakia, H. Hou, B. Williams, H.M. Swartz, T.K. Hunt, et al., *The role of oxygen during fracture healing.* Bone, 2013. **52**(1): p. 220-9.

181. Kelly, K., *The third culture.* Science, 1998. **279**(5353): p. 992-993.

182. Blenman, P.R., D.R. Carter, and G.S. Beaupre, *Role of mechanical loading in the progressive ossification of a fracture callus.* J Orthop Res, 1989. **7**(3): p. 398-407.

183. Morgan, E.F., M.T. Longaker, and D.R. Carter, *Relationships between tissue dilatation and differentiation in distraction osteogenesis.* Matrix biology : journal of the International Society for Matrix Biology, 2006. **25**(2): p. 94-103.

184. Claes, L.E., C.A. Heigele, C. Neidlinger-Wilke, D. Kaspar, W. Seidl, K.J. Margevicius, and P. Augat, *Effects of mechanical factors on the fracture healing process.* Clinical Orthopaedics and Related Research, 1998(355 Suppl): p. S132-47.

185. Ament, C. and E.P. Hofer, *A fuzzy logic model of fracture healing.* Journal of Biomechanics, 2000. **33**(8): p. 961-968.

186. Shefelbine, S.J., P. Augat, L. Claes, and U. Simon, *Trabecular bone fracture healing simulation with finite element analysis and fuzzy logic.* Journal of Biomechanics, 2005. **38**(12): p. 2440-50.

187. Mow, V.C., S.C. Kuei, W.M. Lai, and C.G. Armstrong, *Biphasic creep and stress relaxation of articular cartilage in compression? Theory and experiments.* J Biomech Eng, 1980. **102**(1): p. 73-84.

188. Prendergast, P. and R. Huiskes, *Finite element analysis of fibrous tissue morphogenesis — A study of the osteogenic index with a biphasic approach.* Mechanics of Composite Materials, 1996. **32**(2): p. 144-150.

189. Isaksson, H., C.C. van Donkelaar, R. Huiskes, and K. Ito, *Corroboration of mechanoregulatory algorithms for tissue differentiation during fracture healing: Comparison with in vivo results.* J Orthop Res, 2006. **24**(5): p. 898-907.

190. Garcia-Aznar, J.M., J.H. Kuiper, M.J. Gomez-Benito, M. Doblare, and J.B. Richardson, *Computational simulation of fracture healing: influence of interfragmentary movement on the callus growth.* J Biomech, 2007. **40**(7): p. 1467-76.

191. Geris, L., A. Gerisch, C. Maes, G. Carmeliet, R. Weiner, J. Vander Sloten, and H. Van Oosterwyck, *Mathematical modeling of fracture healing in mice: comparison between experimental data and numerical simulation results.* Medical & biological engineering & computing, 2006. **44**(4): p. 280-9.

192. Geris, L., A.A. Reed, J. Vander Sloten, A.H. Simpson, and H. Van Oosterwyck, *Occurrence and treatment of bone atrophic non-unions investigated by an integrative approach.* PLoS Comput Biol, 2010. **6**(9): p. e1000915.

193. Jacobsson, M., T. Albrektsson, and I. Turesson, *Dynamics of irradiation injury to bone tissue. A vital microscopic investigation.* Acta radiologica. Oncology, 1985. **24**(4): p. 343-50.

194. Listrom, R.D., J.M. Symington, and T. Albrektsson, *A bone chamber for investigation of gas pressure. Oxygen tension measured in rabbits.* Acta orthopaedica Scandinavica, 1988. **59**(4): p. 454-8.

195. Aspenberg, P., T. Albrektsson, and K.G. Thorngren, *Local application of growth-factor IGF-1 to healing bone. Experiments with a titanium chamber in rabbits.* Acta orthopaedica Scandinavica, 1989. **60**(5): p. 607-10.

196. Guldberg, R.E., N.J. Caldwell, X.E. Guo, R.W. Goulet, S.J. Hollister, and S.A. Goldstein, *Mechanical stimulation of tissue repair in the hydraulic bone chamber.* Journal of bone and mineral research : the official journal of the American Society for Bone and Mineral Research, 1997. **12**(8): p. 1295-302.

197. Tagil, M. and P. Aspenberg, *Cartilage induction by controlled mechanical stimulation in vivo.* J Orthop Res, 1999. **17**(2): p. 200-4.

198. de Rooij, P.P., M.A. Siebrecht, M. Tagil, and P. Aspenberg, *The fate of mechanically induced cartilage in an unloaded environment.* J Biomech, 2001. **34**(7): p. 961-6.

199. Geris, L., K. Vandamme, I. Naert, J. Vander Sloten, J. Duyck, and H. Van Oosterwyck, *Application of mechanoregulatory models to simulate peri-implant tissue formation in an in vivo bone chamber.* Journal of Biomechanics, 2008. **41**(1): p. 145-54.

200. Geris, L., K. Vandamme, I. Naert, J. Vander Sloten, J. Duyck, and H. Van Oosterwyck, *Numerical simulation of bone regeneration in a bone chamber.* Journal of dental research, 2009. **88**(2): p. 158-63.

201. Geris, L., H. Van Oosterwyck, J. Vander Sloten, J. Duyck, and I. Naert, *Assessment of mechanobiological models for the numerical simulation of tissue differentiation around immediately loaded implants.* Computer methods in biomechanics and biomedical engineering, 2003. **6**(5-6): p. 277-88.

202. Vandamme, K., I. Naert, L. Geris, J. Vander Sloten, R. Puers, and J. Duyck, *Influence of controlled immediate loading and implant design on peri-implant bone formation.* Journal of clinical periodontology, 2007. **34**(2): p. 172-81.

203. Boccaccio, A., C. Pappalettere, and D. Kelly, *The Influence of Expansion Rates on Mandibular Distraction Osteogenesis: A Computational Analysis.* Annals of Biomedical Engineering, 2007. **35**(11): p. 1940-1960.

204. Hayward, L.N. and E.F. Morgan, *Assessment of a mechano-regulation theory of skeletal tissue differentiation in an in vivo model of mechanically induced cartilage formation.* Biomech Model Mechanobiol, 2009.

205. Merceron, C., C. Vinatier, S. Portron, M. Masson, J. Amiaud, L. Guigand, Y. Chérel, P. Weiss, and J. Guicheux, *Differential effects of hypoxia on osteochondrogenic potential of human adipose-derived stem cells.* American Journal of Physiology - Cell Physiology, 2010. **298**(2): p. C355-C364.

206. Cao, Y., *Angiogenesis modulates adipogenesis and obesity.* The Journal of Clinical Investigation, 2007. **117**(9): p. 2362-2368.

207. Gomillion, C.T. and K.J. Burg, *Stem cells and adipose tissue engineering.* Biomaterials, 2006. **27**(36): p. 6052-63.

208. Roach, H.I., J. Erenpreisa, and T. Aigner, *Osteogenic differentiation of hypertrophic chondrocytes involves asymmetric cell divisions and apoptosis.* J Cell Biol, 1995. **131**(2): p. 483-94.

209. Mente, P.L. and J.L. Lewis, *Elastic modulus of calcified cartilage is an order of magnitude less than that of subchondral bone.* J Orthop Res, 1994. **12**(5): p. 637-47.

210. Frost, H.M., *Skeletal structural adaptations to mechanical usage (SATMU): 1. Redefining Wolff's law: the bone modeling problem.* Anat Rec, 1990. **226**(4): p. 403-13.

211. Rubin, C. and L. Lanyon, *Regulation of bone mass by mechanical strain magnitude.* Calcified Tissue International, 1985. **37**(4): p. 411-417.

212. Hershey, D. and T. Karhan, *Diffusion coefficients for oxygen transport in whole blood.* AIChE Journal, 1968. **14**(6): p. 969-972.

213. Pattappa, G., H.K. Heywood, J.D. de Bruijn, and D.A. Lee, *The metabolism of human mesenchymal stem cells during proliferation and differentiation.* J Cell Physiol, 2010.

214. Hori, R.Y. and J.L. Lewis, *Mechanical properties of the fibrous tissue found at the bone-cement interface following total joint replacement.* J Biomed Mater Res, 1982. **16**(6): p. 911-27.

215. Armstrong, C.G. and V.C. Mow, *Variations in the Intrinsic Mechanical Proterties of Human Articular-Cartilage with Age, Degeneration, and Water-Content.* Journal of Bone and Joint Surgery-American Volume, 1982. **64**(1): p. 88-94.

216. Ochoa, J.A. and B.M. Hillberry, *Permeability of bovine cancellous bone.* Trans. of the 38th ORS, 1992: p. 162.

217. Cowin, S.C., *Bone poroelasticity.* J Biomech, 1999. **32**(3): p. 217-38.

218. Schaffler, M.B. and D.B. Burr, *Stiffness of compact bone: effects of porosity and density.* J Biomech, 1988. **21**: p. 13–16.

219. Gómez-Benito, M.J., J.M. García-Aznar, J.H. Kuiper, and M. Doblaré, *Influence of fracture gap size on the pattern of long bone healing: A computational study.* Journal of Theoretical Biology, 2005. **235**(1): p. 105-119.

220. Sheehy, E.J., C.T. Buckley, and D.J. Kelly, *Oxygen tension regulates the osteogenic, chondrogenic and endochondral phenotype of bone marrow derived mesenchymal stem cells.* Biochem Biophys Res Commun, 2012. **417**(1): p. 305-10.

221. Yin, M., C. Gentili, E. Koyama, M. Zasloff, and M. Pacifici, *Antiangiogenic treatment delays chondrocyte maturation and bone formation during limb skeletogenesis.* J Bone Miner Res, 2002. **17**(1): p. 56-65.

222. Vinardell, T., R.A. Rolfe, C.T. Buckley, E.G. Meyer, M. Ahearne, P. Murphy, and D.J. Kelly, *Hydrostatic pressure acts to stabilise a chondrogenic phenotype in porcine joint tissue derived stem cells.* Eur Cell Mater, 2012. **23**: p. 121-34.

223. Bian, L., D.Y. Zhai, E.C. Zhang, R.L. Mauck, and J.A. Burdick, *Dynamic Compressive Loading Enhances Cartilage Matrix Synthesis and Distribution and Suppresses Hypertrophy in hMSC-Laden Hyaluronic Acid Hydrogels.* Tissue Eng Part A, 2012. **18**(7-8): p. 715-24.

224. Steward, A.J., S.D. Thorpe, T. Vinardell, C.T. Buckley, D.R. Wagner, and D.J. Kelly, *Cell-matrix interactions regulate mesenchymal stem cell response to hydrostatic pressure.* Acta Biomater, 2012. **8**(6): p. 2153-9.

225. Garcia, P., A. Pieruschka, M. Klein, A. Tami, T. Histing, J.H. Holstein, C. Scheuer, T. Pohlemann, and M.D. Menger, *Temporal and spatial vascularization patterns of unions and nonunions: role of vascular endothelial growth factor and bone morphogenetic proteins.* J Bone Joint Surg Am, 2012. **94**(1): p. 49-58.

226. Ma, T., W.L. Grayson, M. Frohlich, and G. Vunjak-Novakovic, *Hypoxia and stem cell-based engineering of mesenchymal tissues.* Biotechnol Prog, 2009. **25**(1): p. 32-42.

227. Burke, D.P. and D.J. Kelly, *Substrate Stiffness and Oxygen as Regulators of Stem Cell Differentiation during Skeletal Tissue Regeneration: A Mechanobiological Model.* PLoS One, 2012. **7**(7): p. e40737.

228. Oganesian, A., L.C. Armstrong, M.M. Migliorini, D.K. Strickland, and P. Bornstein, *Thrombospondins use the VLDL receptor and a nonapoptotic pathway to inhibit cell division in microvascular endothelial cells.* Mol Biol Cell, 2008. **19**(2): p. 563-71.

229. Armstrong, L.C., B. Bjorkblom, K.D. Hankenson, A.W. Siadak, C.E. Stiles, and P. Bornstein, *Thrombospondin 2 inhibits microvascular endothelial cell proliferation by a caspase-independent mechanism.* Mol Biol Cell, 2002. **13**(6): p. 1893-905.

230. Lopes, N., D. Gregg, S. Vasudevan, H. Hassanain, P. Goldschmidt-Clermont, and H. Kovacic, *Thrombospondin 2 regulates cell proliferation induced by Rac1 redox-dependent signaling.* Mol Cell Biol, 2003. **23**(15): p. 5401-8.

231. Prasad, J., B.P. Wiater, S.E. Nork, S.D. Bain, and T.S. Gross, *Characterizing gait induced normal strains in a murine tibia cortical bone defect model.* J Biomech, 2010. **43**(14): p. 2765-70.

232. Colnot, C., Z. Thompson, T. Miclau, Z. Werb, and J.A. Helms, *Altered fracture repair in the absence of MMP9.* Development, 2003. **130**(17): p. 4123-33.

233. Kosaki, N., H. Takaishi, S. Kamekura, T. Kimura, Y. Okada, L. Minqi, N. Amizuka, U.I. Chung, K. Nakamura, H. Kawaguchi, et al., *Impaired bone fracture healing in matrix metalloproteinase-13 deficient mice.* Biochem Biophys Res Commun, 2007. **354**(4): p. 846-51.

234. Colnot, C., *Skeletal cell fate decisions within periosteum and bone marrow during bone regeneration.* Journal of bone and mineral research : the official journal of the American Society for Bone and Mineral Research, 2009. **24**(2): p. 274-82.

235. Matsubara, H., D.E. Hogan, E.F. Morgan, D.P. Mortlock, T.A. Einhorn, and L.C. Gerstenfeld, *Vascular tissues are a primary source of BMP2 expression*

during bone formation induced by distraction osteogenesis. Bone, 2012. **51**(1): p. 168-80.

236. Burke, D., M. Dishowitz, M. Sweetwyne, E. Miedel, K.D. Hankenson, and D.J. Kelly, *The role of oxygen as a regulator of stem cell fate during fracture repair in TSP2-null mice.* Journal of orthopaedic research : official publication of the Orthopaedic Research Society, 2013.

237. Isaksson, H., C.C. van Donkelaar, R. Huiskes, and K. Ito, *A mechano-regulatory bone-healing model incorporating cell-phenotype specific activity.* Journal of Theoretical Biology, 2008. **252**(2): p. 230-46.

238. Appeddu, P.A. and B.D. Shur, *Molecular analysis of cell surface beta-1,4-galactosyltransferase function during cell migration.* Proceedings of the National Academy of Sciences of the United States of America, 1994. **91**(6): p. 2095-9.

239. Checa, S., Byrne, D. P., Prendergast, P. J., *Predictive modelling in mechanobiology: Combining algorithms for cell activities in response to physical stimuli using a lattice-modelling approach.* Advanced Structured Materials, 2012. **1**(1): p. 423-435.

240. Marlovits, S., P. Zeller, P. Singer, C. Resinger, and V. Vecsei, *Cartilage repair: generations of autologous chondrocyte transplantation.* Eur J Radiol, 2006. **57**(1): p. 24-31.

241. Guo, S. and L.A. Dipietro, *Factors affecting wound healing.* Journal of dental research, 2010. **89**(3): p. 219-29.

242. Nomi, M., A. Atala, P.D. Coppi, and S. Soker, *Principals of neovascularization for tissue engineering.* Molecular aspects of medicine, 2002. **23**(6): p. 463-83.

243. Shweiki, D., A. Itin, D. Soffer, and E. Keshet, *Vascular endothelial growth factor induced by hypoxia may mediate hypoxia-initiated angiogenesis.* Nature, 1992. **359**(6398): p. 843-5.

244. Gerhardt, H., M. Golding, M. Fruttiger, C. Ruhrberg, A. Lundkvist, A. Abramsson, M. Jeltsch, C. Mitchell, K. Alitalo, D. Shima, and C. Betsholtz, *VEGF guides angiogenic sprouting utilizing endothelial tip cell filopodia.* The Journal of cell biology, 2003. **161**(6): p. 1163-77.

245. Checa, S. and P.J. Prendergast, *Effect of cell seeding and mechanical loading on vascularization and tissue formation inside a scaffold: a mechano-biological model using a lattice approach to simulate cell activity.* Journal of Biomechanics, 2010. **43**(5): p. 961-8.

246. Oest, M.E., K.M. Dupont, H.J. Kong, D.J. Mooney, and R.E. Guldberg, *Quantitative assessment of scaffold and growth factor-mediated repair of critically sized bone defects.* Journal of orthopaedic research : official publication of the Orthopaedic Research Society, 2007. **25**(7): p. 941-50.

247. Boerckel, J.D., K.M. Dupont, Y.M. Kolambkar, A.S. Lin, and R.E. Guldberg, *In vivo model for evaluating the effects of mechanical stimulation on tissue-engineered bone repair.* Journal of biomechanical engineering, 2009. **131**(8): p. 084502.

248. Ochoa, M.C., G.D. Vogelsang, J.T. Lum, P.F. VonVoigtlander, and M.F. Piercey, *Effect of the anticonvulsant U-54494A on cortical neuron excitability: comparison to the kappa agonist U-50488H.* Life Sci, 1992. **50**(17): p. 1225-33.

249. Roshan-Ghias, A., A. Terrier, P.E. Bourban, and D.P. Pioletti, *In vivo cyclic loading as a potent stimulatory signal for bone formation inside tissue engineering scaffold.* European cells & materials, 2010. **19**: p. 41-9.

250. Topol, L., W. Chen, H. Song, T.F. Day, and Y. Yang, *Sox9 inhibits Wnt signaling by promoting beta-catenin phosphorylation in the nucleus.* The Journal of biological chemistry, 2009. **284**(5): p. 3323-33.

251. Harrison, L.J., J.L. Cunningham, L. Stromberg, and A.E. Goodship, *Controlled induction of a pseudarthrosis: a study using a rodent model.* Journal of orthopaedic trauma, 2003. **17**(1): p. 11-21.

252. Maes, C., P. Carmeliet, K. Moermans, I. Stockmans, N. Smets, D. Collen, R. Bouillon, and G. Carmeliet, *Impaired angiogenesis and endochondral bone formation in mice lacking the vascular endothelial growth factor isoforms VEGF164 and VEGF188.* Mechanisms of development, 2002. **111**(1-2): p. 61-73.

253. Jackson, T. and X. Zheng, *A cell-based model of endothelial cell migration, proliferation and maturation during corneal angiogenesis.* Bulletin of mathematical biology, 2010. **72**(4): p. 830-68.

254. Thorpe, S.D., T. Nagel, S.F. Carroll, and D.J. Kelly, *Modulating gradients in regulatory signals within mesenchymal stem cell seeded hydrogels: a novel strategy to engineer zonal articular cartilage.* PLoS One, 2013. **8**(4): p. e60764.

255. Sengers, B.G., C.C. van Donkelaar, C.W. Oomens, and F.P. Baaijens, *Computational study of culture conditions and nutrient supply in cartilage tissue engineering.* Biotechnology progress, 2005. **21**(4): p. 1252-61.

256. Haselgrove, J.C., I.M. Shapiro, and S.F. Silverton, *Computer modeling of the oxygen supply and demand of cells of the avian growth cartilage.* The American journal of physiology, 1993. **265**(2 Pt 1): p. C497-506.

257. Brighton, C.T., J.L. Schaffer, D.B. Shapiro, J.J. Tang, and C.C. Clark, *Proliferation and macromolecular synthesis by rat calvarial bone cells grown in various oxygen tensions.* Journal of orthopaedic research : official publication of the Orthopaedic Research Society, 1991. **9**(6): p. 847-54.

258. Boilly, B., A.S. Vercoutter-Edouart, H. Hondermarck, V. Nurcombe, and X. Le Bourhis, *FGF signals for cell proliferation and migration through different pathways.* Cytokine & growth factor reviews, 2000. **11**(4): p. 295-302.

259. Zohar, R., S. Cheifetz, C.A. McCulloch, and J. Sodek, *Analysis of intracellular osteopontin as a marker of osteoblastic cell differentiation and mesenchymal cell migration.* Eur J Oral Sci, 1998. **106 Suppl 1**: p. 401-7.

260. Iwaki, A., S. Jingushi, Y. Oda, T. Izumi, J.I. Shida, M. Tsuneyoshi, and Y. Sugioka, *Localization and quantification of proliferating cells during rat fracture repair: detection of proliferating cell nuclear antigen by immunohistochemistry.* J Bone Miner Res, 1997. **12**(1): p. 96-102.

Appendices

Appendix I: cell model

MSCs both migrate [259] and proliferate [260] within the fracture callus. It was assumed that the net process of these effects can be modeled via a diffusion model [10]:

$$\frac{dn}{dt} = D\nabla^2 n \qquad \text{(Equation.A1)}$$

where D is the stem cell diffusion coefficient and n is the current stem cell concentration. Stem cells originated from the marrow of the medullary cavity [161], the inner cambial layer of the periosteum [147] and from the surrounding muscle tissues. Before the influx of MSCs into the callus, the fracture callus is initially full of granulation tissue.

Appendix II: rule of mixtures

The gradual change of an element from one tissue type to another is accounted for in the model of the element material properties. The material properties are calculated *via* the rule of mixtures:

$$E = \frac{n^{\max} - n}{n^{\max}} E_{granulation} + \frac{n}{n^{\max}} E_{tissue} \qquad \text{(Equation.A2)}$$

The Young's Modulus of an element, E, is calculated as a function of the element's cell density (n), the maximum cell density (n^{max}), the Young's Modulus of granulation tissue ($E_{granulation}$) and the Young's Modulus of the tissue the element is differentiating towards. The rule of mixtures is applied to the other material properties in a similar manner.

Appendix III: temporal smoothing procedure

A temporal smoothing procedure is included in the model in order to avoid any numerical instability that might occur as a result of rapid changes in material properties. An array of k values is defined and initially the properties of granulation tissue are inputted into this array. After the first iteration (i = 1), the material property of the predicted tissue phenotype is placed at the end of the array. All existing properties are moved along one position and the i^{th} value in the array is deleted. Should this be performed a second time the array would look like:

$$E = \left[E_{granulation}, E_{granulation}, \cdots, E_{i=1}, E_{i=2}\right] \quad \text{(Equation.A3)}$$

At the k^{th} iteration ($i = k$):

$$E = \left[E_{i=1}, E_{i=2}, \cdots, E_{i=n-1}, E_{i=n}\right] \quad \text{(Equation.A4)}$$

The material properties for each iteration were calculated via:

$$E = \frac{1}{k}\sum_{j=1}^{k} E_j \quad \text{(Equation.A5)}$$

For this study k was taken to be 10. The other material properties are calculated in a similar manner.

Appendix IV: supplementary figures (Chapter 6)

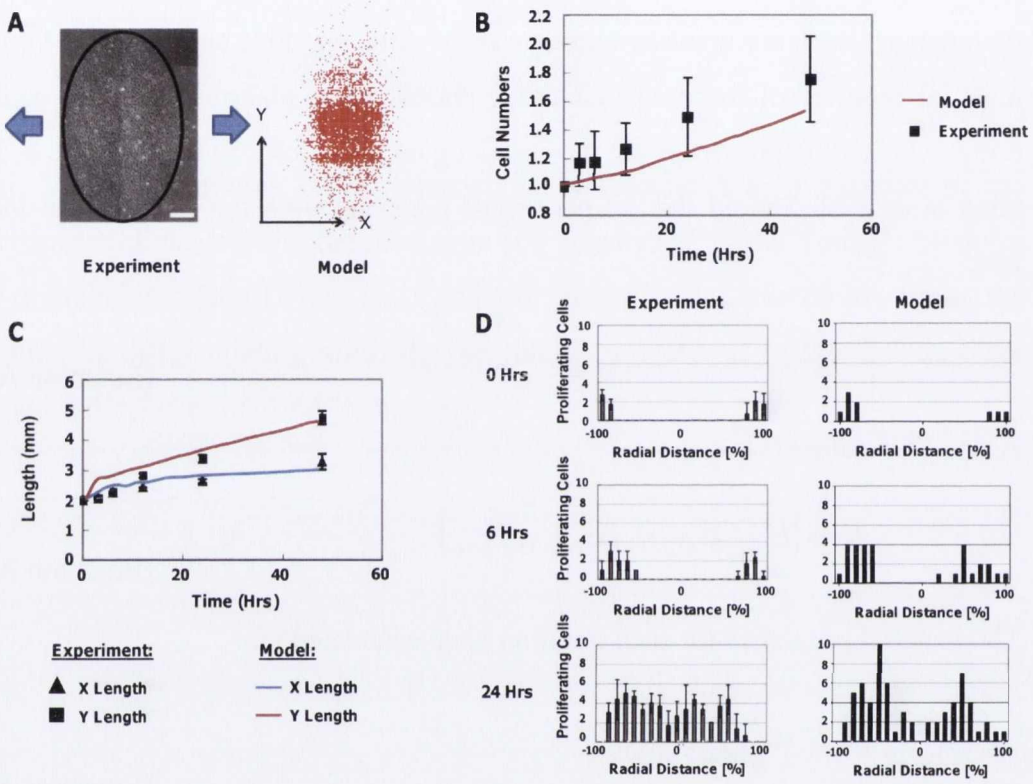

Figure S1. Model Predictions: Strain increases the rate of EC migration and leads to directionally biased migration. (a) Model prediction of the final distribution of the endothelial cell population compared to that observed experimentally. (b) Model prediction of the change in the total cell number over time compared to that observed experimentally. (c) Model prediction of the variation in the X and Y lengths of the endothelial cell region over time compared to that observed experimentally. (d) Model predictions of the number of proliferating cells at various radial distances (Y direction) from the centre ('0') of the EC population at the 0 hour, 6 hour and 24 hour time points compared to that observed experimentally.

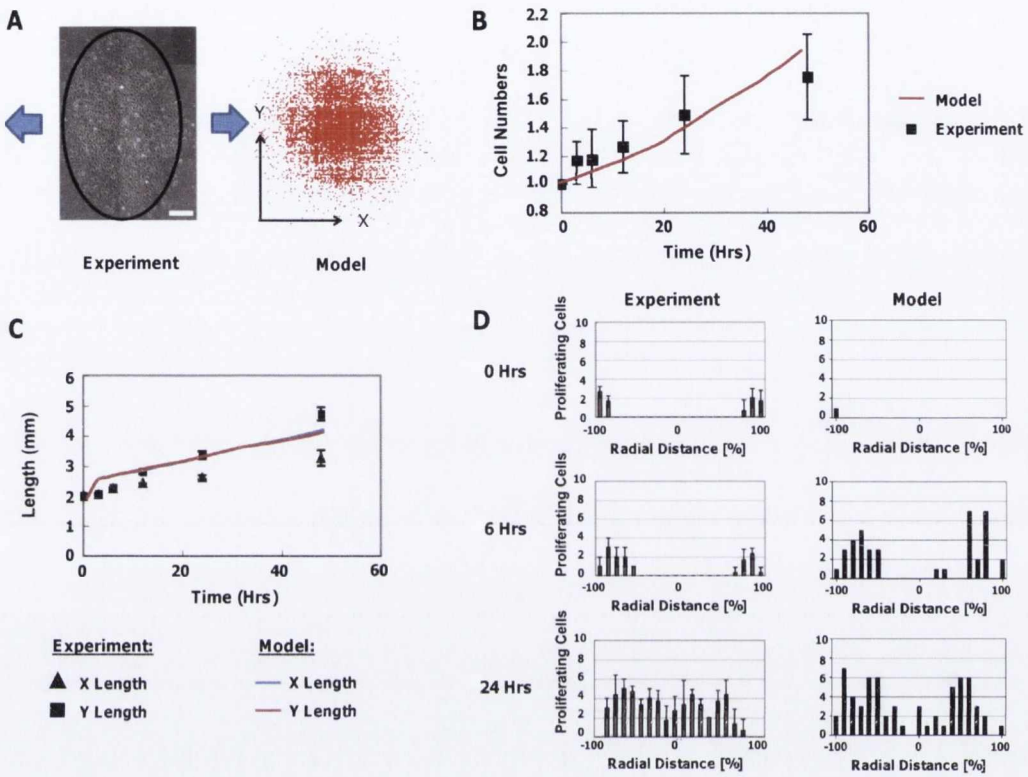

Figure S2. Model Predictions: Strain increases the rate of EC migration and proliferation. (a) Model prediction of the final distribution of the endothelial cell population compared to that observed experimentally. (b) Model prediction of the change in the total cell number over time compared to that observed experimentally. (c) Model prediction of the variation in the X and Y lengths of the endothelial cell region over time compared to that observed experimentally. (d) Model predictions of the number of proliferating cells at various radial distances (Y direction) from the centre ('0') of the EC population at the 0 hour, 6 hour and 24 hour time points compared to that observed experimentally.

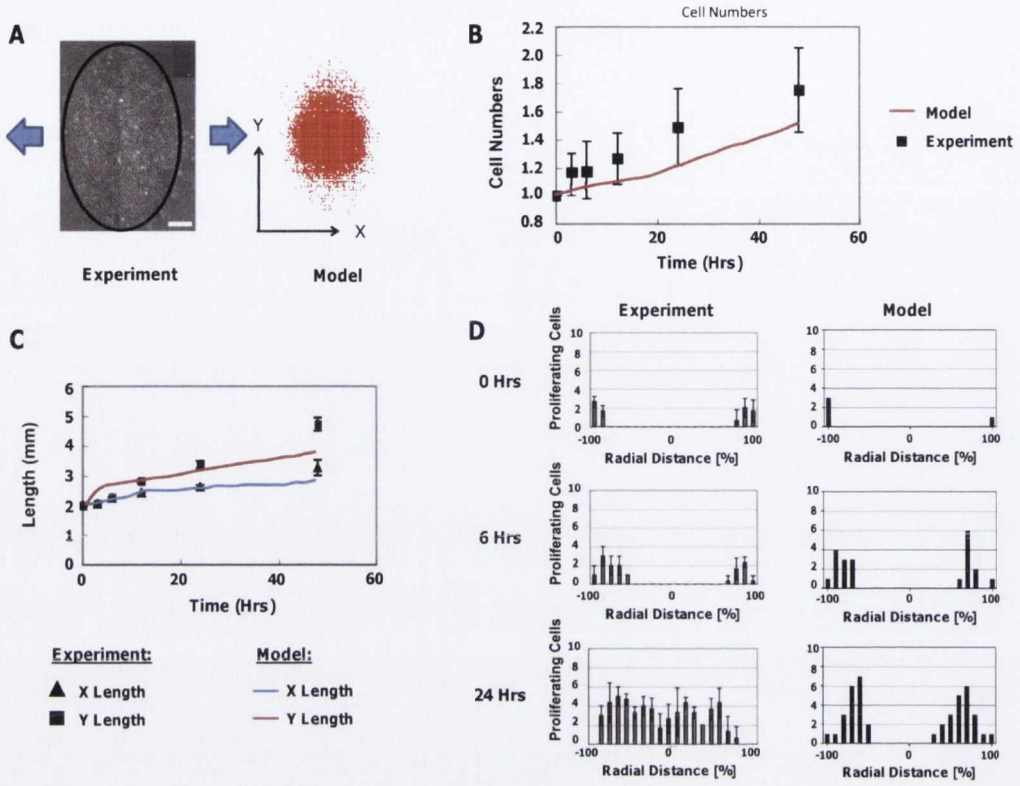

Figure S3. Model Predictions: Strain increases the rate of EC proliferation and leads to directionally biased migration. (a) Model prediction of the final distribution of the endothelial cell population compared to that observed experimentally. (b) Model prediction of the change in the total cell number over time compared to that observed experimentally. (c) Model prediction of the variation in the X and Y lengths of the endothelial cell region over time compared to that observed experimentally. (d) Model predictions of the number of proliferating cells at various radial distances (Y direction) from the centre ('0') of the EC population at the 0 hour, 6 hour and 24 hour time points compared to that observed experimentally.

Appendix V: Determination of element location of each lattice point for an irregularly shaped mesh

A plane is created for each side of an element using the equation of a plane:

$$s = Ax + By + Cz + D$$

Where the normal vector is (A,B,C) (see Figure S4 below). For three points (x_1, y_1, z_1), (x_2, y_2, z_2) and (x_3, y_3, z_3) the equation of the plane is calculated from the following determinants:

$$A = \begin{vmatrix} 1 & y_1 & z_1 \\ 1 & y_2 & z_2 \\ 1 & y_3 & z_3 \end{vmatrix}, B = \begin{vmatrix} x_1 & 1 & z_1 \\ x_2 & 1 & z_2 \\ x_3 & 1 & z_3 \end{vmatrix}, C = \begin{vmatrix} x_1 & y_1 & 1 \\ x_2 & y_2 & 1 \\ x_3 & y_3 & 1 \end{vmatrix}, D = -\begin{vmatrix} x_1 & y_1 & z_1 \\ x_2 & y_2 & z_2 \\ x_3 & y_3 & z_3 \end{vmatrix}$$

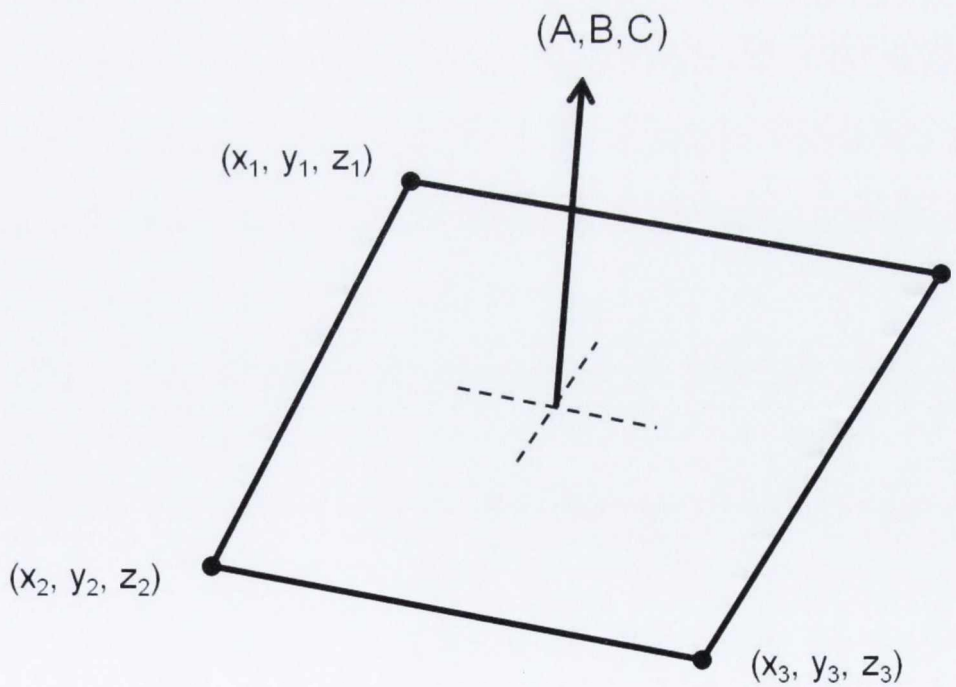

Figure S4. Normal vector (A,B,C) to the plane

For a given lattice point (x, y, z) to be included as part of an element, the lattice point must be inside each of the 6 sides of the element. The sign of s determines which side the lattice point lies with respect to the plane. If s is greater than zero, the point is on the same side as the normal. If s is less than zero, the point is on the opposite side to the normal. If s is equal to zero, the lattice point lies on the plane. To ensure correct interpretation of the direction of the normal vector, the lattice point is being calculated on the correct side of the plane, the centre point of the element is subjected to the same calculations ensuring the correct sign of s.